Development and in vitro testing of liposomal gadolinium-formulations for neutron capture therapy of glioblastoma multiforme

Dissertation zur Erlangung des Grades
„Doktor der Naturwissenschaften“

im Promotionsfach Pharmazie

am Fachbereich Chemie, Pharmazie und Geowissenschaften
der Johannes Gutenberg-Universität Mainz

Tanja Peters
geb. in Oldenburg (Oldb.)

Mainz, 2013

1. Berichterstatter:
2. Berichterstatter:

Tag der mündlichen Prüfung: 29.10.2013

D77

Somewhere, something incredible

is waiting to be known.

Carl Sagan

Acknowledgements

Table of contents

Abbreviations

API	active pharmaceutical ingredient
BBB	blood brain barrier
BC(A)	bicinchoninic acid (assay)
BCNU	bis-chlorethyl-nitrosourea (carmustine)
BCRA1	breast cancer 1 gene
BER	base excision repair
BNCT	boron neutron capture therapy
Bp	base pairs
BPA	boronophenylalanine
BSH	sodium borocaptate
CED	convection enhanced delivery
CF	5,6-carboxyfluorescein
CFA	colony forming assay
CHEMS	cholesteryl hemisuccinate
CME	clathrin-mediated endocytosis
CL	cardiolipin, cardiolipin-containing liposome formulation
CvME	caveolin-mediated endocytosis
Da	Dalton
DAOS	*N*-Ethyl-*N*-(2-hydroxy-3-sulfopropyl)-3,5-dimethoxyaniline sodium salt
DAPI	4',6-Diamidino-2-Phenylindole
DLS	dynamic light scattering
Dsb	double strand break

DMEM	Dulbecco's modified eagle medium
DNA	deoxyribonucleic acid
DOPC	dioleoylphosphatidylcholine
DOPE	dioleoylphosphatidylethanolamine
DOTAP	dioleoyltrimethylammoniumpropane
DSPC	distereoylphosphatidylcholine
DTPA	diethylenetriaminepentaacetic acid
EE	encapsulation efficiency
EGF	epithermal growth factor
EGFR	epithermal growth factor receptor
ER	endoplasmic reticulum
Er-DTPA	erbium-DTPA
EPR	enhanced permeation and retention
FDA	food and drug administration
FoI, foIS	folate-PEG2000-distearoylphosphatidylethanolamine – containing liposome formulation
FolPEG2000	folate-PEG2000-distearoylphosphatidylethanolamine
FR α	folate receptor alpha (synonym to FR 1)
FRβ,γ	folate receptor beta, gamma
GBM	glioblastoma multiforme
Gd-DTPA	gadolinium-DTPA (as in Magnevist® solution)
Gd-DTPA-NV	gadolinium-DTPA (in tris-acetate buffer, from Nanovel)
GPC	gel permeation chromatography
Gy	Gray
HER2	human epidermal growth factor receptor 2

HPC	hydrogenated phosphatidylcholine
HR	homologous repair
ICP-MS	inductively coupled plasma mass spectrometry
LET	linear energy transfer
Linac	linear accelerator
LQ	linear-quadratic
Lu-DTPA	lutetium-DTPA
MCNP5	Monte Carlo N-Parcticle Code 5
MRI	magnetic resonance imaging
MTT	3-(4,5-dimethylthiazol -2-yl)-2,5-diphenyltetrazolium bromide
MWCO	molecular weight cut-off
NBD-PE	*N*-(7-Nitrobenz-2-Oxa-1,3-Diazol-4-yl)-1,2-Dihexadecanoyl-*sn*-Glycero-3-Phosphoethanolamine
NC	neutron capture
NCE	neutron capture element
NCT	neutron capture therapy
NER	nucleotide excision repair
NHEJ	non-homologous end joining
NPR1	natriuretic peptide receptor 1
OD	optical density
PBS	phosphate-buffered saline
PCR	polymerase chain reaction
PDGFR (β)	platelet-derived growth factor receptor
PEG	polyethylene glycol

PEG-PE	polyethylene glycol-phosphoethanolamine
P-gp	P-glycoprotein
PTEN	Phosphatase and tensin homolog
Q	Q-value for nuclear reactions (energy release)
RBE	relative biological effectiveness
RES	reticuloendothelial system
RFC	reduced folate carrier
RNA	ribonucleic acid
mRNA	messenger RNA
siRNA	silencing RNA
RT-PCR	reverse transcriptase PCR
Ssb	single strand break
TEER	transepithelial electrical resistance
Tf	transferrin
TfR (1)	transferrin receptor (1)
VEGFR	vascoendothelial growth factor receptor
XRT	external beam radiation therapy
Z	atomic number

Figures

Tables

1 Introduction

1.1 Liposomes

1.1.1 Structure and composition

Liposomes are nano-sized particulate systems made of a lipid bilayer and an aqueous core. The vesicles are mainly composed of phospholipids, amphiphilic molecules with a hydrophilic headgroup and a lipophilic tail. Due to their amphiphilic nature, the formation of a bilayer is energetically favored in water. By arrangement of the hydrophilic headgroups toward the aqueous surrounding and clustering of the hydrophobic tails together, so that the contact with water is minimized, the phospholipids are able to spontaneously form an ideal structure in regard to their energetics: the liposome, a closed structure without any interfaces between water and hydrophobic molecule parts.

Small liposomes have a size of 20-50 nm, while large liposomes range from 50 to several hundred nanometers. Liposomes can also be categorized according to their lamellarity; unilamellar liposomes exhibit only one bilayer, multilamellar liposomes have several lipid bilayers arranged in an onion-like manner and multivesicular liposomes consist of a large liposome containing several smaller vesicles (fig. 1-1) [1]. The phospholipid bilayers may consist of a single lipid species or be composed of a mixture from several different lipid families (see below). Cholesterol often serves to add more rigidity to liposomes consisting of unsaturated lipids such as DOPC or to preserve fluidity in bilayers of saturated lipids like DSPC [2, 3]. Phospholipids like phosphoglycerides and sphingolipids as well as sterols are the most common lipids for drug carrier design, although synthetic lipids like the cationic DOTAP and synthetic lipid-polymer compounds like the shielding lipid PEG-DSPE have been fashioned for the application in new liposomal transporters for drug delivery and diagnostic purposes. Since their lipid bilayer composed of phospholipids closely resembles biological membranes, liposomes have also been used widely to mimic cellular membranes and study their characteristics and interactions with other membranes in vitro [4, 5]. Furthermore, cellular transport vesicles such as endosomes or lysosomes exhibiting the typical lipid bilayer- and aqueous core - structure can also be described as naturally occurring liposomes.

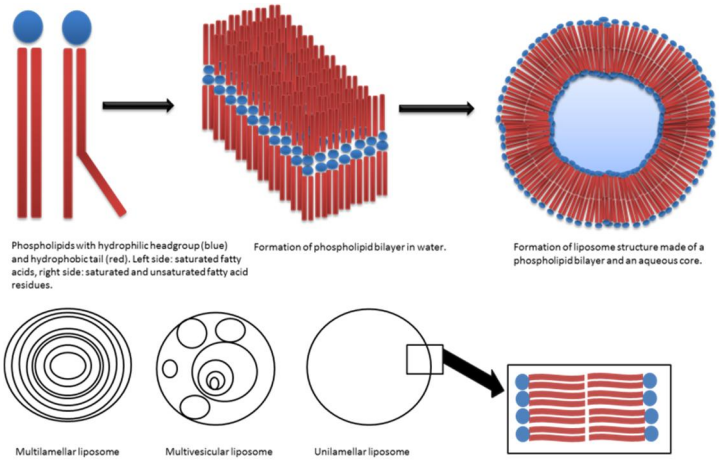

Figure 1-1 Phospholipids and liposome structures (according to Jesorka and Owar [1])

Phospholipids can be divided in two main groups: phosphoglycerides and sphingolipids. Phosphoglycerides consist of a glycerin backbone which has two fatty acids ester-bound to two hydroxyl-groups (hydrophobic tail) and a phosphate-group on the last hydroxyl-group (hydrophilic headgroup). The phosphate-group is ester-bound to alcohols such as ethanolamine, choline, inositol or serine. Sphingolipids can be divided into further subgroups, but for liposomes the phosphorus-containing species, the sphingomyelins, are the most important. Sphingomyelins derive from the amino alcohol sphingosin which is ester-bound to the phosphate-group (which itself is bound to an additional alcohol) and amide-bound to a fatty acid.

Cellular membrane lipids consist generally of phosphocholines (lecithins), phosphoethanolamines (cephalins), phosphatidylserine and sphingomeylins as well as membrane proteins and glycolipids making up the carbohydrate layer of the membrane surface [6]. The membrane lipids differ primarily through the alcohol which is ester-bound to the phosphate-group. The length of the fatty acids and their saturation status are important factors regarding the characteristics of the liposomal carrier, since highly saturated lipids exhibit a higher transition temperature from gel-state to liquid-crystalline state. Shorter chain lengths ensure higher fluidity of the membrane, since the interaction between the chains is lower and lateral movement of the molecules is thus facilitated. Liposomes composed of phospholipids with saturated fatty acids form much more rigid bilayers than unsaturated phospholipids and exhibit different ion permeability across the liposome membrane [7, 8]. Due to the kink caused by the double bonds in their carbon tail, the unsaturated fatty acids prevent a packing as tight as for the saturated, straighter fatty acids and therefore show higher permeability and fluidity. Biological membranes normally contain phospholipids in the liquid-crystalline state, thus preserving the fluidity of the membrane. Furthermore, sterols are included into the bilayer for regulation of membrane fluidity [9]. Phosphatidylcholine is the most abundant lipid in cellular membranes, while cholesterol is also contained to a high amount, namely 20% by weight of all membrane lipids [6]. Therefore, DOPC, a phosphocholine with two unsaturated groups was combined with cholesterol and this composition was chosen as the principal lipid mixture for this study. The phase transition temperature of DOPC is -20°C, thus ensuring the liquid crystalline state at room temperature.

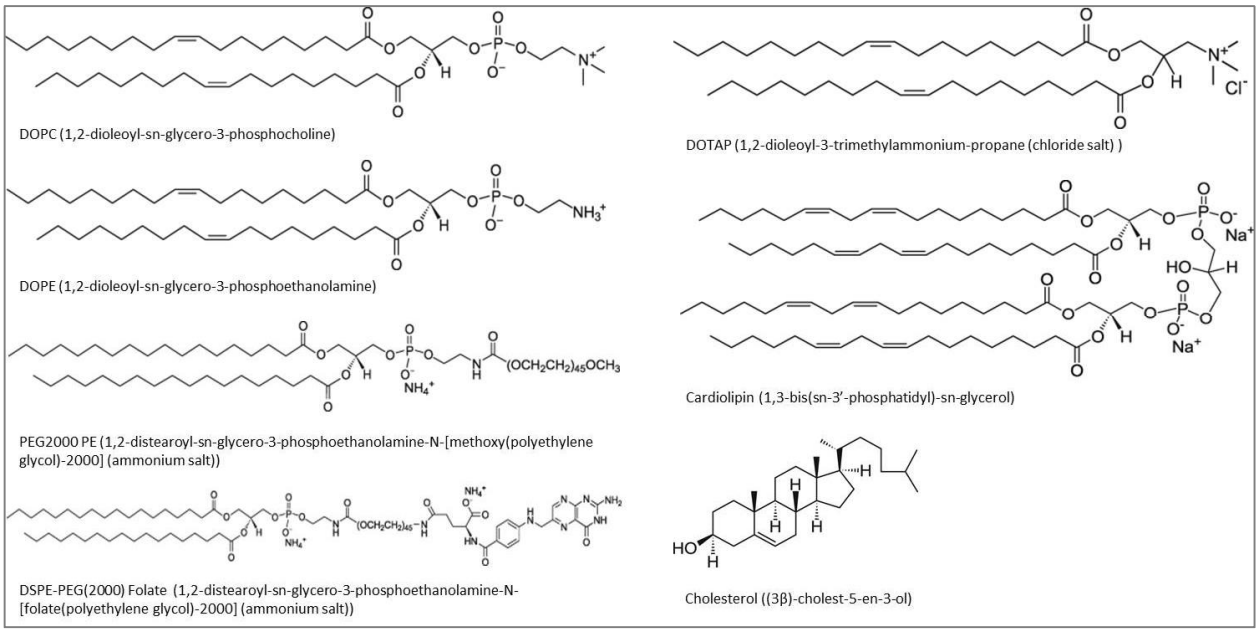

Figure 1-2 Overview of different lipid species (from Avanti Polar Lipids, see references: additional websites)

1.1.2 Manufacture of liposomes

The manufacture of liposomes makes use of a wide variety of different processes, a few of which will be described here briefly. The formation and the size of liposomes can be regulated by the use of downsizing devices or by adjustment of parameters for 'spontaneous' liposome formation techniques. The most common methods using downsizing devices are extrusion (extruder), ultrasound (bath or tip sonicator) and homogenization (homogenizer). These manufacturing methods normally begin with preparation of a lipid film from an organic lipid solution and evaporation of the solvent according to Bangham et al [4]. Rehydration of the film with respective drug solution causes formation of multilamellar liposomes. These large liposomes are then subjected to a particular downsizing method to obtain the desired size distribution. Except for the extrusion technique which uses a specially sized pore membrane, the size of liposomes may vary significantly for these methods [3]. Subsequent filtration or centrifugation steps can be added to obtain a monomodal size distribution of liposomes [10].

Manufacture of spontaneously forming liposomes may for example be done by reverse-phase evaporation, dehydration-rehydration method or detergent depletion technique. Most of these methods involve the use of organic solvents in one or more steps of the process, as in the reverse-phase evaporation. Here, the lipids are dissolved in organic solvent and the aqueous drug solution is added before the mixture is set into a bath sonicator. The resulting emulsion is then kept under vacuum for evaporation of the organic phase and in the residual water phase, liposomes form spontaneously [11]. The main drawback of this technique is the uneven size distribution of the obtained vesicles. For different batches, the size distribution has therefore to be monitored closely and subsequent steps for size adaption may be needed.

The dehydration-rehydration method involves a freeze-drying step after preparation of multilamellar, pre-formed liposomes. The lyophilized liposomes are then reconstituted with rehydration solution and in some cases, extruded in a final step. This technique ensures high entrapment efficiency even for macromolecules, but is on the other hand very extensive and time-consuming due to the multiple preparation steps.

In contrast to the above mentioned manufacturing methods, the detergent depletion technique is suitable for the liposomal encapsulation of labile and sensitive molecules, such as enzymes and proteins. For the formation of liposomes, a colloidal solution of mixed micelles consisting of detergent and lipid is prepared. Then, the detergent is removed from the mixture and liposomes are formed. Depletion of detergent can be carried out by different methods such as dilution, dialysis and gel filtration. Although this technique allows handling of many different lipids and substrates for liposome formation, the detergent removal is considered a slight disadvantage. Complete subtraction of the detergent is time-consuming and in case of dialysis often requires tremendous amounts of buffer solutions, but may be the only means to obtain reasonably homogenous liposomes encapsulating fragile enzymes and proteins [12].

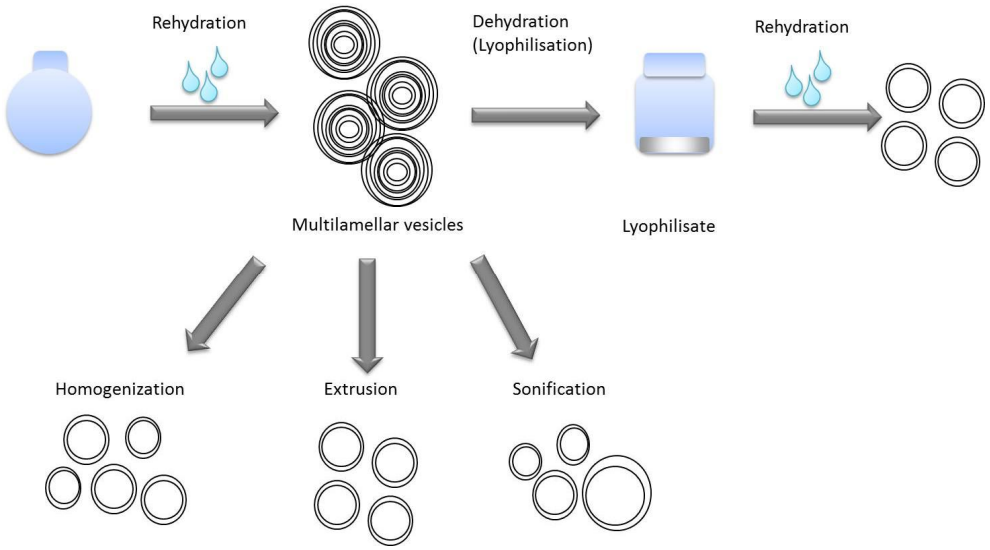

Figure 1-3 Liposome manufacture techniques using downsizing devices and dehydration-rehydration method (according to Jesorka and Owar [1], Lasch et al. [12] and Szoka [11])

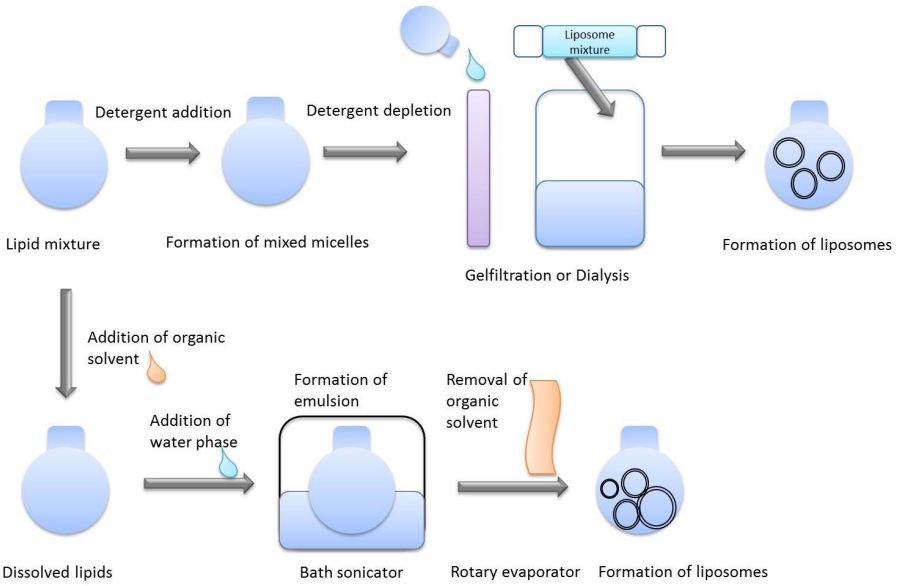

Figure 1-4 Liposome manufacture techniques: detergent-depletion and reverse-phase evaporation method (according to Lasch et al. [12] and Szoka [11])

1.1.3 Liposomes as drug carrier systems

The idea to use liposomes as drug carrying systems developed shortly after the beginning of liposome research in 1965, but it was only in the late 1980s that the full potential of the liposomal drug application was discovered and clinical studies were initiated [4, 13]. The employment of a liposomal nanoparticulate system for drug delivery of highly active substances offers several important advantages over the application of the free drug:

- Liposomes shield entrapped drugs from the biological environment and thus prevent drug degradation by enzymes and adverse conditions in the human body.
- The patient also is protected from unwanted side effects of the API, such as action of the drug at non-target structures (e.g. similar to doxorubicin, see below).
- The high payload of large vesicles enhances accumulation of drug at the target site, particularly in the case of actively targeted liposomes.
- The possibility to control the drugs' side of action by simple variation of the carrier (e.g. liposome composition and/ or addition of a targeting moiety).
- Poorly soluble drugs can be inserted in the lipid bilayer, thus increasing the solubility and bioavailability of the drug.
- The biodegradability and low toxicity of natural and synthetic phospholipids offers no restrictions for their application in vivo.
- Multilamellar liposomes can be used as a sustained release system, especially in the case of lipophilic drugs which can be embedded in the multiple lamellar structures.

For the above mentioned reasons, liposomes have been and are still a promising way to improve drug delivery and bioavailability. The great success of the first liposomal anticancer drug doxorubicin (Doxil®, FDA approval 1995) which showed higher effect on cancer cells and less cardiotoxic side effects than the free drug, prompted many trials for other liposomal drug formulations [14-16]. Until now, it has been mostly anticancer drugs for which liposomal formulations were developed, although there are some examples for other groups, such as antibiotics (e.g. Ambisome® against fungal infections) and vaccines (e.g. Epaxal®, immunization against hepatitis A) [17].

Name	API	Indication
Abelcet®	Amphotericin B	Fungal infections in immunocompromised patients
Ambisome®	Amphotericin B	Fungal infections in immunocompromised patients
Daunoxome®	Daunorubicin	Kaposi's sarcoma
Depocyte®	Cytarabine	Lymphomatous meningitis
Depodur®	Morphine	Pain treatment after surgery
Doxil®/LipoDox®/Evacet®	Doxorubicin	Kaposi's sarcoma Mulitple myeloma Ovarian cancer
Epaxal®	Hepatitis A Virus, inactivated	Hepatitis A vaccine
Inflexal® V	Influenza Virus surface antigens, inactivated	Influenza vaccine
Marqibo®	Vincristine	Acute lymphoblastic leukemia
Visudyne®	Verteporfrin	Age-related macular degeneration Pathologic myopia Presumed ocular histoplasmosis

Table 1 Overview over selected FDA approved liposomal drugs (according to Immordino et al. [14] and Chang and Yeh [17])

Several thoroughly different kinds of liposomes besides the conventional and pegylated species are applied in drug delivery. The aforementioned vaccines are composed of phospholipids and virus surface components forming a virosome. These virosomes mimic a natural occurring virus infection and thus enhance the immune response [17]. For gene delivery, cationic liposomes or lipoplexes were developed. The cationic lipid interacts with anionic DNA or RNA and forms a complex structure which is then used for gene therapy and RNA applications [14, 18, 19]. In addition to their use for transfection, cationic lipids have gained attention for their ability to target tumor vasculature and are therefore an interesting carrier for anti-angiogenetic drugs [17, 20, 21]. Another example for the wide-spread applicability of liposomes is their new-found role in lymphatic targeting. In this case, the liposomal formulation is applied mostly subcutaneously or intra-muscular [22]. The liposome surface can be modified with structures such as avidin and biotin which are known to aggregate after application and thus serve to enhance retention in lymphatic structures like lymph nodes [23]. Furthermore, the imaging of body structures and organs is very helpful for treatment planning, in particular for cancer treatment where the identification of the sentinel lymph node and possible metastases is important for further therapy [24]. Liposomes serve here as imaging agents by carrying MRI contrast agents (e.g. Magnevist®(Gd-DTPA)) and dyes into the respective area, thereby increasing retention time of the marker and facilitating for example surgical removal of tumors and their metastases [25].

Their flexibility in drug encapsulation and drug retention make liposomes a versatile carrier for a broad range of applications in modern treatment strategies. Liposome composition and surface modifications are an easy and promising way to address a multitude of diseases and target sites. At present, applications for liposomes include many different areas, in particular approaches for cancer and gene therapy, lymphatic targeting (against e.g. HIV or metastases [26]), imaging and immunization, and very likely will be expanded to further medical employments in the near future.

1.1.4 Targeting aspects

To improve drug delivery to the site of interest, liposomes can be equipped with targeting moieties such as antibodies (e.g. anti-EGFR) and receptor substrates (e.g. folate, transferrin). The main advantage of employing target structures on the liposome surface is the possibility to address only cells exhibiting the counterpart of the targeting structure, such as cancer cells which overexpress special receptors.

Targeting of conventional liposomes to tumors after intravenous injection relies primarily on passive targeting, the so-called enhanced permeation and retention of liposomes (EPR-effect) in tumor tissue. The effect was first described by Matsumura and Maeda [27] who noticed that macromolecules were preferably accumulated in tumors rather than in normal tissue, whereas low-weight molecules were not. Furthermore, the lymphatic clearance in tumor tissues was very small, therefore, the retention of particles inside the tumor was prolonged in comparison to normal tissues. The authors ascribed this effect to high vascularization of solid tumors and enhanced vascular permeability ('leakiness'), as well as the observed slow or hindered lymphatic clearance in these tissues. Nevertheless, to achieve a sufficient delivery of liposomes to tumor tissue, it is necessary to give liposomes enough time to extravasate and remain trapped inside the tissue. Unfortunately, liposomes tend to attract the human immune defense system, more precisely macrophages. Conventional liposomes are easily cleared from the bloodstream by the reticuloendothelial system of the liver before they can reach their destination. Consequently, prevention of liposome uptake into macrophages and prolongation of their circulation time have been

made the subject of further investigation. First experiments introduced monosialoganglioside and phosphatidylinositol in the lipid bilayer, changed the lipid composition to smaller and more rigid structures and in fact achieved considerably higher blood circulation and tumor concentration [28]. However, the most successful strategy so far was the introduction of long-chain hydrophilic polymers such as polyethylene glycol (PEG), polyvinylalcohol, chitosan or dextranes into the liposome bilayer, thus promoting the circulating time regardless of liposome composition [14, 29-31]. PEG offers several advantages for the use in liposomal formulations. It is biocompatible and non-toxic, if the molecular weight is above 400 Da, has a low immunogenicity and above all, it is already approved by FDA for internal administration [30]. The mechanism for prolonged circulation for so-called pegylated liposomes was attributed to the positioning of a strong steric barrier between liposome and macrophages by branches of PEG-PE molecules inserted into the outer liposome membrane. Another explanation for the effective shielding of liposomes after pegylation is lesser opsonization of the surface and thus less attraction of macrophages [29, 30]. Despite the rather bulky appearance of pegylated liposomes, it was found that the accumulation in tumor tissue exceeded those of normal (conventional) and even of targeted (folate) liposomes. Nevertheless, the uptake of pegylated liposomes is relatively low due to the steric hindrance of the PEG-chains and a target moiety is therefore still necessary to promote uptake of the liposome into target cells after extravasation from the bloodstream [32]. Doxil®, the first liposomal doxorubicin was also designed as a pegylated formulation [16].

Besides the shielding of liposomes against macrophages via pegylation, researchers sought to enhance uptake of the vesicles into target cells while non-target cells should be spared, especially in the case of cancer treatment. The idea was to find characteristics of cancer cells that normal cells did not possess, such as surface markers or receptors. Since receptor expression is almost never constricted to only one cell or tissue type, an abnormal high expression of receptors became the lead target structure instead. Here, epithermal growth factor receptors (EGFR, HER2), the folate receptor 1 (FRα), transferrin receptor (TfR) and others were chosen as promising targets, since different cancer types were found to overexpress one or more of these receptors [33-36]. Although the simplest way would be to address the target via offering the respective ligand as a counterpart on the liposome surface, this approach took hold primarily for FR alpha and TfR. For the other receptors, an additional objective was the coupling of anti-EGFR and anti-HER2 antibodies to liposomes [13]. These immunoliposomes target the respective receptor via antigen-antibody binding, thus effectively delivering their cargo to the target cell. The antibodies, as well as folate, are normally linked to the liposome surface via a PEG-spacer, since it was found that, in spite of their targeting moiety, conventional liposomes were still cleared rapidly from the blood stream [34].

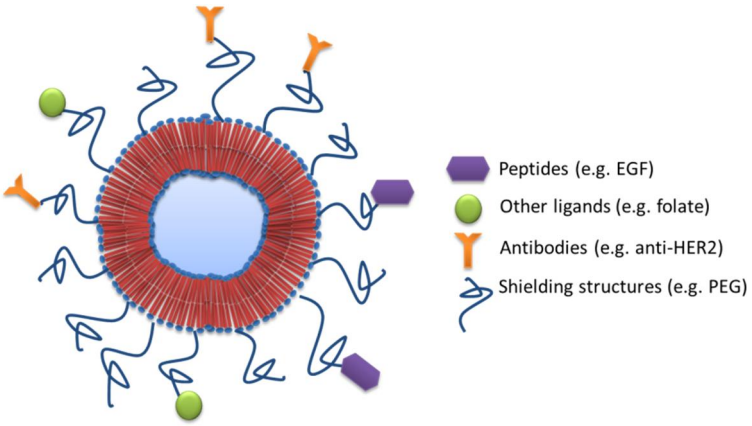

Figure 1-5 Liposome equipped with targeting and shielding structures (according to Torchilin [13])

A special case for the need of targeting structures is the blood brain barrier (BBB). This impenetrable barricade between blood and brain cells is composed of capillary endothelial cells effectively sealed against invasion by their tight junctions. The BBB is strictly controlled by astrocytes which attach to the basal lamina of the endothelial cells [37, 38]. The transport of molecules through this barrier is restricted by the aforementioned tight junctions and mechanisms such as P-glycoprotein (P-gp) efflux pumps. P-gp has been identified as a major component in multi-drug resistance of tumor cells and effectively exports for example anticancer drugs from the intracellular space [39]. Hence, the successful delivery of (hydrophilic) drugs to the brain needs a strategy to overcome the BBB and ensure sufficient drug accumulation to induce an effect. As for tumor targeting, liposomes can be equipped with receptor ligands for brain endothelial cells. Transferrin seemed to be an appropriate ligand, since TfR was found to be expressed by these cells [40]. Furthermore, the inhibition of P-gp was reported in addition to high uptake by Gao et al. [39] after application of dual-targeted liposomes to a BBB model, accounting for the suitability of the chosen targeting moieties. Besides the application of targeting structures, the BBB can also be circumvented by hyperosmotic disruption (e.g. through hyperosmotic mannitol solution opening the tight junctions), intra-arterial injection and convection-enhanced delivery (CED) [41, 42]. CED uses local infusion of a bulk drug solution via catheter in the region of interest. However, aside from CED, these methods are either non-specific for the applied drug (hyperosmotic disruption) or the bypassing of the BBB is strongly dependent on the time allowed for drug-cell interaction and the actual uptake of drug may therefore be uncertain (intra-arterial injection) [42]. The highest delivery and, consequently, the highest uptake of drug into brain cells is still achieved via direct injection; either intrathecal, intraventricular or in case of tumors, intratumoral and intracavitary [43].

1.1.5 Liposome uptake into cells

Liposomes are believed to enter cells by endocytosis and primarily via the clathrin-mediated pathway [44]. The uptake mechanisms of cells can be divided into at least four different pathways: uptake via clathrin-coated pits, caveolae-mediated uptake, macropinocytosis and phagocytosis. The question if membrane fusion also contributes to liposome uptake is still discussed controversially [44, 45].

The pathway by which a particle enters a cell is dependent on its size, surface charge and composition, as well as the up-taking cell type. In general, the clathrin-coated pits allow a cargo with a size of about 100nm, while bigger particles (500nm) are taken up via caveolae-mediated route [44, 46]. The uptake pathway can decide over the intracellular fate of the cargo, therefore the investigation of endocytotic mechanisms is of great importance for the development of nanoparticulate drug formulations. After internalization via clathrin-coated pits, the clathrin-coated vesicles become early endosomes where the cargo is sorted, in some cases recycled and send back to the membrane (e.g. receptors). Then the vesicles turn into late endosomes which already provide an acidic pH and finally into lysosomes where the cargo is degraded by lysosomatic enzymes. The uptake of particles via clathrin-mediated endocytosis may also be stimulated by ligand binding (e.g. EGF) while other receptors such as transferrin receptor are constitutively internalized [47]. For the caveolae-mediated uptake, an alternative route besides the degradation in lysosomes leads to the endoplasmatic reticulum (ER). This pathway is being used by some viruses, for example the Simian Virus 40 (SV40). The virus enters the cell via caveolin-mediated endocytosis (CvME), after which it is transported to the ER and finally to the nucleus [48]. In addition, CvME may also be receptor-mediated and ligands thought to use this pathway are folate, albumin and cholesterol [48].

Macropinocytosis is a non-specific entry route for molecules dissolved in the extracellular fluid. Here, the fluid flows into a cavity formed by membrane protrusions which then break down and fuse with the membrane, thus internalizing the fluid [44]. The further progress of the cargo in the cell is not yet fully understood. For some cells, the internalized vesicle proceeds to lysosomes, although in others their contents are recycled [45]. Phagocytes such as macrophages, dendritic cells and monocytes possess another means for particle uptake, the phagocytosis [49]. Here, membrane extensions envelop large particles (e.g. bacteria, apoptotic bodies, dead cells) which were previously marked as cargo by opsonins. The opsonized cargo binds to receptors on the macrophages' surface and is internalized when the cell extensions close around the particle. Direct receptor binding of cargo to the cell surface without the aid of opsonins is also known as an uptake mechanism. The internalized particles are led to lysosomes where degradation of the vesicle's contents takes place [45].

The fate of endocytosed carriers and their cargo is of special interest for drug delivery purposes. Particularly in the case of labile molecules, such as RNA or DNA for gene therapy, an ending in lysosomes under the influence of degradation enzymes and highly acidic pH has to be avoided at all cost [50]. To preserve the activity of the compound, an escape route from the endosomal compartment (where conditions are still mild in comparison to lysosomes) needs to be established. For liposomes, this has been accomplished for example through introduction of pH-sensitive lipids into the bilayer. Liposomes composed of dioleoylphosphatidylethanolamine (DOPE) and cholesteryl hemisuccinat (CHEMS) as a helper lipid are subjected to conformational changes under acidic conditions [51]. Low pH as in endosomes induces destabilization of the liposome membrane, primarily through phase change of DOPE from lamellar to inverted hexagonal phase [52, 53]. It is believed that consequently to these changes and eventual pore formation, fusion of the liposome with the endosomal membrane occurs, followed by emptying of liposome contents into the cytosol [54].

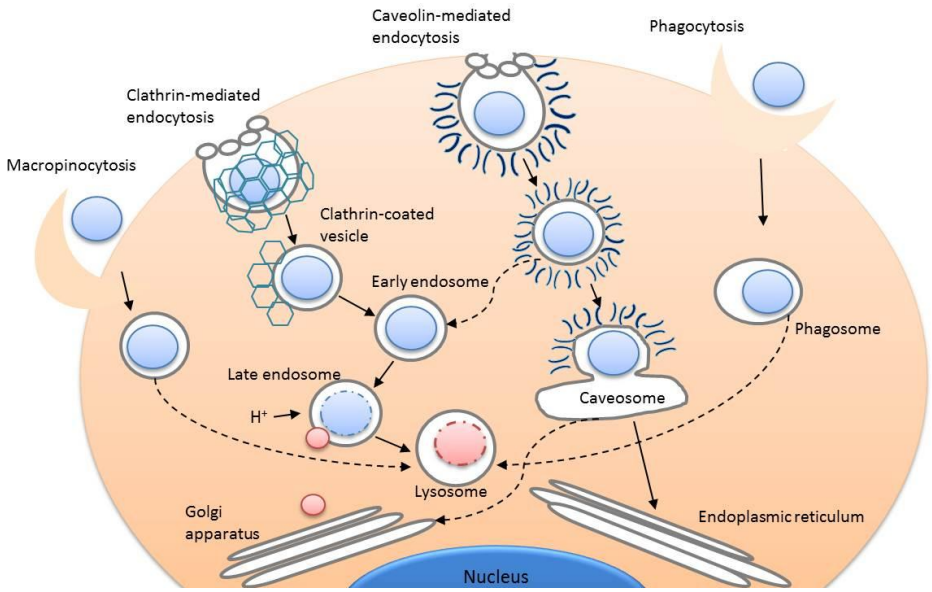

Figure 1-6 Overview over endocytotic pathways (according to Hillaireau and Couvreur [49], MacMahon and Boucrot [47] and Xiang et al. [45])

1.2 Cancer therapy: glioblastoma multiforme

Aside from cardiovascular diseases, cancer is the most common cause of death in Europe and the USA. The cancer types with the highest incidence in Europe are breast cancer (women) and lung and prostate cancer (men) [55]. In the USA, the age-adjusted incidence of lung and bronchial cancer was 61.4 cases per 100,000 people. Brain cancer in contrast has a relatively low incidence with 6.5 cases per 100,000 people [56], but these cases include some of the most aggressive cancer types known. The prognosis for high grade glioma, a type of brain cancer accounting for roughly 40% of all primary brain tumors, is exceptionally poor. As few as 10% of the patients diagnosed with glioblastoma multiforme are still alive 5 years after diagnosis and the median survival under standard treatment is only 14.6 months [57].

Glioma is the general term for all tumors arising from the supportive tissue of the brain (glial cells) in contrast to the neuronal cells. Astrocytomas derive from degenerated astrocytes, star-shaped cells that present the glue-like part of the brain. Gliomas are the most prevalent primary brain tumors and high grade glioma, including glioblastoma multiforme (also: astrocytoma grade IV, GBM), represent 60-75% of all gliomas [58]. Due to high proliferation of the cells and an extensive blood supply from a close network of blood vessels, the tumor is very aggressive and highly malignant. It grows infiltrating into healthy brain tissue, thus rendering complete surgical removal of the tumor extremely difficult. Although the tentacle-like extensions of the tumor invade into normal brain tissue, the tumor usually does not form metastases and spread into other body parts than the brain. Most astrocytomas in adults arise in the cerebrum, but the tumor may also be located in the other parts of the brain, such as the brainstem and the cerebellum. The blood brain barrier is often disrupted at the tumor site which facilitates drug uptake into the cancer cells as well as tumor imaging, especially with MRI contrast agents like Gd-DTPA. Glioblastoma can also form from previously low-grade astrocytomas which grow more slowly, but are nevertheless very aggressive; this type is classified as secondary glioblastoma. Symptoms from glioblastoma may be unspecific such as headache or nausea, but dependent on the tumor location, seizures, personality changes, visual field defects and other neurological deficits may occur [59].

The treatment of glioblastoma is difficult, since the tumor mass often contains necrotic cells and a heterogeneous mixture of anaplastic astrocytes [59]. Some of these cells may not respond to certain treatment options, therefore, the therapy consists normally of a combination of two or more treatments. The first step is to remove as much of the tumor mass as possible to lessen the cranial pressure that derives from the tumor and to preserve neurological function and reduce the impact of the tumor on the healthy brain [57]. During surgery, chemotherapeutics can already be applied to the former tumor cavity; this will be done by so-called wafers which contain the cytotoxic drug carmustine (BCNU). The alkylating agent is supposed to prevent tumor regrowth from residual cancer cells which could not be removed surgically. The surgical debulking is usually followed by radiotherapy and chemotherapy with temozolomide, another DNA-alkylating agent.

Radiotherapy is after surgery the most effective treatment of glioblastoma [60]. The standard treatment is fractionated external beam radiation, for example 1.8 Gy, five times a week over 5 or 6 weeks (total dose of about 60 Gy). Other radiation treatments are stereotactic surgery (single high-dose fraction from a very narrow beam directed at the lesion), brachytherapy (radioactive isotopes are placed directly into brain tumor), proton beam and boron neutron capture therapy.

Besides the standard therapy with temozolomide, further options for GBM treatment include courses of other chemotherapeutic drugs such as cisplatin, carboplatin, etoposide and irinotecan [57, 59, 61, 62]. Some of these drugs are also given concurrent to radiotherapy, as is temozolomide. Despite all these efforts to cure GBM, the probability of tumor reappearance is high and the median time to recurrence is approximately 7 months after standard therapy treatment. For tumor recurrence, the treatment options are practically similar to first therapy: resection of the tumor in selected patients and concomitant radio- and chemotherapy with temozolomide or another anticancer drug.

Despite the advances in cancer research in the last decades, the diagnosis of glioblastoma still leads to fatal outcome in nearly all cases. Although glioblastoma has been studied extensively to reveal potential points of action, few strategies have proven to prolong survival for more than some weeks. Among these, the use of tenascin C-siRNA was very successful, the median survival of GBM patients treated with this option was 106 weeks in comparison to 48 weeks [63]. Tenascin-C is a proliferation-stimulating protein which is often overexpressed in glioma and the siRNA was used to silence the respective gene. Further RNA applications are the knock-down of DNA repair gene O6-methylguanine-DNA methyltransferase (MGMT) which causes resistance to temozolomide [64, 65]. Other strategies base on targeting glioma cells via their overexpression of growth factor receptors such as EGFR, VEGFR, PDGFR or other receptors like transferrin [57]. Natural toxins are then conjugated to the respective ligand proteins and transferred into glioma cells. Additionally, the angiogenesis of tumor-supporting blood vessels can be counteracted by the application of monoclonal antibodies such as bevacizumab and other anti-angiogenic drugs. Unfortunately, not all glioblastoma cells, particularly the tumor stem cells, respond to treatment. Tumor stem cells in glioblastoma have the ability to provoke cancer while displaying the characteristics of somatic stem cells. It seems that especially the genetic profile of the cells, including for example the status of tumor suppressor gene PTEN, the expression of P-glycoprotein and the multidrug resistance-related protein 1, has a major influence on the efficacy of the treatment [61, 66]. Therefore, the exact classification of the tumor and its genetic profile has become a very important part in the treatment planning and the choice of therapeutic strategy for glioblastoma patients. However, due to tumor inhomogeneity and subsequent different cellular effects, improvements of current treatment options such as radiotherapy are crucial for the amelioration of long-term survival of GBM patients.

Figure 1-7 MRI image of a glioblastoma (from ABTA brochure [57])

1.3 Radiation therapy

1.3.1 Cellular response to ionizing radiation

1.3.1.1 Characteristics of ionizing radiation

Radiation effects on cells are based on the direct or indirect ionization of molecules in the cell, thus leading to lesions of cellular structures as proteins, membranes and DNA. Ionizing radiation can consist of many different particles, such as neutrons, protons, electrons, heavy ions (carbon), α-particles or photons (x- and γ-rays), the latter exhibiting both characteristics of particles and waves. The particles can be divided into groups according to their ability to ionize atoms along their pathway. Ions and fast neutrons are highly (or densely) ionizing particles while electrons have a low linear energy transfer (LET) and are sparsely ionizing. The linear energy transfer describes the energy deposit of a particle along its path in tissues and is expressed as [67]:

(1) $$LET\ \left(\frac{keV}{\mu m}\right) = \frac{\Delta E}{\Delta D}$$

ΔE= energy loss

ΔD= distance traveled

Table 2 gives an overview over LETs of different types of radiation. The biologic effect of high-LET-radiation is greater than of low-LET-radiation, because its energy is deposited over a much smaller distance and induces therefore more ionization around and direct hits on target structures (e.g. cellular DNA) in a defined area. Consequently, equal doses of high and low-LET radiation result in different biological effects. For comparison of different radiation types, the term of relative biological effectiveness (RBE) was introduced. Here, the effect of a dose from 60-Co or a 250 kV Roentgen source is compared with the dose from another radiation source giving the same effect (e.g. 50% reduction of cell survival):

(2) $$RBE = \frac{Dose\ (Gy) from\ 60{-}Co\ or\ 250kV\ Source}{Dose\ (Gy) from\ other\ radiation\ source\ to\ produce\ the\ same\ biological\ effect}$$

In general, radiation with high LET also has a high RBE. On the other hand, high-LET radiation has a smaller penetration depth than low-LET radiation. In addition to the dependence on the LET of the radiation, the RBE factor is also related to the kind of cells that are irradiated (i.e. radiosensitive or radioresistant) and further influenced by other factors such as the oxygenation status of the respective tissue.

Table 2 Overview over LETs of different types of radiation (according to Hermann and Baumann, [62] and Richter and Feyerabend [63]).

	Radiation	Energy (MeV)	LET (keV/µm)
high LET	α-particle	5.0	90
	fast neutrons	6.2	21
	thermal neutrons	0.025 eV	10
	protons	2.0	17
low LET	x-rays	0.2	2.5
	electrons	2.0	0.2

Charged particles like alpha particles, protons and electrons can ionize molecules directly while neutral particles ionize indirectly (e.g. neutrons via products of the neutron capture reaction). X-rays also belong to indirect ionizing radiation, since their interactions with cellular atoms result in charged particles which are then able to ionize further molecules.

Indirect ionization takes place via induction of diffusible radicals and the radiation energy is secondarily deposited in the target molecule (e.g. the DNA). The effect bases largely on the ionization of water molecules which are ubiquitous in biological systems [67]:

i) Ionization of water molecule $H_2O \rightarrow H_2O^+ + e^-$

ii) Decay of the positive ion $H_2O^+ \rightarrow H^+ + OH^\bullet$

iii) Electron interacts with another water molecule $e^- + H_2O \rightarrow OH^- + H^\bullet$

The reaction results in oxidizing OH-radicals, reducing H-radicals, hydrated electrons and peroxides (if O_2 is present). These products can induce among others oxidation of thiol-groups, for example of amino acid cysteine, protein denaturation, base damages and alterations and single and double-strand breaks (ssb and dsb) of the cellular DNA. Chromosome aberrations like dicentric and acentric chromosomes and interstitial deletions result from two nearby located dsb. The damage caused to a cell by application of 1-1.5 Gy has been estimated to consist of as much as 1000 ssb and 50-100 dsb [68].

Among the radiation-induced lesions to cells, un- or misrepaired DNA double strand breaks are thought to be the most important for the radiation effect and subsequent cell death [60, 69]. While single strand breaks and base damages can be repaired via enzymatic base or nucleotide excision repair, the more challenging double strand breaks are mended by homologous recombination repair (HR) or nonhomologous end joining (NHEJ) [60, 70]. However, if the repair of dsb fails or the DNA is mismatched and important genetic information is consequently lost in the process, the cell will perish eventually.

1.3.1.2 Cell cycle

Cells exhibit different phases in their proliferation cycle which are distinguished by the cellular activity (fig. 1-8). In the mitosis phase, the cell divides into two similar daughter cells. The following G1 phase is a gap-phase during which the cell grows and increases in volume, before entering the S-phase for DNA

replication. The G0-phase (a possible junction in G1) represents an arrest in the cycle with lower metabolic activity where cells can remain for different lengths of time. Differentiated cells in organs sometimes stay permanently in G0-phase. However, the quiescent cells may re-enter the cell cycle after their rest in G0 phase. The G2 phase represents another gap for cell growth and preparation for the following mitosis.

The radiosensitivity of cells is cell-cycle dependent. The S-phase is the most radioresistant phase of the cycle while the mitosis and the G2 phase are most susceptible to radiation [67, 69, 71]. For the ongoing cell cycle, there exist several checkpoints (e.g. G1/S, G2/M and spindle checkpoint in M) at which the cycle can be stopped and, if necessary, repair mechanisms can be activated. The G2 arrest after irradiation seems to be present in all eukaryotic cells and the length of the G2 block is cell type dependent, but as an approximation, 2 h per applied Gy or 10% of the cell cycle are estimated for the delay [67]. A G1 arrest is more seldom, while an S-phase delay can be observed usually after irradiation with doses above 5 Gy [72].

The homologous recombination repair mechanism for dsb is believed to take place in M, G2 and S-Phase when there is a sister chromatid to the broken DNA strands present [60, 73]. The second dsb-repair path, NHJR is more prone to errors since no homologous strand is used for the repair. Here, the ends of the broken strands are brought together and ligated, usually under deletion of a few nucleotides [6]. This repair mechanism can be activated throughout the whole cell cycle (i.e. also in the G1 phase) [60, 64]. Cells that fail to repair dsb accurately are destined for either apoptosis or mitotic death (also clonogenic death or reproductive cell death). After suffering severe damage from radiation, morphologically intact cells still may divide several times, before the lesions on the chromosomes prevent the completion of the mitosis and the cells finally die [67, 68, 74]. However, in some cases cells suffer mutations, but are nonetheless able to divide or cells become quiescent and cease to proliferate altogether (G0 phase).

While the mitotic death is the most common fate of irradiated cells, a small part of tumor cells may undergo radiation-induced apoptosis [74]. This kind of cell death is thought to take place without induction of mitosis and is therefore called interphase death [68]. In contrast to necrosis, apoptosis is a programmed cell death which is induced by apoptosis signals such as the absence of growth factors [75]. At the end of a signal cascade involving caspases, the cell shrinks and apoptotic bodies containing intact mitochondria, ribosomes and DNA are built. These bodies are phagocytosed by macrophages or adjacent cells [75]. Necrosis on the other hand leads to cell swelling and rupture and results from exposition to non-physiological conditions or agents that damage the cell membrane, thus leading to loss of cellular integrity. Due to the uncontrolled cell lysis, the cellular contents are set free into extracellular space, where they may provoke inflammations [75].

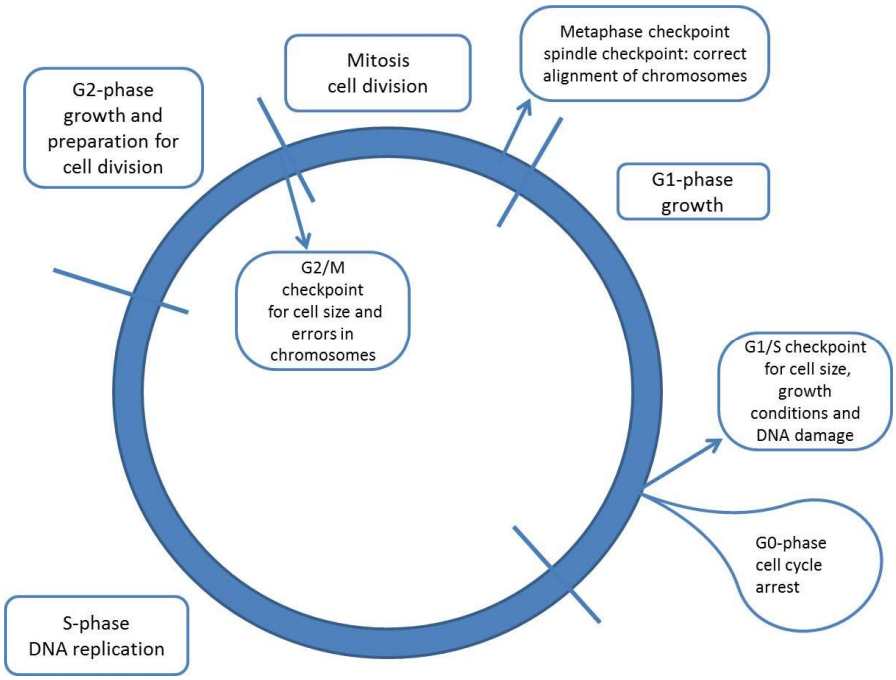

Figure 1-8 Cell cycle overview (according to Alberts et al. [6], Hermann and Baumann [67] and Washington and Leaver [69]).

1.3.1.3 Survival curves of cells after irradiation

Due to the reactions described above, irradiated cells have lower proliferation than non-irradiated cells. The difference in proliferation is assessed with clonogenic or MTT assay, giving the surviving fraction (survival) of irradiated cells in relation to non-treated cells. The cell survival can be plotted as a survival curve showing the surviving fraction of cells against applied dose.

A typical survival curve of photon-treated cells shows a shoulder region for low doses and an exponential part for higher doses. The best fit for this curve shape was found to be a mathematical equation which takes into account both parts of the curve by assigning two factors, α and β to describe the initial slope and the curvature of the line, respectively. This model for survival curves is called linear-quadratic model (LQ-model) and cell survival is defined as:

(3) $$SF = e^{(-\alpha D - \beta D^2)}$$

α=factor describing initial slope (single hit)

β=factor describing curvature (multi hit)

D= dose

Cell survival is clearly dependent on dose, but also on the probability of hitting a target whose destruction will actually lead to cell death. As mentioned before, the main target for cell destruction is the DNA. Dsb can occur either through one particle striking at two points of the molecule (one time per strand) or through two particles each breaking a single DNA strand in close proximity. The first scenario is described by the linear component of the formula (-αD) where the probability of the event is increasing linearly with the dose. The second component stands for sublethal events which only lead to cell death because two or more lesions interact and prevent effective repair by cellular repair

mechanisms. The probability of this event increases proportionally to the dose squared ($-\beta D^2$). The two sections of the curve present therefore two different ways of cell killing. The first type of cell killing (represented by α) is predominant at lower doses and results from a single-hit lesion which is non-repairable. The second type (β) results from multi-hit events which would be repairable if the lesions did not accumulate. Yet, the sum of the accumulated sublethal lesions finally leads to cell death and this type of cell killing predominates at higher doses [76].

Interestingly, it was found that neutron-irradiated cells do not exhibit an (extensive) shoulder region [69, 77] . As described above, high-LET neutrons have a higher probability to induce lethal damage to the cellular DNA, therefore the dose to achieve the same biological effect as photons is smaller. Furthermore, through densely ionizing radiation, two or more sublethal DNA damages accumulate more easily than for sparsely ionizing radiation and consequently, the cell survival now solely depends on the square of the dose (i.e. the β-term). Additionally, the relative biological effectiveness of neutrons is higher for low doses than for high doses, because the shoulder is less pronounced for neutrons than for photons [67].

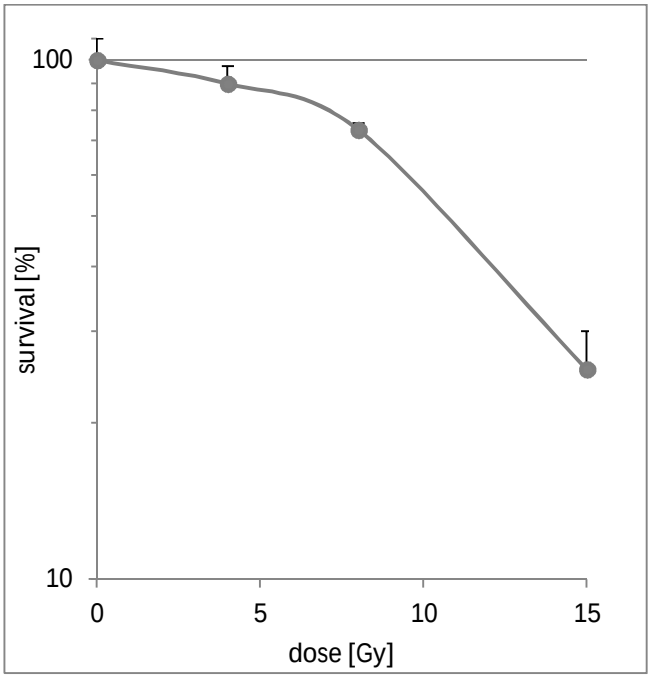

Figure 1-9 Survival curve of irradiated F98 cells (synchrotron, exp. MD 485 A)

1.3.2 Overview over different radiation techniques

Radiation has been used for cancer treatment since the late 19th century, shortly after Wilhelm Roentgen discovered X-rays. In 1913, the first radium tubes were established for the routine use in tumor therapy. Earliest linear accelerators (linacs) have been constructed in 1948 and the first medical linac was installed 1953 in Hammersmith hospital in London. The linear accelerator produced high-energy photons in range of 6-20 MV, thus finally allowing treatment of deeply seated tumors [78]. Since these early days of radiotherapy, the technique has been majorly improved by computer-aided dose calculations, treatment planning and 3D-modeling of the tumor. Better dose distribution could be

achieved by computer tomography-based calculations and the beam could be modulated to 3D-structures, thus focusing the radiation dose to the target alone and avoiding other organs. Intensity modulated radiotherapy (IMRT) allowed further modulation of the beam intensity during fractions. The invention of stereotactic radiotherapy (using ^{60}Co-sources) was especially useful for the treatment of brain cancer or metastases, because a very high dose could be administered to an exactly defined location by using a stereotactic frame [69].

An additional radiation method for tumor treatment is brachytherapy, where either a radiation emitting seed is planted into the tumor volume or a radiation tube is set directly into the tumor bed, for example after excision of a mammalian tumor (x-ray brachytherapy).

Besides photons, other ionizing particles were also used for medical purposes: electrons, protons, carbon ions and neutrons. Electrons are used for treatment of superficial cancers, because the particles do not penetrate very deep into tissues. Protons have an advantageous dose profile over x-rays with less energy deposited in non-target (healthy) tissues, but the main obstacle to their application in clinical cancer treatment is the proton source itself which is usually very large and costly. Carbon ions display the same useful dose profile as protons and a higher biological effectiveness. However, as in the case with protons, the cost of the therapy needs to be minimized in order to allow the treatment to be established as a possible standard therapy [78, 79].

Neutron radiotherapy of cancer relies on high linear energy transfer of neutrons. The biological effect is, depending on neutron energy and type of tissue, approximately three times higher than for x-rays [79]. The dose distribution in tissue is similar to photons and side effects on healthy tissue have also ever since been a problem in neutron beam as in photon therapy [80].

Apart from radiotherapy with photons, none of the above mentioned radiation treatments are yet established for standard cancer therapy. However, clinical trials are ongoing and promising results are being obtained continuously, for example for salivary gland malignancies with fast neutron irradiation [79].

1.3.3 Photon radiation therapy (XRT)

The radiation therapy most widely used for cancer treatment is external beam radiation therapy with photons. For conventional radiation therapy the treatment is planned by a simulator which targets the volume to be irradiated. Newer methods use a photon beam which can be intensity modulated (IMRT) and the doses applied are calculated individually, sculpted to the 3D model of the target (i.e. the tumor) (3DCRT). The dose is measured in Gy which describes the energy dose of ionizing radiation as the absorbed energy per mass:

(4) $$Gy = \frac{J}{kg}$$

Gy= Gray

J= Joule

kg= kilogram

Dose calculations have to comply with individual tissue characteristics and respect the radiosensitivity of nearby organs to reduce damage to healthy tissues. The tolerated dose for organs and healthy tissues differs vastly from under 1 Gy for mature lymphocytes and 4 Gy for eyes (lens) to 60 Gy for bones of the adult and finally astonishing 100Gy for the uterus [67]. The tolerated dose of organs limits the dose which can be given to the tumor, since the x-rays generally also reach a certain amount of the tumor-surrounding healthy tissue. In most cases, the total dose is fractionated. Fractionation allows normal cells to repair sublethal radiation damage and to recuperate between fractions (i.e. at least 6 hours). Hypoxic tumor regions may reoxygenize if temporary sealed capillaries are reopened or microcirculation is ameliorated through lower tumor pressure. Furthermore, since radiosensitivity is cell-cycle dependent, tumor cells may enter a more radiosensitive phase before the next fraction is applied, thus improving cell killing. Typical conventional fractionation schemes are 1.8-2 Gy per fraction, 5 times a week. The period over which the patient receives radiation treatment depends on the total dose which will be applied, the tumor type, the tumor status and the further medication/ treatment of the patient. Hyperfractionation is thought to be more conservative for healthy tissues, because the doses are divided again into smaller fractions of 1.15 Gy, twice a day for the same period of time. Hypofractionation schemes in contrast schedule fewer fractions of higher doses, while the total dose is also reduced. The treatment is for the most part reserved for palliative radiation, since chronic side effects occur more frequently in this schedule [67].

1.3.4 Radiosensitizer and radioenhancer

Many attempts have been made to modify and improve radiation therapy, be it conventional photon irradiation or the less practiced neutron therapy. Most strategies base on the idea of increasing the radiation effect on cells in situ by employment of radiosensitizing agents such as nitroimidazoles, halogenated pyrimidines and platinum compounds. Radiosensitizers in general are substances that render cells more susceptible to radiation treatment while radioenhancer act as intensifier of the initial radiation, for example by photoelectric interaction and subsequent release of Auger-electrons. The radiomodifying effect of these substances can be divided in several classes, such as hypoxic sensitizers, S-Phase sensitizers and cytotoxic chemotherapy agents. Imidazoles serve as hypoxic sensitizers (or more precisely, enhancers) which enhance radiation effects in anoxic cells by providing radical adducts [81]. Oxygen is the most potent radioenhancer and its level in tumor tissues strongly affects the radiation outcome, due to the production of reactive oxygen species [69]. The oxygen enhancement ratio (OER) is a term to describe the effect of radiation in hypoxic cells in comparison to oxic cells and usually gives a factor of 2-3 (i.e. the dose required to kill hypoxic cells is 2-3 times higher than for normally oxygenized cells) [82]. S-Phase sensitizers include halogenated pyrimidines (e.g. bromodeoxyuridine) which are incorporated into the DNA during cell division. After the introduction of these compounds, the DNA is at higher risk to suffer ssb from formation of free radicals and at the same time, the repair ability of cells decreases [62, 81]. Platinum compounds are examples for cytotoxic agents as radiosensitizer, although they have also enhancing effects, as described below. These drugs are thought to hinder DNA repair after radiation and additionally, platinum compounds have a direct cytotoxic effect as DNA-intercalating agents. Other drugs of the cytotoxic agent group are taxanes (mitosis inhibition) and temozolomide (alkylating agent) [62]. Another class of radiomodifiers is used relatively seldom: high-Z elements such as gadolinium, platinum and iodine which act as radioenhancers. These elements are known for their ability to interact photoelectrically with photon beam-radiation. In these processes, the interaction leads to ejection of electrons from K-shell or other electrons which can produce high-LET Auger and

internal conversion electron cascades [83, 84]. The cellular DNA is susceptible to such high-LET particles and severe lesions like DNA dsb can be induced if the particle is in close enough proximity to the DNA [85, 86]. Other high-Z elements, such as the lanthanides lutetium and erbium may also be applied as radioenhancer.

Although some of the radiosensitizing substances were thought to be a valuable addition to standard radiation therapy, most of the compounds ultimately fell short of expectations, especially in brain cancer therapy [60, 62, 87]. For GBM, only temozolomide has entered standard clinical application until now. Nevertheless, the research on substances for enhancement of cell killing under irradiation is still ongoing and also includes several new approaches, such as the DNA damage repair pathways, transcript down-regulations of for example, BCRA1 and again EGF receptor inhibitors [60].

1.3.5 Neutron capture therapy

In neutron capture therapy, the effect of radiation damage is sought to be amplified by neutron capture agents. Neutrons as high-LET radiation already perform superior to photon irradiation in cell survival reduction and their relative biology enhancement factors are reported to be 3 - 3.5 for most tissues [79, 88]. Furthermore, the radiation effect of neutrons is less influenced by cell cycle and oxygen status of the tissue [67, 89]. Notwithstanding these already established advantages, the addition of a neutron capturing agent can lead to even better results of neutron therapy. The concept of neutron capture therapy (NCT) involves the use of an element with a high probability to interact with a neutron (= high neutron cross section), thus engaging in neutron capture reaction and emitting charged particles with a high LET. These high-LET products then increase the effect of neutron irradiation in biology material. Of all elements of the periodic system, boron and gadolinium appear to be the most promising candidates. ^{10}B and ^{157}Gd offer several advantages, including a high cross section for thermal neutrons (3,840 barn for ^{10}B and 255,000 barn for ^{157}Gd), the availability of suitable non-toxic complexes (e.g. BSH and BPA for boron, Gd-DTPA and other MRI compounds for Gd) for the therapy and the elements are not radioactive themselves. The natural abundance of ^{10}B is 19.8%, while ^{157}Gd content is only 15.6% of the natural Gd isotope mixture. The remaining Gd isotopes (7 in total) have much lower cross section for neutron capture than ^{157}Gd; therefore the median value for the natural mixture results in 49,000 barn for thermal neutrons. Nevertheless, the higher cross section of Gd, especially of the ^{157}Gd isotope (66 times higher than for ^{10}B) is the most important advantage of GdNCT over BNCT. Another one is the possibility of using Gd as magnetic resonance imaging (MRI) contrast agent under radiation therapy, thus leading to higher accuracy of the irradiation (as in XRT, see above)[90]. The compound Gd-DTPA which was used in this study is a FDA-approved MRI contrast agent, known under the brand name Magnevist®. Furthermore, it is under discussion if the long-range gamma rays from a Gd-neutron capture (Gd-NC) event are more helpful for the treatment than short range fission products from B-NC, especially if the compound cannot enter the target cell to induce DNA lesions or the distribution is slightly uneven in a heterogeneous tumor mass [91-94].

The neutron capture reactions for ^{10}B and ^{157}Gd are given below (fig. 1-10 and 1-11). For boron, the neutron capture event results in a recoil ^{7}Li nucleus and the emission of an α-particle (^{4}He). These fission products have respective energies of 0.85 and 1.5 MeV [95]. Their path lengths in tissue are no longer than 5-9 µm and thus shorter than the diameter of an average cell [96].

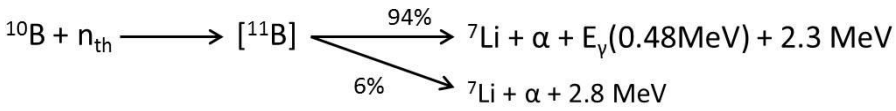

Figure 1-10 Neutron capture reaction for boron (^{10}B isotope) (adapted from Salt et al. [98])

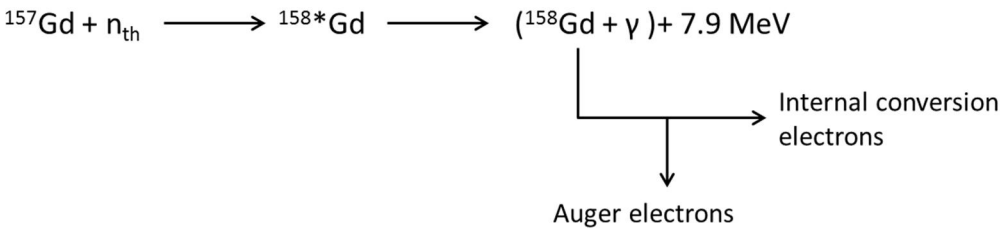

Figure 1-11 Neutron capture reaction for gadolinium (^{157}Gd isotope) (adapted from Salt et al. [98])

The reaction of ^{157}Gd and thermal neutrons is more complex. First, the capture generates an excited ^{158}Gd isotope, whose excess energy is then set free as gamma rays and via emission of electrons (Auger and internal conversion). The neutron capture reaction of ^{157}Gd yields 4.9 Auger electrons, 0.7 internal conversion electrons, 0.84 x-rays and 1.83 γ-rays [97].The overall energy released from the reactions is approximately three times higher than for boron (Q = 7.9 MeV, boron NC: Q = 2.3 MeV) [98]. The gamma rays with average energy of 2.2 MeV possess long range in tissues (several centimeters) and occupy most of the energy released (~99%) [98]. Only a small part of the energy is made up of Auger and internal conversion electrons (0.066 MeV) [95]. Auger electron emission is a consequence of internal conversion, electron capture or photoelectric interactions. If an electron is ejected, the vacancy is filled with an electron from a higher shell. The energy difference is equaled by emission of x-rays or an electron. The new vacancies from these electrons are also filled, thus a cascade of electrons will be emitted (ten or more), until all vacancies are in the valence shell [95]. Since the average energy of the Auger electrons from the Gd-NC event is 4.2 keV, their pathway is limited to the dimensions of a cell (published values range from 12.5 nm to 1 µm [95, 98-101]) [97]. In addition, the gamma rays produced by the neutron capture reaction of one Gd-atom may interact with other surrounding Gd-atoms inside or outside the target cell, thereby inducing further electron cascades from these Gd-atoms and inflicting additional damage to cellular structures.

It was found that the high-LET Auger electrons from Gd-NC event induce DNA lesions (dsb) when in close proximity to the nucleus [102]. Furthermore, the contribution of Auger electrons to cellular damage after irradiation is believed to be of highest importance for the neutron capture reaction [99]. The infliction of dsb from these electrons was calculated by Goorley and Nikjoo 2004 [103]. They reported an average number of 140 dsb per cell for a concentration of 1 g Gd/g tissue and a dose of 10 Gy, which was much more than from thermal neutrons alone (27 dsb). However, photons and internal conversion electrons from the Gd-NC produced approximately 350 dsb per cell in a 1 cm radius head phantom. Since these photons and electrons have a longer range than Auger electrons, their energy deposition may be located outside the original Gd-containing cell (i.e. in adjacent cells). Consequently, Auger electrons may indeed play a significant role in cell killing during GdNCT due to the local energy

deposition in Gd-containing cells, but other components from the reaction should be considered as well in the estimation of Gd-NCT effectiveness [103].

Further interaction of neutrons with biologic materials/ tissues consists mainly of scattering with hydrogen and capture in hydrogen and nitrogen. Although the cross sections of these elements are small in comparison with boron and gadolinium, their abundance in tissue results in relatively high contribution to the total dose from neutron irradiation. Figure 1-12 lists reactions of neutrons with H- and N-atoms of biological material. For the hydrogen capture reaction, the released energy is 2.23 MeV (gamma rays) while the nitrogen capture results in 0.63 MeV (protons)[104].

$^{1}H\ (n, n')\ ^{1}H$

$^{1}H\ (n, \gamma)\ ^{2}H$

$^{14}N\ (n, p)\ ^{14}C$

Figure 1-12 Interactions of neutrons with elements from biological material (according to Miller et al. [95])

In order to spare healthy tissues, the neutron dose to normal cells should be minimized to extremely low residuary values. For neutron capture therapy, this means selective application of NC-element (in this case B and Gd) to target cells while surrounding healthy tissue ideally should not incorporate the NC-element. Thus, the dose from the NC-element is the main dose component in target cells, while normal cells are at the most subjected to radiation generated by hydrogen and nitrogen neutron capture.

In practice, the selective and/ or high uptake of boron and gadolinium for neutron capture therapy has been addressed by development of various NC-element-containing compounds. For BNCT, the amino acid-coupled boronophenylalanine (BPA) is a well-characterized representative. Cancer cells are known to have a high metabolic rate and require therefore great amounts of amino acids. The BPA molecule is recognized by these cells as an amino acid and therefore taken up in high quantity. Other compounds are sodium borocaptate (BSH), carborane cages, porphyrin-derivatives, targeted boron-conjugates of monoclonal antibodies and boron-containing liposomes [96, 104, 105]. Currently, BPA and BSH are in clinical use, but neither compound effectively fulfills all requirements for BNCT (e.g. high tumor accumulation (~ 20 µg ^{10}B/g tissue), low distribution in healthy tissue and blood, persistence in tumor during BNCT) [96, 106].

For GdNCT, the development of suitable Gd-containing compounds is also still ongoing. Besides the approved MRI contrast agents Gd-DTPA and -DOTA, gadoteridol, motexafin-gadolinium, gadolinium-oxide and gadolinium-chitosan particles as well as other carriers are under investigation [91, 93, 106, 107]. However, as in the case with BNCT, the optimal Gd-providing agent is still missing and few of the newly developed compounds enter clinical trials for cancer treatment.

In spite of the difficulties in finding an ideal NC-compound, the NCT research still concentrates on treatment strategies of the most malignant cancer types. At present, BNCT and GdNCT research is set on therapy improvement of amongst others radioresistant melanoma, thyroid and liver cancer, head and neck cancer and brain tumors, including GBM [108-113]. Neutron capture therapy facilities are presently installed in several European countries as well as in Argentina, USA, Taiwan and Japan [106, 110, 114-118].

2 Aim of the thesis

Radiation therapy is after surgery the most promising treatment option for a multitude of cancer diseases. However, the treatment efficacy of radiation is limited by the necessity to spare the healthy tissue surrounding the irradiation area. To prevent severe damage to normal cells, the radiation has to obey to strict rules concerning dose and fractionation schemes for the various tissues and organs in the vicinity of the target, that is the tumor. Yet, side effects cannot always be avoided completely and patients may suffer from skin conditions, nausea and other unwanted reactions, even though the applied radiation dose may not be high enough to kill all remaining tumor cells. The aim of this study was to develop a liposomal formulation of the radioenhancer and neutron capture agent Gd-DTPA to improve the efficacy of radiation therapy as a part of the BMBF-funded project "Indirect radiation therapy IRT of cancer with target nanoparticles" (grant number: 05KS7UMA).

The application of the enhancer/ NC-element is expected to significantly enhance the radiation effect on cancer cells in regard to cell survival. Thus, the radiation dose might be reduced while resulting in the same effect as without enhancer/NC-element, but minus severe side effects as under the higher radiation dose. Simultaneously, if the influence on healthy tissue is acceptable, an enhanced effect for the usual dose would unquestionably also be beneficial for cancer treatment.

The main challenge of the treatment with radioenhancers/NC-elements is similar for all drug-involving treatments: the selective targeting and accumulation of the drug at the target site. Therefore, the application of the drug should take place via a specially designed carrier that improves the accumulation and uptake of the drug into the target tissue. In case of Gd-DTPA, the molecule should also arrive in close proximity to the cell's nucleus for optimal enhancing conditions under irradiation. As biodegradable carriers which can be adapted to different conditions by adjustment of the lipid composition and if needed, targeting structures on their surface, liposomes were estimated to fulfill the requirements for a suitable carrier of Gd-DTPA.

For the successful development of liposomal radioenhancer/NC-elements, the formulation had to fulfill several conditions as among others exhibiting low toxicity and sufficient encapsulation of the drug, ensuring high uptake into target cells and performing satisfactorily under actual radiation treatment. Furthermore, the manufacturing process should result in reproducible nanoparticles of a defined size and encapsulation efficiency of the drug and a sufficient stability of the liposome suspension.

Since the prognosis for high grade glioma is very poor and patients' life span after diagnosis is in spite of steadily ongoing research still only about a year, the current work has the aim to improve the radiotherapeutic treatment options for glioblastoma multiforme. For this purpose, an in vitro cell model should be established for uptake, toxicity and performance studies. Two cell lines (rat and human glioma) were chosen to ensure universal practicability of the newly developed formulations. The formulations should then be tested under clinical conditions (linear accelerator) as well as with alternative radiation techniques (neutron capture therapy) in both cell culture models to establish a proof-of-principle for the use of gadolinium as radioenhancer/neutron capture agent and to evaluate the effectiveness of the radioenhancer/NC-element approach for the therapy of glioblastoma.

3 Materials and methods

3.1 Materials

3.1.1 Reagents and solvents

All chemicals, reagents and solvents were of analytical grade or higher.

3-(4,5-Dimethylthiazolyl-2)-2,5-diphenyl-2H-tetrazoliumbromide (MTT)	Carl Roth GmbH & Co. KG, Karlsruhe, Germany
4-(1,1,3,3-Tetramethylbutyl)phenyl-polyethylene glycol (Triton™ X-100)	Sigma Aldrich Co., Buchs, Schweiz
5(6)-Carboxyfluorescein	Sigma Aldrich Co., St. Louis, Missouri, USA
Ammonium hydroxide, 29%	Merck KGaA, Darmstadt, Germany
β-mercaptoethanol	Sigma Aldrich Co., Buchs, Schweiz
BC-Assay Protein Quantitation Kit	Uptima, Interchim, Montluçun, France
Double-distilled Water	VE-water, double-distilled, Destamat Bi 18E
Bisglyceroborate	Nanovel Ltd. & Co. KG, Langenlonsheim, Germany
Boric acid	Merck KGaA, Darmstadt, Germany
Butanol	Merck KGaA, Darmstadt, Germany
Cell Mask ™ Deep Red	Life Technologies GmbH, Darmstadt, Germany
Chloroform	Merck KGaA, Darmstadt, Germany
Coulter ® Isoton® II Diluent	Beckmann Coulter, Krefeld, Germany
Dimethylsulfoxid (DMSO)	Carl Roth GmbH & Co. KG, Karlsruhe, Germany
EDTA	Sigma Aldrich Co., St. Louis, Missouri, USA
Er-DTPA formulation (Er-DTPA in tris-acetate buffer)	Nanovel Ltd. & Co. KG, Langenlonsheim, Germany
Europium Standard 1000±3µg/ml, in 2% HNO3	High-Purity Standards, Charleston, South Carolina, US
Fast Start Taq Polymerase Kit	Roche Applied Sciences, Roche Diagnostics Deutschland, Mannheim, Germany

Gd-DTPA-NV (Gd-DTPA Nanovel in tris-acetate buffer)	Nanovel Ltd. & Co. KG, Langenlonsheim, Germany
Hydrogen Peroxide, 35%	Carl Roth GmbH & Co. KG, Karlsruhe, Germany
LabAssay ™ Phospholipid	Wako Pure Chemical Industries, Osaka, Japan
Lu-DTPA (in tris-acetate buffer)	Nanovel Ltd. & Co. KG, Langenlonsheim, Germany
Methanol	Merck KGaA, Darmstadt, Germany
Magnevist® (Gd-DTPA dimeglumin)	Bayer Vital GmbH, Leverkusen, Germany
Nitric acid, 65%	Carl Roth GmbH & Co. KG, Karlsruhe, Germany
ProLong®Gold antifade reagent with DAPI	Life Technologies GmbH, Darmstadt, Germany
RNEasy Mini Kit	Qiagen Sciences, Germantown, Maryland, USA
Sephadex™ G-25 Medium	GE Healthcare, Uppsala, Sweden
Sodium borate	Carl Roth GmbH & Co. KG, Karlsruhe, Germany
Transcriptor high fidelity cDNA Synthesis Kit	Roche Applied Sciences, Roche Diagnostics Deutschland, Mannheim, Germany
Tris-borate	Nanovel Ltd. & Co. KG, Langenlonsheim, Germany
Trometamol (tris)	Carl Roth GmbH & Co. KG, Karlsruhe, Germany

3.1.2 Lipids

3.1.2.1 Neutral lipids and cholesterol

1,2-Dioleoyl-*sn*-glycero-phosphoethanolamine (DOPE)	Lipoid GmbH, Ludwigshafen, Germany
1,2-Dioleoyl-sn-glycero-3-phosphocholine (DOPC)	Sigma Aldrich Co., St. Louis, Missouri, USA
Cholesterol	Sigma Aldrich Co., St. Louis, Missouri, USA

3.1.2.2 Charged lipids

1,2-Dioleoyl-3-trimethylammonium-propane (DOTAP)	Lipoid GmbH, Ludwigshafen, Germany
Cardiolipin (CL)	Sigma Aldrich Co., St. Louis, Missouri, USA

3.1.2.3 Pegylated and functionalized lipids

1,2-distearoyl-*sn*-glycero-3-phosphoethanolamine- N-[methoxy(polyethylene glycol)-2000] (mPEG-2000-DSPE)	Lipoid GmbH, Ludwigshafen, Germany
1,2-distearoyl-*sn*-glycero-3-phosphoethanolamine- N-[folate(polyethylene glycol)-2000] (DSPE-PEG(2000) Folate)	Avanti Polar Lipids, Alabaster, Alabama, US
N-(7-Nitrobenz-2-oxa-1,3-diazol-4-yl)-1,2 Dihexadecanoyl-sn-glycero-3-Phosphoethanolamine (NBD-PE)	Life Technologies GmbH, Darmstadt,Germany

3.1.3 Laboratory disposables

Spectra/Por®Biotech Cellulose Ester Dialysis Membranes MWCO 3,500-5,000D	Spectrum Laboratories, Rancho Dominguez, CA, USA
Polycarbonate membrane (Extrusion)	Nuclepore™ track- etched polycarbonate membranes 0,1µm and 0,08µm, Whatman, Kent, UK
Sterile syringe filter , hydrophobic	PTFE filter 0,2µm, Carl Roth GmbH, Karlsruhe, Germany
Sterile syringe filter, hydrophilic	Cellulose Acetate filter 0,2µm, VWR International, Darmstadt, Germany
Syringe	Braun Inject 2ml Luer solo, B. Braun , Meslsungen, Germany

3.1.4 General Equipment

Double-distillation apparatus	Destamat Bi-Destillierapparat Bi 18E, Heraeus Quartzglas GmbH, Klein Ostheim, Germany
Centrifuge	Centrifuge 5804R, Eppendorf, Hamburg, Germany
Extruder	Avanti ®Mini Extruder, Avanti Polar Lipids, Alabaster, Alabama, US
Flow through cell, USP apparatus 4	Sotax CE7 smart, Sotax AG, Allschwil, Switzerland
Inductively coupled plasma mass spectroscopy	Agilent ICP-MS 7500 ce, Agilent Technologies, Santa Clara, California, US
Microplate reader	Tecan infinite™ F200, Tecan Group Ltd., Männedorf, Switzerland
Plate Shaker	Ika Vibrax VXR basic, Ika-Werke, Staufen, Germany
PCR Cycler	BioRad T100 heatable lid, Biorad laboratories Munich, Germany
Rotary evaporators	RotavaporR-3 with vaccuum pump V-700, Büchi Labortechnik, Flawil, Switzerland
Size measurement and zeta potential measurement	Zetasizer Nano ZS, Malvern Instruments, Malvern, England For early size measurements: Custom-made DLS, Nanovel, Langenlonsheim, Germany
Ultrasound bath	RK 510, Brandelin, Berlin, Germany
Ultrasound tip (conical micro tip)	Branson sonifier®B12, Branson Ultrasonics, Dietzenbach, Germany
Vortex	Agitateur Top-Mix 11118, Bioblock Scientific, Frenkendorf, Switzerland
Water Bath	SV 15, Gerhardt, Bonn, Germany

3.1.5 Data progression

Excel	Microsoft Corporation, Redmont, Washington, US
Mass Hunter Workstation	Agilent Technologies, Santa Clara, California, US

MCNP5	Los Alamos National Security, Los Alamos, New Mexico, USA
Prism 3.0	GraphPad Software, La Jolla, California, US
Zen 2009 Light Edition	Carl Zeiss MicroImaging GmbH, Jena, Germany
Zetasizer Software	Malvern Instruments, Malvern, England

3.1.6 Cell culture

3.1.6.1 Cell lines

For cell culture experiments, the F98 (ATCC number CRL-2397™) and the LN229 cell line (ATCC number CRL-2611™) were used. Both cell lines were purchased from LGC/American Type Culture Collection, Middlesex, UK.

Anaplastic glioma cell line F98 was derived in 1971 by Koestner and Wechsler from a pregnant CD Fischer rat which was treated with a single dose of N-ethyl-N-nitrosourea. The cell line is widely used in brain tumor research and has been proven to be consistent in morphology and state of differentiation for a high number of passages [119]. Its close resemblance to human glioblastoma in growth pattern as well as sensitivity to therapy adds to the importance of the F98 model for undifferentiated malignant glioma [120]. F98 cells have been used successfully in boron NCT and photon irradiation studies for both in vivo (following inoculation in rat brain to form a tumor) and in vitro irradiation since 1990 [121-123].

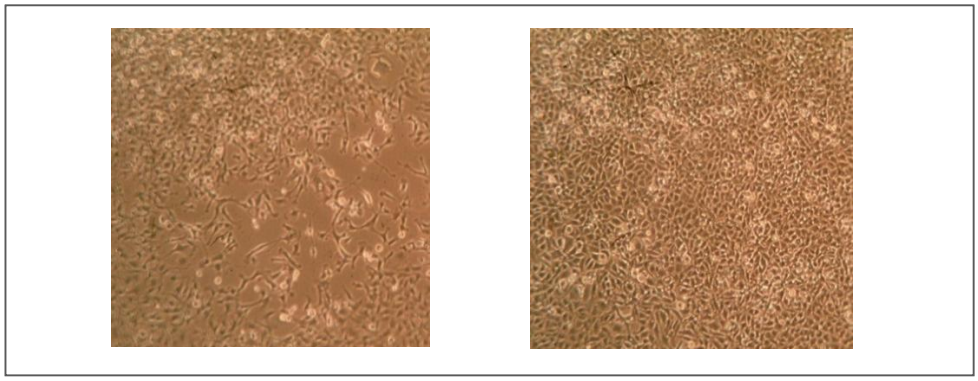

Figure 3-1 Microscopic images of cultured F98 cells, left side: 4 days in culture, right side: confluent state (7 days in culture)

The LN229 glioblastoma cell line is of human origin [124]. It was isolated in 1979 from a female patient with glioblastoma located in the right frontal cortex. In our studies, this human cell line was enclosed to ensure the transferability of our findings from the rat glioma cell line to human glioblastoma.

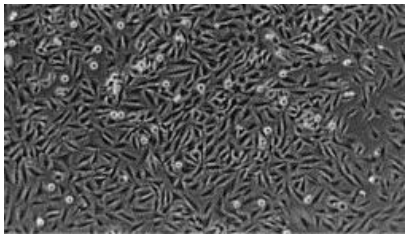

Figure 3-2 Microscopic image of cultured LN229 cells (from Frei et al. [124]

3.1.6.2 Cell culture media

Cell culture media and supplements were purchased from Life Technologies GmbH, Darmstadt, Germany.

Growth medium F98 cells	Dulbecco's modified eagle medium: GlutaMax-I, 4.5 g/l glucose, w/o Na-pyruvate, supplemented with 10% FBS and 1% PenStrep.
Growth medium LN229 cells	Dulbecco's modified eagle medium: GlutaMax-I, 4.5 g/l glucose, w/o Na-pyruvate, supplemented with 5% FBS and 1% PenStrep.
Fetal bovine serum (FBS)	Fetal bovine serum standard, qualified, E. U. approved, South America origin
Buffer	Dulbecco's phosphate-buffered saline w/o Ca^{2+} and Mg^{2+} (PBS)
Trypsin	0.25% trypsin and 0.02%-EDTA, with phenol red
Antibiotics	PenStrep, 10000 U/ml penicillin/ 10000 µg/ml streptomycin
Growth media without phenol red	Dulbecco's modified eagle medium: w/o phenol red, 4.5 g/l glucose, w/o L-glutamin, w/o Na-pyruvate

3.1.6.3 Cell culture equipment and disposables

Laminar Flow	Herasafe HSP12, Heraeus, Germany
Incubator	Incubator MCO-17AI, Sanyo Electric, Co., Japan
Centrifuge	Centrifuge 5804, Eppendorf, Hamburg, Germany
Microscope	Wilovert®203147, Hund Wetzlar, Wetzlar, Germany
Hemocytometer	Thoma, Marienfeld, Germany
Cell counter	Coulter® Z2 Coulter Particle Count and Size Analyzer, Beckmann Coulter, Krefeld, Germany
Microplates	96well microplates, clear, Greiner Bio One, Frickenhausen, Germany
	96well microplates, black, clear bottom, Greiner Bio One, Frickenhausen, Germany
	6well microplates, clear, Greiner Bio One, Frickenhausen, Germany
Cell culture flasks	Cell culture flasks with filter cap, surface area 25 and 75 cm², Greiner Bio One, Frickenhausen, Germany
Petri dishes	100 x 20 mm, Greiner Bio One, Frickenhausen, Germany

3.2 Methods

3.2.1 Liposome manufacture

3.2.1.1 Lipid film preparation

Lipid films were prepared by dissolving lipids in chloroform and/ or methanol according to their respective solubility. Required amounts of lipid solution were mixed in round bottom flasks and left under vacuum on a rotary evaporator. To ensure complete solvent removal, the round bottom flasks were kept under high vacuum for an additional two hours after all visible traces of solvents had been evaporated. Lipid films were stored under nitrogen atmosphere at -20°C until usage.

3.2.1.2 Manufacture by ultrasound

In some early experiments, liposomes were manufactured by ultrasound. The lipid film was rehydrated with PBS and radioenhancer solution before being vortexed and sonified in turn for one minute to ensure complete suspension of lipids. The lipid suspension was then subjected to sonification by a conical ultrasound micro tip (35 Watt) under nitrogen atmosphere while being cooled in an ice bath for 6 minutes.

Metal shards from the ultrasound tip have been removed by short centrifugation at 180 g.

3.2.1.3 Extrusion

Liposomes were prepared by lipid film/-extrusion method. Lipid films were produced as described above. For lipid film rehydration, required amounts of PBS and radioenhancer or NC-element solution were added, allowed to rehydrate for 30 min and subjected to repeated vortexing until lipid was completely removed from the glass wall of the round bottom flask.

Lipid suspension was then vortexed for one minute and extruded eleven times through a 0.1 µm polycarbonate membrane.

For freeze-thaw (ft) preparations of liposomes, lipid suspensions were frozen in liquid nitrogen for one minute, thawed in a 37°C water bath for five to six minutes and vortexed shortly. The freeze-thaw cycle was repeated five times, after which lipid suspensions were vortexed again for one minute and extruded as described above.

For cell culture experiments, liposome suspensions were sterilized by filtration through a 0.2 µm sterile PTFE filter.

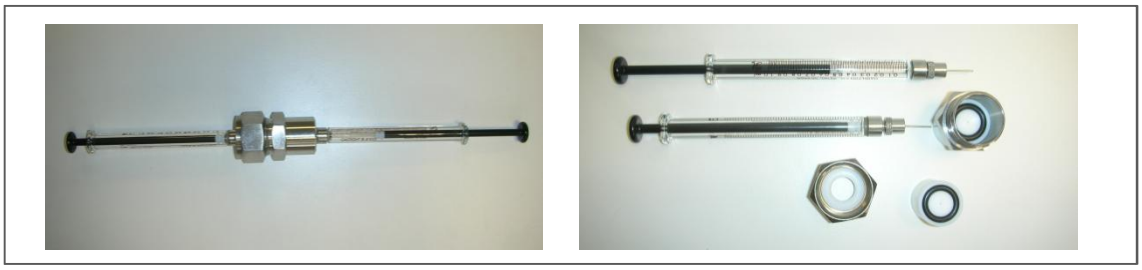

Figure 3-3 Mini-Extruder (Avanti Polar), left side: assembled extruder, right side: single parts of the device

3.2.1.4 Removal of non-entrapped material from liposome suspension

Removal of non-entrapped radioenhancer/ NC-element material from extruded liposomes was performed by adapted minicolumn centrifugation method [12]. The technique has been first described by Fry, White and Goldman in the 1970s as a simple method to subtract non-entrapped small molecules from liposomal preparations without dilution [125]. The method is based on size exclusion

chromatography in which small molecules, such as the radioenhancer/NC-element are hold back by the permeable sepharose beads whereas bigger complexes, for example liposomes, are forced through the column without retention.

Sepharose G-25 medium was left to swell in PBS for at least 24 hours, before being packed into the barrel of a 2 ml plastic syringe containing a filter disc to prevent the sepharose from leaking out. The syringe is then placed into a centrifugation tube and spun for 3 min at 1000 g to remove excess buffer. After transferring the syringe to a fresh tube, the liposome suspension was applied onto the sepharose gel bed. Next, the syringe is spun for 10 minutes at 50 g to allow interaction of non-entrapped material with the gel, before the syringe is centrifuged again for 3 min at 1000 g to expel the liposome suspension from the column. Non-entrapped material is held back by the gel bed. The eluate volume was measured to determine potential dilution of liposome formulation in the centrifugation process.

3.2.2 Liposome characterization

3.2.2.1 Size measurements

Size measurements of liposome suspensions were performed by dynamic light scattering (DLS). Dynamic light scattering or photon correlation spectroscopy is a technique based on the fluctuation of light scattered by dispersed particles. The suspended particles are illuminated with a laser and the intensity fluctuations in the scattered light allow the calculation of the particle size.

Due to the Brownian motion of molecules, dispersed particles are in constant movement. Consequently, their light scatter pattern changes over time, leading to an intensity fluctuation. The fluctuation of light intensity versus time is used to calculate a correlation function. A digital correlator measures the similarity between two signals in short time spans. Since large particles move slowly and small particles move more quickly, the fluctuation of intensity is affected by the particle size. For small particles, the correlation function decays faster, as smaller particles move more quickly than larger ones. Thus, the different decay rates can be used to calculate the size distribution of the sample.

To minimize effects of contaminants, such as dust, and to reduce multiple scattering in the samples, the intensity of the scattered light was measured at an angle of 173° (backscatter detection).

For DLS measurements, samples were diluted with PBS to yield a final lipid concentration of 0.25 mg lipid/ml. All measurements were done in triplicates, of which the Z-average (arithmetic mean) and the SD are stated.

3.2.2.2 Zeta potential measurements

Measurement of the zeta potential of liposomal formulations has become a useful tool for describing their stability. As a rule of thumb, a zeta potential above 25-30 mV, either positive or negative, ensures a sufficient stability of the formulation. Aggregation of the colloidal particles is then overcome by electrical repulsion due to their respective surface charge.

The occurrence of a zeta potential derives from surface groups on colloidal particles which can ionize and subsequently adsorb ions to the particle surface. The surrounding solution counterbalances the charge on the particle with ions of the opposite sign. Thus, a layer attaches itself around the more stable charges on the particle surface. The inner region of the layer is called the Stern layer, where ions are relatively strongly bound, while the outer region is more of a diffuse nature. Inside the diffuse layer there exists a boundary separating the contingent of ions which form a stable attachment and move with the original particle, and those staying behind. At this point, namely the surface of hydrodynamic shear, the electrostatic potential is the zeta potential. Measurement of this potential is performed by electrophoresis and determination of particle velocity by Laser Doppler Velocimetry. In practice, two electrodes are connected to the sample and an electric field is applied. The particles are forced to wander to the electrodes accordingly to their charge, during which their velocity is measured via the intensity fluctuation of the light the particles scatter. The velocity of a particle in an electric field equates to the electrophoretic mobility, finally allowing calculation of the zeta potential.

For the zeta potential measurements, samples were diluted in bi-distilled water to yield a concentration of 0.25 mg lipid/ml. All measurements were performed in triplicates, quoted are the arithmetic means and the SD.

3.2.2.3 Analysis of lipid content after extrusion

Since the extrusion procedure of liposomes may dilute the lipid suspension due to buffer excess from pre-wetted membranes and syringes, lipid content must be determined again after the manufacture process is finished.

The LabAssay™ Phospholipid Assay allows a rapid determination of the amount of choline-containing phospholipids such as dioleoylphosphatidylcholine in liposome suspensions [126-128]. The enzyme phospholipase D catalyzes the hydrolysis of these phospholipids to choline. The second enzyme, choline oxidase, oxidizes choline to hydrogen peroxide, which in turn is needed for the quantitative oxidation of *N*-Ethyl-*N*-(2-hydroxy-3-sulfopropyl)-3,5-dimethoxyaniline sodium salt (DAOS) and 4-Aminoantipyrine. This reaction is catalyzed by peroxidase and leaves the reagents to form a blue pigment. Measurement of the absorption of the blue color gives the amount of choline-containing phospholipids in the sample.

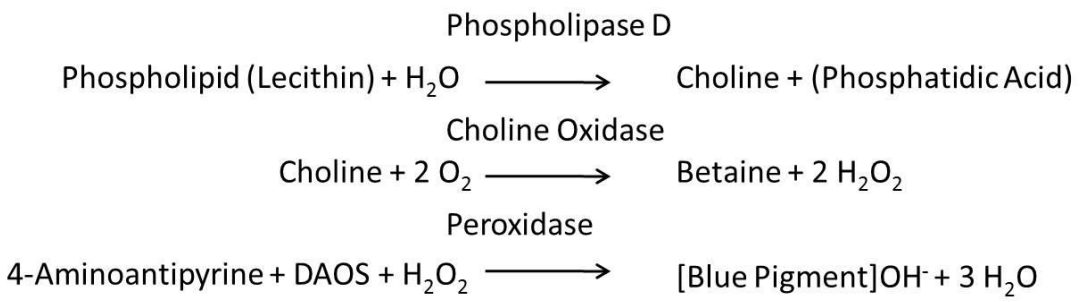

Figure 3-4 Reactions in Phospholipase D Assay (modified according to instruction leaflet of LabAssay™Phospholipid, Wako Pure Chemical Industries, Ltd., Osaka, Japan, see references: additional websites).

Liposome samples were diluted 1:1 with bi-distilled water. 2 µl of each sample were pipetted in triplicates onto a 96 well clear microplate. 280 µl of enzyme working solution were added to each well and the mixture was incubated for 5 min at 37°C in an incubator. The kit contained choline chloride as a calibration substance. Absorption was then read out in a microplate reader at 560 nm, reference wavelength 690 nm. Since the assay gives back only phosphocholine content, the amounts of other lipids are calculated based on their ratio to dioleoylphosphatidylcholine in the lipid mixture.

3.2.2.4 Determination of encapsulation efficiency

The encapsulation efficiency (EE, also: entrapment efficiency) of liposomes was determined fluorimetrically (entrapment of carboxyfluorescein (CF), excitation wavelength 492 nm, emission 517 nm) or by using ICP-MS for NC-element Gd-DTPA (Magnevist®).

Carboxyfluorescein was applied as a model substance for water-soluble drugs for the majority of liposomal formulations, before NC-element Gd-DTPA was used. CF solution was prepared by dissolving CF under addition of 0.1 N NaOH in bi-distilled water and subsequent pH-adjustment by drop-wise adding of 0.1 N HCl. Final concentrations of CF solution were 15 - 20 mM. Liposomes were prepared as described above, except for CF as the encapsulated substance instead of the radioenhancer or NC-element.

Extruded liposome suspensions underwent GPC-treatment as described in section 3.5.1.4 for removal of non-entrapped CF. Liposomes were then dissolved in a 2% Triton-X solution and diluted appropriately for fluorimetric measurement of CF-concentration on a microplate reader (filter: excitation 465 (35) nm, emission 535 (25) nm). The CF-contents were compared with those of non-GPC treated liposomes (extruded liposome solution before the minicolumn centrifugation). The EE is expressed as percentage of total substance concentration, calculated from the amount of CF in GPC purified liposomes divided by the original CF-concentration in the extrusion suspension:

(5) $$EE\ (\%) = \frac{[CF]purified}{[CF]original} * Df * 100\%$$

EE: encapsulation efficiency

[CF] original: CF-concentration of extruded liposome suspension

[CF] purified: CF-concentration of GPC-treated liposome suspension

Df: dilution factor (taking in account the dilution via GPC-treatment)

For Gd-DTPA containing liposomes, the determination of the EE was accomplished in the same manner; with the analysis of NC-element content of non-purified and GPC-treated liposomes performed by ICP-MS measurement (cf. section 3.2.3.7).

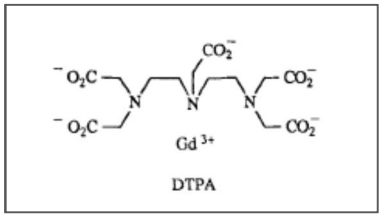

Figure 3-5 Gd-DTPA complex (adapted from Oksendal and Hals [129])

3.2.2.5 Release of NC-element from liposomes

The release of NC-element Gd-DTPA (Magnevist®) from liposomal entrapment was examined by flow through dissolution in a USP apparatus 4, using dialysis adapter devices for dispersed system dosage forms.

The USP apparatus 4 consists of seven dialysis chambers which can be operated separately. Each chamber is connected to the pump and its own media vessel, either on flow through or recirculation modus.

The flow through cell, USP apparatus 4, offers several advantages over dialysis sac method which is usually used for release studies of liposomes. The USP 4 method can provide sink conditions in the flow through cell, whereas this may not be the case at all times for the dialysis sac method [130, 131]. Bhardwaj and Burgess [132] showed that the USP 4 method was able to distinguish between several dosage forms and liposome formulations of dexamethasone. However, neither the reverse dialysis sac method nor the dialysis sac method accomplished to discern the differences between all formulations tested. Furthermore, in the adapter method, dissolution media can be exchanged or altered by addition of other compounds like serum components far more easily than in the dialysis sac method [132].

Liposomes were prepared by lipid film/extrusion method, together with freeze-thaw treatment, and subsequent removal of non-entrapped material via minicolumn centrifugation method. Liposome adapter devices were equipped with a cellulose-ether dialysis membrane, MWCO 3500-5000D. 450 µl of liposome formulation were then pipetted carefully into the liposome adapter device and positioned in a 22.6 mm tablet flow through cell. To ensure laminar flow in the cells, small glass beads were filled into the base of each container. A glass fiber filter was placed into the filter holder of the dissolution cells. Dissolution media consisted of 50 ml PBS for each formulation and was circulated with a flow rate of 16.2 ml/min. Samples of 1 ml volume were extracted at defined times and replaced with fresh media. The experiments were performed over 24 hours at 37°C.

Sample preparation for ICP-MS analysis of NC-element Gd:

To 100 µl of each sample, 2 ml of a 1:1 mixture of nitric acid and hydrogen peroxide were added. Samples were then diluted with bi-distilled water to obtain a total volume of 7.5 ml and 50 µl of 10ppm Eu for internal standardization were pipetted into each tube (cf. section 3.2.3.7).

Figure 3-6 Left side: dissolution apparatus Sotax CE7 smart (USP apparatus 4). Right side: tablet dissolution cell equipped with liposome adapter.

3.2.3 Cell culture experiments

3.2.3.1 General procedures

Both cell lines were kept under recommended growth conditions (5%CO_2, 99% humidity, 37°C) and subcultured once a week. For growth media, LN229 cells required DMEM high glucose supplemented with 5% FBS and F98 cells DMEM high glucose, supplemented with 10% FBS. Culture medium was replaced every 3 to 4 days.

Subcultivation procedure involved washing the cells two times with PBS to remove all traces of trypsin-inactivating agents such as Ca^{2+}, Mg^{2+} and other serum components. Cells were then trypsinized, incubated for 5 min and trypsin was inactivated by adding complete growth medium. After cell counting via hemocytometer, the cell suspension was centrifuged at 180g and the supernatant was aspirated off. Cells were resuspended in an appropriate amount of complete growth medium and seeded in flasks at a density of 800 cells/cm² and of 2133 cells/ cm², for F98 and LN229 cells, respectively.

3.2.3.2 Polymerase chain reaction experiments for determination of folate receptor alpha and other receptors in F98 and LN229 cells

The polymerase chain reaction (PCR) is a tool for detection of specific DNA or RNA (reverse transcriptase PCR, also RT-PCR) from biological samples by multiple amplification of the chosen material. The method uses DNA (or RNA which has to be transcripted into DNA first) to gain a variety of genetic information, for example genotype, receptor expression or enzyme profiles from any kinds of cells. In the PCR reaction, the DNA of interest is amplified using appropriate primers adapted to the respective DNA strands and DNA polymerase enzyme. Resulting PCR mixtures are brought onto a gel on which samples are separated electrophoretically by their mass (in base pairs, bp).

As some other receptors were considered for targeting of liposomes in the early stage of the study, the expression of EGFR, PDGFR β, NPR1 and TFR1 was also analyzed for F98 and LN229 cells. Sequences for mRNA corresponding to the chosen receptors were derived from PubMed, NCBI sequence viewer v 2.0 individually for humans and rats.

Primers were designed for both species together where possible and otherwise individually for human and murine receptors:

NPR1; product size: 245
hNPR1.ss ATTGGCATCCACACAGGAC
rNPR1.ss ATTGGCATCCACACAGGTC
hrNPR1.as TAGGTCCGAACCTTGCCTTT

PDGFRB ; product size: 320
hrPDGFRB.ss ATCTTCAACAGCCTCTACACCAC
hrPDGFRB.as TCACTCCTCAGAAACTCCTCATC

TFR1 ; product size: 196
hrTFR1.ss AGCAACTTCAAGGTTTCTGC
hrTFR1.as AACAGAAAGAAACTGCTGGGATT

FOLR1
human; product size: 234
hFOLR1.ss TTCTAGTGTGGGTGGCTGTAGTAG
hFOLR1.as CACAGTGGTTCCAGTTGAATCTAT

rat; product size: 485
rFOLR1.ss AACTTCTCAATGTCTGCATGGAT
rFOLR1.as GTGTCTTGGATAAAGTGACGTTTG

EGFR
human; product size: 262
hEGFR.ss ACTCCTTCACACATACTCCTCCTC
hEGFR.as TTTCCTGAAATTATCACATCTCCA

rat; product size: 334
rEGFR.ss GAAGATGGAGTCAGCAAGTGTAAA
rEGFR.as TTGTTCTGCCACGAATTATTTCTA

For qualitative analysis of receptor expression in F98 and LN229 glioma cell lines, total RNA was isolated from cells using RNEasy Mini Kit from Qiagen, transcripted into DNA and amplified via polymerase chain reaction.

Cells were grown in cell culture flasks under recommended growth conditions until fluency was reached. Cells were then washed three times with 5 ml PBS and 0.35 ml lysis buffer RLT (RNEasy Mini Kit), supplemented with 0.01 ml β-mercaptoethanol was added. Cells were then stored at -80°C until PCR was performed. For mRNA-extraction, full cell lysate was centrifuged through Qiashredder column and washed with ethanol 70%. The eluat was centrifuged on RNEasy columns, which hold back RNA. Columns were washed, RNA was eluated and OD was measured at 260nm.

2 µg RNA were used for DNA synthesis with Transcriptor high fidelity cDNA synthesis Kit, random primer, PCR cycle: 65°C, 10 min. In the meantime, the standard RT-PCR mixture (4 µl RT reaction buffer,

0.5ml Protector RNAse inhibitor, 2 µl DNT mix, 1 µl DTT, 1.1 µl Reverse Transcriptase) was prepared. Both mixtures were united and run in PCR cycler for 30 min at 50°C and 5 min at 85°C. Finally, 2 µl of the newly synthesized DNA-samples were added to the mixture for the standard procedure protocol of Fast Start Taq polymerase-Kit (5 µl PCR buffer, 0.2 µl DNTP mix, 5 µl ss-primer, 5 µl as-primer, 0.4 µl Taq polymerase, 28.6 µl water PCR-grade). This mixture was left in the PCR cycler to run through 1 cycle activation/denaturation (4 min, 95°C), 35 cycles denaturation (30 sec, 95°C), annealing (30 sec, 55°C), elongation (55 sec, 72°C), 1 cycle final extension (7 min, 72°C) and 30 min cooling at 4°C.

Products were subjected to gel-electrophoresis (80 volt) on a 2% agarose gel including 0.1% ethidium bromide in tris-acetate-EDTA (TAE) buffer. TAE consisted of 40 mM tris, 20 mM acetic acid and 1 mM EDTA. For the gel electrophoresis, the gene ruler 1kb was used as a DNA ladder. 5 µl of the DNA probes were loaded together with 25 µl loading buffer in gel bags. The experiment was repeated six times.

3.2.3.3 Uptake of fluorescence-labeled liposomes into F98 and LN229 cells

As a fluorescent probe for fluorescence spectroscopy measurements, NBD-DHPE was chosen for its relatively small fluorescent headgroup and comparable chain length to the main lipid of the liposome formulations, DOPC.

Fluorescence of a molecule is caused by the interaction of the fluorophore and a photon of a defined energy. The energy of the photon can be absorbed by an electron of the molecule which will then be raised from the ground state to an excited state. The electron undergoes several conformational changes in its excited state and may interact with its molecular environment, while the initially absorbed energy will decrease. Some of these interactions (collisional quenching, fluorescence energy transfer and intersystem crossing) may deplete all of the absorbed energy without the emission of a photon. However, with a certain probability, the electron will return to its ground state under the emission of a photon. The fluorescence light is of a longer wavelength than the excitation photon due to the energy-dissipating effects mentioned above.

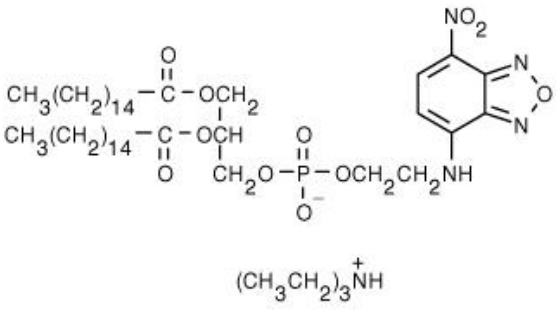

Figure 3-7 Formula of NBD-PE [133]

Fluorescence spectroscopic measurements were carried out as follows:

Liposomes were prepared from NBD-PE (0.5% mol/mol) containing lipid films. F98 and LN229 cells were seeded in black, clear bottom 96 well microplates at a density of 4000 cells/well and allowed to grow

under recommended growth conditions for at least 24 hours. Cells were then incubated with 2 to 4 mg lipid/ml liposome formulation for up to 24 hours. At the end of incubation time, liposome-containing growth medium was aspirated off and cells were washed three times with 300 µl ice-cold PBS. A 2% solution of Triton X-100 in PBS was used to solubilize cells, which were then left in the dark to dissolve on a plate shaker for 45 min. Plates were read out on a microplate reader using excitation wavelength 465 (35) nm and emission wavelength 535 (25) nm.

Results were expressed as µg lipid per µg cell protein. Cell protein quantity was determined via BC-assay, which was done in parallel to uptake experiments at all times.

3.2.3.4 Determination of total cell protein by bicinchoninic acid assay

For exact quantification of NBD-PE liposome uptake into F98 and LN229 cells, total cell protein was determined by BC-Assay simultaneously to uptake experiments for the two cell lines.

The quantification of cell protein is based on the Biuret reaction, in which Cu^{2+} ions are reduced to Cu^{1+} by proteins in an alkaline medium. Bicinchoninic acid forms a purple colored Cu^{1+} chelate, whose absorption can be read out at 562 nm. Smith et al. [134] improved the original assay for protein determination (Lowry-Assay [135]) by replacing the detection reagent Folin-Ciocalteau with bicinchoninic acid (BC). The final BC-complex proved to be less susceptible to buffer salts and detergents. At the same time, the assay allowed a higher flexibility of the protocol, since the method could be adjusted to the expected protein concentration by simple alteration of the reaction temperature.

$$\text{Peptidic bonds} + Cu^{2+} \xrightarrow{OH^-} Cu^{1+}$$

$$Cu^{1+} + \text{BCA} \longrightarrow \text{BCA-}Cu^{1+}\text{- complex [purple]}$$

Figure 3-8 Reaction scheme for BC-assay (modified according to Smith at al. [134]).

F98 and LN229 cells were seeded at a density of 4000 cells/well in 96 well clear microplates and allowed to grow for 24 hours in parallel to cells for uptake experiments. Cells were washed three times with 300 µl of ice-cold PBS at the same time as cells from uptake experiments, and 200 µl bicinchoninic acid working solution was added to each well [136]. Cells were incubated 30 min at room temperature on a plate shaker and transferred to a heating chamber to incubate for another 30 min at a temperature of 60°C. For calibration, bovine serum albumin, which was included in the kit, was used. Plates were allowed to cool down for ten minutes and absorption was read by a microplate reader at 560 (10) nm wavelength.

3.2.3.5 Fluorescence microscopy

Confocal laser scanning microscopy has proved to be a useful tool for the imaging of cellular liposome uptake. The technique enables the researcher to examine different levels of a cell by dividing it into many cross-sections which can be viewed individually. This 'stacking method' is made possible by the employment of a pinhole (confocal aperture) which excludes light coming from areas out of focus. This way, only light from planes in focus reaches the detector while the probe is scanned point by point. The out-of-focus areas are therefore invisible in the image and it is possible to view into the depth of thicker objects.

Experiments were carried out as follows:

Cells were seeded in 6 well plates on 20 x 20 mm cover slips at a density of 8000 cells/well and kept under recommended growth conditions for 48 hours. Medium was changed again, before cells were incubated with 1.5-1.65 mg/ml DOTAP-liposomes marked with 0.5% NBD-PE for 1.5 hours. The DOTAP-liposomes were prepared as described above and given directly to the wells containing the cell growth medium. After the incubation period, cells were washed three times with 1.5 ml ice-cold PBS. For cell membrane staining, cells were covered with 1 ml of a 5 µg/ml solution of Cell Mask Deep Red for 10 minutes and subsequently rinsed once with 1.5 ml PBS.

Fixation protocol included incubation with 1 ml of PBS containing 4% formaldehyde for 20 minutes. Cover slips were then washed again three times with 1.5 ml ice-cold PBS, immersed shortly in bi-distilled water and mounted with one droplet of ProLong Gold antifade reagent with DAPI. The slides were left to dry overnight at 4°C and examined microscopically on the following day.

Microscopic imaging was performed at the Confocal Laser Scanning Microscope Core Facility, University Medical Center of the Johannes Gutenberg University Mainz, Mainz, Germany. The facility offers a Zeiss Confocal LSM 510-UV equipped with four channels. The Argon Laser (458, 488 nm) was used for excitation of DAPI (460 nm for excitation, 500 nm as emission wavelength) and NBD-PE (excitation 463 nm, emission 536 nm), the Helium Neon Laser (633 nm) for Cell Mask Deep Red (excitation 649 nm, emission 666 nm). Slides were examined through a Plan-Apochromat 63 x oil objective, giving a total magnification of 63 x 1.4.

3.2.3.6 Uptake of NC-element gadolinium into F98 and LN229 cells

The investigation of cellular uptake of NC-element-containing liposomes is based on uptake experiments with both cell lines and the subsequent analysis of cellular content, regarding potentially internalized Gd.

Cells were seeded in 100 x 20mm petri dishes at densities of 1.4 million cells/dish and 1.6 million cells/dish for F98 and LN229 cells, respectively. After allowing cells to grow under recommended growth conditions for 2 days, growth media was changed. Cells were incubated with Magnevist® or liposomal formulations containing Magnevist®, all of which were added directly to the culture medium, for a specified amount of time. Gd-containing media was then aspirated off and cells were washed three times with 8 ml ice-cold PBS, trypsinized and counted. Cell suspensions were centrifuged at 180 g for 8

min and the supernatant was aspirated off thoroughly. The remaining cell pellet was frozen at -20°C and stored until ICP-MS measurements could be performed.

3.2.3.7 Analysis of NC-element gadolinium in cell pellets via ICP-MS

Inductively coupled plasma mass spectroscopy is a highly sensitive method for discovering trace amounts of elements in complex sample matrices.

For the measurement, samples must be presented in liquid form.The first step then is the nebulization of the sample in a spray chamber. From there, the aerosol droplets escape into the inductively coupled plasma, where the droplets are vaporized to gas, atomized to obtain single atoms and finally, ionized. The resulting ions are separated according to their mass-charge-ratio. Thus, all isotopes of one element can be detected separately.

The cell pellet from uptake experiments (section 3.2.3.6) was thawed, dissolved in 3 ml of a mixture of concentrated (65%) nitric acid and concentrated (35%) hydrogen peroxide. Sample tubes were put in an ultrasound bath for 30 min to ensure complete dissolution of cell remainders. 2 ml of the clear solution were pipetted into a sample tube and 5.5 ml bi-distilled water as well as 50 µl of Europium-Standard (Eu-Standard, 10ppm) were added.

Corresponding Gd-containing media were diluted with bi-distilled water, mixed with 2 ml of the nitric acid/ hydrogen peroxide solution and filled up with bi-distilled water to give a final volume of 7.5 ml. 50µl of Eu-Standard was added to each sample.

Measurements were performed on an Agilent ICP-MS 7500 ce, using a concentric 0.05 ml/min nebulizer and a cyclone spray chamber. All samples were measured 9 times of which the mean for all Gd-Isotopes was calculated automatically by MassHunter Workstation program. Rinsing between samples was done with solutions consisting of i) (1.25% w/w) HNO_3 ii) butanol (2.5% w/w), concentrated ammonium (1% w/w), EDTA (0.05% w/w), Triton X-100 (0.05% w/w) iii) (1.25% w/w) HNO_3 .

3.2.3.8 Cytotoxicity and cell proliferation assay (MTT assay)

The MTT assay is widely used for determination of cytotoxicity and viability of cells. It is based on reduction of the yellow tetrazolium salt 3-(4,5-Dimethylthiazolyl-2)-2,5-diphenyl-2H-tetrazolium-bromide to form a deep blue colored formazan whose absorption can be easily measured in microplates via plate reader. The cellular reduction of MTT depends highly on enzymes of the endoplasmic reticulum, involving the reduced pyridine nucleotides NADH and NADPH. Mitochondria also play a role in MTT reduction by providing succinate as electron donor for MTT [137, 138]. Mosmann et al. developed the test as a fast and simple assay for growth and chemosensitivity testing of cells [139].

MTT assay was performed as follows:

MTT stock solution was prepared by dissolving 5 g/l tetrazolium salt in double-distilled water under vigorous stirring for at least 2 hours, and subsequent sterile filtration through a 0.22 µm cellulose-

acetate filter. For preparation of the working solution, the stock solution was diluted with DMEM w/o phenol red to a final concentration of 0.5 g/l.

Cells were grown in 96 well microplates and subjected to irradiation after incubation with different formulations of radioenhancer/NC-element. MTT assay was usually performed every day, beginning one day after irradiation, for at least 4 days [140]. Cell growth media was aspirated off, replaced with 100 µl of 0.5 g/l MTT working solution and incubated for 30 min. In the next step, MTT working solution was carefully removed and exchanged against 180 µl DMSO which were also left to incubation for 30 min. The resulting blue colored extract was pipetted into a fresh microplate for the read-out in a plate reader (absorption wavelength 560 nm, reference wavelength 690 nm).

3.2.3.8.1 Multiple MTT assay

As a variation of the MTT test, a multiple MTT assay could be applied. In this case, the usual MTT assay was performed every day as described above, and the results were combined to form a growth or proliferation curve of the respective cell group (i.e., treated with liposomes, free metal solution or control)[141]. The growth curve was then fitted via nonlinear regression and exponential growth of the Prism program to obtain the doubling time, a start value and the K constant for each treatment group.

(6) $$y = start * exp^{(K*x)}$$

start: start value of absorption

K: rate for exponential increase

For further calculations, the optical density value y was set to 1 as fix point to be reached. The time span necessary for the cells to give absorption of 1 was used for the calculation of the delay time, giving the relative lag, the proliferative survival of cells and the inhibition (I) (cf. [142]).

(7) $$Relative\ lag = \frac{Delay}{Doubling\ time}$$

(8) $$Proliferative\ survival\ (S) = 2^{-\ relative\ lag}$$

(9) $$Inhibition\ (I) = 1 - S$$

delay: time difference in reaching absorption 1 of control group to treated group

doubling time: period of time in which cells divide and therefore double their number (= one cell cycle)

The cell survival calculated by this formula is the proliferative survival of cells, that is, only dividing cells are counted, while non-dividing cells are subtracted from the equation (= start value) and can be analyzed separately. In contrast, colony forming and one-point MTT assays show the overall survival, the sum of proliferative cells and quiescent cells. In colony forming assay, the latter remain uncounted, since they do not form a colony and therefore, cannot be observed. In single-point MTT assay, the quiescent cells which are alive, though not dividing, add to the overall MTT absorption through their still working metabolism. In the following sections, the overall survival is given, if not otherwise stated.

3.2.3.8.2 Correlation between MTT absorption and cell number

The use of MTT assay for the determination of cell survival after irradiation is based on the assumption that formazan production and cell number show a linear relationship. Although a good correlation between MTT absorption and cell number was described by Carmichael et al. [140], it was found later that for higher cell densities or some fast-growing cell lines the relationship was not necessarily linear [143, 144].

Therefore, the correlation between MTT reduction and corresponding cell number was examined for both cell lines F98 and LN229 over the respective time span of radiation experiments.

LN229 and F98 cells were seeded into 96 well microplates, with cell densities of 2500 and 4000 cells/well for each cell line. Cells were allowed to attach for 24 hours and MTT assay was performed for 8 wells, every 24 hours for 4 or 5 days (for F98 and LN229 cells, respectively). Simultaneously, 8 or 16 wells, according to cell number, were trypsinized, united and counted via Coulter Particle Count and Size Analyzer (measurement between 7.5 and 20 µm).

Cell number and MTT absorption were correlated according to cell seeding density (2500 and 4000 cells/well).

3.2.3.8.3 Correlation between MTT assay and colony forming assay

The MTT assay has been proven to offer a good reproducibility and comparable results to the standard test for irradiation experiments, the colony forming assay (CFA) [145, 146]. However, the cells had to be seeded at an appropriate density and still be in the exponential growth phase for this to be the case. In addition, the test settings had to allow enough time for mitotic cell death to occur, that is approximately four days after treatment [145, 147].

Therefore, the suitability of the multiple MTT assay for determination of cell survival after irradiation was examined and compared with the standard test, the colony forming assay [141].

Two different procedures were applied for the study: the plating before the irradiation treatment and the plating afterwards [146, 148, 149]. In the first case, LN229 cells were seeded in growth flasks, allowed to reach confluency, and irradiated with doses from 1-15 Gy from the linear accelerator at the University Medical Center Mainz (cf. section 3.2.4.2). Growth medium was replaced with fresh medium and cells were splitted and plated the next day. 250 and 500 cells/ dish were seeded in petri dishes for

the CFA, while 2500 and 4000 cells were seeded in 96 well plates for the MTT assay. The CFA was evaluated at day 20 after irradiation; MTT was done every day for 5 days as described before.

For the colony-staining in the CFA, the growth medium was aspirated off and cells were washed one time with PBS. The plates were then incubated for 30 minutes with a solution of 0.5% crystal violet in methanol/water (50/50% vol/vol). After the incubation, culture plates were rinsed thoroughly with water and left to dry overnight. The next day, all colonies of more than 50 cells or larger than 1 mm were counted under the light microscope.

For the second part of the study, cells were already plated for the irradiation. Briefly, F98 and LN229 cells were seeded in 96well plates for MTT assay at a density of 2500 and 4000 or 2500 and 5000 cells/well, respectively. For the colony forming assay, both cell lines were also seeded in 6 well plates at densities of 75 and 100 cells per well for the F98 cell line and 100 and 200 cells/well for the LN229 line. Cell culture plates were irradiated with 1-15 Gy as described above. Medium was changed and the plates were left in the incubator under recommended growth conditions. CFA was analyzed 8 days after irradiation, while the MTT assay was done every day after the irradiation for 5 days.

Survival of the cells in the CFA was calculated as follows [148]:

(10) $$Plating\ efficiency\ (PE) = \frac{No.of\ colonies}{No.of seeded\ cells} * 100\%$$

(11) $$Surviving\ fraction\ (SF) = \frac{No.of\ colonies\ after\ treatment}{No.of\ seeded\ cells * PE}$$

3.2.4 Cell irradiation experiments

3.2.4.1 General procedure

Cells were seeded in 96 well microplates and kept under recommended growth conditions for 24-48 hours. Prior to irradiation, cells were incubated for 1 to 24 hours with different liposomal or 'free metal' formulations of radioenhancer (Gd-DTPA(-NV), Lu-DTPA, Er-DTPA) or neutron capture elements (tris-borate, bisglyceroborate, Gd-DTPA). The culture plates were sealed with adhesive tape to prevent CO_2 loss before being transported to the radiation facility.

When irradiations were completed, the cell culture plates were transported back to the cell culture laboratory and the liposome- or free metal-containing medium was replaced with fresh culture medium. Meanwhile, the control plates (0 Gy or 0 kW·min) were kept under the same conditions regarding incubation, transport, temperature and medium change. Cells were allowed to recuperate for approximately 24 hours, before MTT proliferation assays were first performed.

For determination of significant differences between cell survivals, one way-ANOVA and subsequent Tukey-test were run for all formulations (Prism program).

3.2.4.2 Photon irradiation by linear accelerator

The irradiation with photons or x-rays produced by linear accelerators continues to be the standard in radiation therapy until today. Patients were treated with x-rays from linear accelerators since the early 1950s, employing photons with energy of 6-20 MeV[78].

The linear accelerator generates x-rays by raising the velocity of electrons through oscillating electric potentials along a linear beamline. When the electrons impact on a target (for example water-cooled tungsten), x-rays are created by bremsstrahlung or x-ray fluorescence. Electrons which are scattered by the strong electric field of the tungsten nuclei produce a continuous spectrum of x-rays, the bremsstrahlung. X-ray fluorescence occurs when electrons have enough energy to push an electron from an inner shell of a metal. The position will be occupied again by an electron of a higher energy and x-ray photons are emitted. These x-rays form the spectral x-ray lines which represent the transitions from a higher energy shell to K-shell (K-lines) or to L-shell (L-lines).

Photon irradiation of cells was performed at the University Medical Center, Department for Radiooncology and Radiation Therapy, using the linear accelerator Mevatron MD2 (6 MV), Siemens. The radiation field was set to either 20 x 20 cm or 40 x 40 cm. For human tissue phantom material, RW3 plates (white polystyrene) were used because the dose absorption of the material is approximately equivalent to water. Cell culture plates were placed in the radiation field and usually three RW3 plates served as build-up material (cf. [142]). The dose rate for the applied doses was 1.8 Gy/min.

Cells were incubated with radioenhancer solution or liposomal formulations thereof. Both cell lines were subjected to radiation doses ranging from 1 to 15 Gy. The non-irradiated control plate is referred to as '0 Gy'. MTT tests were performed for up to 145 h after irradiation of cells.

3.2.4.3 Photon irradiation by synchrotron radiation

Synchrotrons use a high energy electron beam to generate x-rays. The electrons are accelerated to a high speed and injected into the storage ring where bending magnets hold them on their circular path. The magnetic fields cause the electrons to emit electromagnetic radiation which is then channeled to the different beamlines connected to the ring.

Synchrotron radiation offers one primary advantage over the x-rays generated by a linear accelerator. From the provided spectrum in GeV range, distinct energies can be singled out and used for irradiation with a monochromatic beam. Further, synchrotron radiation is known for its brilliance and high intensity. Since the users of the beamline can select their preferred wavelength for their experiments, the application area of synchrotron radiation is a very wide-set field ranging from crystallography to different medical applications of x-rays.

Synchrotron irradiation of cells was performed at ID 17, Medical Beamline of the European Synchrotron Radiation Facility (ESRF), Grenoble, France. Cells were prepared as described above (cf. section 3.2.4.1). For the irradiation procedure, the 96 well plates were set up in a plate holder at an angle of approximately 45° and placed directly onto a 2 % agar gel (5 mm thickness) serving as a tissue phantom. The synchrotron beam had to pass through the agar gel, before it reached the underside of wells. Similar to the set-up at the University medical center, the application of a phantom was necessary, since the

absorbed dose depends on the depth profile for x-rays in matter. To ensure the maximum energy deposition on the level of the cells and not in the medium or air above the cell monolayer, the beam had to pass through a gel of a defined width, located in front of the 96 well plates (cf. figure 3-9 B). Thus, the air above the medium in the wells and the medium itself could not interfere with the beam. During the irradiation process, the plate holder was moved slowly up and down to ensure the application of the exact same doses to each well. Preliminary experiments investigated the build-up effect of a 2 cm agar gel based on its position in the beam, that is in front of or behind the cells which were irradiated. These experiments were conducted with lutetium-DTPA as the radioenhancing agent. Lutetium as well as erbium may be used as radioenhancer, because both lanthanides are high-Z elements. Therefore, the elements offer the possibility to induce Auger-electron cascades as a result of photoelectric interaction with x-rays, similar to Gd.

The x-ray energy applied was chosen to fit the respective K-edge of the lutetium or gadolinium used in the experiment. In some cases, an additional energy below the K-edge was selected to examine the effect of the x-ray wavelength on the survival of the cells treated with Gd- or Lu-formulations.

Usually, the dose rates for all applied doses were higher than 1 Gy/ min (approximately 1.2 - 1.8 Gy/min) for synchrotron experiments. However, for the first experiment, MD 442, the dose rates were only 0.1 - 0.11 Gy/ min, due to the respective user mode of the synchrotron facility.

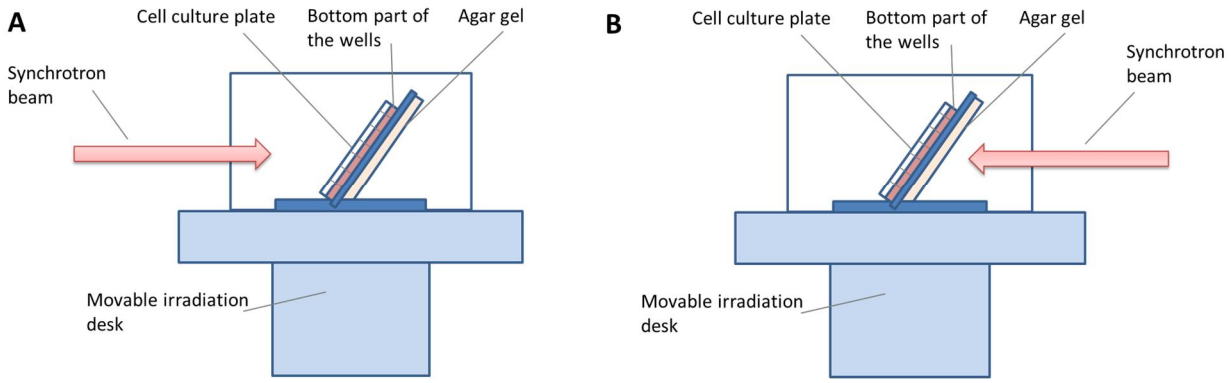

Figure 3-9 Irradiation set-up at ID17, ESRF. A) Agar gel behind cells. B) Agar in front of cells. Set-up B) was chosen for further irradiation experiments.

3.2.4.4 Neutron irradiation

The irradiation of cancer with neutrons is for the most part based on the application of neutron capture elements such as boron or gadolinium. Fissure products of the neutron capture event of these elements are high linear energy transfer particles or gamma rays. Thus, molecules in the cell can be ionized and damage the cellular DNA, finally leading to mitotic cell death or apoptosis of the cancer cell.

3.2.4.4.1 Irradiation experiments at Institute Laue-Langevin (ILL)

Neutron irradiation experiments at ILL, Grenoble, were performed at the D22 beamline, a small angle neutron scattering instrument. The instrument provides a high flux of cold neutrons (energies lower than 0.025 eV), wavelength selection (monochromator) and a large area multidetector with high resolution for scattering experiments (figure 3-10). Therefore, the neutron beam can be used for cell irradiation experiments as well as for structural analysis of, for example, liposome formulations. The neutron flux for the homogeneous, very brilliant neutron beam is reported to be $1.2 \cdot 10^8$ n/(cm²·s) for wavelengths of 0.45 to 4 nm.

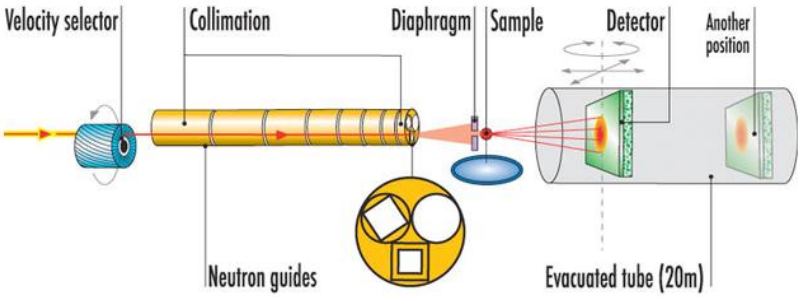

Figure 3-10 Instrument layout of D22 beamline, ILL, Grenoble (retrieved from: http://www.ill.eu/instruments-support/instruments-groups/instruments/d22/description/instrument-layout).

Furthermore, the cross section for neutron capture elements is at least 2-3 times greater for the cold neutrons provided from the neutrons source at ILL than for thermal neutrons [150]. The cross section for Gd (natural occurring mixed isotopes) for cold neutrons was reported to be approximately 10.7 Mb instead of 49 kb for thermal neutrons [151, 152].

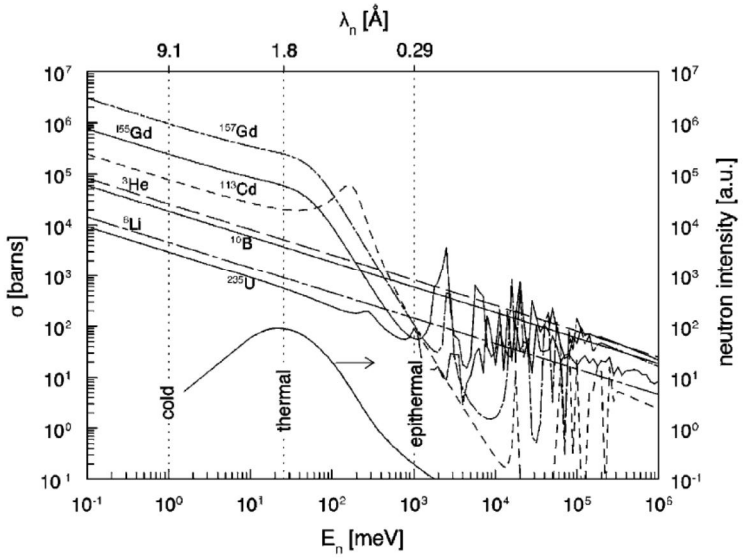

Figure 3-11 Cross sections of selected atoms in relation to neutron energy (from van Eijk et al. [152])

Figure 3-12 shows the set-up for neutron irradiation experiments of glioma cells. 96 well plates were placed at a 45° angle in the neutron beam, on a movable irradiation desk similar to the set-up at ESRF, ID 17. In the experiments at D22, the influence of Er-DTPA as a supplement in liposomal formulations of Gd-DTPA-NV and bisglyceroborate was studied. Er-DTPA was included to determine if an additional radioenhancer may further improve the radiation effect of the neutron capture reaction. As another high-Z element, erbium is expected to interact photoelectrically with the gamma rays deriving from the NC-event of Gd-DTPA-NV. The gamma ray spectrum of the prompt gamma ray emission for the 157Gd-neutron capture event provides suitable energies for the absorption at Er-K-edge (cf. figure 3-13) [153]. Thus, the latter element may also produce a high-LET Auger-cascade which should further enhance the radiation effect, in addition to the original neutron capture event. This aspect of the neutron capture therapy with Gd, a 'build-up effect' from interaction of gamma rays with other atoms (e.g. lanthanides) was also investigated by using a Gd-loaded agar gel, placed behind the cells during irradiation. Consequently, the gamma rays and secondary electrons derived from the Gd-neutron capture event in the gel may further interact with lanthanide elements and/ or cellular structures in the wells of the 96 well plate.

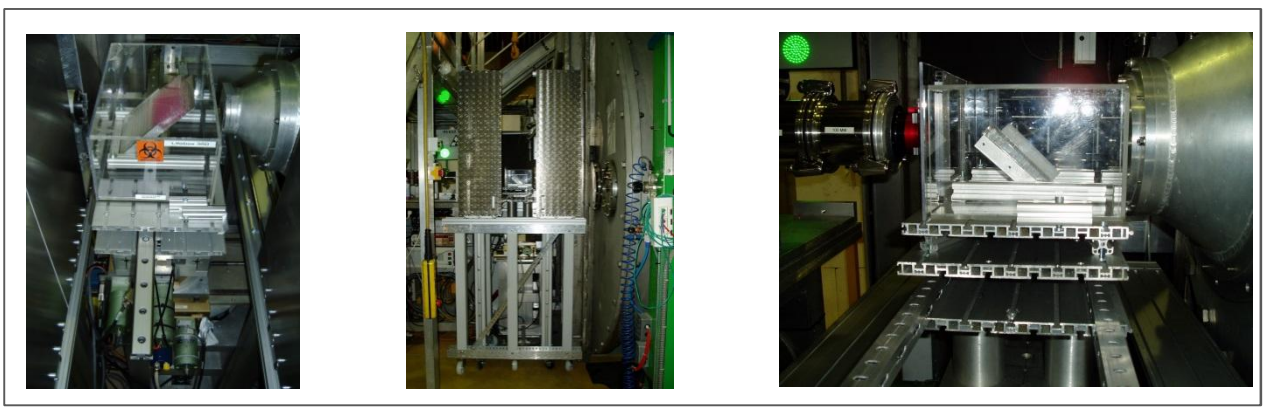

Figure 3-12 Irradiation set-up for cell experiments at D22, ILL.

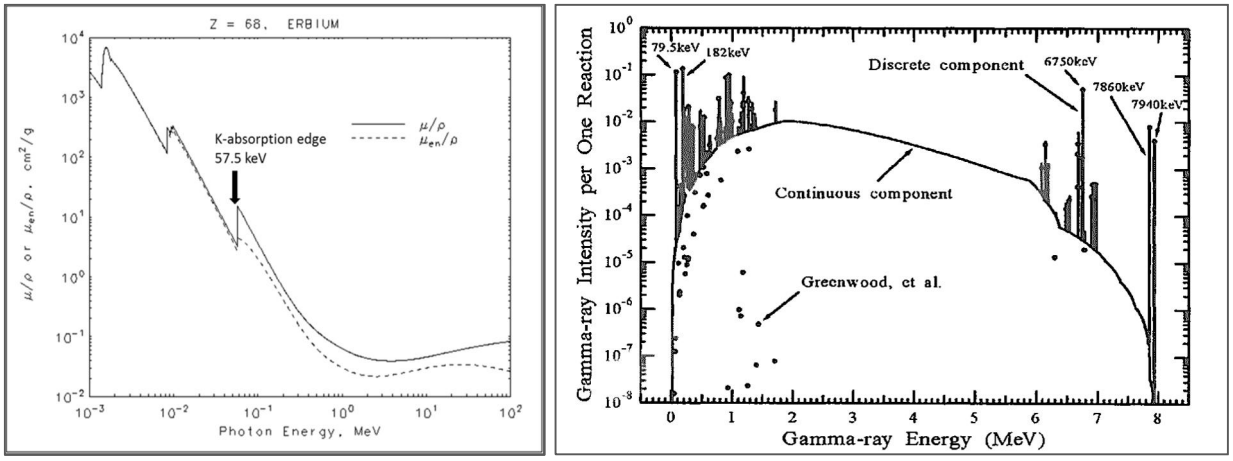

Figure 3-13 Left side: X-ray mass coefficient spectrum for Erbium (from: http://physics.nist.gov/PhysRefData/XrayMassCoef/ElemTab/z68.html). Right side: energy spectrum from the prompt gamma rays from ^{157}Gd (n, γ) ^{158}Gd (from: Sakurai [153]).

3.2.4.4.2 Irradiation experiments at TRIGA reactor

Further neutron irradiation experiments with F98 and LN229 cells were performed at the thermal column of the TRIGA Mark II reactor, Institute for Nuclear Chemistry, Johannes Gutenberg-University Mainz, Germany.

The TRIGA Mark II reactor is a pool-type reactor which uses a special hydrogen-enriched uranium-zirconium fuel. The mixture of the fuel ensures the safety of the reactor, since it provides a prompt negative temperature coefficient of reactivity. Thus, an involuntary increase of the fuel temperature leads to a very quick self-shutdown of the reactor [154].

The Mark II in Mainz is equipped with four horizontal beam ports and a graphite thermal column. The column provides the thermal neutrons which were used for the irradiation experiments [155]. Figure 3-14 shows simulated fields for neutrons and gamma rays in the thermal column [156]. The neutron flux per Watt in the central channel of the thermal column is shown in figure 3-15 (see figure 3-19 for the position of the channel in relation to the irradiation chamber).

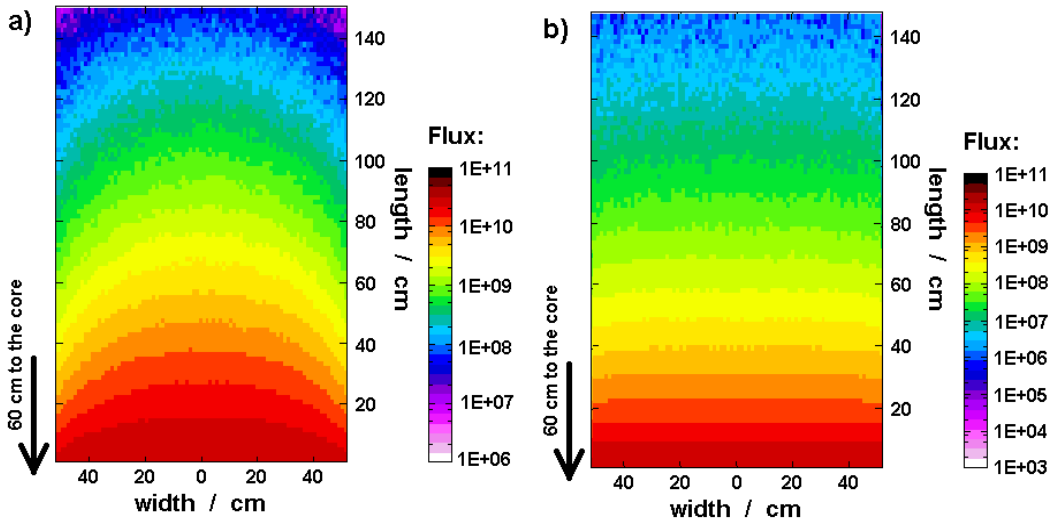

Figure 3-14 Neutron flux (a) and photon flux (b) at 100 kW in the thermal column. The point of origin is 60 cm away from the core (from: Schmitz et al [155]).

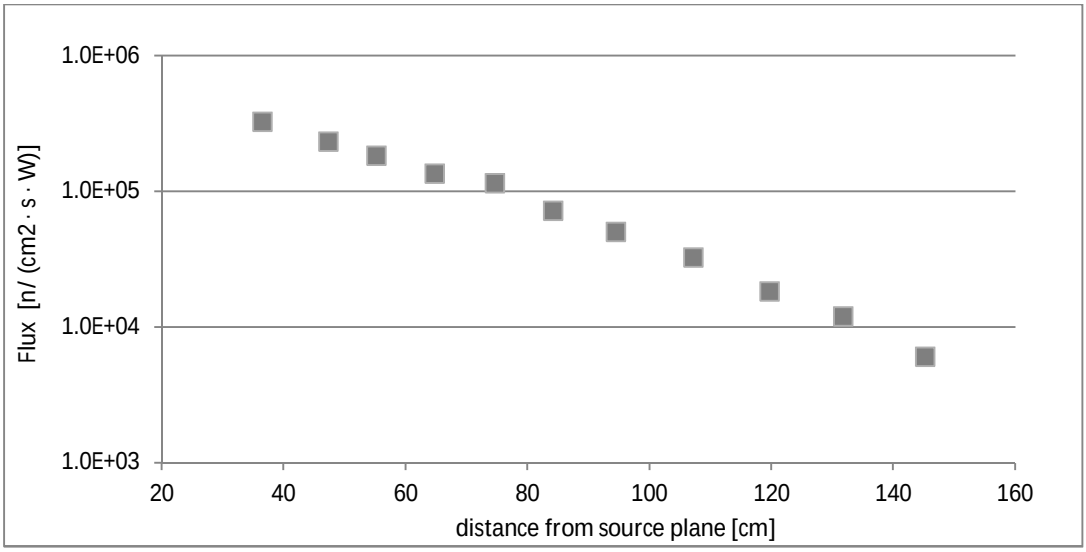

Figure 3-15 Neutron flux per Watt measured in air in the central 10·10 cm channel using gold foil activation, distance from the core = distance from source plane + 60 cm. (Data acquired by T. Schmitz, Institute for Nuclear Chemistry, Johannes Gutenberg-University Mainz).

Cells were prepared as described in section 3.2.4.1. Usually, 10 plates were used: 1 dummy plate (i.e. an empty 96 well plate) on top, 4 plates with cells and 5 dummy plates at the bottom. The cell culture plates were piled in this order and positioned in the center of an irradiation box made of polyethylene, which was entirely filled with polystyrene foam as a diffusor. The box was then introduced into a 20·20 cm irradiation chamber of the thermal column (figure 3-16 and 3-17), approximately 92 cm from the core [157], and irradiated for 10 to 60 min at a reactor power of 10 to 100kW$_{th}$. A period of approximately 45 min was needed to allow the radiation dose to decrease, before the irradiation box could be removed from the beam port of the thermal column. The irradiated media was aspirated off immediately to remove activated sodium and chloride isotopes from the culture plates. After replenishment with fresh media, the 96 well plates were transported back to the cell culture laboratory and treated as mentioned above.

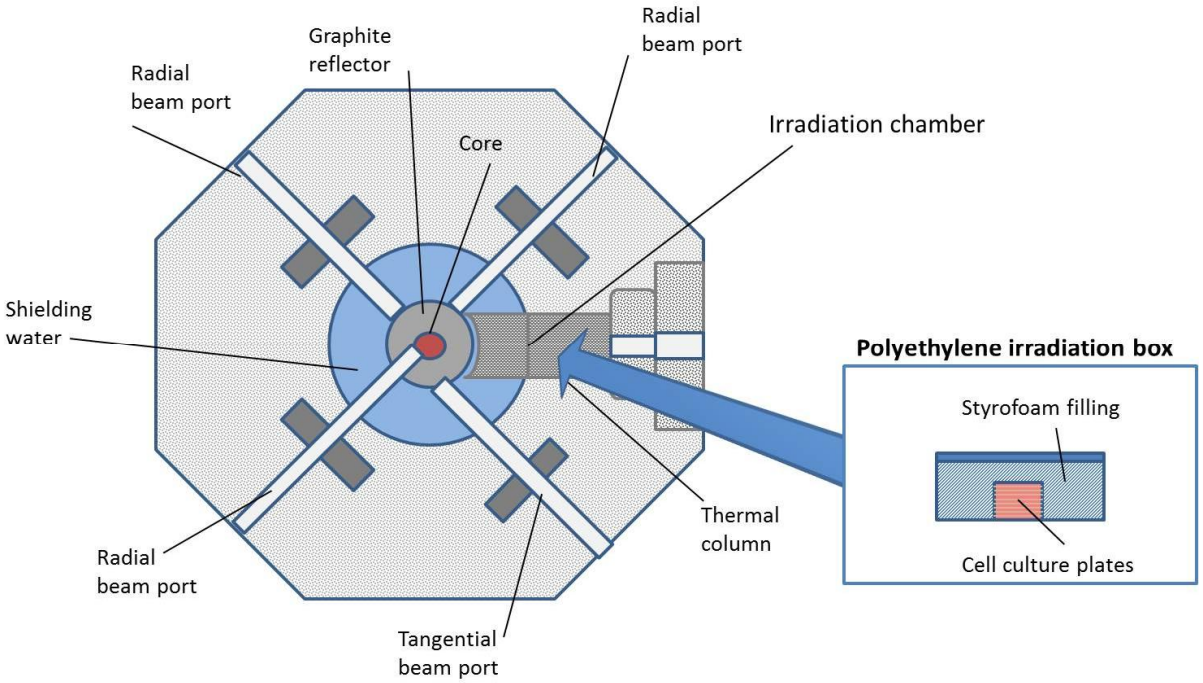

Figure 3-16 Cell irradiation settings at the TRIGA reactor, Mainz (simplified view, according to Hampel et al. [145]).

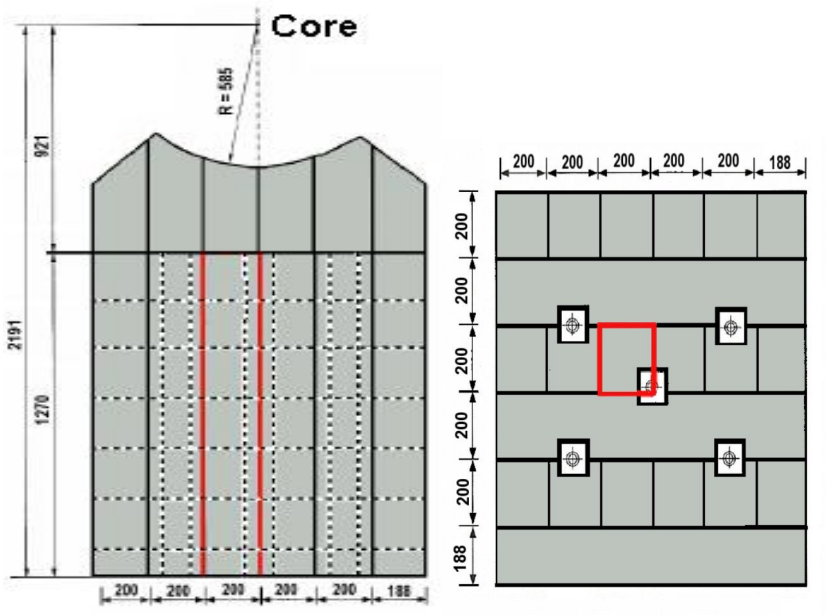

Figure 3-17 Top view (left side) and view from cold end (right side) of thermal column with 20·20 cm irradiation chamber marked in red. Black marked squares (right side) show position of other channels. All dimensions in cm. (From: Vogtländer [156]).

3.2.5 Calculation of gadolinium dose during neutron irradiation via Monte Carlo simulations

Since the direct measurement of the dose applied to cells in 96 well plates is not feasible in the neutron irradiation experiments, the dose was calculated by Monte Carlo simulations. Monte Carlo N-Particle code (MCNP) is used for particle transport calculations, for example photons, neutrons and electrons, in radiation dosimetry. With the aid of Monte Carlo simulation, the neutron field from the thermal column is calculated according to stochastic principle. Taking into account the three dimensional geometric proportions, material constants of the irradiation box and the plates and the composition of cell culture media, the neutron and photon dose per well can be derived from the simulation.

The neutron and photon dose were calculated using MCNP5 and the neutron field was simulated using a source plane at the front of the thermal column. The agreement of the model used in Monte Carlo simulation with the actual conditions at TRIGA reactor had before been confirmed by experimental investigations of the irradiation environment [155, 156, 158, 159]. Figure 3-18 shows the neutron and photon spectra at the selected source plane.

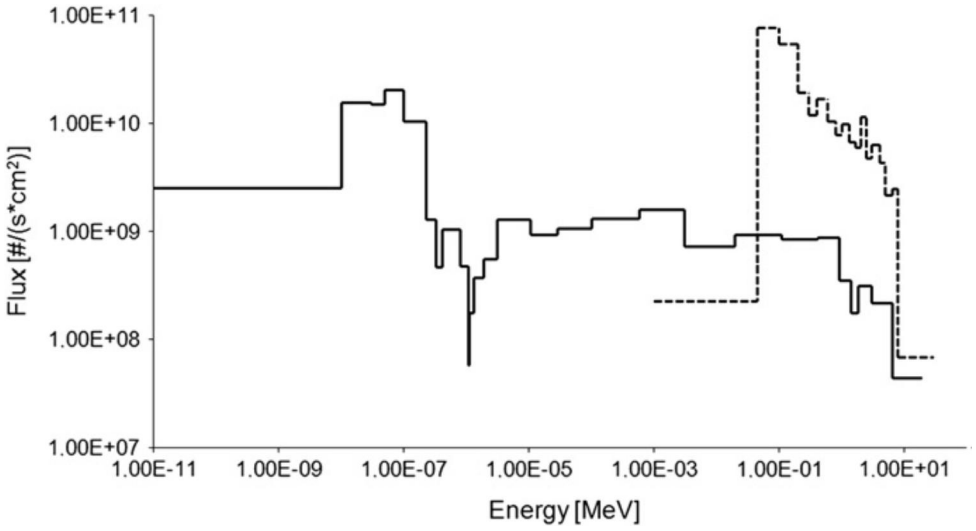

Figure 3-18 Neutron and photon (dotted line) spectrum at the source plane at the front of the thermal column of TRIGA reactor, Mainz (from: Blaickner et al. [158]).

4 Results

4.1 Liposomal formulations

4.1.1 Size

The manufacture of liposomes by ultrasound tip proved to be unsatisfactory in regard to size distribution and reproducibility of the manufacturing process. As shown in figures 4-1 and 4-2, liposome size varied over a wide range, including vesicles of more than 500 nm in diameter. Since these large particles pose a risk of causing thrombosis when injected, ultrasound was finally ruled out as an appropriate means of producing liposomes.

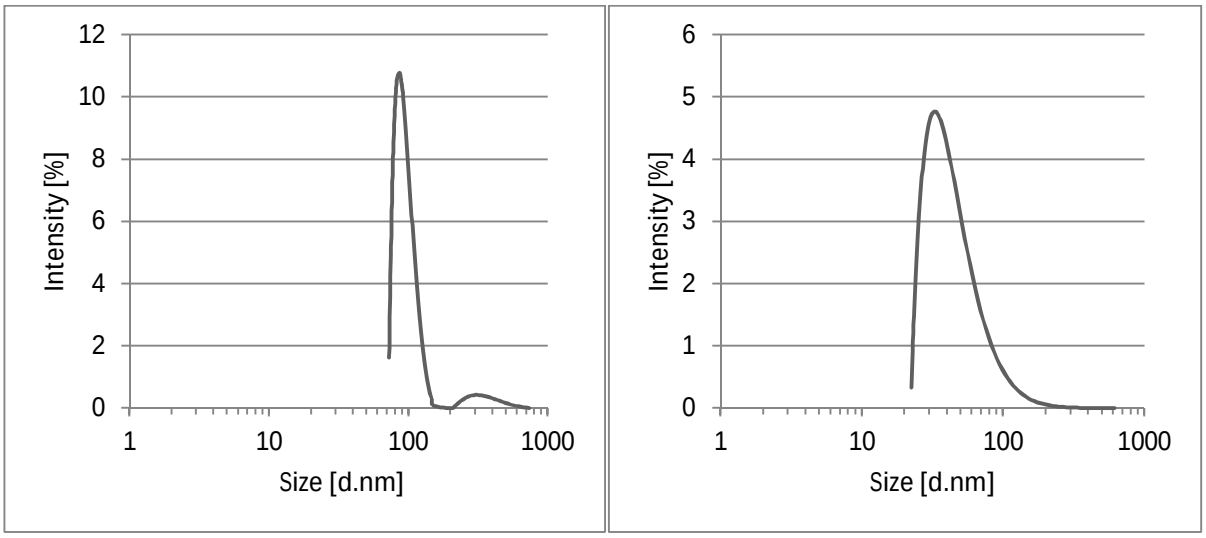

Figure 4-1; Figure 4-2 Size distributions by intensity of two batches of sonicated DOPC liposomes containing Gd-DTPA, after GPC treatment

In contrast, the extrusion method lead to reproducible, monomodal size distributions after 11 passages of lipid suspension through a 100nm polycarbonate membrane (fig.4-3; 4-4). Accordingly, all further formulations were manufactured by extrusion process.

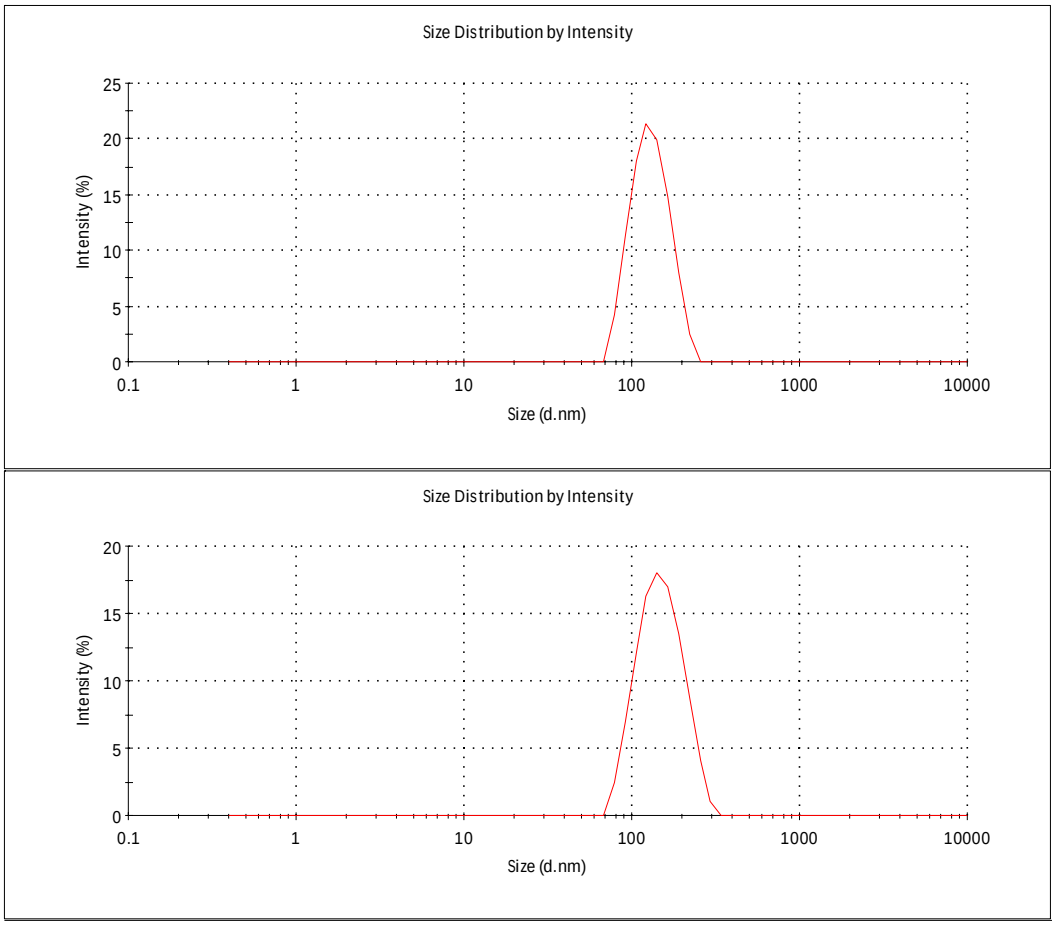

Figure 4-3; Figure 4-4 Size distributions of two batches of extruded DOPC-Chol-DOPE liposomes containing Magnevist, after GPC treatment.

Due to the employment of a polycarbonate membrane with a defined pore size of 100 nm, all lipid formulations yielded very similar size distributions of liposomes. Only the liposome formulation containing Cardiolipin was of slightly larger size than neutral or cationic formulations (table 3). However, the introduction of FolPEG-2000 and other long-chained PEGs also resulted in nearly the same size distribution as for the other formulations.

Sterile filtration did not affect the size of the liposomes; neither did the GPC treatment as confirmed by size measurements before and after the operations (data not shown).

4.1.2 Zeta potential

As expected, liposomes containing charged lipids showed a negative zeta potential for anionic and a positive potential for cationic lipids, respectively. The size and zeta potential of the main formulations used in fluorimetric uptake studies are shown in table 3. Since measurements were done in double distilled water, the zeta potential of neutral/-zwitterionic lipids such as DOPE or DOPC should theoretically quantify to zero at pH 7. In practice, most measurements yielded results in the lower negative range.

For liposome formulations containing NBD-PE, the zeta potential is shifted to more negative regions, due to additional negatively charged groups in the NBD-PE molecule. The same mechanism applies for formulations containing FolPEG2000 and other PEGs (see section 4.3, table 8).

Table 3 Size and zeta-potential of liposome formulations used in NBD-uptake experiment

Formulation (including 0.5% NBD-PE)	Size [d.nm] ± SD	Zeta Potential [mV] ± SD
DOPC-Chol-DOTAP	137.42 ± 2.70	49.51 ± 4.59
DOPC-Chol-CL	142.40 ± 10.42	-57.98 ± 3.09
DOPC-Chol-DOPE	152.97 ± 10.82	-23.82 ± 1.77
FolS-DOPC-Chol (FolPEG2000)	137.79 ± 6.17	-17.5 ± 8.11
DOPC-DOPE (50mg/ml)	129.44 ± 8.14	-20.78 ± 6.04

Zeta-potential was also determined after entrapment of the radioenhancer/NC-element Gd-DTPA. The DOTAP formulation including 9% (mol/mol) DOTAP showed a high enough zeta potential to ensure sufficient stability of the liposomes in suspension (> ± 30 mV), as did the CL-formulation (table 4)[160].

Table 4 Size and zeta potential values for main formulations (50mg lipid/ml, encapsulating Gd-DTPA, after GPC treatment)

Formulation	Size [d.nm] ± SD	Zeta Potential [mV] ± SD
DOPC-Chol-DOTAP	136.20 ± 8.07	41.25 ± 2.49
DOPC-Chol-CL	152.11 ± 10.22	-67.77 ± 2.70
DOPC-Chol-DOPE	133.19 ± 5.76	-15.53 ± 7.53
FolS-DOPC-Chol (FolPEG2000)	136.77 ± 8.81	-24.70 ± 3.10
DOPC-DOPE	138.54 ± 10.17	-17.78 ± 6.04

4.1.3 Encapsulation efficiency

Examination of the encapsulation or entrapment efficiency of Carboxyfluorescein revealed differences between the formulations, dependent on the lipid composition. DOTAP-containing liposomes appeared to have the highest EE for all formulations (2.99%). This is caused in part by the opposing charges of

DOTAP and the entrapped model substance, Carboxyfluorescein, whose carboxyl group is deprotonated in neutral solution. Remarkably, Cardiolipin containing liposomes also showed a high EE for CF, despite their negative charge.

All other formulations entrapped a very small amount of CF (1.8-2.5%). Therefore, the liposome manufacture process was changed from 'normal' room temperature extrusion to the freeze-thaw and subsequent extrusion method, which was previously found to enhance the encapsulation efficiency [161-163].

The application of five freeze-thaw cycles before extrusion improved the encapsulation efficiency significantly. For all tested formulations, the EE could be increased by a factor of 2, although the size of the vesicles was reduced simultaneously (cf. table 5).

Further improvement of the EE was achieved by increasing the amount of extruded lipid. The 50 mg/ml formulation of DOPC-Chol-DOTAP yielded both in normal and freeze-thaw extrusion an EE twofold higher than for the 25 mg/ml formulation. Consequently, the other lipid formulations were also adapted to the higher lipid amount for the manufacturing.

Table 5 Liposome formulations and their respective size and encapsulation efficiency

Formulation	Size [d.nm] ± SD	Encapsulation Efficiency [%]
DOPC-Chol n	154.43 ± 2.97	2.51 ± 0.00
DOPC-Chol ft	139.77 ± 3.55	6.24 ± 0.27
DOPC-Chol-CL n	139.67 ± 2.26	2.24 ± 0.10
DOPC-Chol-CL ft	124.20 ± 2.55	9.35 ± 0.32
DOPC-Chol-DOPE n	140.73 ± 1.42	1.81 ± 0.03
DOPC-Chol-DOPE ft	130.43 ± 0.47	4.21 ± 0.08
DOPC-Chol-DOTAP n	135.37 ± 1.72	2.99 ± 0.07
DOPC-Chol-DOTAP ft	123.80 ± 1.57	9.35 ± 0.14
DOPC-Chol-DOTAP 50mg/ml n	141.50 ± 1.9	7.08 ± 0.26
DOPC-Chol-DOTAP 50mg/ml ft	122.37 ± 0.55	15.13 ± 0.7

4.1.3.1 Encapsulation efficiency for Gd-DTPA

Determination of the encapsulation efficiency of Gd-DTPA (Magnevist®) in 50mg/ml freeze-thaw and extrusion liposomes was performed by ICP-MS measurement of the liposome formulations before and after gel permeation chromatography. The EE of Magnevist was highest in DOTAP and DOPC-DOPE

liposomes (10.2% of initially employed Magnevist® solution). The CL-formulation held only 6.6%, while the DOPE and the FolPEG2000 formulation entrapped 9.4 and 9.6%, respectively.

Table 6 Liposome formulations and their respective EE for Gd-DTPA (Magnevist®)

Formulation	Encapsulation Efficiency [%]
DOPC-Chol-DOTAP	10.24 ± 4.85
DOPC-Chol-CL	6.56 ± 1.74
DOPC-Chol-DOPE	9.37 ± 2.83
FolS-DOPC-Chol (FolPEG2000)	9.60 ± 1.75
DOPC-DOPE	10.21 ± 2.53

4.1.4 In vitro release studies (flow-through cell)

The cumulative percent Gd-DTPA-release values for DOTAP-liposomes and DOPC-DOPE-liposomes over 24 hours are shown in fig. 4-5. For comparison, the figure also includes the release of free Gd-DTPA under the same conditions. The in vitro release of Gd-DTPA from the liposome formulations shows different phases until it is, in case of the DOPC-DOPE liposomes, nearly complete (liberation 96%) after 24 hours of dissolution.

In the first five minutes, the release of Gd-DTPA shows an initial burst (fig. 4-6). The second stage is also a relatively rapid liberation. Since the burst occurs for liposomal as well as for non-entrapped Gd-DTPA and the slope is nearly identical for the three formulations, this phenomenon can be ascribed to free Gd-DTPA leaked out from the liposomes. The semi-logarithmic plot shows distinctly two stages of release. Between 5 and 10 min after start of the experiment, there appears a slight inconsistency in the curves, which might indicate another stage. However, this phenomenon may also be ascribed to variation in the Gd-detection. Interestingly, the further release of the free Magnevist solution from the dialysis tube is only slightly higher than that of the liposomal Magnevist (40% after 60min in comparison to 30% for PEPC and 28% for DOTAP liposomes). After 180 min, the percent Gd release from the free Magnevist solution is equal to the release from DOPC-DOPE liposomes (60%).

The further release profiles of the three formulations are similar, indicating that they all follow the same release kinetic. The curves follow the shape of a saturation curve, approaching a maximum value. The most simple curve fitting with the equation for a first order kinetic, the one phase exponential association (Prism Software, equation 11), leads to a very good correlation based on the determination coefficients (R^2= 0.9830, R^2= 0.9907 and R^2= 0.9909 for non-entrapped Gd-DTPA, Gd-DOPC-DOPE- and Gd-DOTAP-liposomes, respectively). To account for two or more different stages of release, equation 11 can be modified via introduction of a second and third term (equation 12), describing the second and third phase of Gd-DTPA release from liposomes [164].

(11) $$y = y_{max} * (1 - e^{-k*x})$$

(12) $$y = y_0 + a * \left(1 - e^{-k*x}\right) + b * (1 - e^{-m*x}) + c * (1 - e^{-n*x})$$

Y_0= start value

y_{max}= maximal value at time t=∞

k, m, n = rate constants

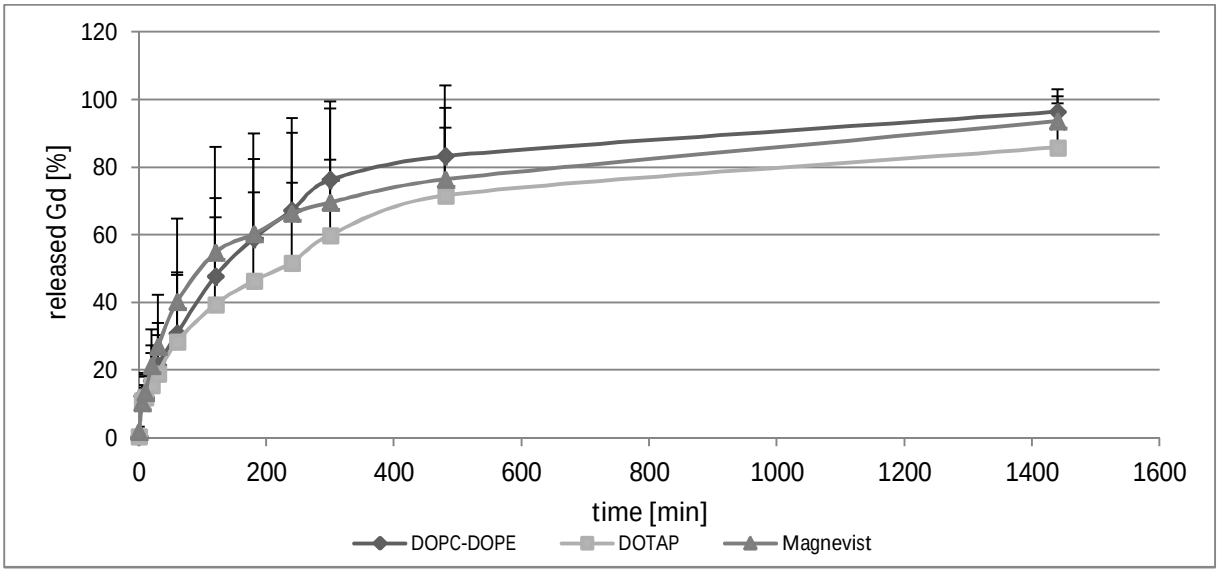

Figure 4-5 Flow-through dissolution profiles of Gd-DTPA release from different formulations. DOPC-DOPE 50 mg/ml ft liposomes containing Magnevist solution (initial concentration 300 mM); DOTAP: DOTAP 50 mg/ml ft liposomes containing Magnevist solution (initial concentration 300 mM); Magnevist: free Magnevist solution (21 mM, equivalent to absolute Magnevist concentration in liposome suspension).

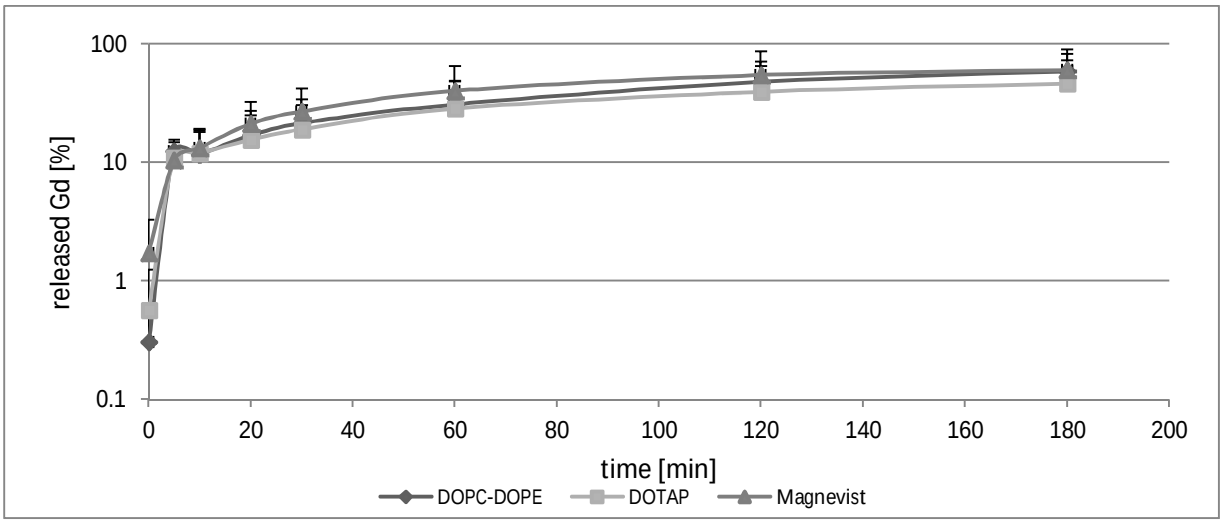

Figure 4-6 Release profile of Gd-DTPA from different formulations: initial burst in first minutes and transition to rapid release. DOPC-DOPE 50 mg/ml ft liposomes containing Magnevist solution (initial concentration 300 mM); DOTAP: DOTAP 50 mg/ml ft liposomes containing Magnevist solution (initial concentration 300 mM); Magnevist: free Magnevist solution (21 mM, equivalent to absolute Magnevist concentration in liposome suspension).

4.2 Detection of FR alpha expression in F98 and LN229 cell line

Reverse Transcriptase polymerase chain reactions were used to gain insight in F98 and LN229 receptor profiles. The folate receptor FR alpha was shown to be expressed in LN229 cells, but not in F98 cells. Figure 4-7 presents a typical picture from gel electrophoresis of the PCR products. LN229 cells exhibit a distinct line for the FR alpha at 485 bp, while F98 cells do not show a band for their respective product at 234 bp. The expression of the other receptors was also analysed, but not followed up in further experiments.

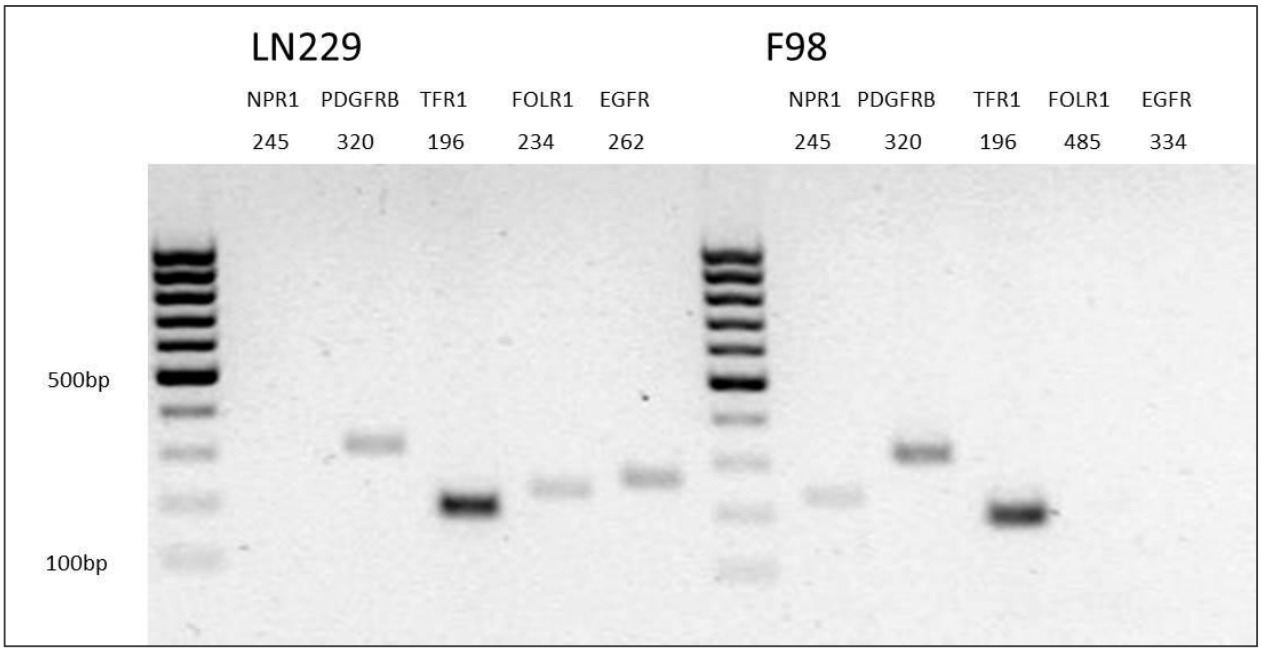

Figure 4-7 Results from receptor screening experiment (RT-PCR), separation of DNA product into distinct bands via gel-electrophoresis. Numbers below receptor abbreviations give the size of the DNA strand in base pairs.

Table 7 gives an overview over receptor expressions found by RT-PCR experiments and states results from respective references, if available.

Table 7 Results from PCR screening of different receptors. First sign reflects findings from our study, second sign and numbers in parenthesis show results from literature research.

	NPR1	PDGFR **β**	TFR1	FR **α**	EGFR
F98 (rodent)	+ n.s.	+ + [165]	+ + [166]	- - [167]	- + [165] – [35, 168-170]
LN229 (human)	- n.s.	+ n.s.	+ n.s.	+ n.s.	+ + [171-174]

In general, the results from PCR experiments and the findings in literature are in accordance. However, the result form the EGFR-screening for F98 cells is controversially discussed in literature, although the majority of publications agree with our findings that EGFR is not expressed.

4.3 Fluorescence spectroscopic uptake experiments for liposomal formulations

The incubation of NBD-fluorescence labeled liposomes with F98 and LN229 cells showed that their uptake is time- as well as concentration-dependent (fig. 4-8). Furthermore, the lipid composition of the liposomes plays a major role in the extent of their uptake.

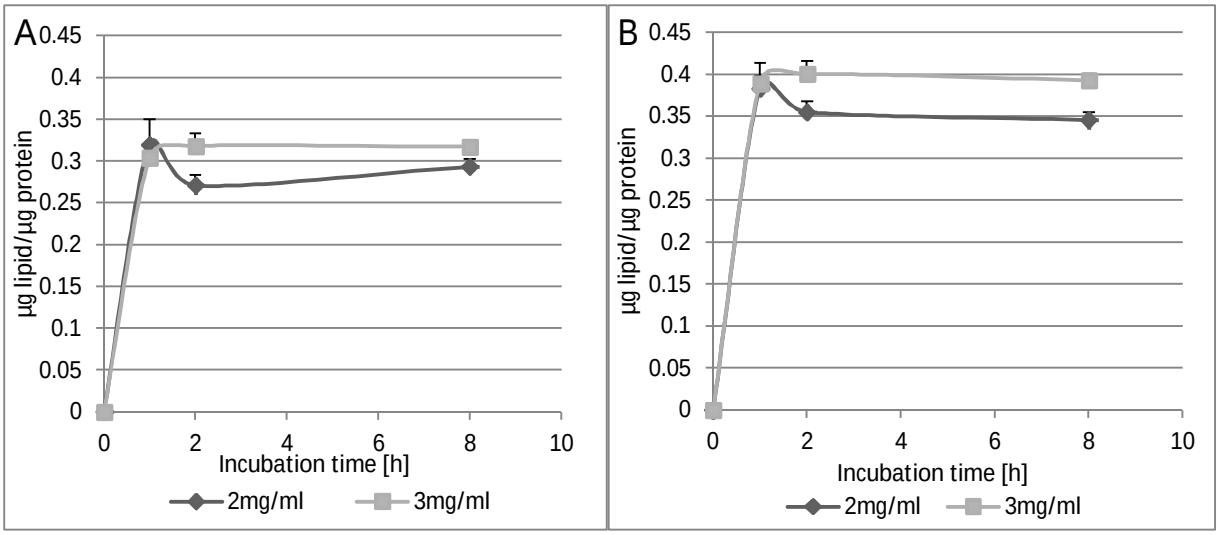

Figure 4-8 Uptake of FolS-DOPC-Chol (FolatePEG2000) liposomes into F98 cells (A) and LN229 cells (B).

As presented in fig. 4-8, folate-targeted liposomes were taken up to high account into F98 cells. Surprisingly, the uptake is nearly as high as into LN229 cells, although the latter were found to express the folate receptor alpha in contrast to F98 cells. The amount of liposome uptake should therefore be much higher in LN229 cells, given that the receptor is known to have a high affinity for folate. Thus, the uptake of folate-targeted liposome into FRα-positive cells, but not into the FR α negative species should be promoted markedly [175].

Of all non-targeted liposome formulations, DOTAP liposomes were taken up to the highest extent. Since these liposomes are charged positively and the cell membrane offers a high number of negatively charged groups, a high liposome cell interaction can occur and thus modulate the liposome uptake. Correspondingly, liposomes carrying negative charges, in addition to zwitterionic mixtures, were taken up to a smaller extent (cf. overview in table 9 and fig. 4-11). DOTAP-liposomes were taken up according to their charge-ratio. Less positive charges in the formulation lead to a lower uptake (fig. 4-9). Although the uptake is qualitatively similar for F98 and LN229 cells, the quantity of lipid taken up is slightly different, accounting for differences in uptake activity or mechanisms in cell lines. Interestingly, the amount of incorporated DOTAP 9% liposomes clearly reaches a maximum after 3 hours, decreases afterwards for the next 2 hours of incubation and increases again, before it settles on a lower level after

24 hours. Other formulations also show this behavior in some cases, although to a lesser extent (cf. fig. 4-10 B)).

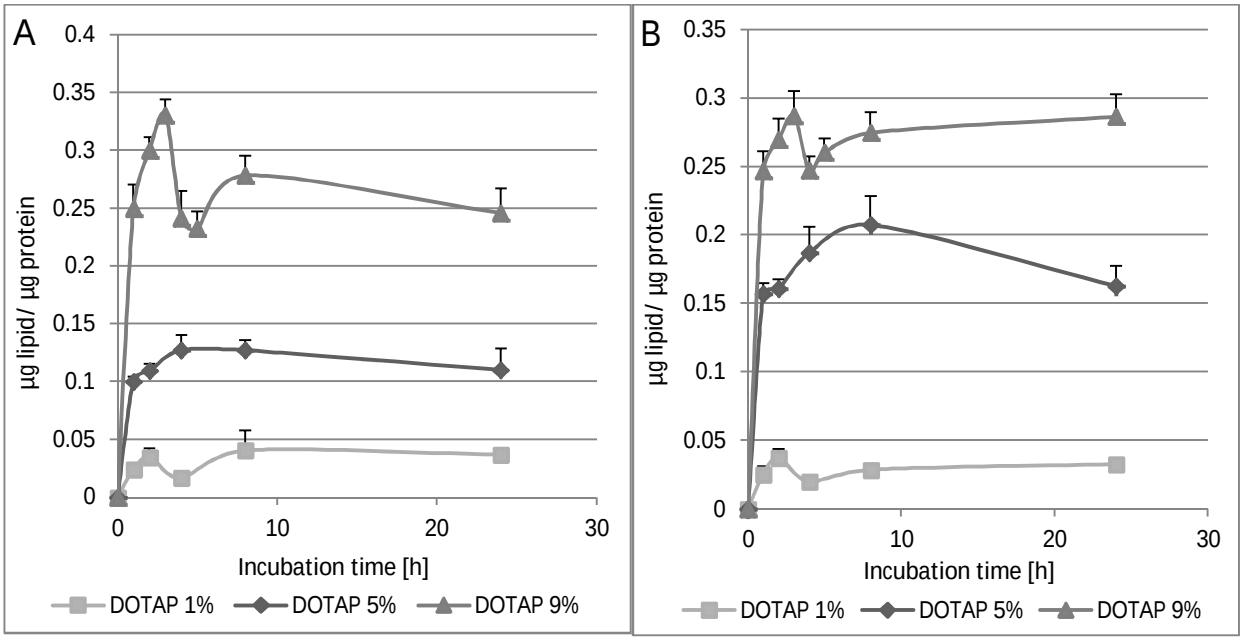

Figure 4-9 Uptake of DOTAP liposomes into glioma cells. A) Uptake into F98 cells, B) Uptake into LN229 cells.

DOTAP 1%: DOPC-Chol-DOTAP liposomes, including 1% (mol/mol) DOTAP; DOTAP 5%: DOPC-Chol-DOTAP liposomes, including 5% (mol/mol) DOTAP; DOTAP 9%: DOPC-Chol-DOTAP liposomes, including 8.5 % (mol/mol) DOTAP.

The incorporation of PEG 2000 into lipid mixtures had a dramatic effect on cellular uptake. As shown in fig. 4-10, inclusion of 1-5% PEG leads to significantly lower uptake of DOTAP-liposomes into LN229 cells. The same phenomena could be observed for the uptake of FolatePEG 2000 (fig. 4-10, B)), Cardiolipin and DOPE-liposomes into LN229 cells after only 1% PEG2000 was added to the mixture. This 'shielding effect' is also visible in the zeta potential values for the respective formulations (table 6). For DOTAP-formulations, the incorporation of PEG2000 leads to a decrease in their zeta potential, the highest fraction of PEG2000 gives the lowest zeta potential and vice versa. There is much less influence on DOPE- and Folate2000-liposomes, although the uptake into glioma cells is distinctly lower for the PEG-bearing formulations. The effect of PEG-incorporation is more pronounced for LN229 than for F98 cells. Here, the uptake of the Folate- and the CL-mixture with PEG2000 after 24 h incubation even increases slightly in comparison to the unshielded composition. Nevertheless, since uptake does not seem to be linear, but reaches a maximum, this may be due to the individual uptake modality of the liposomes. Table 6 gives an overview of the tested formulations and their uptake into both cell lines after 24h incubation. The most efficient liposome-compositions were chosen for neutron irradiation experiments, while some other formulations were still tested in preliminary experiments as well as in the earlier conducted synchrotron- and photon-irradiation experiments.

The zeta potentials of DOPE- and Folate2000-liposomes remain nearly unchanged after PEG-addition. On the other hand, the high negative potential of -60 mV for CL-liposomes is reduced to -44 mV for the CL-PEG-formulation. The size of all formulations is not altered by the addition of the shielding lipid. In some cases, the liposomes even decrease slightly in size after PEG was introduced.

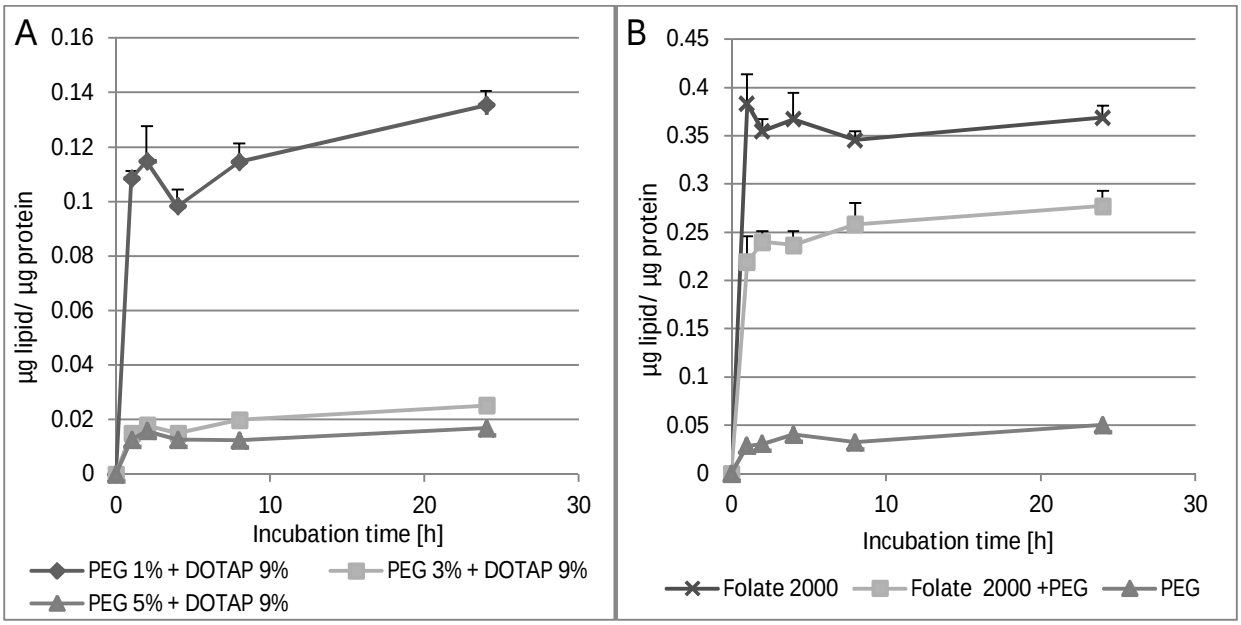

Figure 4-10 A) Uptake of DOTAP-liposomes bearing different fractions of PEG2000 into LN229 cells. B) Uptake of Folate2000– and PEG-containing-liposomes into LN229 cells. PEG 1%, 3% or 5% + DOTAP 9%: DOPC-Chol-DOTAP-PEG2000 liposomes containing 1%, 3% or 5% (mol/mol) PEG2000 and 9% DOTAP. Folate 2000+ PEG: FolS-DOPC-Chol--PEG2000 liposomes, Folate 2000: FolS-DOPC-Chol liposomes, PEG: DOPC-Chol-PEG2000 liposomes.

Table 8 Size and zeta potential values for main formulations before and after introduction of PEG2000-DSPE.

Formulation (including 0.5% (mol/mol) NBD-PE)	Size [d.nm] ± SD	Zeta Potential [mV] ± SD
DOPC-Chol-DOTAP-PEG 5%	134.37 ± 1.17	21.70 ± 0.69
DOPC-Chol-DOTAP-PEG 3%	129.67 ± 1.08	28.70 ± 0.75
DOPC-Chol-DOTAP-PEG 1%	135.53 ± 0.35	38.43 ± 0.76
DOPC-Chol-DOTAP	137.42 ± 2.70	49.51 ± 4.59
DOPC-Chol-CL	135.03 ± 0.86	-60.17 ± 1.39
DOPC-Chol-CL-PEG2000	132.87 ± 0.81	-44.40 ± 0.79
DOPC-Chol-DOPE	159.18 ± 1.44	-23.82 ± 1.77
DOPC-Chol-DOPE-PEG2000	141.70 ± 0.17	-25.47 ± 1.04
FolS-DOPC-Chol (FolPEG2000)	144.20 ± 0.52	-22.83 ± 0.55
FolS-DOPC-Chol-PEG2000 (FolPEG2000)	137.27 ± 0.91	-21.50 ± 0.44

Table 9 Overview of tested formulations and their respective uptake into F98 and LN229 cells after 24h incubation.

Formulation (including 0.5% (mol/mol) NBD-PE)	Uptake into F98 cells [µg lipid/ µg protein]	Uptake into LN229 cells [µg lipid/ µg protein]
DOPC-Chol-DOTAP 9%	0.272 ± 0.03	0.337 ± 0.059
DOPC-Chol-DOTAP 5%	0.11 ± 0.019	0.162 ± 0.015
DOPC-Chol-DOTAP 1%	0.037 ± 0.003	0.033 ± 0.003
DOPC-Chol-DOTAP-PEG 5%	0.011 ± 0.001	0.017 ± 0.001
DOPC-Chol-DOTAP-PEG 3%	0.019 ± 0.001	0.025 ± 0.001
DOPC-Chol-DOTAP-PEG 1%	0.118 ± 0.009	0.135 ± 0.005
DOPC-Chol-CL 4.5%	0.02 ± 0.002	0.043 ± 0.005
DOPC-Chol-CL-PEG2000 (4.5%)	0.032 ± 0.001	0.038 ± 0.004
DOPC-Chol-CL 10%	0.037 ± 0.004	0.041 ± 0.003
DOPC-Chol-DOPE 8.7%	0.032 ± 0.002	0.041 ± 0.005
DOPC-Chol-DOPE-PEG2000 (8.7%)	0.022 ± 0.000	0.028 ± 0.0013
DOPC-Chol-DOPE 10%	0.208 ± 0.056	0.201 ± 0.052
FolS-DOPC-Chol (FolPEG2000)	0.3 ± 0.006	0.309 ± 0.055
FolS-DOPC-Chol-PEG2000 (FolPEG2000)	0.307 ± 0.008	0.278 ± 0.016
DOPC-DOPE (4mg/ml)	0.174 ± 0.046	0.279 ± 0.026
DOPC-Chol-PEG2000 1%	0.052 ± 0.003	0.05 ± 0.004

Figure 4-11 presents an overview of liposome uptake after 4 and 24 hours for formulations which were chosen for further experiments. The uptake was highest for Folate20000-, DOTAP- and DOPC-DOPE-liposomes. Although the PEPC liposomes were only tested in a concentration of 4mg/ml, their uptake was deemed high enough to justify further tests. All other formulations were tested in a concentration of 2mg/ml.

Cardiolipin liposomes were included in follow-up tests because of their negative charge. While the uptake was generally low in F98 and LN229 cells, the mixture provided a very high zeta potential and, at least for CF, a high EE (9%).

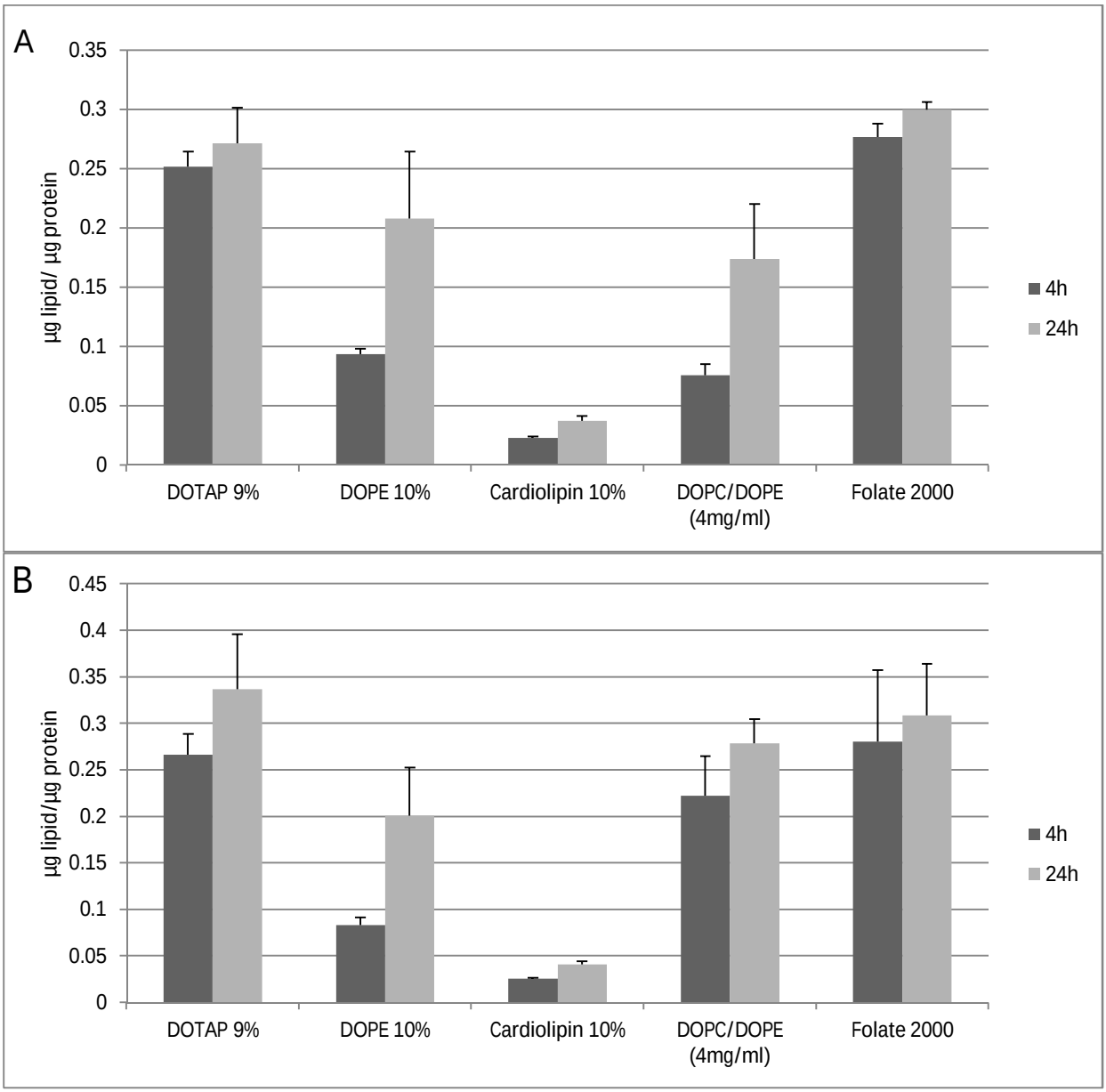

Figure 4-11 Overview over uptake of liposomal formulations after 4h and 24h. A) F98 cells B) LN229 cells. Except for DOPC/DOPE liposomes, all formulations were applied in a concentration of 2mg/ml.

4.3.1 Fluorescence microscopic uptake of liposomes

Fluorescence microscopic experiments were performed to examine liposome attachment to and/or uptake into F98 and LN229 cells. The uptake of Gd into the cell is a crucial point in the radioenhancer and NCE-therapy, since the element has to be close to the cellular DNA to induce lethal damage to the cell in the course of irradiation.

In this case, the microscopic technique is limited to the labeling of the liposomal shell with the green fluorescent NBD-PE, while the NC-element Gd-DTPA in the core remains invisible due to the lack of

appropriate labeling methods. Nevertheless, the images provide a first idea of the suitability of the liposomal carrier in a radiation therapy.

Microscopic images of cellular liposome uptake show co-localization of green labeled DOPC-Chol-DOTAP-liposomes with the cell body. Apparently, the liposomes attach preferably to the point where two cell membranes meet, or at the juncture of dividing membranes during mitosis (fig. 4-12). However, the confocal images (slides of different levels in the cell depth) reveal the spatial orientation of liposomes in the cell, which seems to be inside the cytosol as well as on the outer membrane (fig. 4-13 and 4-14). Since the red color from the cell membrane staining was overly present in the cells, the green liposome label was not very distinguishable in the pictures and therefore, the exact position of the liposomes in the cellular body could not be clarified. Nonetheless, at least the cell attachment was confirmed and the uptake seen as very likely. Additionally, it has to be noted that the incubation time was only 1 hour instead of the 3h incubation which was chosen later in the neutron irradiation experiment. Since the Gd-DTPA as content of the liposomes could not be seen at the images, the fate of the liposomes, possible disrupture or inclusion into endosomal compartments, was not determined.

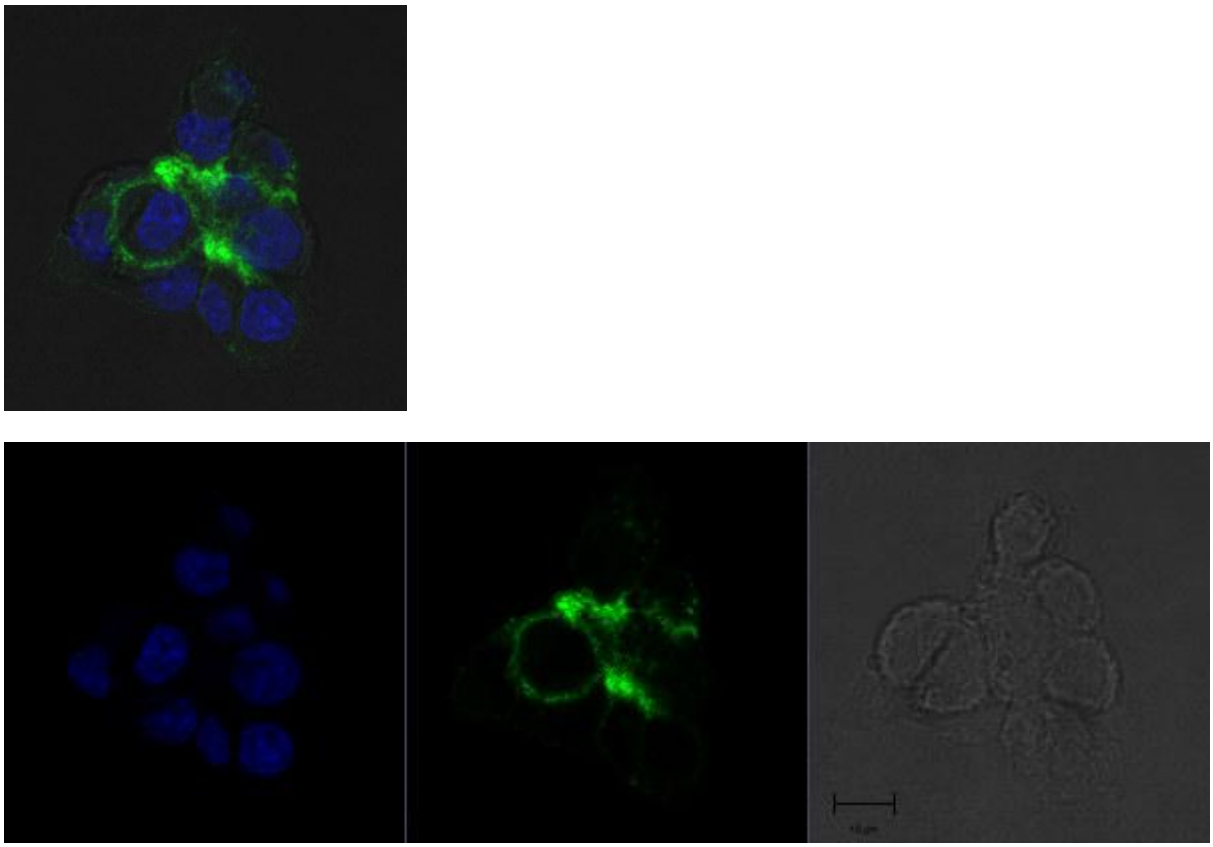

Figure 4-12 Fluorescence images of F98 cells: merged channels, single channels, series cut through different levels. Blue: nucleus (DAPI), green: DOPC-Chol-DOTAP liposomes (NBD-PE). Scale bar represents 10 µm (last plane of images).

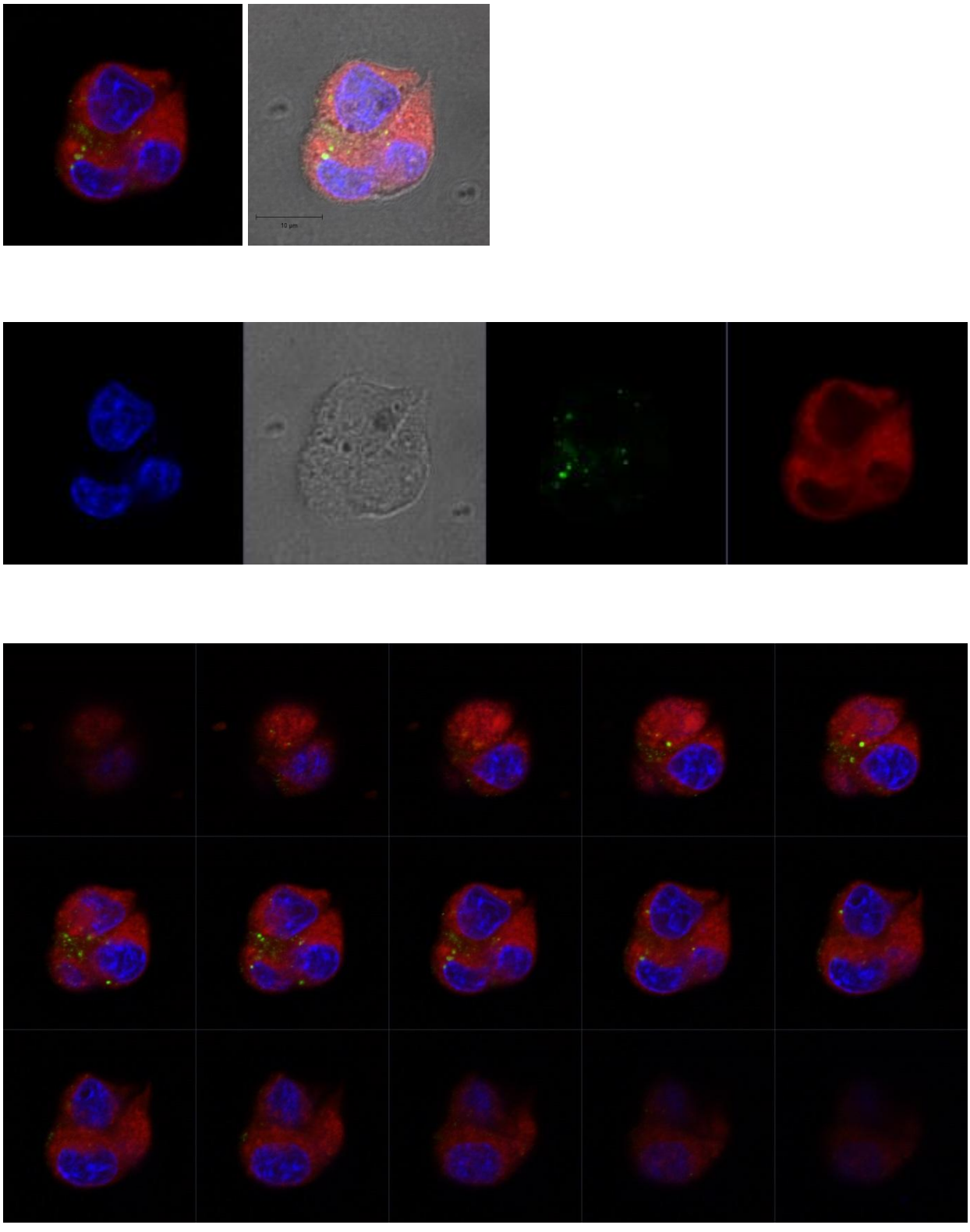

Figure 4-13 Fluorescence images of F98 cells: merged channels, single channels, series cut through different levels. Blue: nucleus (DAPI), red: cytosol/cell membrane (Cell Mask Deep Red), green: DOPC-Chol-DOTAP liposomes (NBD-PE). Scale bar in second image (first plane) represents 10 µm.

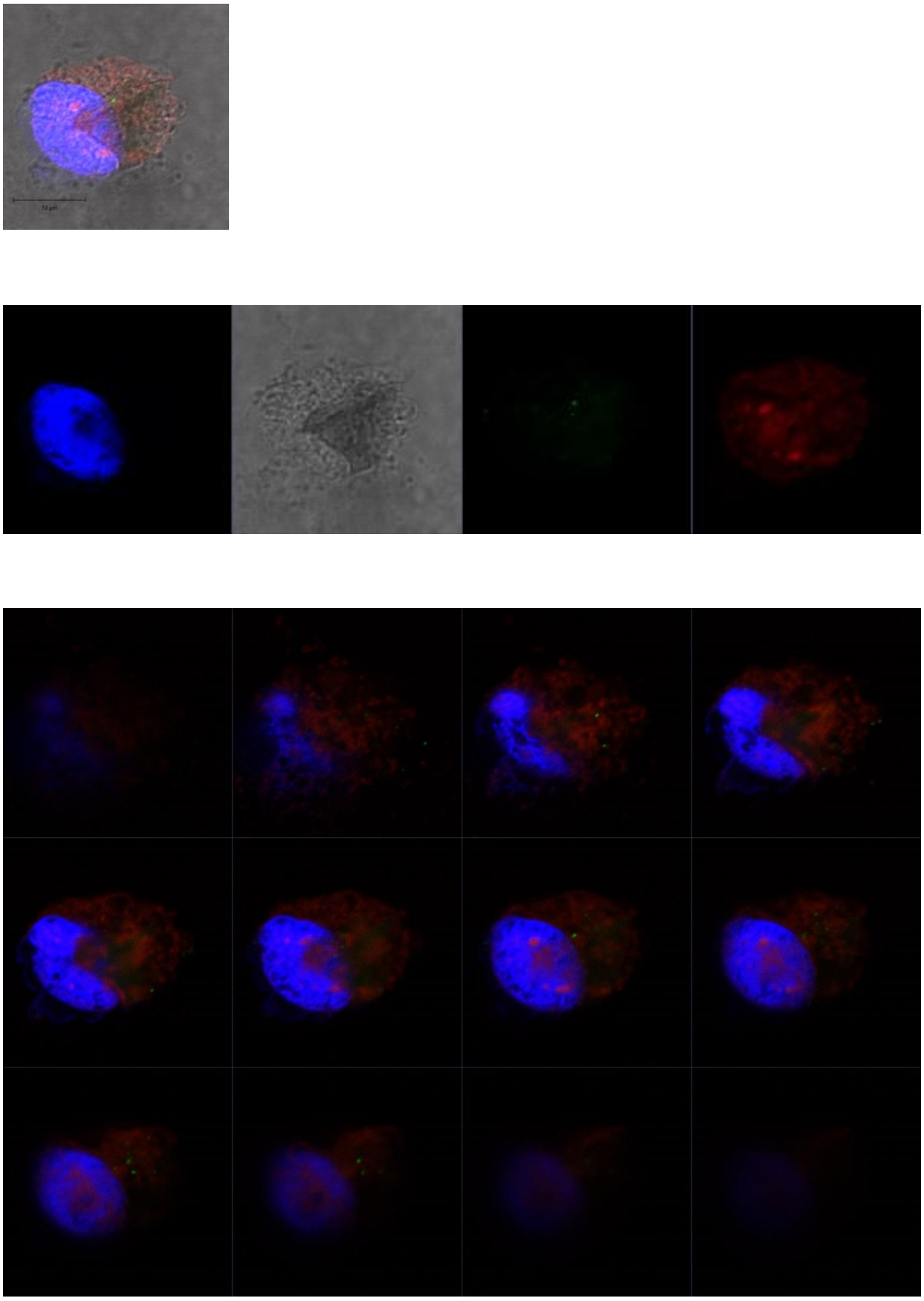

Figure 4-14 Fluorescent images of LN229 cell: merged channels, single channels, series cut through different levels. Blue: nucleus (DAPI), red: cytosol/cell membrane (Cell Mask Deep Red), green: DOPC-Chol-DOTAP liposomes (NBD-PE). Scale bar in first image (first plane) represents 10 µm.

4.4 Uptake of Gd-DTPA into F98 and LN229 cells

For the neutron irradiation experiments, five main lipid mixtures were used as liposomal carriers of Gd-DTPA. The liposomal formulations and their respective EE for Gd, as measured via ICP-MS are listed in table 10.

Table 10 Overview of liposomal formulations and their respective EE for Gd.

Liposome formulation	Encapsulation efficiency [%]	Gd-content [mg/ml]
FolS-DOPC-Chol 0.13:63:37	9.6 ± 1.75	4.48 ± 0.69
DOPC-Chol-Cl 70:20:10	6.56 ± 1.74	3.33 ± 0.42
DOPC-Chol-DOPE 70:20:10	9.37 ± 2.83	4.54 ± 1.02
DOPC-DOPE 50:50	10.21 ± 2.53	5.76 ± 1.59
DOPC-Chol-DOTAP 57:33:9	10.24 ± 4.85	5.91 ± 1.74

Gadolinium from non-encapsulated Magnevist solution was taken up by cells in a time- and concentration-dependent manner. Both cell lines accumulated Gd-DTPA (concentration: 340 µg/ml cell medium) over 24 hours linear proportional to incubation time and without signs of saturation (fig. 4-15 A). For F98 cells, the incubation time was expanded to 48 hours and different concentrations of Magnevist were tested. Figure 4-14 B shows the concentration-dependent uptake of Gd-DTPA into F98 cells for 24 and 48 hours incubation time. While for the 24 hour incubation the Gd-content in cells advances nearly in a linear proportion to the medium concentration of Gd-DTPA, the 48 hour incubation seems to approach saturation near a concentration of 902 µg Gd /ml medium.

Liposomal Gd-DTPA formulations (DOTAP- and DOPE-DOPC-liposomes) also show a time- and concentration- dependency of their uptake. DOTAP-liposomes delivered significantly more Gd-DTPA into cells than PEPC liposomes or free Magnevist solution. While the latter formulations carried 137 and 89 ng Gd/ 10^6 cells into F98 cells after 24 hours incubation, DOTAP-liposomes transported a multiple of this Gd-quantity (740 ng). It is noteworthy that the amount of Gd-DTPA in F98 and LN229 cells after incubation with DOTAP-liposomes does not increase linearly with the incubation time. After 3-4 hours, the Gd-DTPA content reaches a maximum and then settles to a lower level (fig. 4-16). This has also been noted for DOTAP-liposomes in the fluorescence uptake experiments. Furthermore, the concentration-dependent uptake of DOTAP-liposomes over 24 hours also did not follow linearity. In contrast, the uptake of DOPC-DOPE-liposomes over time and their different concentrations could be described as linear proportional in both cases (cf. fig 4-16 and 4-17).

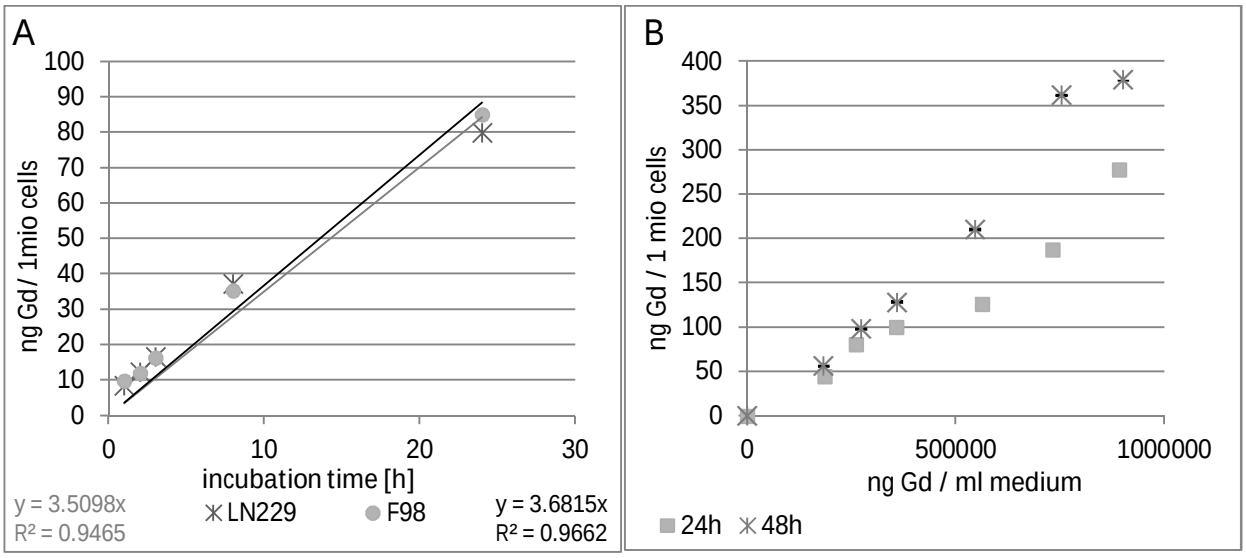

Figure 4-15 A) Uptake of Gd-DTPA (free Magnevist solution, 340µg Gd/ml cell medium) into F98 (●) and LN229 cells (✳), B) Gd-DTPA uptake (free Magnesvist solution) into F98 cells, incubation time: 24 hours (■), 48 hours (✳).

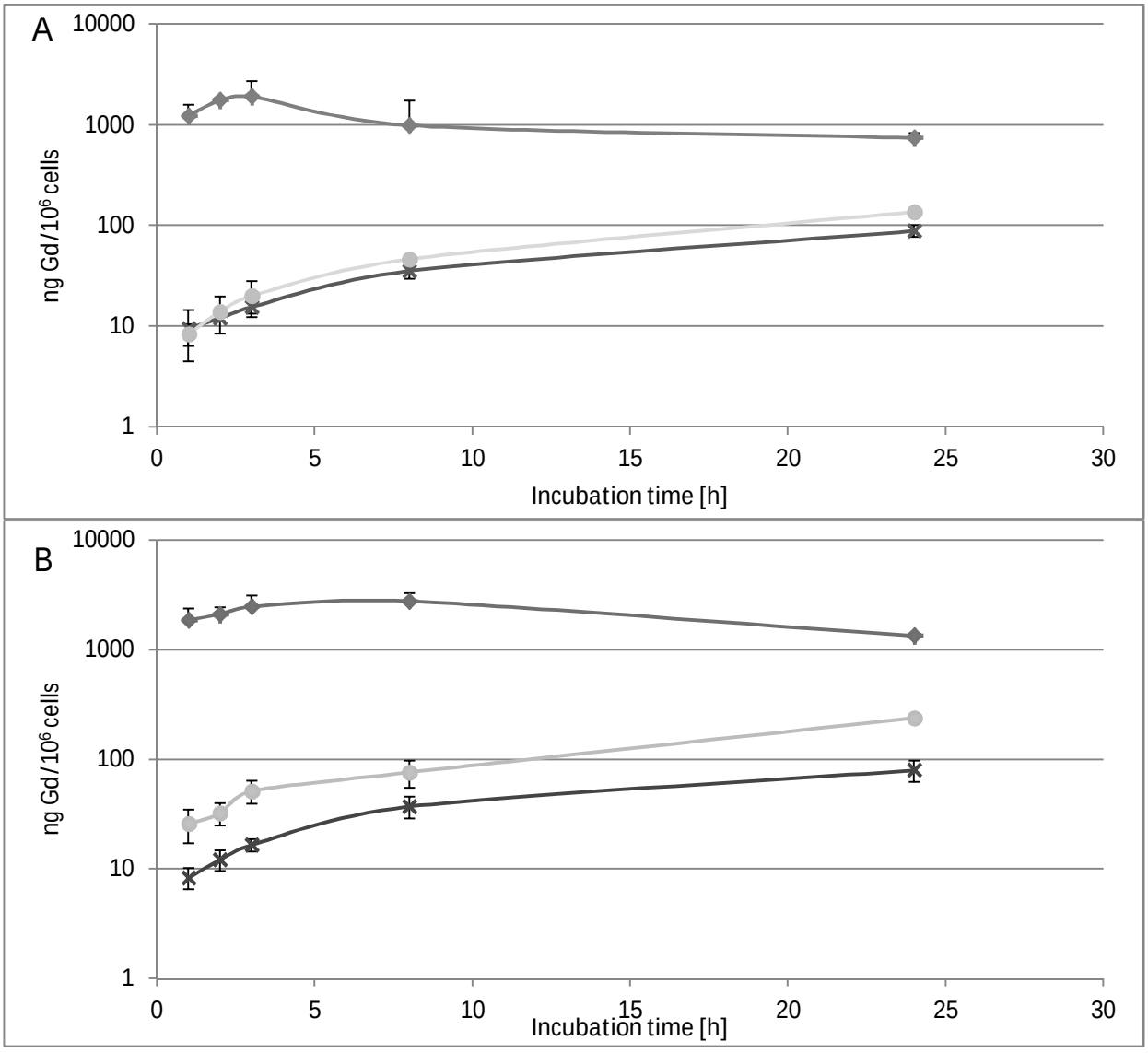

Figure 4-16 Gd-DTPA uptake into F98 and LN229 cells. A) F98 cells. B) LN229 cells. DOTAP-liposomes(◆), free Magnevist solution (x), DOPC-DOPE-liposomes (●).

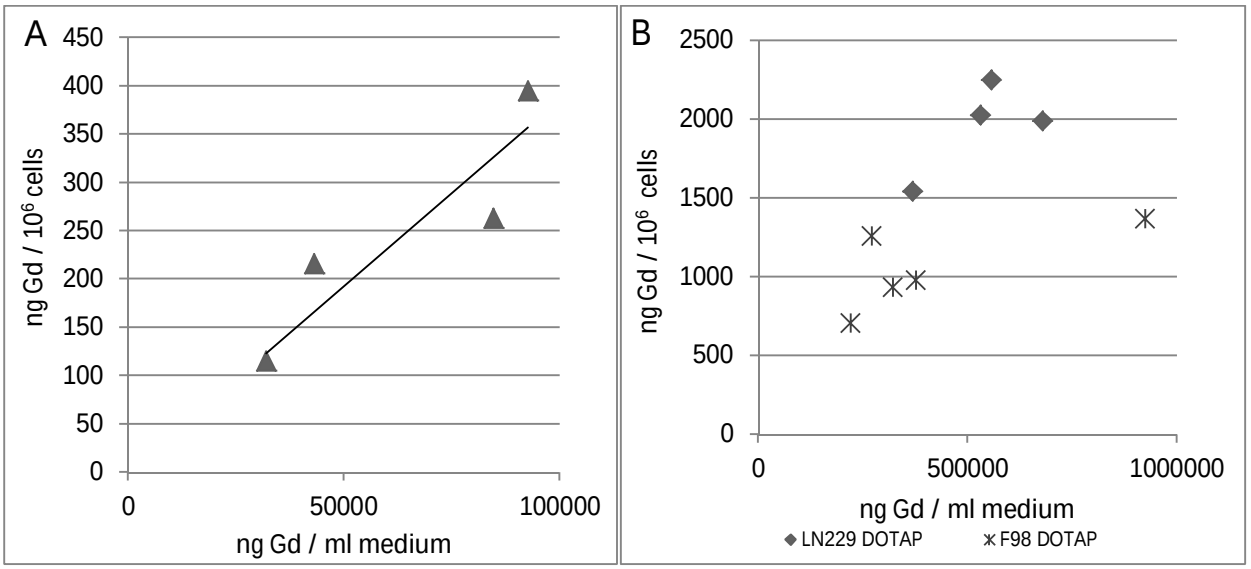

Figure 4-17 A) Concentration-dependent uptake of DOPC-DOPE-liposomes into F98 cells (incubation time: 24 h). B) Concentration-dependent uptake of DOTAP-liposomes (24 hour incubation) into F98 (✳) and LN229 cells (◆).

The uptake of Gd-DTPA into glioma cells was also studied for three other formulations: Cardiolipin-, Folate2000PEG- and DOPE-liposomes. The Gd-content in the glioma cells after 3 hour incubation with the respective formulations is shown in figure 4-18 (Fol = folate2000PEG-, CL = cardiolipin-, DOPE = DOPE-, DOTAP = DOTAP-containing liposomes). All liposomal formulations performed superior to free Magnevist solution, indicating the benefit of a liposomal carrier for Gd-DTPA.

As mentioned before, the DOTAP-liposomes carried by far the highest Gd-amount into both cell lines and results in highly significant differences to all other formulations ($P < 0.001$). For F98 cells, the DOPE liposomes performed better than the other mixtures, but Folate also achieved high uptake of Gd: DOPE > Folate > CL > DOPC-DOPE. The Gd-content delivered by liposomes for LN229 cells decreases in the following order: Folate > CL > DOPE > DOPC-DOPE. However, the differences between these formulations are not significant. Surprisingly, CL-liposomes performed for both cell lines better than DOPC-DOPE liposomes, which was not expected after low uptake results in fluorimetric experiments.

Altogether, results from fluorimetric uptake were not in agreement with ICP-MS measurements. Of course, the DOPE-formulation was applied in higher concentration in fluorimetric experiments; therefore, the uptake might be out of proportion. More than that, the time point of the read-out is different in both experiments, since the uptake of Gd was measured after 3h. In the earlier fluorimetric measurements, the uptake was only measured after 4h, and the graph shows in most cases a maximum of uptake after 2-4h and a decline after this time point.

Interestingly, the EE of the formulations and therefore, the Gd-content per ml do not seem to have an effect of the Gd-amount accumulated in cells. Although the cationic DOTAP-formulation has the highest EE and delivers the highest amount of Gd into both cell lines, the other formulations do not follow this order (with EE decreasing as follows: DOTAP > DOPC-DOPE > Folate > DOPE > CL). This may be due to the differences in the EE being small in comparison to the final amount of Gd taken up into the cells.

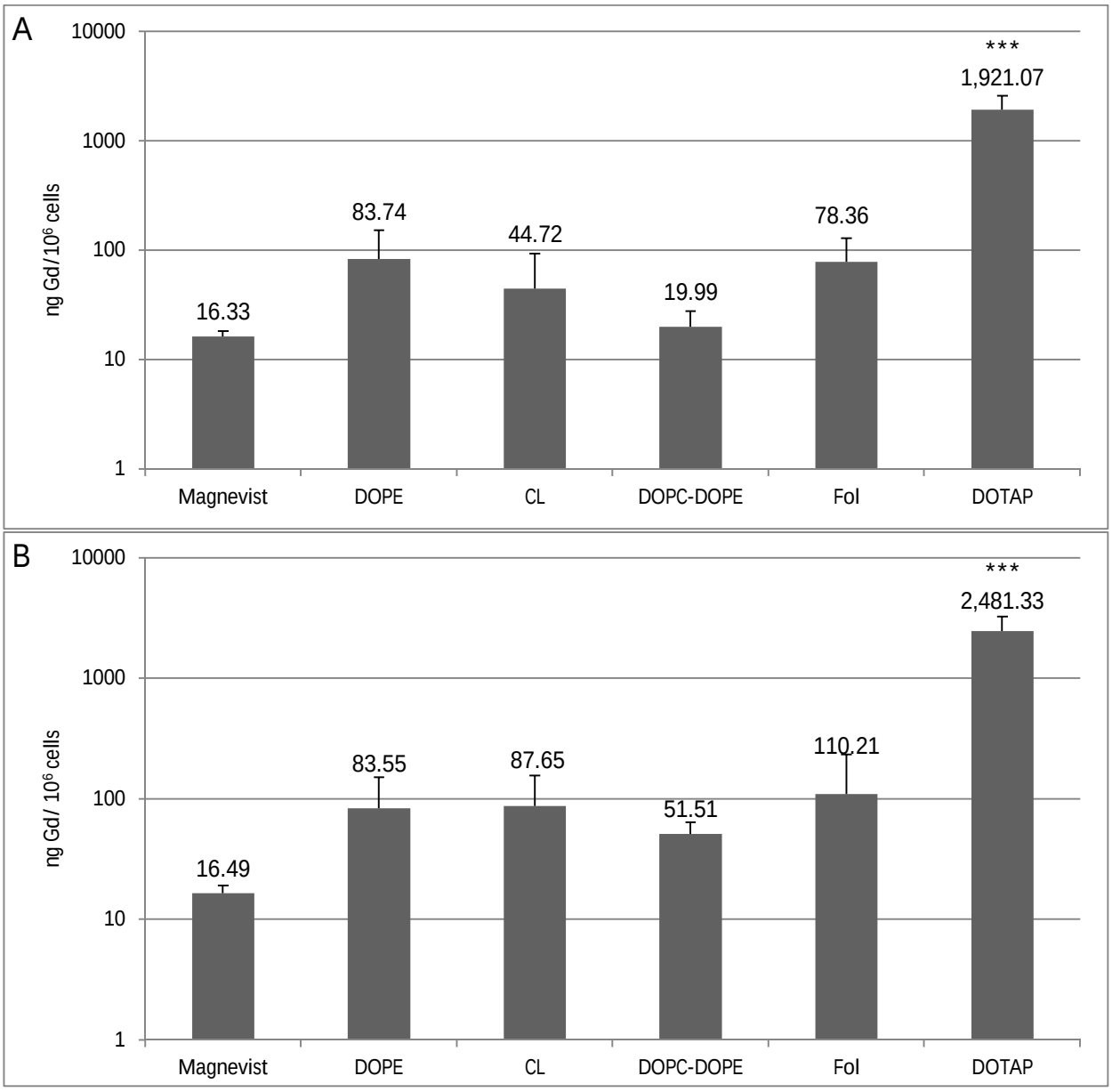

Figure 4-18 Overview over Gd-content after 3h incubation with respective formulations. A) F98 cells, B) LN229 cells. $P < 0.001$ = (***).

4.5 MTT assay

4.5.1 Correlation of cell number and optical density

The correlation between MTT absorption and cell number was examined for both cell lines. For LN229, the proportion is linear for the examined range (R^2=0.9596), as shown in figure 4-19. F98 cells also showed a linear dependence of OD to cell number over a wide range, although the graph seems to follow a more logarithmic curve for higher cell densities and OD > 0.6. Nevertheless, the fit for a linear trend line is still satisfactory (R^2= 0.8575).

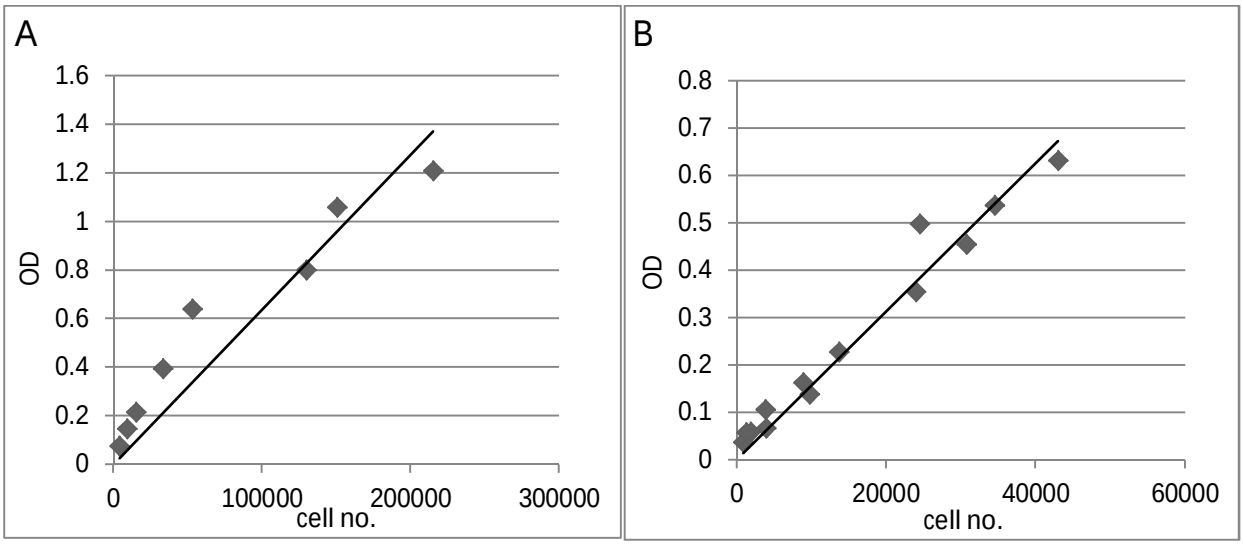

Figure 4-19 Correlation of cell number with optical density (MTT absorption). A) F98 cells, B) LN229 cells.

4.5.2 Comparison of MTT assays and colony forming assay

Our study for the comparison of MTT multiple assay and colony forming assay found that the multiple MTT assay can present an alternative to the more extensive colony assay for the interpretation of cell survival after x-ray irradiation(cf. [141]). However, data analysis could be simplified further by using only two or three of the assigned six time points of the multiple MTT assay. Figure 4-20 shows the survival rates of F98 cells after irradiation for the multiple points assay (proliferative survival) and for two chosen single time points in comparison to the CFA (survival). The irradiation was done after cells were already plated. The multiple MTT assay generates a similar curve to the MTT single time points late in the experiment. As shown in fig. 4-21, the corresponding correlation data of all three assay variants with the CFA produce similar results for the linear regression. Here, the goodness of fit (R^2) is even better for the single point MTT assays than for the multiple MTT assay.

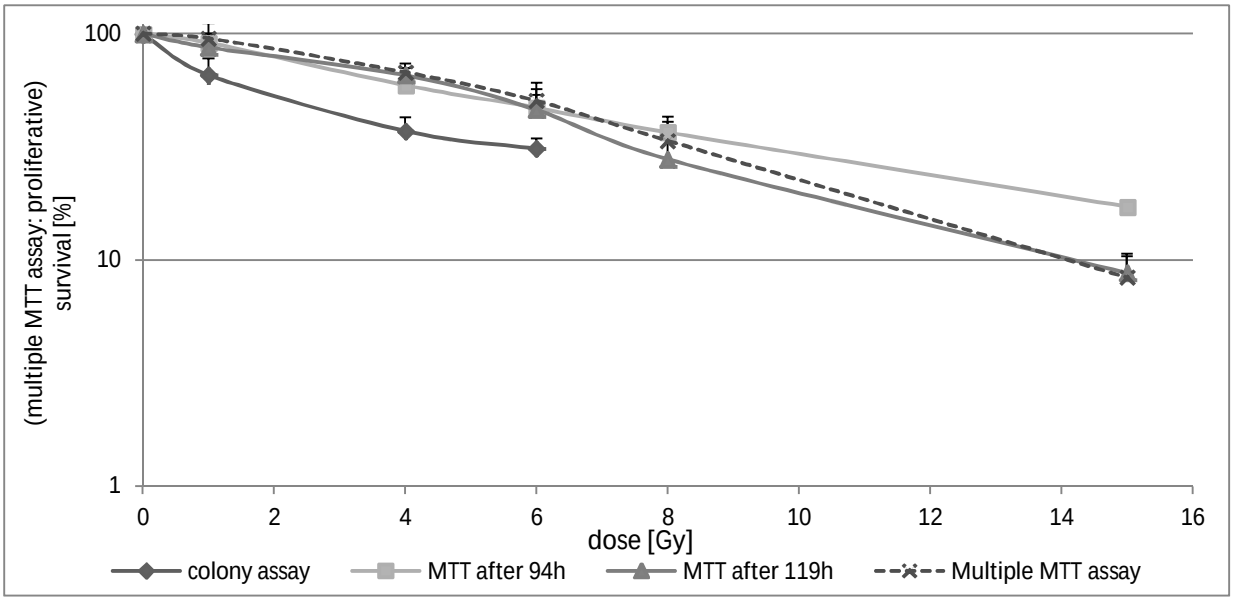

Figure 4-20 Survival curves for F98 cells after X-ray irradiation (plating before irradiation), generated from colony forming assay (◆), single point MTT assays after 94h (plating time) (■) and 119h (▲), and multiple point MTT assay(∗).

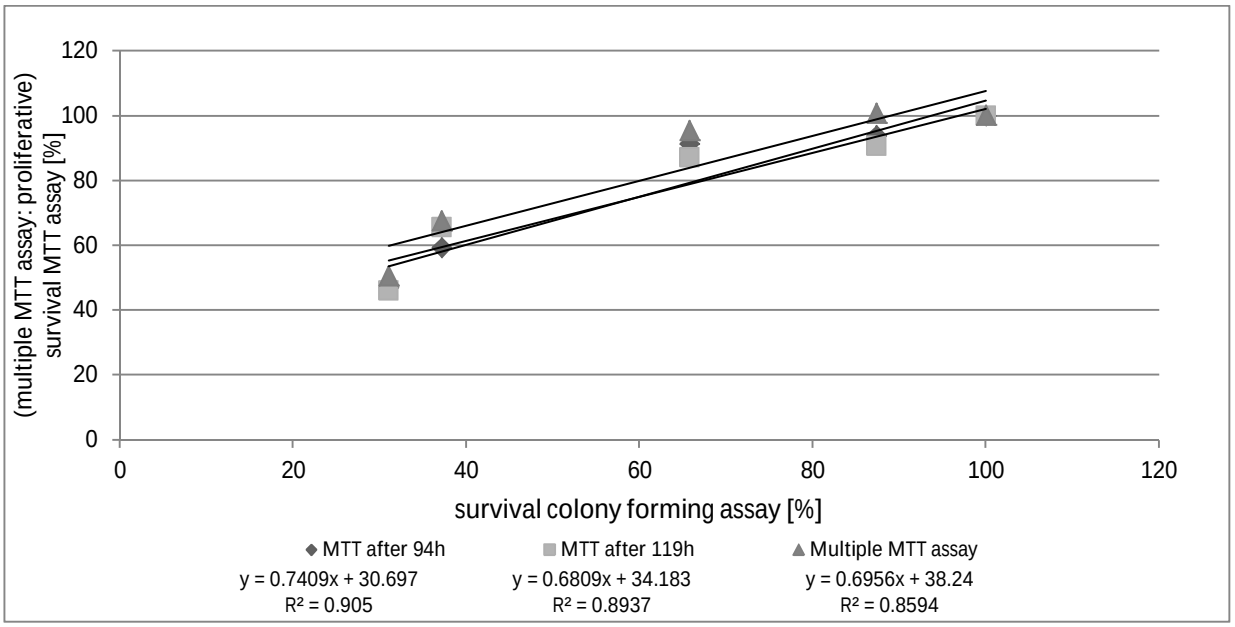

Figure 4-21 Correlation of survival data of F98 cells from MTT single point assays 94h (■) and 119h (▲) after plating and multiple MTT assay to survival of cells generated from colony forming assay.

The same principle applies for the human cell line LN229. Figure 4-22 shows the survival curves after irradiation and the correlation of MTT survival data with CFA. The cells were also plated before the irradiation took place. Survival curves of single point MTT assays are in accordance to the survival curve of multiple MTT assay, except the latter assesses a survival slightly too low for higher radiation doses. Correlation between the MTT assays and the CFA is, based on the coefficient of determination, inferior to the correlation calculated for F98 cells. Nevertheless, both single time point MTT assays (after 145 and 166 h) yield nearly the same R^2 as the multiple assay for the correlation between MTT and CFA (R^2= 0.7963 and R^2= 0.7765 in comparison to R^2= 0.7863 for the multiple assay, respectively).

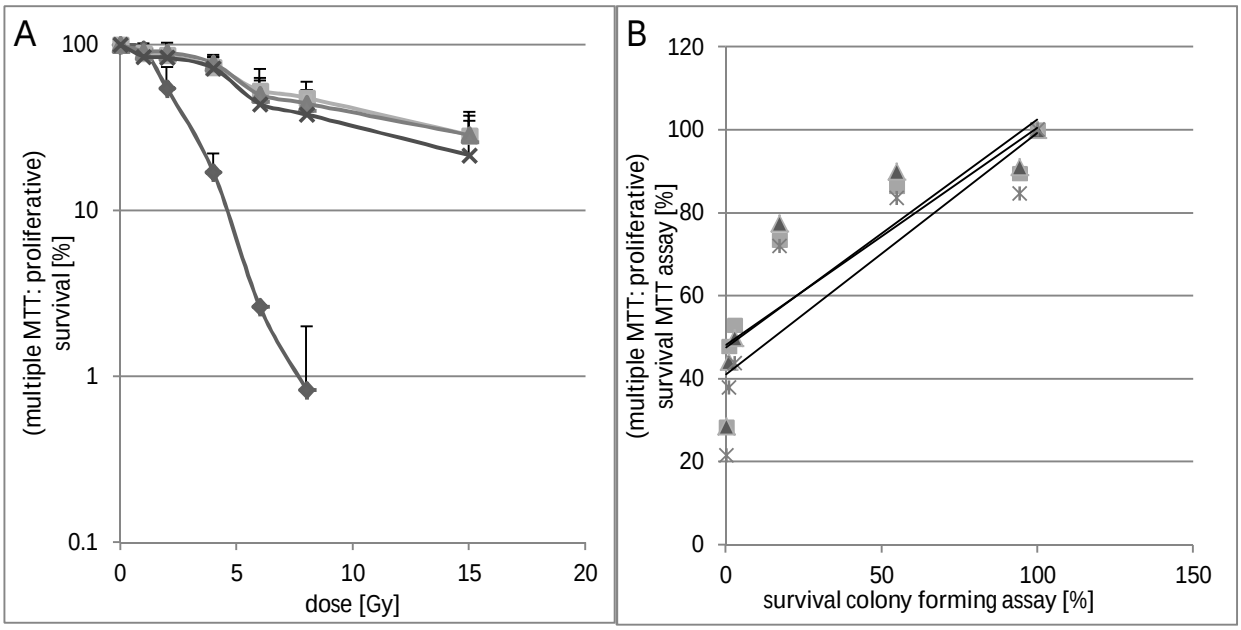

Figure 4-22 A) Survival curves for LN229 cells irradiated with x-rays. B) Correlation of MTT assays to colony forming assay for LN229 cells. Colony forming assay (◆), single point MTT assays after 145h (plating time) (■) and 166h (▲), and multiple point MTT assay(✱).

For the comparison of MTT assays and CFA with plating of cells done after irradiation, the outcome is qualitatively the same as for plating before irradiation. The experiment was conducted only with LN229 cells, which showed good linear correlation between multiple MTT assay and CFA (R^2=0.9557). Additionally, the single point MTT assays (i.e. MTT 97h, 116h and 140h after seeding) show also a very good correlation to the CFA (R^2=0.9801; 0.9708 and 0.9675, respectively). As shown in figure 4-23 A, all the survival curves generated from MTT assays are similar in form, though the multiple assay again tends to overestimate the irradiation effect on the cell survival for higher doses in comparison to the single time point MTT assays.

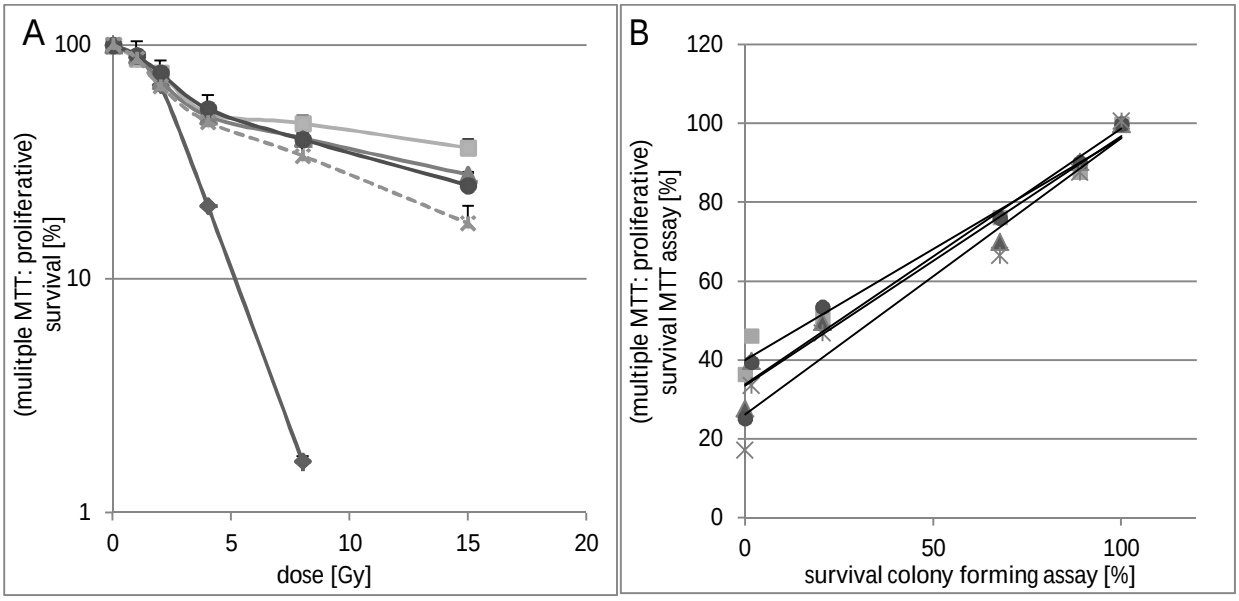

Figure 4-23. A) Survival curves for LN229 cells irradiated with x-rays, where cell plating was done after irradiation. B) Correlation of MTT assays to colony forming assay for LN229 cells Colony forming assay (◆), single point MTT assays after 97h (plating time) (■), 116h (▲), 140h (●)and multiple point MTT assay(∗).

4.5.3 Single point MTT assay and multiple MTT assay

The single point MTT assay was done as a series of MTT tests at defined time points, whereas for the multiple MTT assay the previously acquired data was converted with non-linear regression to gain information on doubling time and growth rates of the cells. The growth curves of cells after irradiation and treatment with radioenhancer or NC-elements were fitted through the equation of exponential growth, assuming the idealized case in which cell cultures were still undergoing the cycle of lag-phase, log-phase and plateau similar to untreated cell cultures. Figure 4-24 presents growth curves and the according best-fit curves of untreated cells in different seeding densities (2500 and 4000 cells). The goodness of fit based on R^2 was in all cases very good (R^2= 0.975 and 0.972 for the different seeding densities of F98 cells, and R^2= 0.958 and 0.954 for LN229 cells, respectively). Doubling times varied slightly between the cell densities, with higher densities requiring more time to reduplicate. F98 cells needed 25 to 29 hours, a value corresponding well to previous findings of Ko et al. [176] (26h). LN229 cells reduplicated in 44 to 47 hours, also depending on seeding density. For irradiation experiments, a seeding density of 4000 cells/ well was finally chosen, given that preliminary experiments exhibited very high variation in standard deviations for the lower seeding density of 2500 cells.

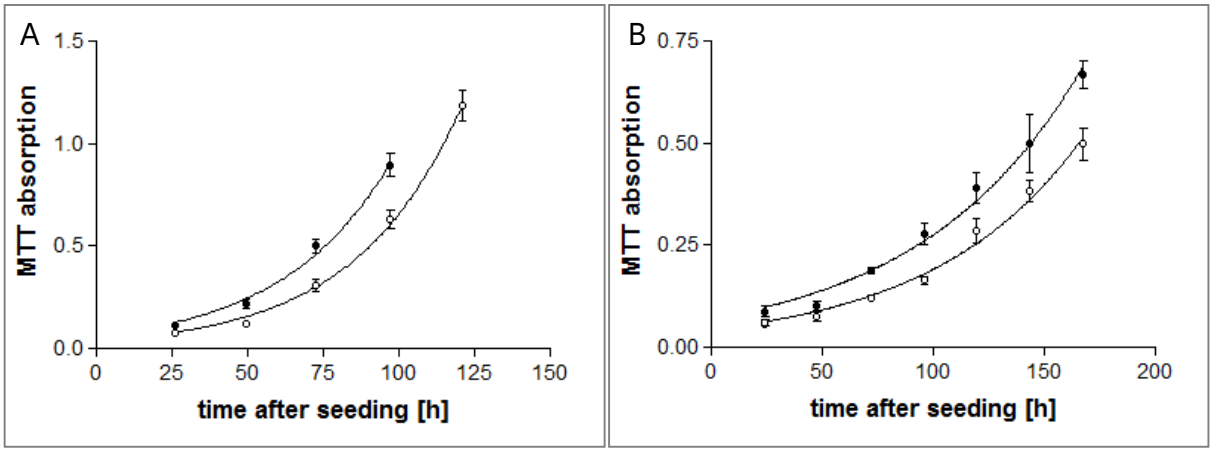

Figure 4-24 Growth curves for F98 (A) and LN229 cells (B). Open circles present seeding density of 2500 cells/well (96well plate), closed circles stand for 4000 cells/well.

In some cases, the exponential curve fit for growth curves after irradiation was not satisfying in regard to correlation coefficient and outcome of doubling times. Here, the analysis produced negative doubling times for certain formulations, which were not usable for further interpretation. Therefore, it was necessary to dispense with the multiple MTT assay and rely again on several single point MTT tests. Instead of the calculation for delay and survival for the multiple assay, the single point MTT tests were simply transformed to percent survival of the (non-)irradiated control. This operation needs less data modification and consequently seems to be more reliable, when the exponential growth does not fit the growth curves exactly. Figure 4-25 shows an preliminary experiment with boron as NC-agent in which two out of three curves did not follow exponential growth after irradiation (R^2 and doubling time (DT) are given in the legend). The experiment outcome in regard to the efficiency of the boron NCT approach will be discussed in section 4.6.2.5.

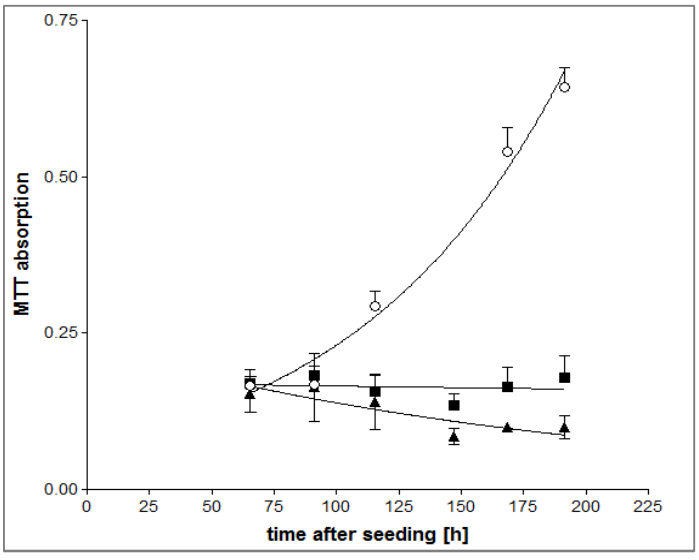

Figure 4-25 Curve fits for neutron-irradiated F98 cells ($8.28 \cdot 10^{12}$ n/cm²). Applied formulations: tris-borate 1 mM (❍) (R^2= 0.9645, DT= 59.44h), bisglyceroborate DOPC-liposomes (■)(R^2=0.0067, DT= -2128h), bisglyceroborate CL-Chol-DOPC-liposomes (▲) (R^2=0.4116, DT= -135.6h).

Figure 4-26 shows the same experiment interpreted by multiple MTT assay and three single point MTT tests. The percent survival was calculated based on the irradiated medium control for both analyses. Thus, only the effect of the formulation is presented in the survival data. The differences between the formulations are most pronounced for the multiple assay (A), though the original data from single point MTT does not suggest such strong differences (B). Additionally, the survival for cells treated with Tris-borate is significantly higher than the survival for the other two formulations in the multiple assay. In contrast, the single point assays prove this to be true only for one time point (MTT after 115 h). Overall, the survival data based on analysis of multiple MTT assay is much lower than the original data from single point assays. The outcome is distorted by the calculation process, thus leading easily to misinterpretation of the results.

It was therefore necessary to prove the applicability of the multiple assay for each experimental setup, including the critical inspection of the goodness of fit and the doubling time given from the exponential growth curve. Especially for higher doses, the growth curve does not follow necessarily the ideal exponential growth usually seen for proliferation curves (fig. 4-27). Since consequently for several parts of the subsequent irradiation experiments the curve fitting was poor, further investigations were mostly based on single point MTT, allowing for better comparison between the individual tests.

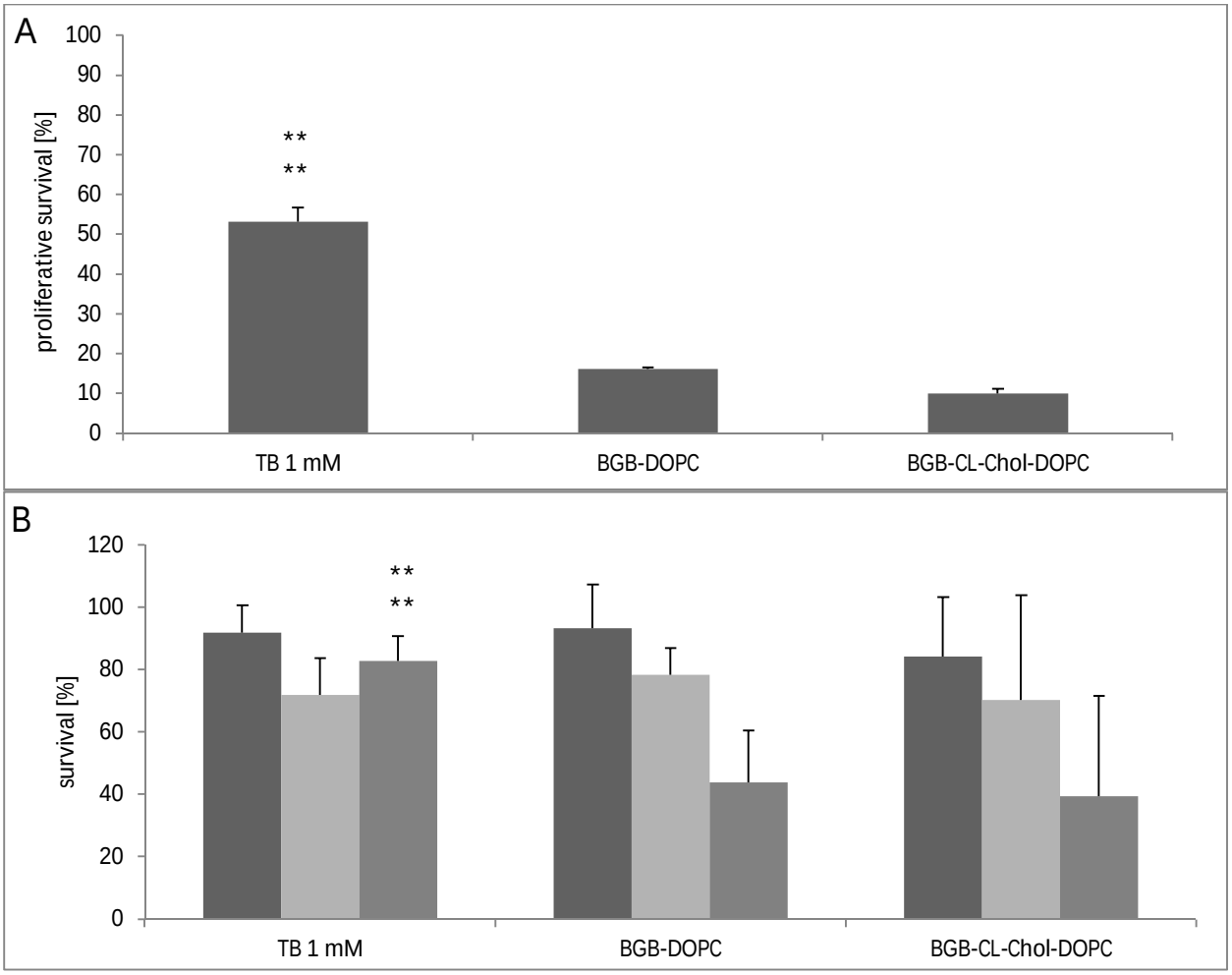

Figure 4-26 Results from MTT assays of neutron irradiated F98 cells ($8.28 \cdot 10^{12}$ n/cm²). A) Multiple MTT assay. B) Single point MTT analysis. Dark grey columns: MTT was done 65 hours after plating, light grey: 91 h, grey: 115h. Presented are arithmetic means and SD. ** results differ significantly from other formulations ($P < 0.001$).

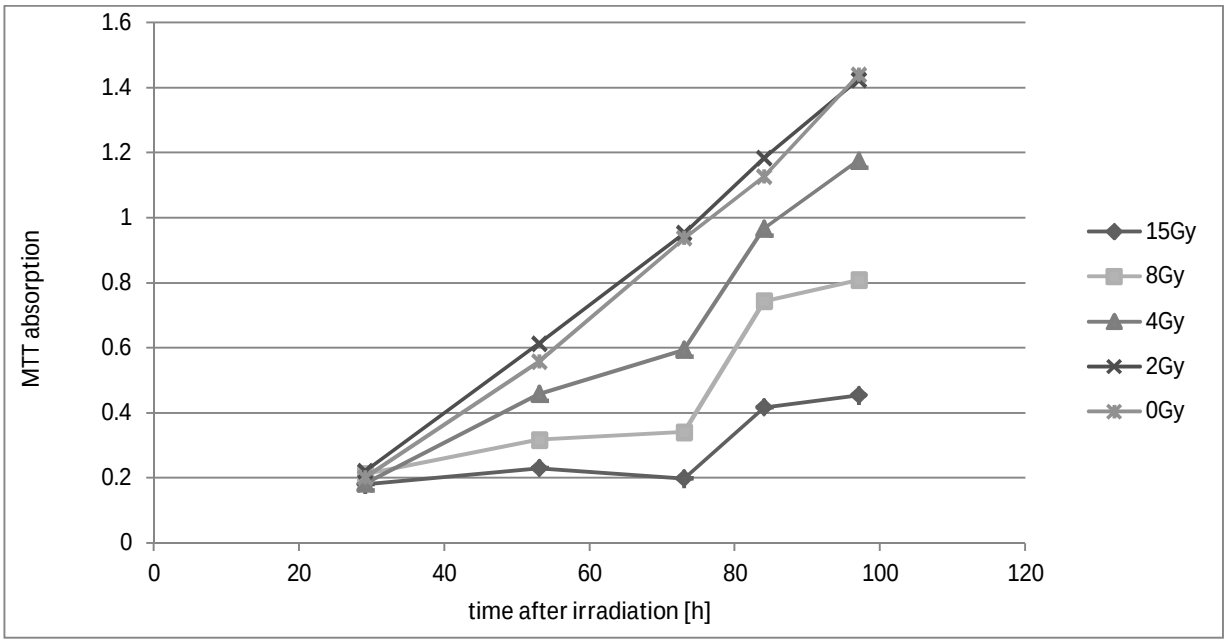

Figure 4-27 Proliferation curve of F98 cells, treated with different doses of synchrotron radiation (51.2 keV), seeding density 4000 cells/well, plated 1d before irradiation.

4.6 Radiation experiments

4.6.1 Photon irradiation experiments

4.6.1.1 Irradiation experiments using synchrotron radiation

Synchrotron experiments were conducted to gather information about the principle mechanism of radioenhancer application in radiation therapy. The influence of energy (wavelength) of the synchrotron radiation on cell survival treated with the radioenhancer Gd-DTPA has been investigated based on the K-absorption edge of Gd. Preliminary experiments were conducted with the lanthanide Lutetium, another potential radioenhancing high-Z element.

4.6.1.1.1 Preliminary experiments with Lu-DTPA as radioenhancer

Several different radiation set-ups were tested at ID 17, the medical beamline at the ESRF, France. To analyze the influence of build-up effect from secondary electrons on cell survival, an agar gel phantom was placed before or behind the cells for the radiation treatment or cells were irradiated without phantom material. Cells were incubated with Lu-DTPA- containing liposomes 1 h before irradiation. In addition, the effect of the wavelength on cell survival through induction of Auger-electrons from Lu-DTPA (absorption of photons at the K-edge of Lu) was investigated. Cells were therefore irradiated with energies above and below Lu-K-edge (above: 64.6 keV, below: 63.6 keV, K-edge was found at 64.35 keV, measured at ID 17). Applied formulations were ultrasound-manufactured pure DOPC-liposomes, entrapping 250 mM Lu-DTPA with an initial lipid concentration of 40 mg/ml. Final lipid concentration in wells was 0.4 mg/ml, non-entrapped material was removed via GPC for one part of the liposomes. Figure 4-28 shows the respective proliferative survival of irradiated F98 cells for the different set-ups.

Interestingly, the differences in proliferative survival between above and below-irradiated cells without agar gel were relatively small. Only the 250 mM Lu-DTPA-liposomes led to significantly lower cell survival after irradiation with the more suitable wavelength for Auger-electron induction, than with the below-energy. On the other hand, the other formulations did contain less Lu-DTPA, which would explain the more pronounced influence of the wavelength for the higher Lu-concentration. Furthermore, the absorption of photons at the L-edge of Lutetium (9.2 keV) will also add to the effect obtained at below-energy. Regarding the position of the agar gel, both positions in front and behind the cells led in general to lower proliferative cell survival than the irradiation without phantom. Although two formulations (Lu-liposomes 250 mM w and w/o GPC) have to be excluded from this observation, the other three Lu-formulations in the 'agar gel-behind' set-up reduce the proliferative cell survival in comparison to the set-up without any phantom. Of course, the impact of the phantom placed in front of the cells during irradiation is still much higher than for the phantom behind the cells (e.g. proliferative survival reduced to 41% and 62% for free Lu-DTPA, respectively). Nonetheless, the phantom gel behind the cells clearly added to the cellular damage done by the synchrotron radiation. These findings indicate a strong influence of secondary electrons induced by synchrotron x-rays in the phantom in front of the cells (forward direction) as well as from the phantom behind the cells (backward direction).

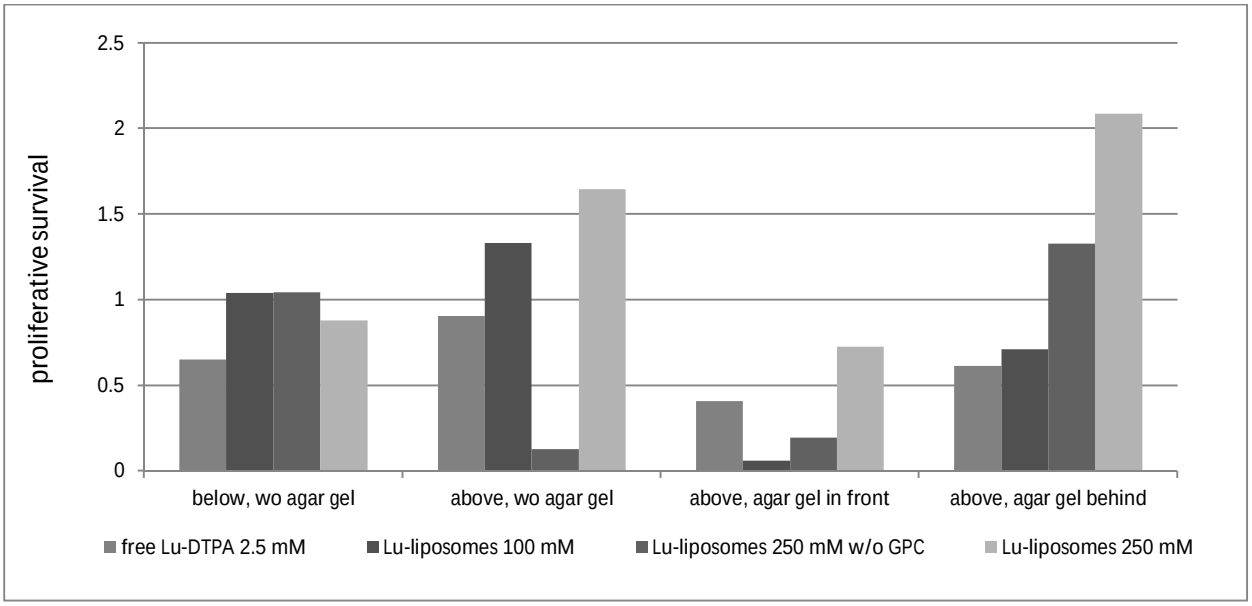

Figure 4-28 Analysis of irradiation conditions at ID 17: set-up with agar gel in front of or behind F98 cells. Dose: 10Gy, proliferative survival (4 time points in multiple MTT assay). W/o GPC: non-entrapped material was not removed. All other liposome formulations were purified by GPC-treatment. Dose: 10 Gy.

4.6.1.1.2 Experiments with Gd-DTPA as radioenhancer

Further experiments were performed with Gd-DTPA as radioenhancer. The suitability and efficacy of Gd-DTPA as radioenhancer was tested by cell irradiation with energies above and below Gd-K-edge, similar to the previous experiment with Lu-DTPA. As the phantom gel in front of the cells had the highest effect on cell survival, this set-up was chosen for the following experiments. For experiment MD 485 A, radioenhancer formulation was composed of Gd-DTPA (Magnevist) encapsulated by DOPC-Chol-CL liposomes, 25 mg lipid/ml, extruded via 100 nm membrane. For experiment MD 485 B, further lipid mixtures were tested, all including Gd-DTPA (Magnevist®) as radioenhancer (table 11).

Table 11 Overview of Gd-liposomal formulations tested in MD 485 B.

Liposomal formulation	Initial lipid concentration during extrusion [mg/ml]	Freeze-thaw preparation	GPC	Lipid concentration in wells [mg/ml]	Gd-concentration in wells [mg/ml]
DOPC-Chol-Cl 60:35:5	40	--	--	1	0.47
DOPC-Chol-DOPE 58:34:9	40	--	--	1	0.47
DOPC-Chol-DOTAP 57:33:9	40	--	--	1	0.47

Toxicity assays showed no toxic effect for all formulations (fig. 4-29 and 4-30) for the period of the experiment (3 h incubation time plus irradiation time). Values are means of four MTT assay time points, error bars represent SD.

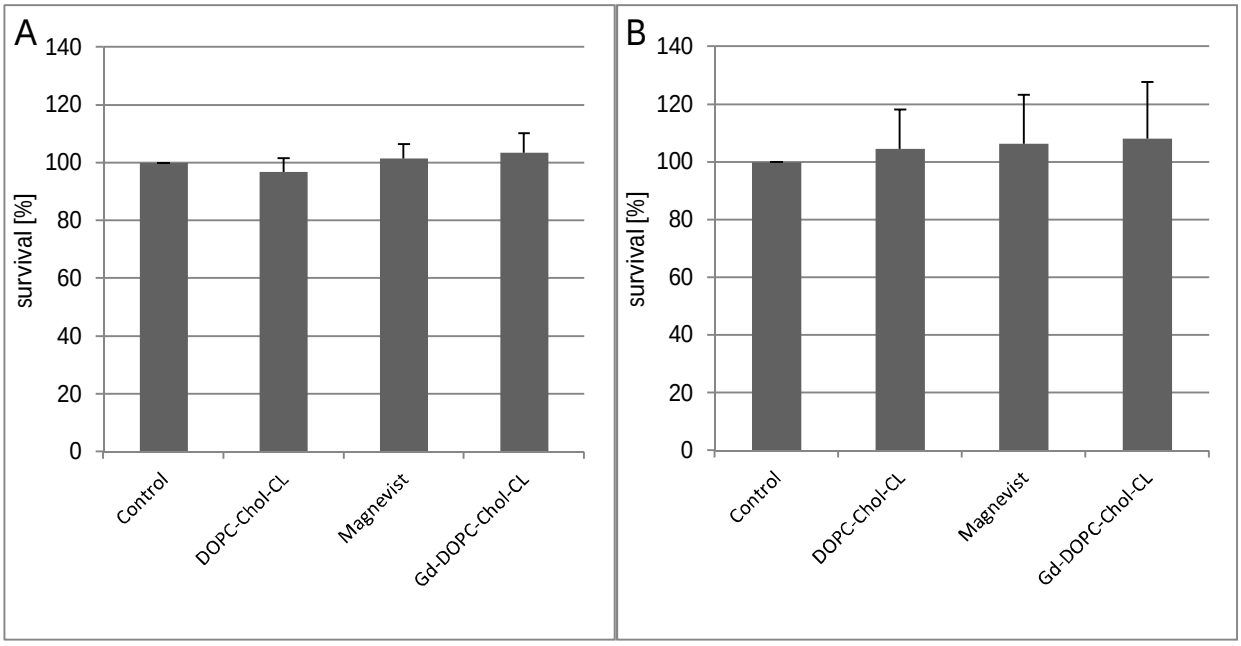

Figure 4-29 Toxicity of different formulations in experiment MD 485 A. (A) F98 cells, (B) LN229 cells.

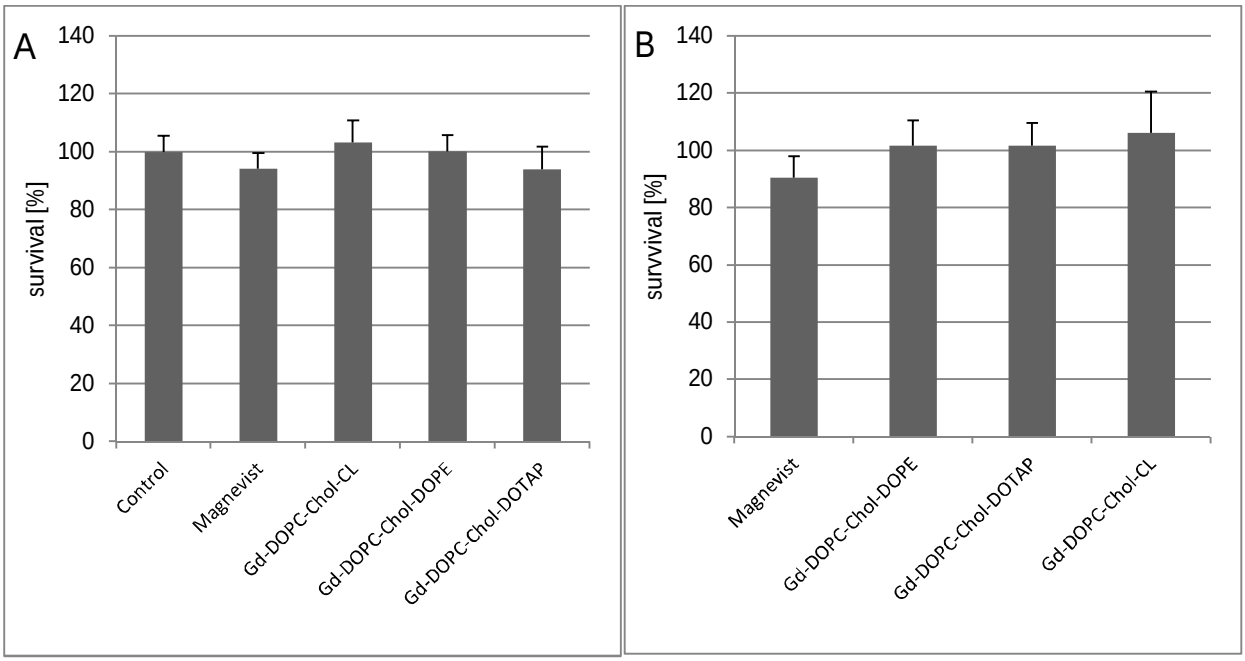

Figure 4-30 Toxicity of different formulations in experiment MD 485 B. (A) F98 cells, (B) LN229 cells.

Survival curves of 'medium control' (i.e. irradiated cells without further treatment) were based on non-irradiated medium. Fig. 4-31 A shows cell survival of F98 cells, irradiated with energy of 51.2 keV (above Gd-K-edge), for several time points after irradiation. The first two time-points (21 and 48 h after irradiation) do not yet show a notable effect of the radiation on F98 cells. Nevertheless, given enough time for further cell divisions and thus for apoptosis induction, the survival decreases significantly at later time points (71 and 106 h after irradiation). LN229 cells exhibit similar behavior, although the effect is not as distinct as for F98 cells, due to prolonged doubling times of LN229 cells (fig. 4-31 B).

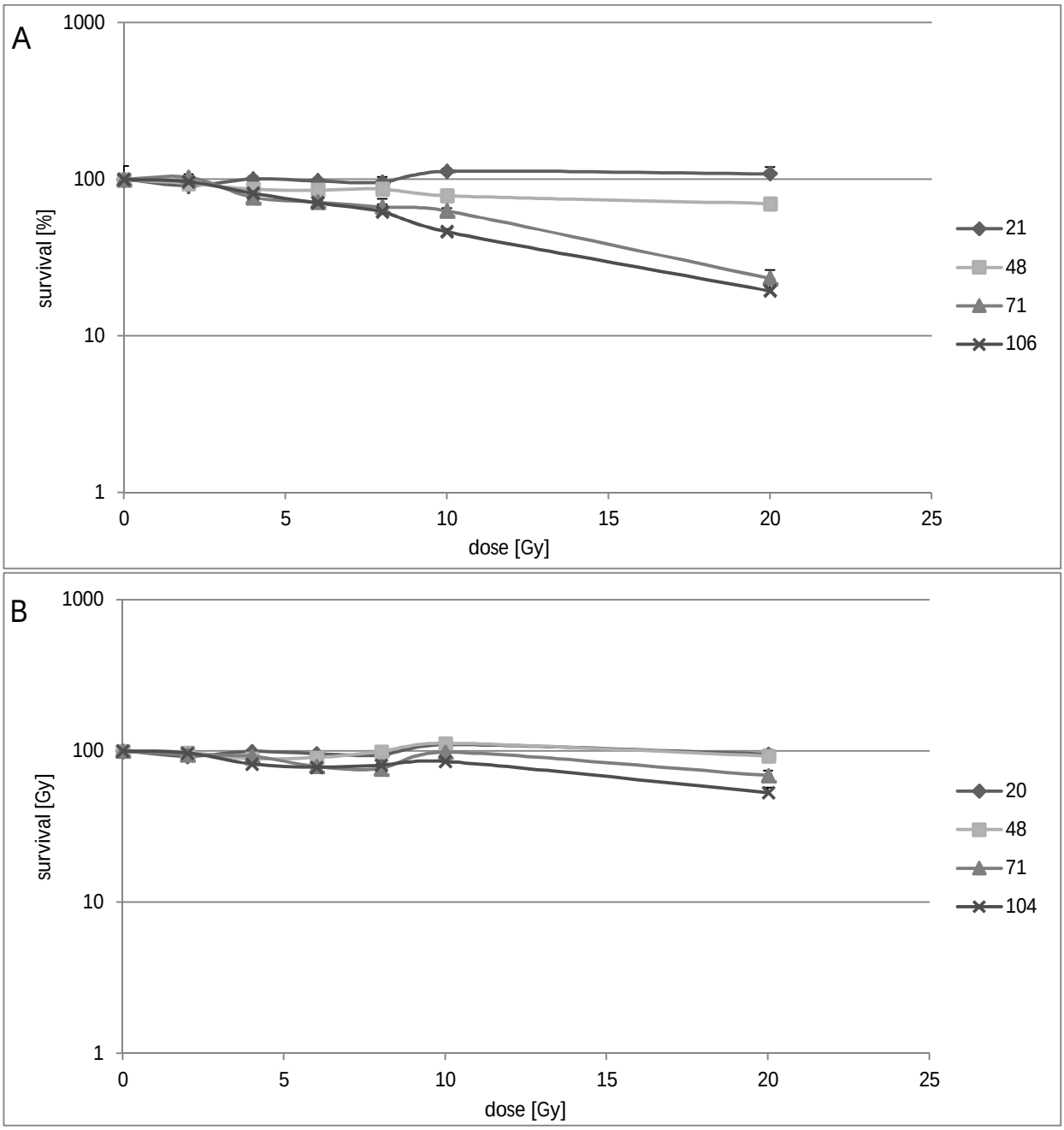

Figure 4-31 Survival curves of F98 (A) and LN229 (B) cells after irradiation with synchrotron radiation of 51.2keV (MD 485 A). Survival of cells without further treatment based on non-irradiated medium control. Legend: values indicate time [h] after irradiation.

4.6.1.1.3 Irradiation above and below Gd-K-edge

The irradiation of F98 cells treated with Magnevist with distinctive energies of synchrotron radiation led to altered outcome in cell survival. Fig. 4-32 shows survival curves for both above and below Gd-K-edge energy at MTT time point 84 h and 97 h after irradiation. The survival is based on the respective irradiated medium control on the same plates. Survival values are given in table 12. For 51.2 keV (above K-edge), the survival is significantly lower than for 49.2 keV (below), although the total radiation dose applied to the cells is the same. At higher doses (8 and 15 Gy), the survival of 'above'- irradiated cells is approximately even 20% lower than for 'below'-irradiated cells. These findings indicate that the applied

energy does indeed have an effect of the potency of the radioenhancer element Gd in irradiation treatment. The 'activation' of the radioenhancing effect depends on the appropriate energy for the K-absorption edge of Gd, thus producing electrons which can induce DNA-damage and lead to cell death. Further experiments (MD 485 B) were therefore conducted with the higher energy 51.2 keV suitable for the absorption at Gd-K-edge.

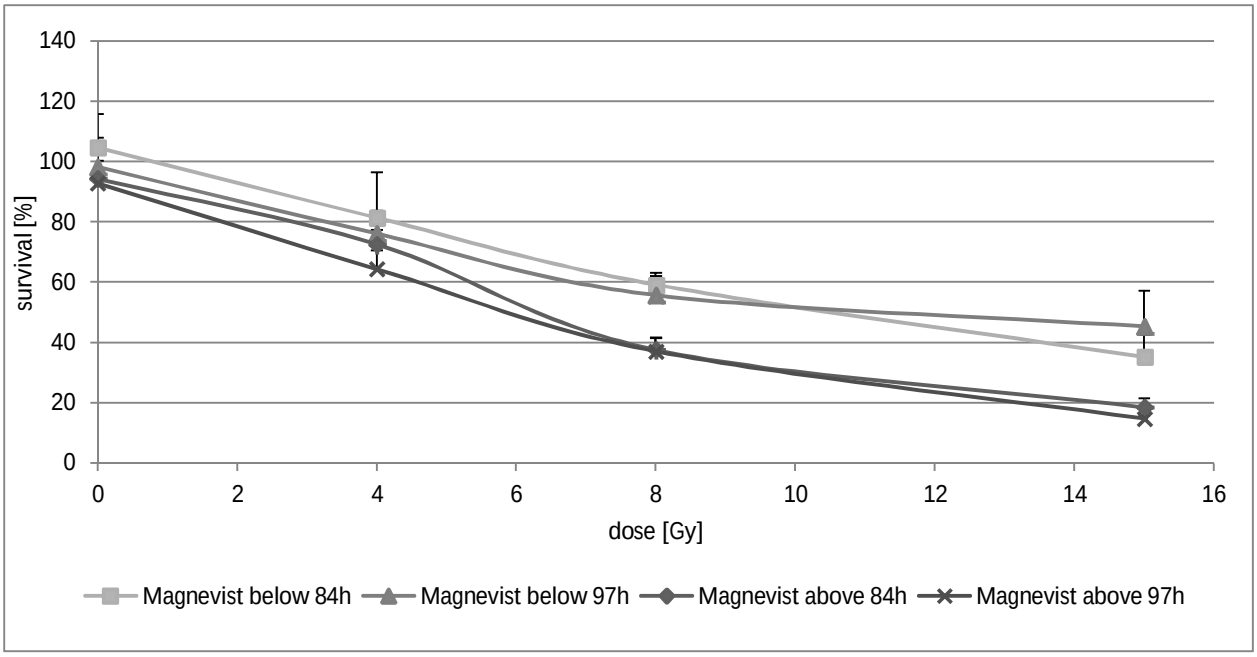

Figure 4-32 Survival curves of F98 cells treated with Magnevist solution and irradiated with energy of 51.2 keV (above) and 49.2 keV (below Gd-K-edge), MTT time points 84 and 97 h after irradiation.

Table 12 Survival data of F98 cells, irradiated with different synchrotron energy/wavelength after treatment with free Magnevist.

Energy	Above K-edge (51.2 keV)		Below K-edge (49.2 keV)	
MTT time point	84h	97h	84h	97h
4 Gy	72.60 ± 4.67	64.38 ± 6.08	81.40 ± 14.69	76.14 ± 7.53
8 Gy	37.61 ± 4.07	37.1 ± 4.39	59.20 ± 2.69	55.77 ± 7.2
15Gy	18.55 ± 2.87	14.77 ± 0.91	35.28 ± 7.23	45.36 ± 11.67

4.6.1.1.4 Irradiation after treatment with liposomal radioenhancer Gd-DTPA

The application of different liposomal formulations containing Magnevist as an enhancer led to lower cell survival after irradiation. Figure 4-33 displays survival curves of F98 cells. Since the survival is based on the respective irradiated medium control, the curves display only the effect of Gd under irradiation. Although every plate has its own medium control, the variation between plates (i.e. different doses) leads to inhomogeneity in survival for the individual formulations. Nevertheless, trends are evident: the cationic formulation Gd-DOPC-Chol-DOTAP and the neutral-fusogenic Gd-DOPC-Chol-DOPE cause lower survival than the anionic Gd-DOPC-Chol-CL mixture. For lower doses, the difference between the formulations is not as pronounced as for higher doses (above 4 Gy). In some cases, the effect of Gd increases with higher dose (Gd-DOTAP-formulation). However, the variations in the other formulations are too wide to draw a definite conclusion from this phenomenon. Table 13 shows the survival values for all tested formulations.

The overall effect of the irradiation treatment (i.e. irradiation plus Gd-enhancing effect) is shown in fig. 4-34. The free Magnevist curve is very similar to the control (medium alone), all other formulations led to lower survival. The DOTAP-formulations performed in the overall effect superior to the other formulations; the respective survival data were 15-20% lower than for control (from 4 Gy to 10 Gy).

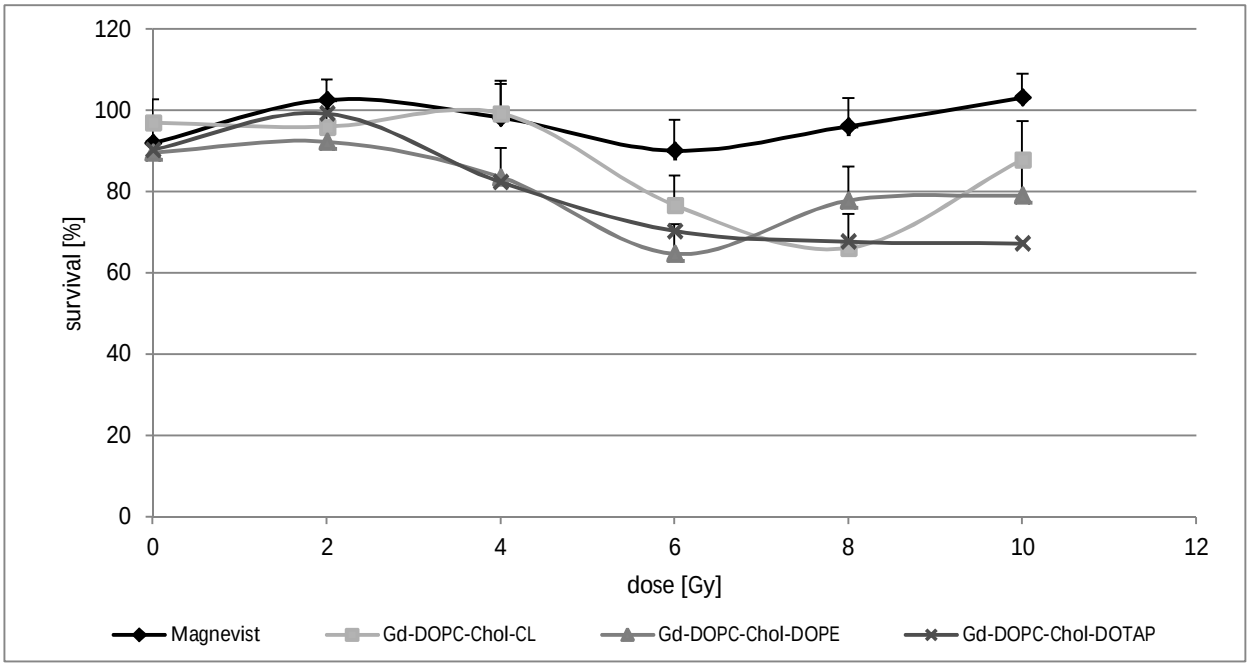

Figure 4-33 Survival of F98 cells, based on irradiated medium control, 106 h after irradiation.

Table 13 Survival data of irradiated F98 cells, based on respective irradiated control (= 100%), 106 h after irradiation.

Dose [Gy]	Magnevist	Gd-DOPC-Chol-CL	Gd-DOPC-Chol-DOPE	Gd-DOPC-Chol-DOTAP
0	92.1 ± 5.1	97.1 ± 5.6	89.7 ± 8.6	90.4 ± 5.6
2	102.7 ± 4.9	96.0 ± 4.3	92.4 ± 2.4	99.3 ± 5.0
4	98.3 ± 8.9	99.4 ± 7.1	83.6 ± 10.2	82.4 ± 11.3
6	90.1 ± 7.5	76.7 ± 7.2	64.8 ± 7.9	70.3 ± 4.8
8	96.2 ± 6.9	66.2 ± 8.3	77.8 ± 7.7	67.8 ± 9.6
10	103.2 ± 5.8	88.0 ± 9.4	79.1 ± 11.5	67.3 ± 10.5

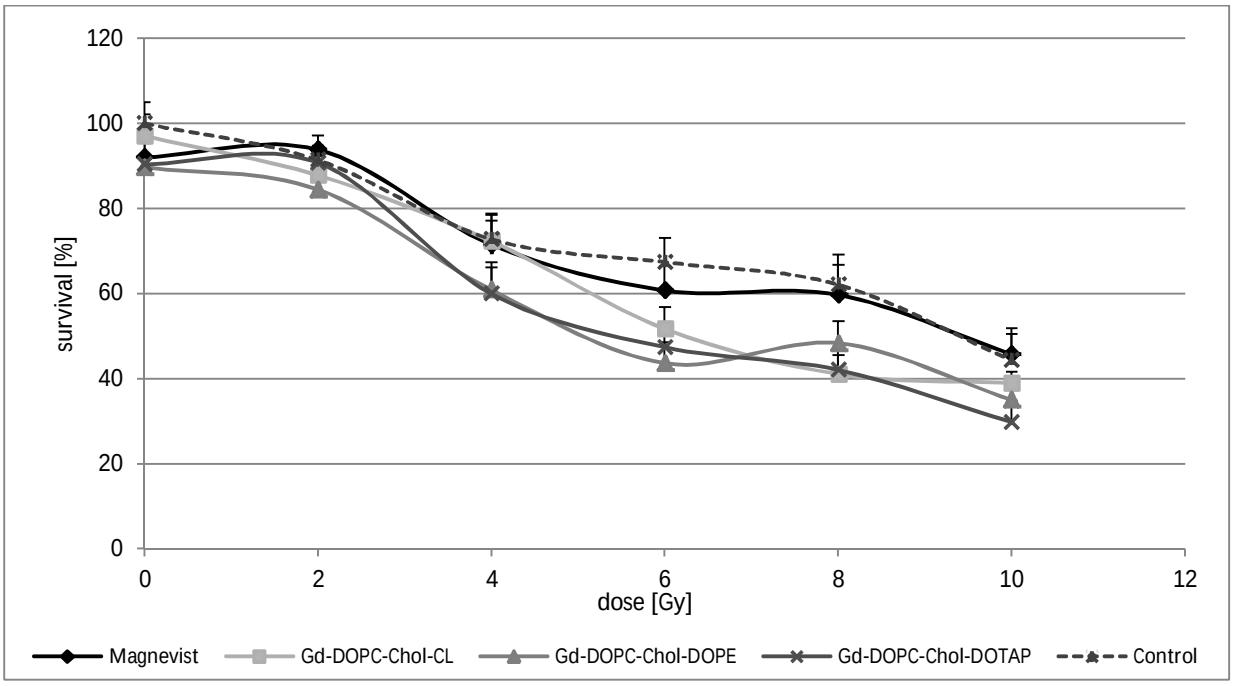

Figure 4-34 Survival of F98 cells, based on non-irradiated medium control, 106 h after irradiation.

LN229 cells reveal comparable results after treatment with Gd-containing liposomes, although not to the same extent as F98 cells. For doses above 6 Gy, liposomal formulations of Gd tend to decrease cell survival in comparison to free Magnevist. Other than for F98 cells, the anionic cardiolipin-containing formulation rather than cationic DOPTAP led to lowest survival for 6, 8 and 10 Gy dose (fig. 4-35 A). Table 14 presents the respective survival values for LN229 cells. In case of the overall effect of irradiation and Gd-treatment, a difference between free and encapsulated Magnevist also only occurs for the Cardiolipin-formulation and for doses above 6 Gy (4-7% less survival). The cationic and fusogenic liposomes (DOTAP and DOPE formulation) perform only slightly better (4 and 2% less survival for 10 Gy, respectively) than free Magnevist (fig. 4-35 B). The survival curves based on non-irradiated control show a slight increase instead of a decrease after 6 Gy, this is due to an aberration in the plates for 8 and 10 Gy which showed uncharacteristically high proliferation in spite of the high dose.

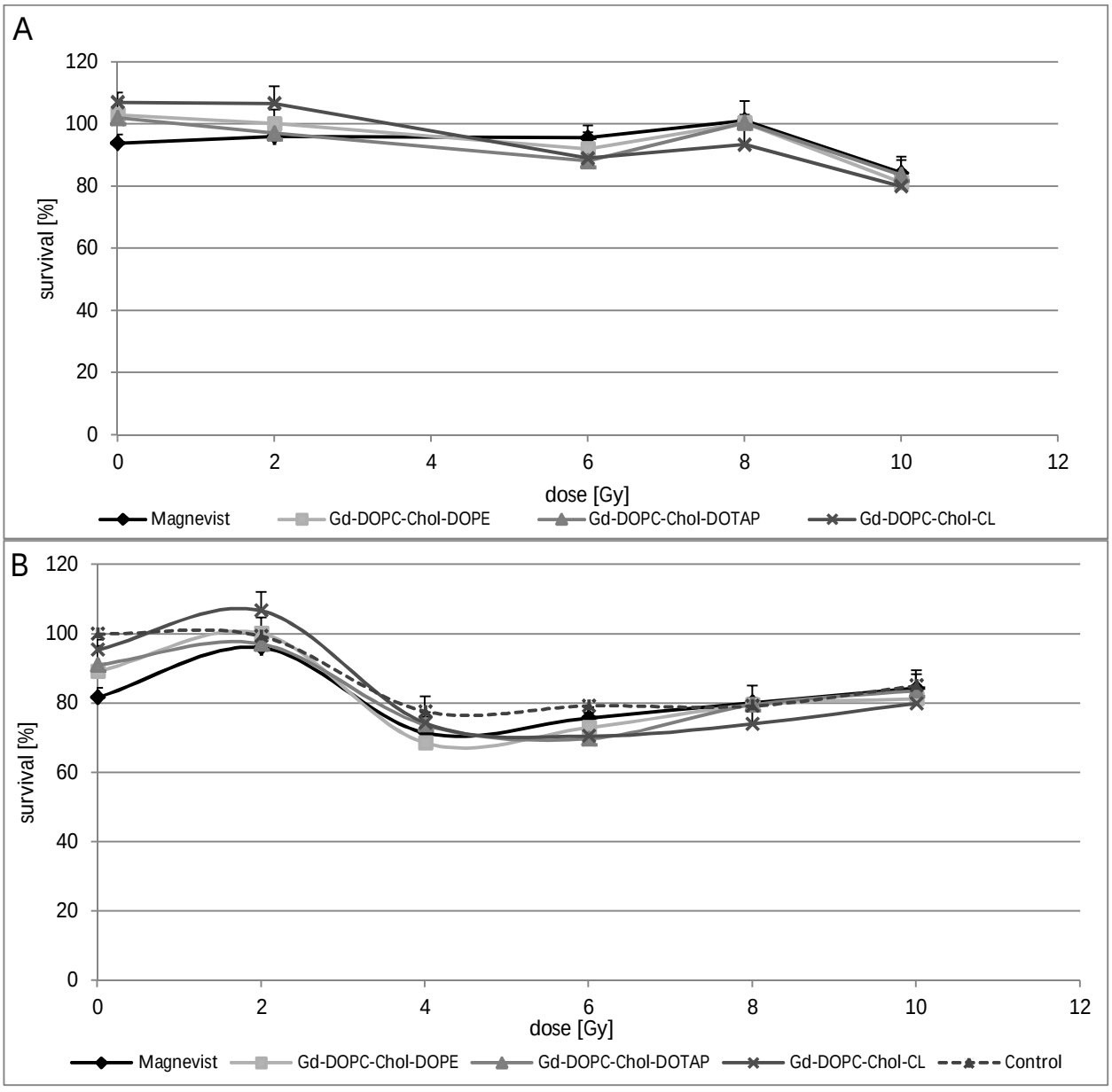

Figure 4-35 Survival curves of LN229 cells after treatment with radioenhancer and irradiation with 51.2 keV, MTT assay at time point 104 h after irradiation. A) Survival based on irradiated medium control. B) Survival based on non-irradiated medium control.

Table 14 Survival values for irradiated LN229 cells, based on respective irradiated medium control (= 100%), 104 h after irradiation.

Dose [Gy]	Magnevist	Gd-DOPC-Chol-DOPE	Gd-DOPC-Chol-DOTAP	Gd-DOPC-Chol-CL
0	93.9 ± 2.6	103.0 ± 1.1	102.0 ± 5.4	107.1 ± 2.9
2	96.0 ± 0.8	100.1 ± 4.5	97.1 ± 4.8	106.7 ± 5.4
6	95.6 ± 3.9	92.1 ± 5.2	88.1 ± 3.9	89.0 ± 4.8
8	101.2 ± 1.7	100.4 ± 7.0	100.4 ± 1.8	93.5 ± 6.1
10	84.3 ± 5.1	81.3 ± 3.1	83.6 ± 4.7	80.0 ± 5.1

4.6.1.2 Irradiation experiments using clinical linear accelerator

The radioenhancer formulations were also tested under clinical conditions with a Siemens MD2 linear accelerator. The respective dose was either applied fully (plates in the center) or the 96 well plates were arranged in the outer sphere of the radiation field. Since the frequency spectrum is different in the corners of the radiation field, the arrangement of the plates in the outer region leads to application of lower energy photons (and lower dose) to the cells than in the middle of the field. Scheithauer [177] described the effect in relation to the radial distance from the central beam (fig. 4-36). Since photons produced at the target of linear accelerators have different energies dependent on the emission angle, the radiation field needs to be homogenized to gain an even dose distribution for the radiation treatment of patients [177]. Through application of a cone-shaped compensating filter, a more homogeneous central field is created, but the outer region of the field is dominated by lower relative spectral energies (cf. fig. 4-36) due to the conical shape of the flattening filter. This lower energy spectrum includes a higher percentage of the required energy for the K-absorption edge of Gadolinium (50.2 keV). Therefore, similar to synchrotron radiation above the K-edge, the effect of the radioenhancer Gd should be more pronounced under the right energy spectrum given in the corners of the radiation field.

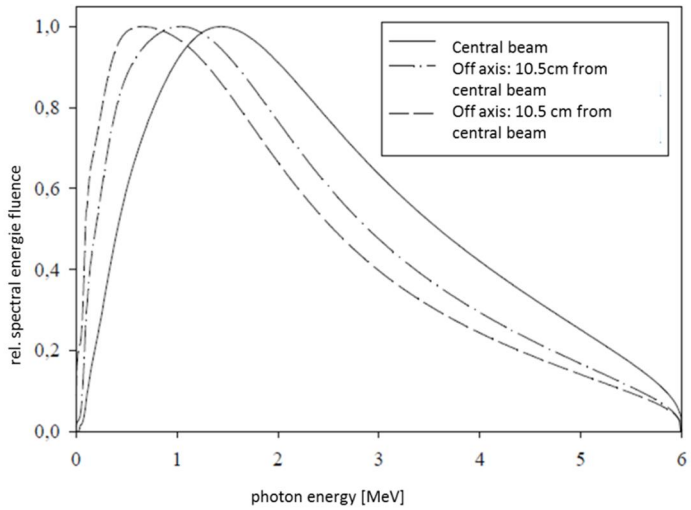

Figure 4-36 Differences in photon energies in relation to the radial distance from the central beam (adapted from: Scheithauer [175]).

Figure 4-37 A shows a normal growth curve of non-irradiated ('medium control') F98 cells and 4-37 B the respective survival curves of irradiated cells at different time points after irradiation, based on the proliferation curve shown in 4-37 A. The growth curve reaches its plateau approximately 98h after the start of the experiment. Consequently, the survival curves after this time point cannot be considered accurate, since the irradiated cells normally exhibit a delay in proliferation and will reach the plateau at a later time point. Their survival curve therefore shows a false negative, that is too high, result if based on non-irradiated control (cf. fig 4-37 A). Here, the survival curves after 68 and 94 hours show the lowest values, whereas later time points (120 and 145 h) exhibit again higher survival due to stagnant cell proliferation in the control group. Therefore, the MTT time points had to be chosen carefully, if the survival was based on non-irradiated control. Curves displaying only the Gd-effect (i.e. based on irradiated medium control) normally do not propose this problem, because every plate has its own medium control irradiated with the same dose. Nevertheless, if the irradiated medium control cells are

already in plateau-state while enhancer-treated cells are not, as it may occur with low-dose plates, comparison of treatment groups has to be exercised with caution.

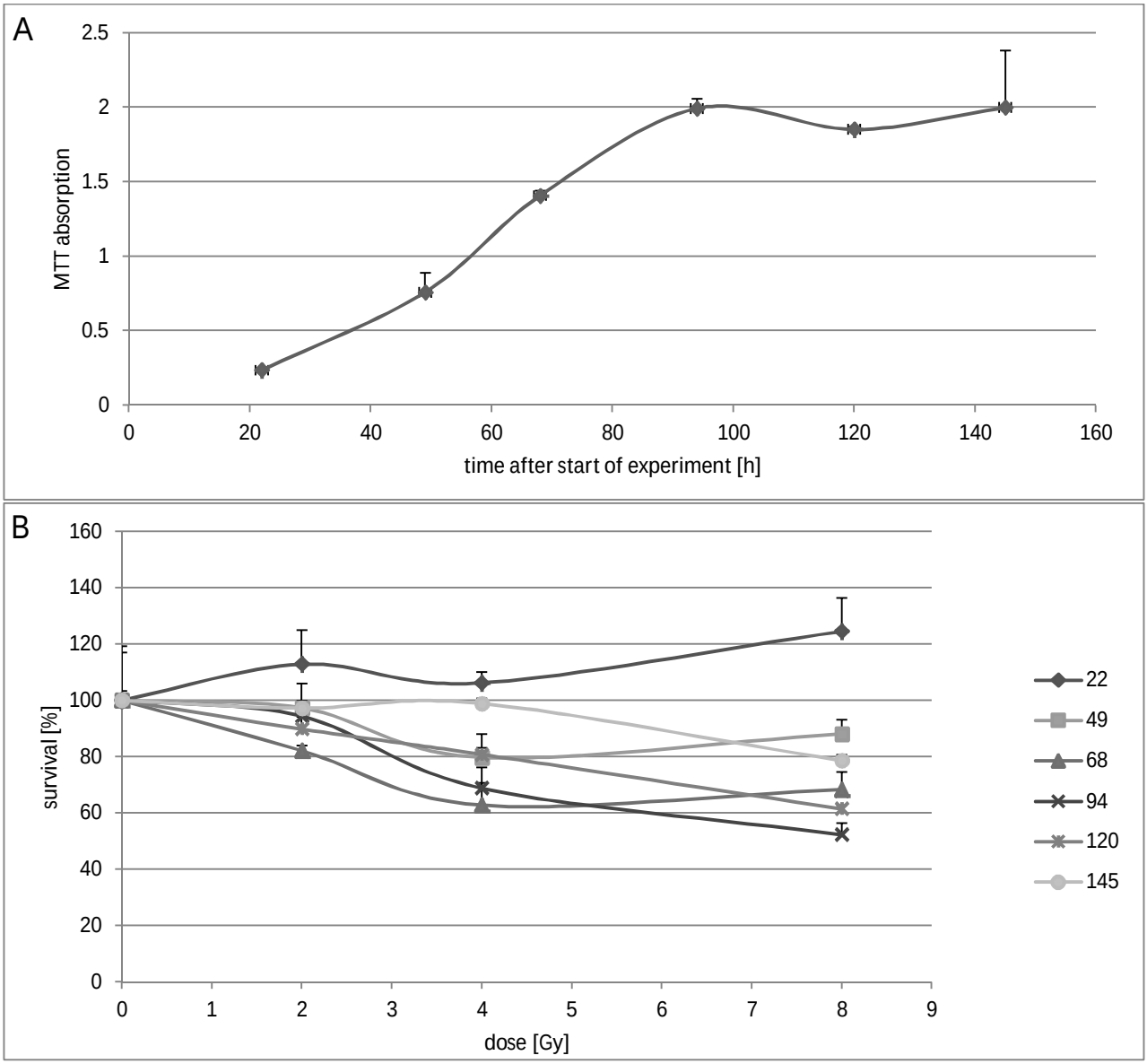

Figure 4-37 A) Growth curve of irradiated F98 cells. B) Survival curves of irradiated F98 cells, based on non-irradiated medium control. Legend: values indicate h after irradiation.

Table 15 shows the composition of the formulations tested in the experiment. The concentration of Magnevist solution equates to the liposomal formulation without GPC treatment.

Table 15 Overview of tested Gd-formulations.

Formulation	Initial lipid concentration during extrusion [mg/ml]	Freeze-thaw preparation	GPC	Lipid concentration in wells [mg/ml]	Gd-concentration in wells [mg/ml]
DOPC-Chol-Cl 60:35:5	40	--	w/o	0.4	0.47
DOPC-Chol-Cl 60:35:5	40	--	w	0.4	approx. 0.011
Magnevist 2	--	--	--	--	1.18

Figure 4-38 displays the toxicity tests of all formulations used in the experiment. Neither the Gd-containing liposomes nor the free Magnevist exhibited a notable effect on the cells.

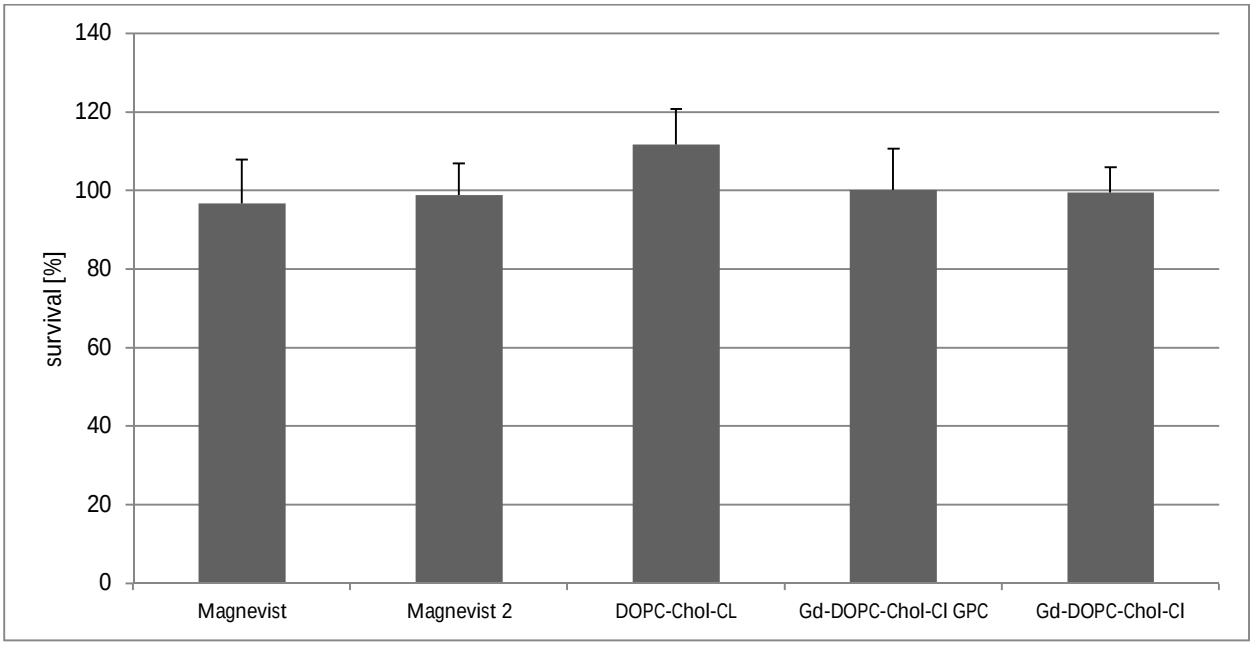

Figure 4-38 Toxicity test of different Gd-formulations on F98 cells, incubation time 1 h.

The irradiation of F98 cells in the outer region of the radiation field was performed accordingly to previous experiments by Buch [142]. 96 well plates in the corners of the Plexiglas template were divided into eight different circles, corresponding to the eight rows of the plate. Circle 1 was the outer circle, circle 8 the inner circle nearest to the center of the radiation field as shown in fig. 4-39.

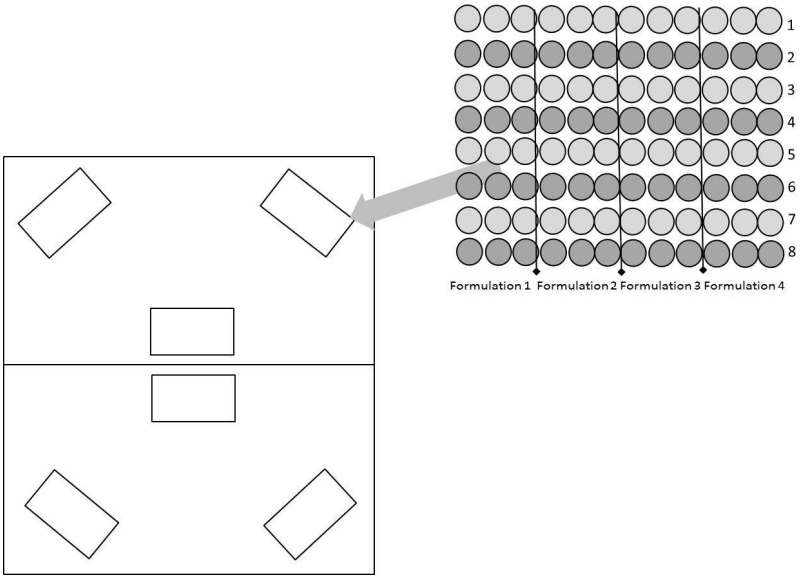

Figure 4-39 Plexiglas form for 96 well plate, 3 cm high with six cavities for 96 well plates. Set-up for the irradiation experiment at the JG-University medical center. 96 well plates were subdivided for different formulations and circles 1-8 as shown in the drawing. Another Plexiglas plate of 2 cm thickness covered the plates from above (in respect to the build-up effect for photons).

Resulting survival curves show the survival of irradiated cells (medium) based on the non-irradiated medium control. Circle 8 displays the lowest and the circle 1 the highest cell survival, in accordance with their respective position in the radiation field (figure 4-40 A). The same outcome is achieved by Magnevist-containing liposomes based on non-irradiated control (B). On the contrary, if survival of liposome-treated cells is calculated on the base of irradiated cells (the respective medium control on each plate), the order changes radically (C). Row 1 presents the lowest survival and row 4 the highest, while row 2 and 3 are in the middle section. Although the differences in survival are small, the trend indicates that the shifting to lower energies has indeed an impact on survival of Gd-treated cells. The dose at position 1 is lower than on position 8. Nevertheless, the survival of Gd-treated cells is lower than on the other positions if set in relation to the respective medium control.

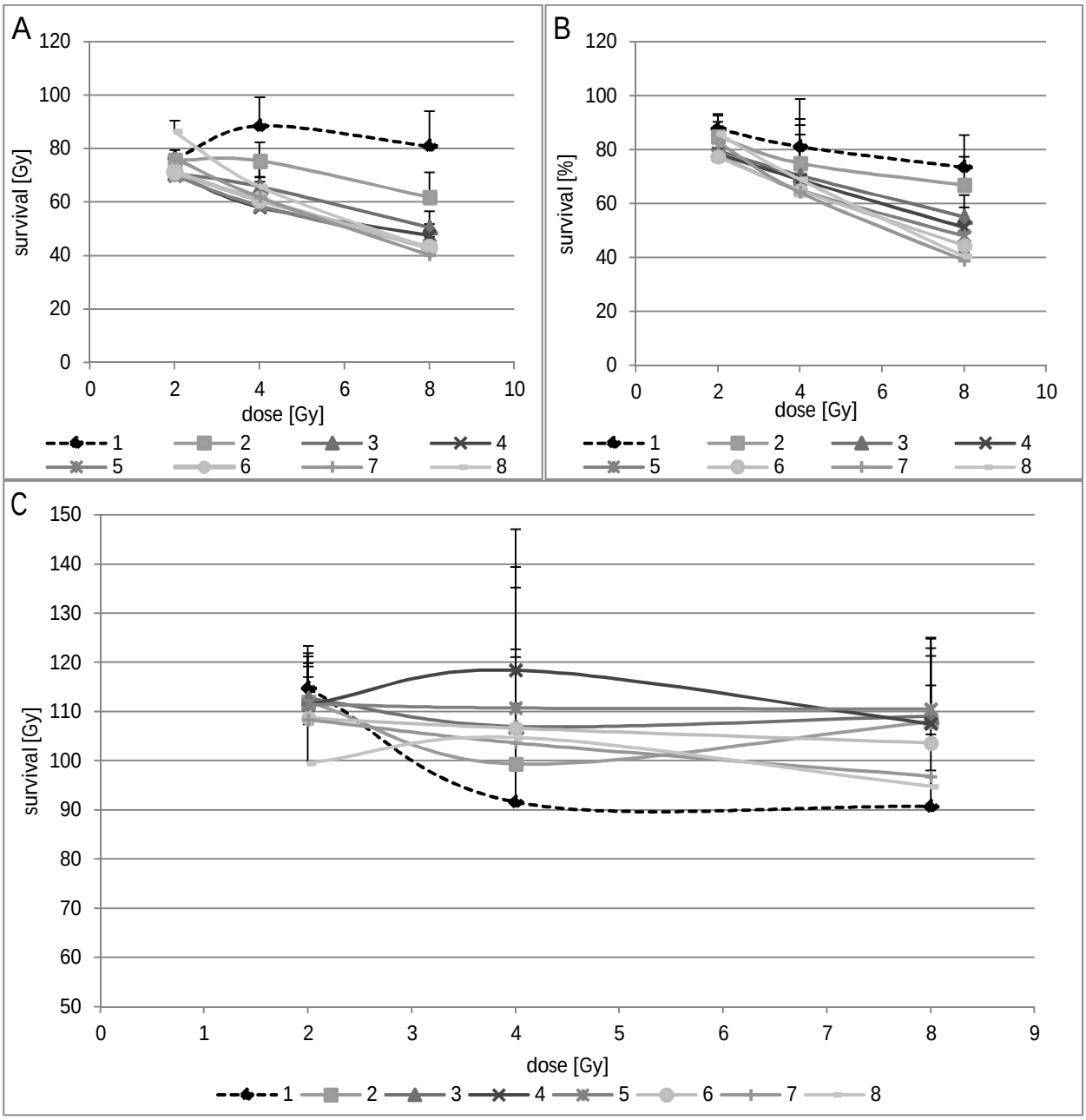

Figure 4-40 F98 cells: survival curves of 'corner' plates. (A) Medium irradiated, based on non-irradiated medium-control. (B) Gd-DOPC-Chol-Cl liposomes, based on non-irradiated medium control. (C) Gd-DOPC-Chol-CL liposomes, based on their respective irradiated medium control. Legend: digits express row number of 96 well plate, with 1 being the outer row and 8 being the row closest to the main irradiation field.

For the main irradiation field, the survival of Gd-treated cells was based on irradiated medium control. Figure 4-41 shows that Gd-liposomes, with or without GPC purification, performed superior to free Magnevist, indicating that the liposomal delivery plays an important role in the uptake. However, the effect is small and the cellular survival is still approximately 100% and therefore equal to medium without radioenhancer. The higher concentration of free Gd-DTPA, Magnevist 2, led to lowest cell survival (88% for a dose of 8 Gy).

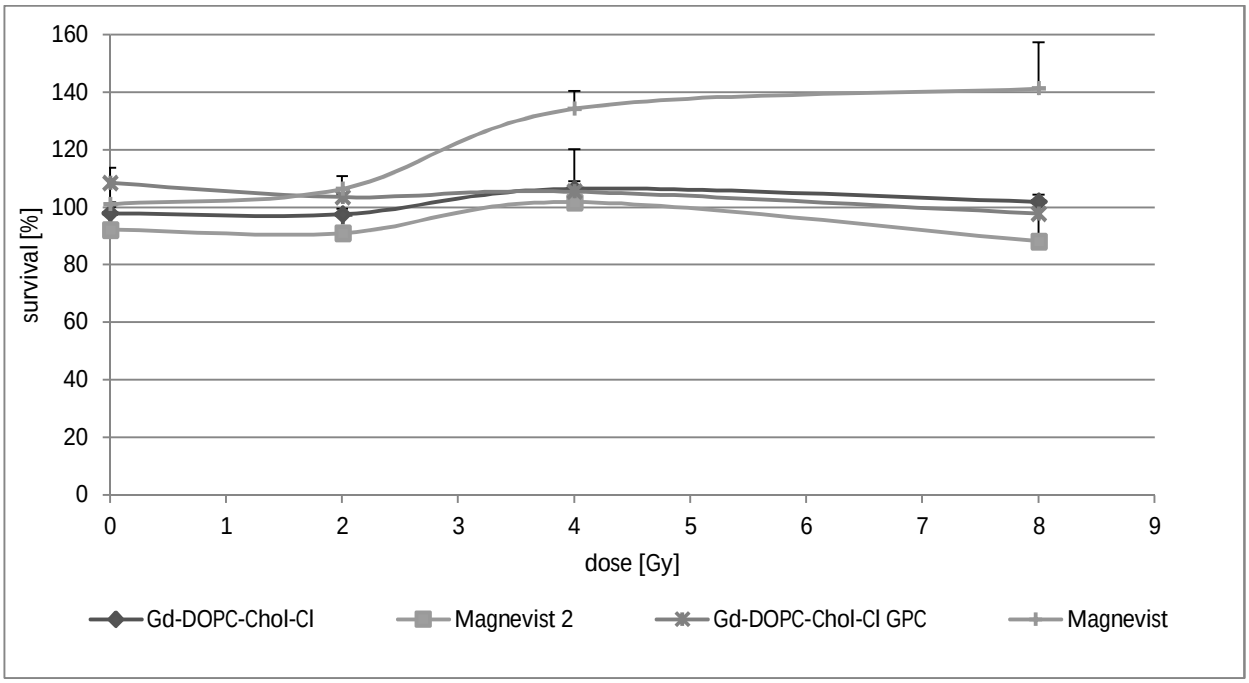

Figure 4-41 Survival curves of F98 cells, 94 h after irradiation.

4.6.2 Neutron irradiation experiments

4.6.2.1 Irradiation experiments at D22 beamline, ILL

First neutron irradiation experiments were carried out with F98 cells at the small angle neutron scattering instrument D22, ILL, Grenoble (experiment no. BAG-8-4). The liposomal formulations applied here contained Gd-DTPA-NV and Er-DTPA (50 mM Gd-DTPA-NV and 200 mM Er-DTPA or 250 mM Gd-DTPA-NV) and were manufactured by ultrasound with an initial lipid concentration of 40 mg DOPC/ml (no additive lipid components). Final lipid concentrations in wells were 0.4 mg/ml and non-encapsulated material was not removed before cell treatment. Cells were incubated for 1 h with liposomal formulations of free NC-elements before irradiation. Figure 4-42 depicts the proliferative survival of irradiated F98 cells. Since an exact dosimetry was very difficult to obtain at D22 beamline, the survival is given in regard to the irradiation time of the cells. For both irradiation spans, the liposomal Gd-DTPA-NV plus Er-DTPA formulation shows a distinctive effect on cell survival (16 and 23% reduction of cell survival compared to non-irradiated cells treated with the same formulation). Gd-DTPA-NV alone as liposomal formulation is not as effective as the mixture of neutron capture agent and radioenhancer Er-DTPA, but still leads to 14 and 8% lower survival (based on non-irradiated cells, equally treated). Free Gd-DTPA-NV is more effective for an irradiation period of 4 min (34% reduction), but for the shorter time span, it only leads to 10% reduction of cell survival.

In short, the supplement of Er-DTPA as an additional radioenhancer leads to higher effects of the applied neutron irradiation than with the NC-agent alone. The interaction of gamma rays induced by Gd-NC event with electrons from Er, resulting in high-LET Auger electron cascades from erbium, seems to be the underlying mechanism. The concentration of Gd-DTPA-NV in the Er-containing formulation is much smaller than in the formulation with Gd-DTPA-NV alone (50 mM instead of 250 mM), but the

survival is considerably lower for Gd-Er-liposomes. Consequently, the higher reduction of cell survival can be attributed to the supplemented Er-DTPA. Due to its the low cross section of 160 barn, it seems unlikely that the erbium-neutron capture event may be responsible for the enhanced radiation effect [178].

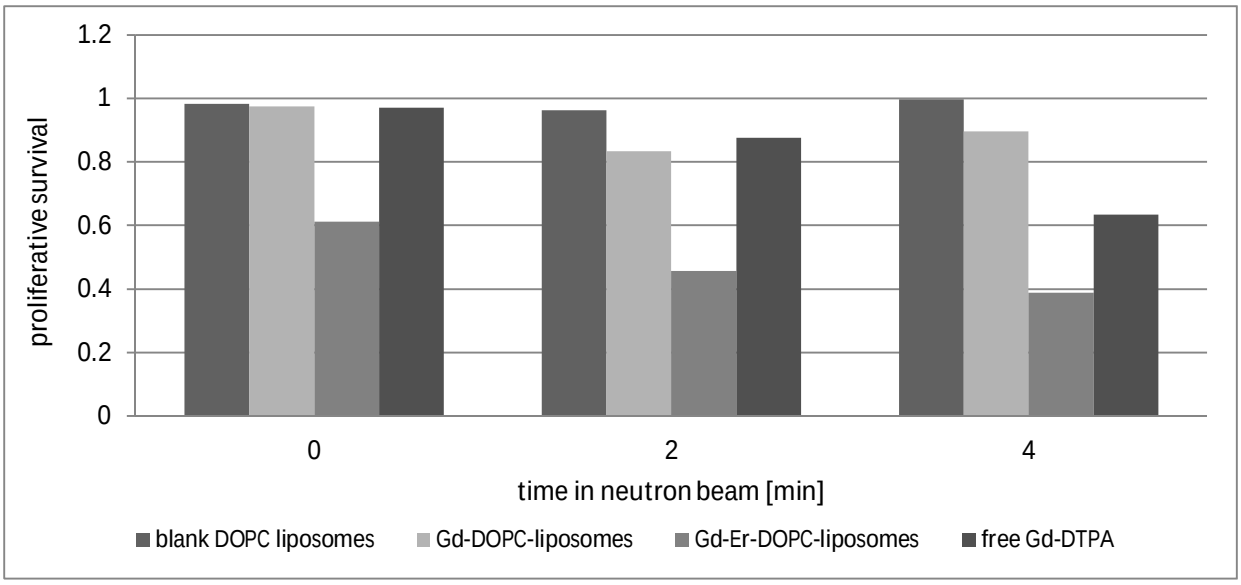

Figure 4-42 Proliferative survival of neutron-irradiated F98 cells (Gd/Gd-DTPA = Gd-DTPA-NV).

Further experiments (experiment number LTP-8-1) used Gd-DTPA-NV and Er-DTPA as well as tris-borate (TB) and bisglyceroborate (BGB), a boric acid-glycerol chelate complex, as liposomal neutron capture agents and radioenhancer [179]. Unfortunately, the good results from BAG-8-4 could not be reproduced in these experiments. Our assigned beamtime fell into a period where the beam intensity was reduced to less than 10% of its original flux. Figure 4-43 shows irradiated F98 cells, treated with different liposomal formulations and irradiated for different time spans at D22 beamline. BGB-liposome-formulation contained 500 mM BGB. Gd-DTPA-NV-, Er-DTPA-, BGB-liposomal formulation contained 100 mM BGB, as well as 50 mM Gd-DTPA-NV and 200 mM Er-DTPA. Besides the previously used pure DOPC liposomes, another liposome formulation, consisting of 5% cardiolipin, 60% DOPC and 35% cholesterol, was introduced. The liposomes were extruded, but the initial lipid concentration of 40 mg/ml remained the same. Although liposome- and NC-agent-concentrations per well were similar to those used in the previous experiment, the survival of F98 cells was not reduced in the same magnitude as before, when irradiation times were much shorter (2 and 4 minutes as opposed to 12 to 120 min). None of the formulations led to significantly lower cell survival after irradiation compared to the non-irradiated control formulation. Some of these findings can be ascribed to the differences between the individual 96 well plates, since control formulations were placed onto a different plate than the respective irradiated formulations and therefore, variations between seeding densities may have occurred. Additionally, it seems possible that the extrusion process for the liposomes led to differences in the encapsulation efficiency and uptake into cells which were not investigated. Nevertheless, the low flux of the neutrons was estimated to be the main reason for the unsatisfactory outcome of the experiments.

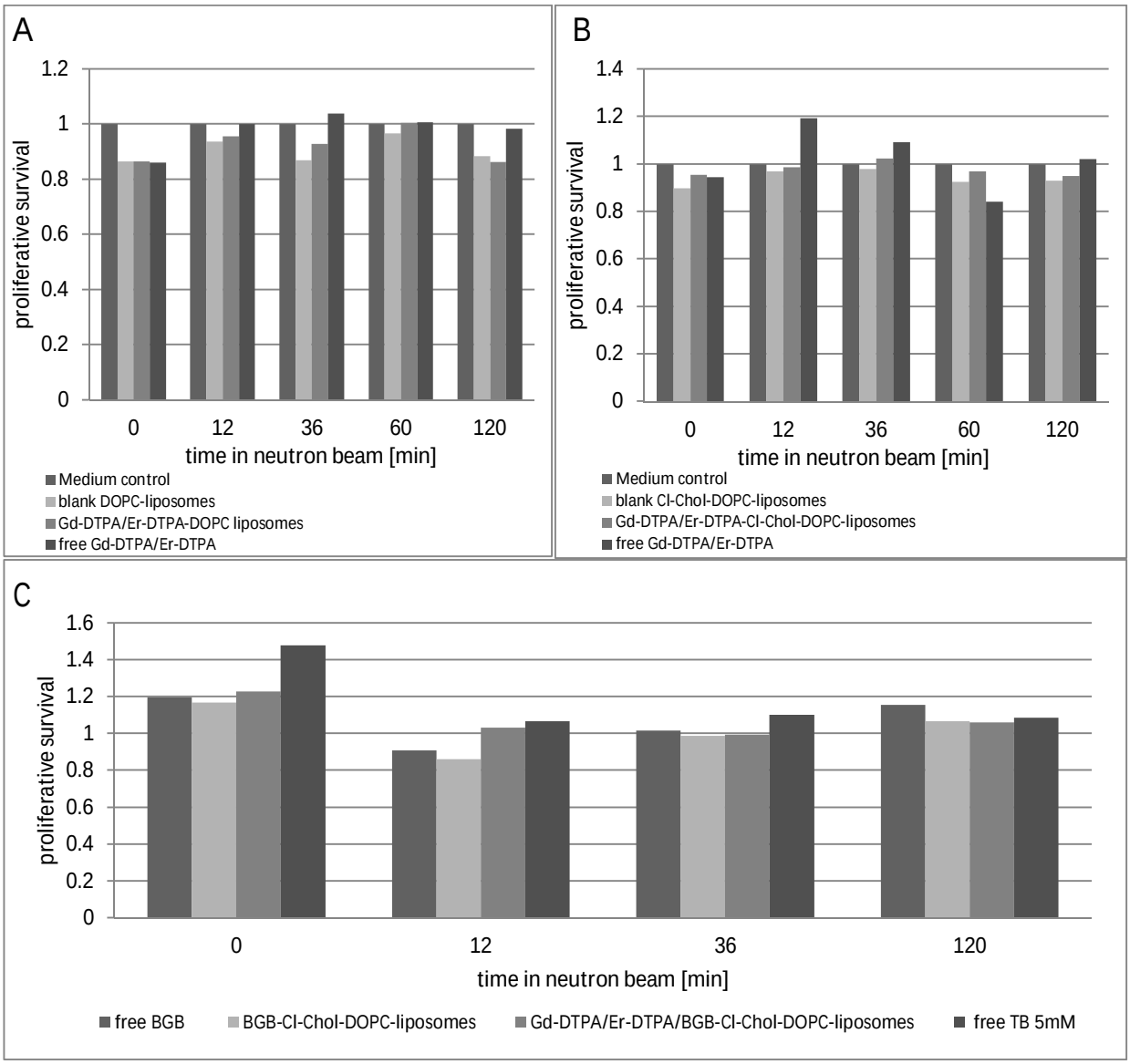

Figure 4-43 Irradiation experiments at D22, ILL, experiment no. LTP-8-1. Graphs A to C show proliferative survival of F98 cells, treated with different liposomal formulations with Gd or B as neutron capture element. In some cases, Er-DTPA was added as an additional radioenhancing element (Gd-DTPA = Gd-DTPA-NV).

Another part of the study had the aim to identify the Gd-related 'build-up' effect under neutron irradiation. This 'build-up' effect of Gd-derived gamma rays (after the neutron capture event has taken place) was examined by irradiation of a cell culture plate surrounded by Gd-containing media. Here, a 2 cm Gd-containing agar gel (100 mM Gd) was placed behind the cell culture plate and empty wells next to cell-containing wells were also filled with Gd-DTPA-NV (100 mM, 200 µl) solution. The neutron beam then reached cells as well as the Gd-gel located behind the cells and the Gd-filled wells next to cell-containing wells. Figure 4-44 shows the results from the experiment with F98 cells. In spite of the low neutron flux, the results show for nearly all formulations a higher reduction of cell survival for cells irradiated in Gd-environment than for cells without Gd in the proximity (table 16). These findings indicate that the long-range gamma rays derived from Gd-neutron capture event may attribute to cellular damage, even if located outside the wells. Through interaction with further radioenhancing elements such as Er or Gd, present inside or outside the target cell, high-LET secondary electrons set free from these atoms may add to the local energy deposition.

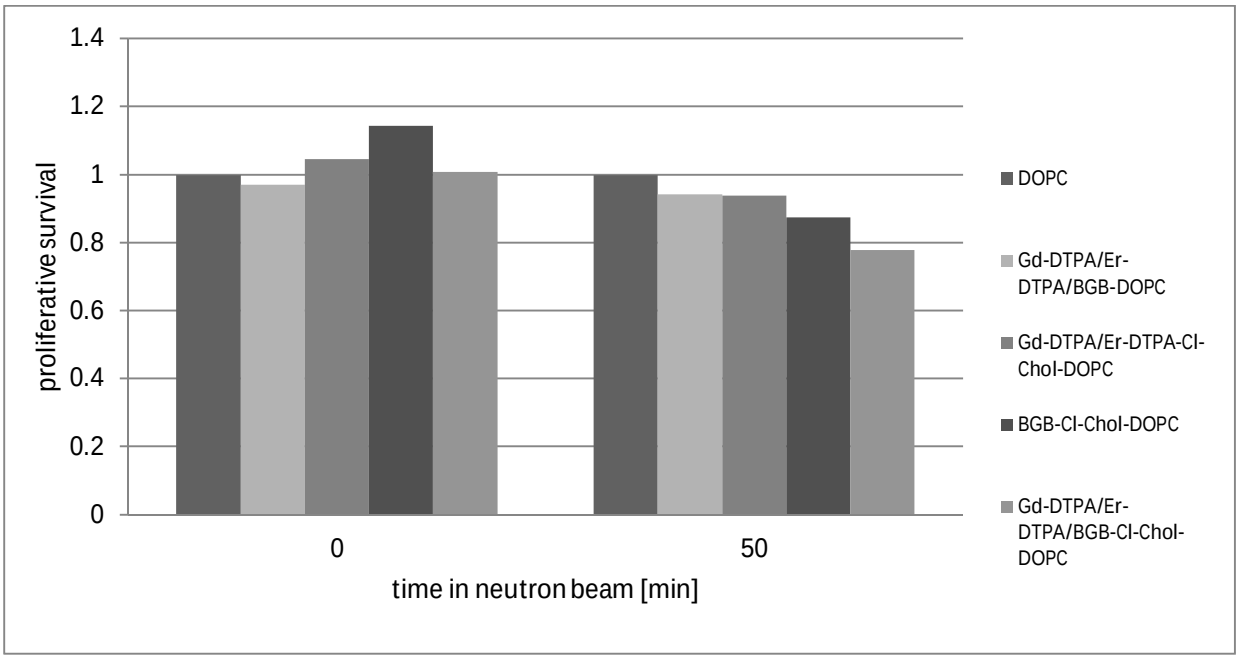

Figure 4-44 Proliferative survival of neutron-irradiated F98 cells, surrounded by Gd-containing media (Gd-DTPA = Gd-DTPA-NV).

Table 16 Reduction of cell survival for irradiated F98 cells, with and without Gd-environment.

Liposomal formulation	With Gd-environment Reduction of cell survival based on non-irradiated formulation [%]	Without Gd-environment Reduction of cell survival based on non-irradiated formulation [%]
Gd-DTPA/Er-DTPA/BGB-DOPC	2.9	9.6
Gd-DTPA/Er-DTPA-Cl-Chol-DOPC	10.4	0.4
BGB-Cl-Chol-DOPC	23.5	8.7
Gd-DTPA/Er-DTPA/BGB-Cl-Chol-DOPC	22.9	13.7

4.6.2.2 Neutron irradiation experiments at TRIGA reactor, Mainz

4.6.2.2.1 Suitability of experimental set-up

Previous studies in the thermal column of the TRIGA reactor in Mainz have shown that the exact position of the individual well of a 96 well plate has an influence of the acquired dose during irradiation. The dose declined from the hot end to the cold end, i.e. the side closer to the reactor core to the side further away from the reactor core, but not notably within individual rows. Sodium-activation analysis showed that the first and last rows (i.e. hot end and cold end) differed considerably from the middle rows. Moreover, the plates at the bottom of the stack added to the inhomogeneity by absorbing more dose than the top plates [180]. Therefore, the dose distribution for the applied neutron doses was examined again for both cell lines.

Fig. 4-45 presents the survival of irradiated (neutron fluence: $4.14 \cdot 10^{12}$ n/cm² and $6.21 \cdot 10^{12}$ n/cm²) and control cells based on the mean of the individual rows from a 96 well plate. Row 1 indicates the row nearest to the cold end, while row 8 stands for the row nearest to the hot end. The values represent the relative survival calculated from all wells in a row based on the arithmetical mean of all rows, that is the whole plate. For the two neutron doses, the pattern of the cell survival is similar, representing a similar dose distribution for both fluences. Surprisingly, the control group also seems to follow this pattern, albeit to a small extent. This indicates an influence of the seeding procedure at the plating time and the resulting seeding density of the cells. Naturally, the number of seeded cells affects the MTT outcome and should therefore be identical in all wells. Cell suspensions were consequently mixed thoroughly during plating preparations.

Despite the dose decline and seeding inconsistency, the overall SD between the rows was only 4, 10 and 8% (control, $4.14 \cdot 10^{12}$ n/cm², $6.21 \cdot 10^{12}$ n/cm²) for F98 cells (93 h after plating) and 5, 6 and 4% (control, $4.14 \cdot 10^{12}$ n/cm², $6.21 \cdot 10^{12}$ n/cm²) for LN229 cells (114 h after plating). The first two rows nearest to the cold end and the last row at the hot end have the highest discrepancy to the mean survival. Without the attribution of these rows, the overall SD was ameliorated to < 4% for all doses used for F98 cells, and < 3% for all doses used for LN229 cells. Consequently, these rows were excluded from the treatment with liposomes or free metal formulations and served as a medium control, which was calculated from their arithmetic mean.

As a consequence of these findings, an experimental set-up in which the respective plates and formulations were always irradiated at exactly the same position was employed (fig.4-46). The special arrangement ensured the comparability of the experiments and formulations. Liposomal and free metal formulations of Gd-DTPA were positioned at the same row of the 96 well plate in each experiment and for each cell line. The position of the 96 well plate in the stack of 10 plates remained the same for each experiment and each cell line.

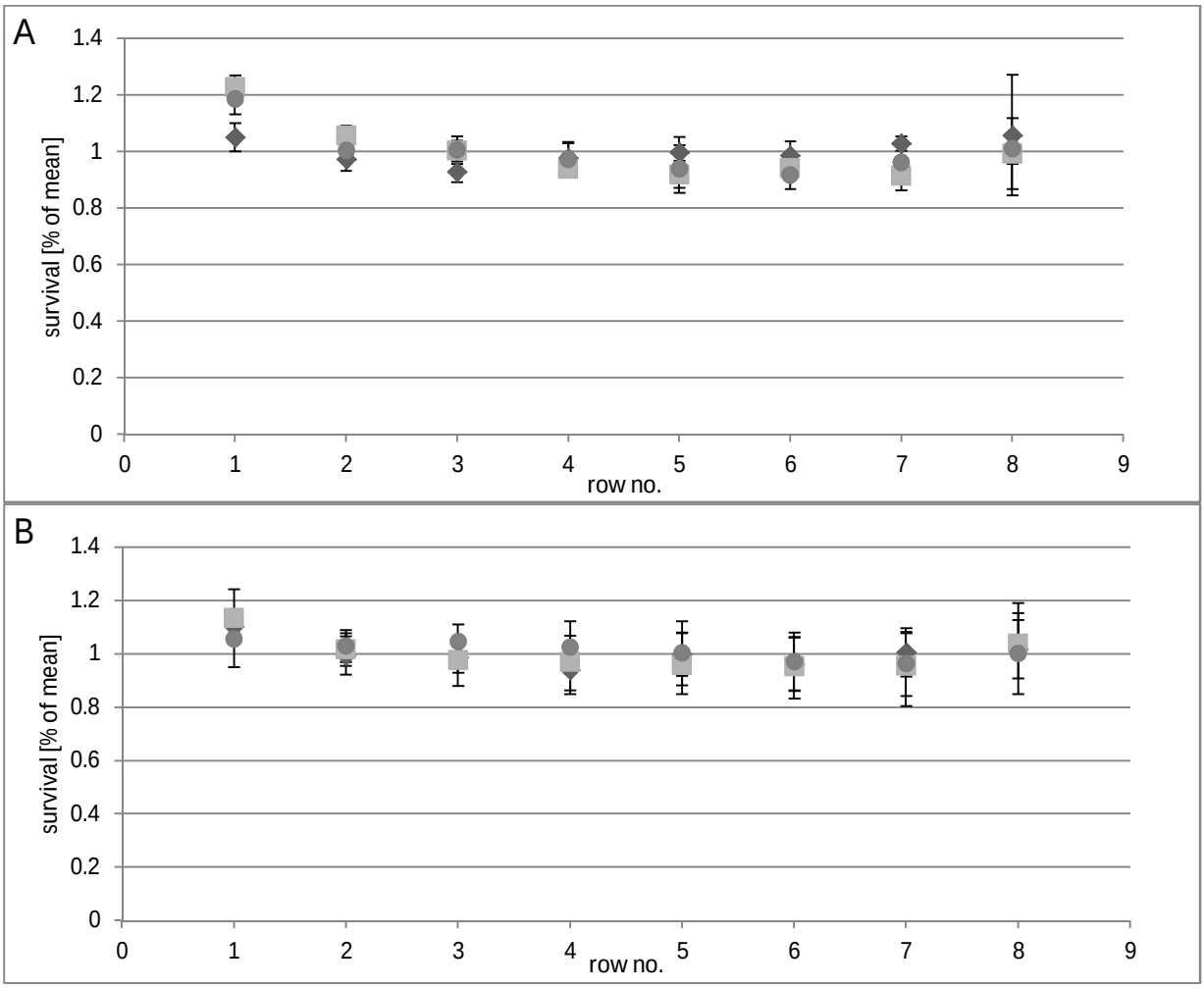

Figure 4-45 Differences of cell survival in rows based on the mean survival of all rows. Row 1= cold end, row 8= hot end. A) F98 cells, MTT 93h after plating. B) LN229 cells, 114h after plating. (◆) control: 0 $\cdot 10^{12}$ n/cm², (■): 4.14 $\cdot 10^{12}$ n/cm², (●): 6.21 $\cdot 10^{12}$ n/cm².

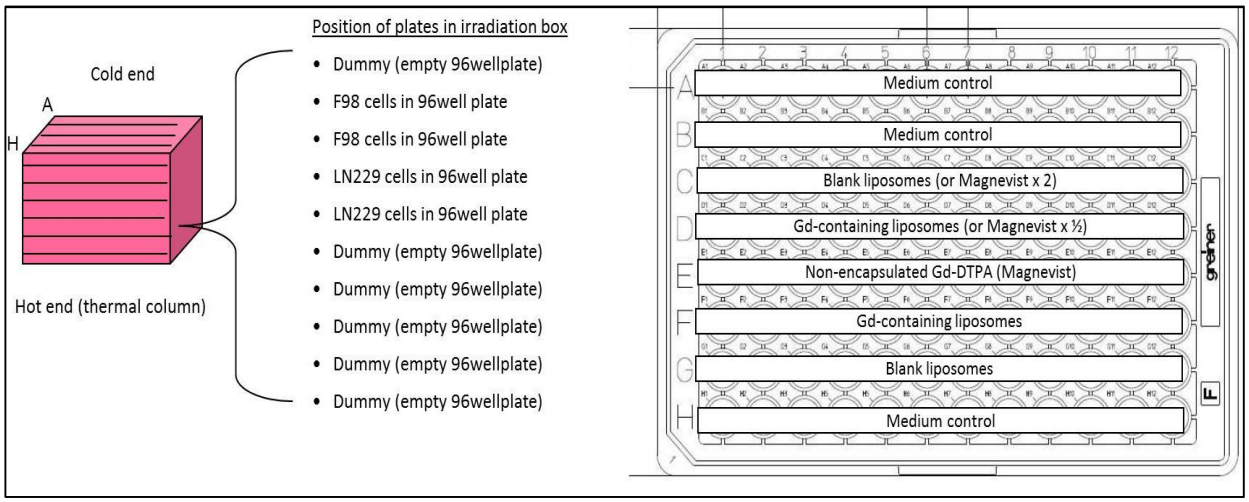

Figure 4-46 Orientation and position of 96 well plates in irradiation box and location of the various NC-element-formulations on the 96 well plates before neutron irradiation, pipetting scheme 1 and 2 (scheme 2 is indicated in brackets).

4.6.2.3 Determination of the optimal neutron dose range for cell irradiation

Since the cell irradiation experiments at the TRIGA Mark II reactor were the first to be performed at this radiation site, the optimal dose range for the irradiation had to be determined for the glioma cells before the NC-formulations could be tested.

The first experiments used reactor energies of 100 to 1000 kW x min, corresponding to fluences of $2.07 \cdot 10^{12}$ to $8.28 \cdot 10^{13}$ n/cm². The respective growth and survival curves are shown in fig. 4-47. Except for the fluence $2.07 \cdot 10^{12}$ n/cm², the cell survival is extremely low. Consequently, differences in survival could not be distinguished very well. Therefore, the fluence was set lower from $2.07 \cdot 10^{12}$ n/cm² up to $8.28 \cdot 10^{12}$ n/cm². Figure 4-48 displays the resulting growth and survival curves. Since the lowest fluence led to little effect on survival in comparison to non-irradiated cells, and the highest fluence $8.28 \cdot 10^{12}$ n/cm² resulted in very low survival (< 50% for both late time points), the doses in-between (4.14 and $6.21 \cdot 10^{12}$ n/cm²) were chosen for optimal cell irradiation dose. Table 17 displays the cell survival values of the experiment for MTT time points 43 and 67 h after irradiation. These two time points exhibited the lowest cell survival values, while later time points showed again higher survival. This phenomenon occurred also for photon irradiated cells and is attributed to the plateau-phase of non-irradiated cells which served as basis for the survival calculation. In following experiments most survival values were therefore calculated on basis of irradiated controls, thus eliminating the problem of outgrowing non-irradiated controls. Here, late time points were selected to give cells enough time to divide and retard fatal DNA lesions leading to cells death, as reported in the following section.

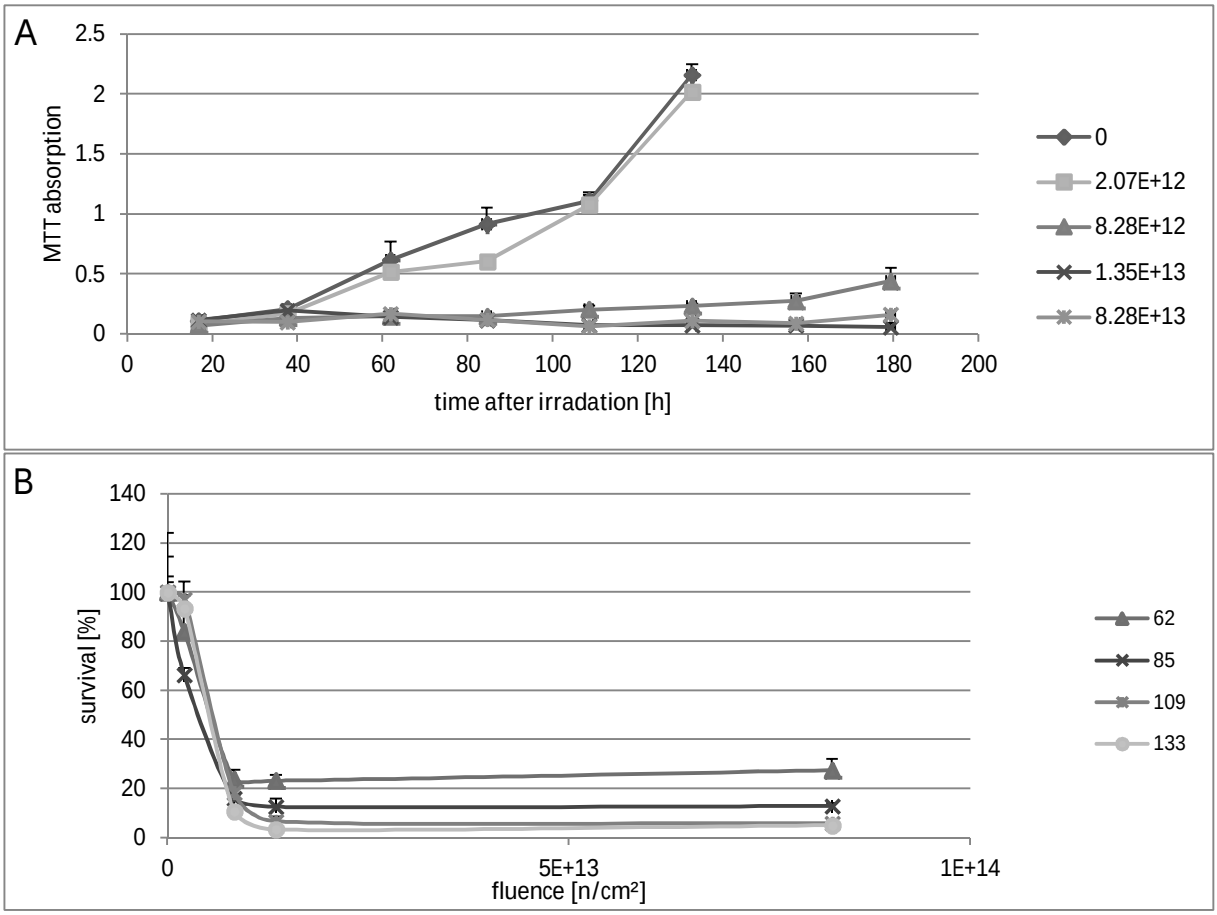

Figure 4-47 Growth and survival curves of irradiated F98 cells. A) Growth curve, Legend: digits represent fluence [n/cm²]. B) Survival curve, legend: digits represent time after irradiation [h].

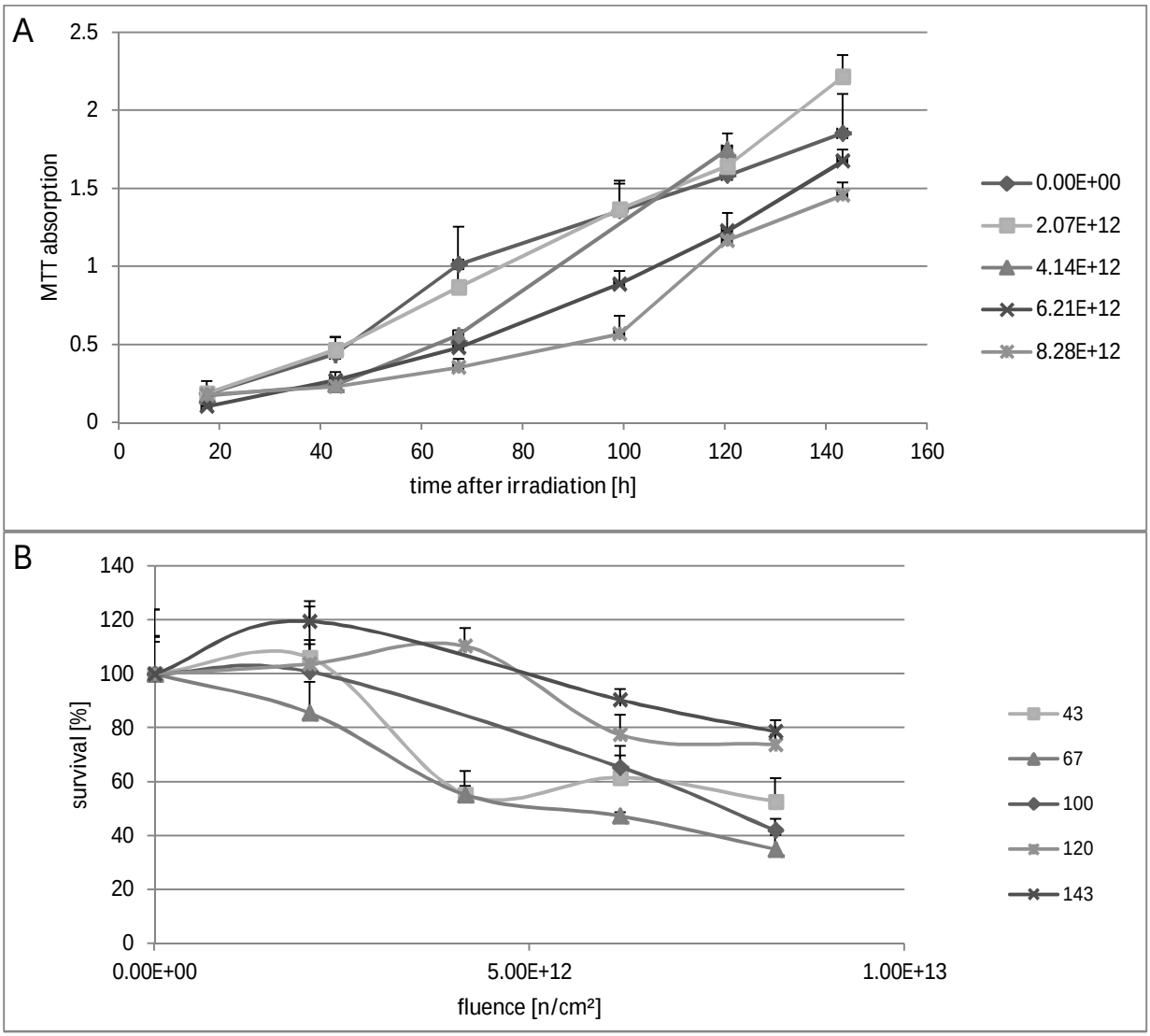

Figure 4-48 Growth and survival curves of irradiated F98 cells. A) Growth curve, Legend: digits represent fluence [n/cm²]. B) Survival curve, legend: digits represent time after irradiation [h].

Table 17 Survival data of neutron-irradiated F98 cells.

Fluence [n/cm²]	Survival after 43h [%]	Survival after 67h [%]
$0.00 \cdot 10^{12}$	100 ± 23.8	100 ± 23.79
$2.07 \cdot 10^{12}$	106.08 ± 18.86	85.54 ± 11.33
$4.14 \cdot 10^{12}$	55.38 ± 8.42	55.21 ± 3.22
$6.21 \cdot 10^{12}$	61.62 ± 11.52	47.32 ± 1.31
$8.28 \cdot 10^{12}$	52.75 ± 8.48	34.94 ± 5.24

4.6.2.4 *Survival of F98 and LN229 cells after neutron irradiation – analysis of survival time and curve shape*

Figure 4-49 shows cell survival curves for F98 and LN229 cells based on non-irradiated medium control. Cells were seeded 2 days prior to the experiment to ensure that cells were in log-phase of exponential growth when treated. Since only three doses (0, 4.14 $\cdot 10^{12}$ and 6.21$\cdot 10^{12}$ n/cm²) were tested, the shape of the graphs does not show clearly if the survival follows the established linear-quadratic model. Nevertheless, a simple model based on exponential curve fit reveals a good correlation regarding the time points 72 and 97h after irradiation. Earlier time points exhibit higher survival, in some cases even a small stimulation for growth after irradiation (cf. figure 4-49 B, LN229 cells at time point 22 h after irradiation). At later time points, cells had more time to divide and consequently, to discover lethal DNA damage leading to cell death. Therefore, further experiments primarily use the later time points for survival analysis.

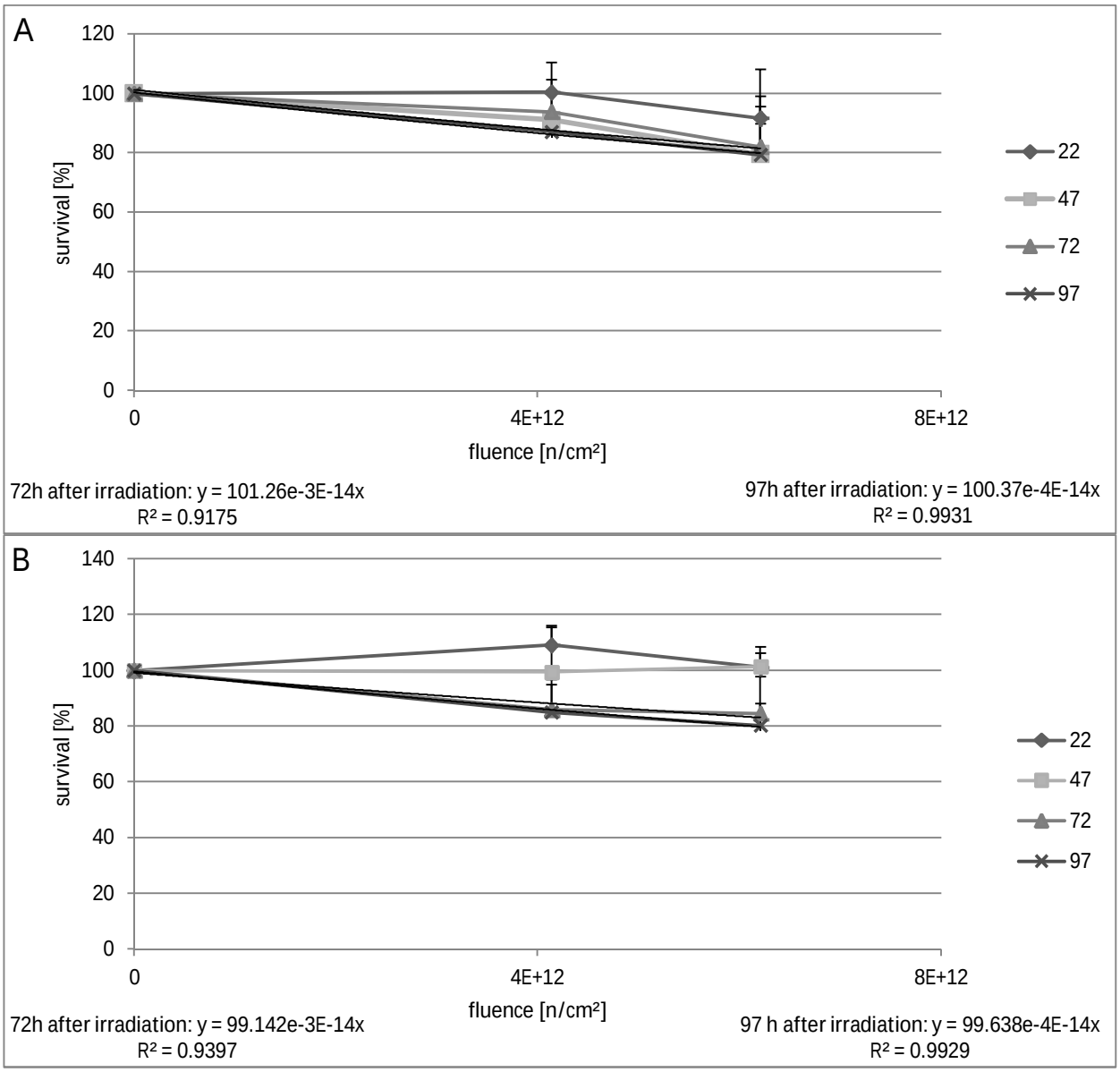

Figure 4-49 Survival curve of F98 cells (A) and LN229 (B) cells, without NC-Element – treatment, MTT at time points 22, 47, 72 and 97 h after irradiation with neutrons.

4.6.2.5 *Irradiation experiments using boron and gadolinium as NC-element –feasibility of NC-element-approach*

In preliminary experiments, the feasibility of the NC-approach in radiation therapy of glioma in the cell culture model was tested for the irradiation with thermal neutrons at TRIGA reactor, Mainz, in contrast to cold neutrons tested at the ILL, Grenoble. For comparison of effects, boron, a long-known and thoroughly studied NC-element, was included into the irradiation experiments otherwise performed with Gd-DTPA.

The first results from initial experiments with boron as neutron capture agent were shown in section 4.5.3, figures 4-25 and 4-26, to illustrate differences between multiple MTT assay and single-point-MTT assay in survival interpretation. The experiments were done with a formerly used set-up (plates were not stacked, but placed at a 45° angle before each other in the irradiation box) and irradiated with a high neutron fluence of $8.28 \cdot 10^{12}$ n/cm². Liposomes were manufactured via ultrasound, lipid contents per well were 0.4 mg/ml and no gel permeation chromatography was performed. Boron was either used 'free' as a tris-borate complex or encapsulated in liposomes in form of the boric acid-glycerol chelate complex bisglyceroborate (BGB). The boron concentration used was 1 and 5 mM for free boron and 500 mM for liposomal formulations and therefore, much higher than the amounts used in the later experiments presented below (which were calculated to be equimolar to Gd in the natural isotope mixture of both elements). The results show significantly reduced cell survival for both liposomal formulations of BGB (cardiolipin-containing liposomes 39% survival and DOPC-liposomes 44%, single point, 115 h after seeding, 60 h after irradiation, respectively).

Hence, the proof-of-concept for boron neutron capture therapy in our model cell line F98 already had been obtained with these experiments at the TRIGA reactor. However, the comparison with Gd-NCT and its effectiveness in both cell lines with equimolar B- and Gd-concentrations, as well as with the more suitable irradiation set-up of stacked plates and lower neutron fluence required further investigation and the next experiments were performed under improved conditions.

For liposomal carriers of the NC-elements, some early state, extruded formulations of anionic (CL), fusogenic (DOPE) and cationic (DOTAP) lipid mixture were used. Table 18 presents an overview of liposomal formulations. 'Free' B- or Gd- formulations were used in the respective concentration to match liposomal formulations. Cells were seeded 1 d prior to the experiment and incubation time was set to 3 h. Figure 4-50 presents toxicity data of applied formulations for both cell lines. The boron glycerol-complex seems to be unstable, if not encapsulated in liposomes. Therefore, the toxicity is here slightly higher, though cell survival is still more than 80% of the medium control. All other formulations displayed no significant toxicity towards both cell lines.

Table 18 Overview of liposomal formulations tested in the experiment.

Liposomal formulation	Initial lipid concentration during extrusion [mg/ml]	FT-Preparation	GPC	Lipid concentration in wells [mg/ml]	Gd-concentration in wells [mg/ml]	B- concentration in wells [mg/ml]
DOPC-Chol-Cl 60:35:5	25	--	--	1	1.89	0.1
DOPC-Chol-DOPE 58:34:9	25	--	--	1	1.89	0.1
DOPC-Chol-DOTAP 57:33:9	25	--	--	1	1.89	0.1

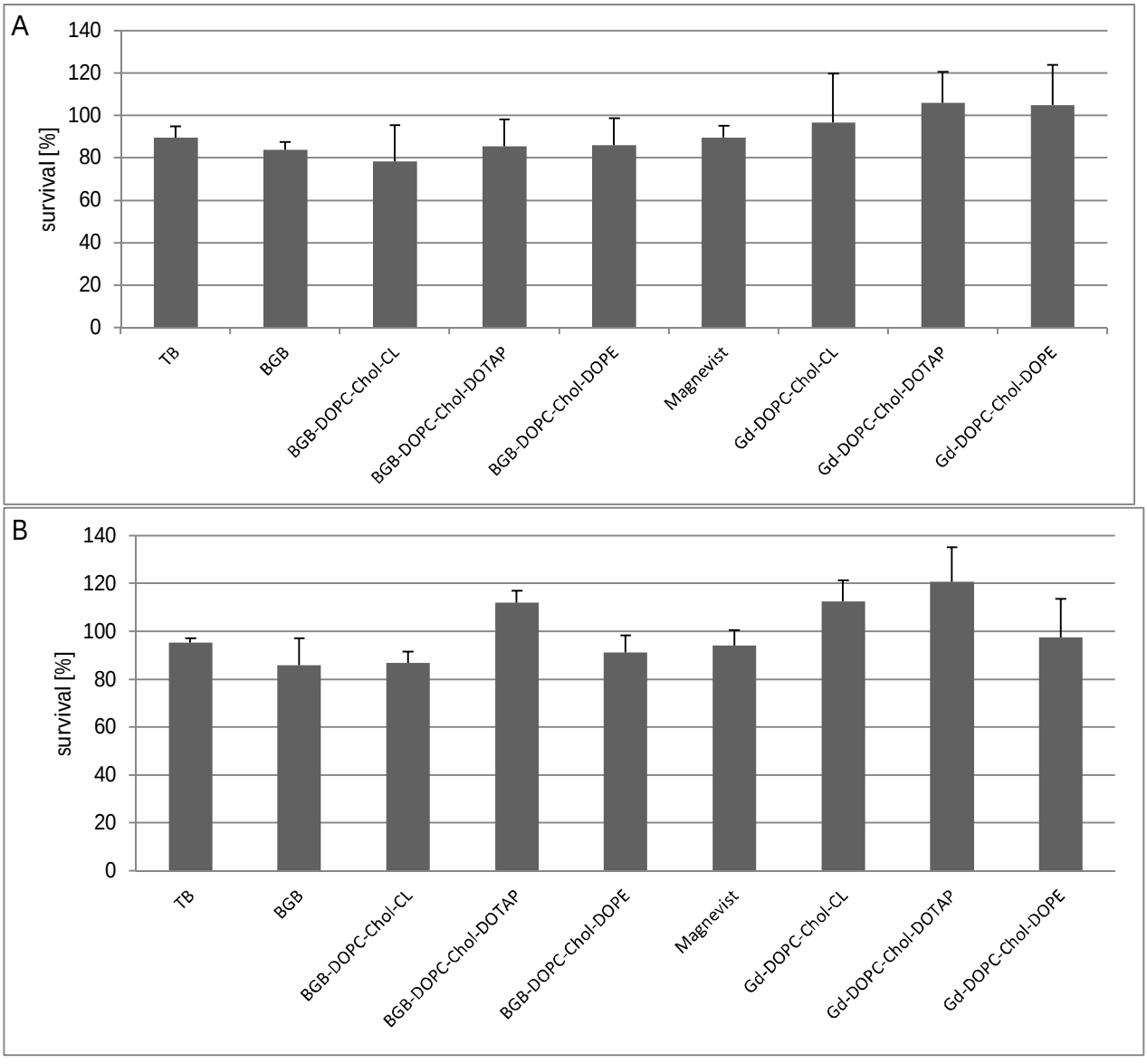

Figure 4-50 Toxicity tests of NC-formulations on F98 (A) and LN229 (B) cells. Mean of both time points (66 and 91h after treatment, incubation time 3h. Error bars represent SD.

In the irradiation experiment, boron containing liposomes performed superior to free boron-glycerol complex, although not to free tris-borate. Nevertheless, all boron-containing formulations led to significantly lower survival than free Magnevist (fig. 4-51). The treatment with Gd-containing liposomes resulted in lower survival of F98 cells than with blank liposome and also than free Magnevist. In fact, the Gd-containing formulations led to survival nearly as low as the BGB-liposomes For $4.14 \cdot 10^{12}$ n/cm², survival was 31 and 27% for the Gd-CL-and Gd-DOPE-formulation, respective to 27 and 26% for the BGB-Cl- and the BGB-DOPE-formulation. Survival values are given in detail in table 19.

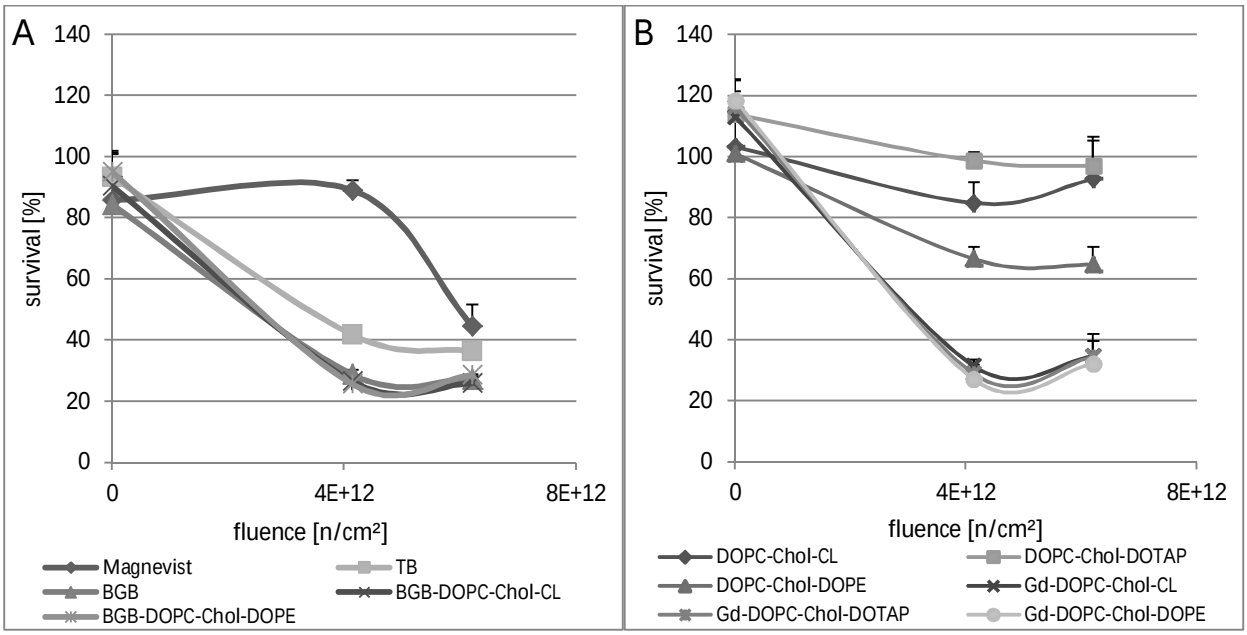

Figure 4-51 Survival curves of irradiated F98 cells, 91h after irradiation, based on irradiated-medium control.

Table 19 Survival data for irradiated F98 cells, based on irradiated control, 91 h after treatment.

Fluence [n/cm²]	Magnevist	TB	BGB	BGB-DOPC-Chol-CL	BGB-DOPC-Chol-DOPE	DOPC-Chol-CL	DOPC-Chol-DOTAP	DOPC-Chol-DOPE	Gd-DOPC-Chol-CL	Gd-DOPC-Chol-DOTAP	Gd-DOPC-Chol-DOPE
$0 \cdot 10^{12}$	85.8 ± 8.2	93.4 ± 7.8	84.4 ± 12.2	90.4 ± 11.5	95.0 ± 5.7	103.2 ± 10.3	113.9 ± 3.9	101.0 ± 14.5	112.9 ± 8.5	116.3 ± 8.7	118.4 ± 6.9
$4.14 \cdot 10^{12}$	89.1 ± 3.1	41.8 ± 2.4	28.8 ± 0.5	26.6 ± 1.3	25.7 ± 1.4	84.8 ± 6.7	98.7 ± 2.7	66.5 ± 3.9	31.4 ± 2.1	28.9 ± 3.0	27.1 ± 1.5
$6.21 \cdot 10^{12}$	44.5 ± 7.0	36.5 ± 0.4	27.3 ± 0.7	25.9 ± 0.8	28.6 ± 0.2	92.6 ± 13.8	96.9 ± 8.4	64.6 ± 5.8	34.6 ± 7.1	34.5 ± 5.0	32.2 ± 3.6

LN2229 cells exhibited also lower survival for boron-containing formulations than for free Magnevist (fig. 4-52). The anionic CL-formulation and the fusogenic DOPE-formulation led to equally low survival (approximately 57 and 45% for $4.14 \cdot 10^{12}$ n/cm² and $6.21 \cdot 10^{12}$ n/cm²). The application of Gd-containing liposomes did not result in cell survival this low, however, the proliferation was still only 58 to 68% of the control (at $6.21 \cdot 10^{12}$ n/cm², fig. 4-53). Free Magnevist was not tested at this fluence in the experiment, but the result from the lower fluence $4.14 \cdot 10^{12}$ n/cm² (76% survival) was slightly superior to the Gd-liposomes (approximately 83% for the CL-and the DOPE-formulation).

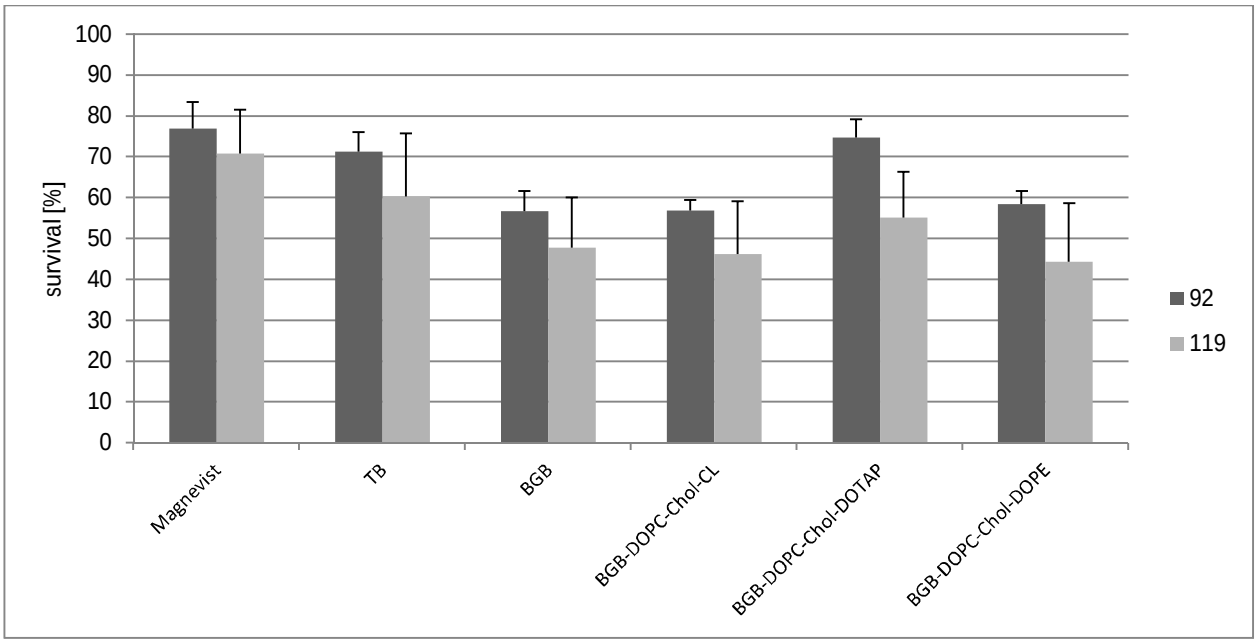

Figure 4-52 Survival of irradiated LN229 cells, fluence: $4.14 \cdot 10^{12}$ n/cm², 92 and 119h after irradiation. Survival is based on irradiated medium control, error bars present SD.

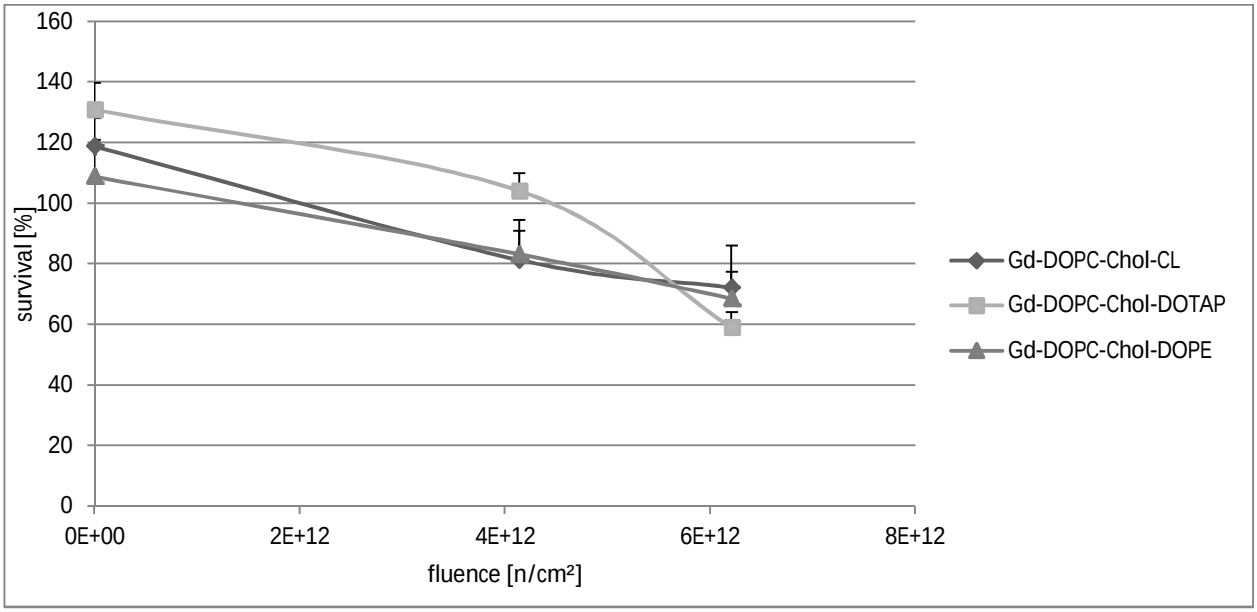

Figure 4-53 Survival curves of irradiated LN229 cells, 92h after irradiation, based on irradiated medium control.

4.6.2.6 *Irradiation experiments after cell treatment with main liposomal formulations of NC-element Gd-DTPA*

Neutron irradiation of F98 and LN229 cells with thermal neutrons, after application of liposomal NC-element formulations, was performed to study the effectiveness of liposomal carrier and gadolinium neutron capture treatment in glioma therapy. Five main liposomal formulations were tested, including cationic DOPC-Chol-DOTAP, fusogenic DOPC-DOPE and DOPC-Chol-DOPE, anionic DOPC-Chol-CL and the folate-targeted FolS-DOPC-Chol. All preparations were tested as blanks as well as loaded with Gd-DTPA (Magnevist®). Additionally, Magnevist® was tried for efficiency in survival reduction in three concentrations (Magnevist, Magnevist 0.5 and Magnevist 2, see table 20). Neutron fluence was $4.14 \cdot 10^{12}$ and $6.21 \cdot 10^{12}$ n/cm² and MTT was performed approximately every 24 hours after irradiation for four days. Irradiation took place 46-48 hours after plating of cells. Survival was calculated for each time point based on irradiated medium control. The Gd-containing formulations tested (either liposomal or 'free' Magnevist) are listed in table 20.

Table 20 Overview of tested liposomal and free Gd-containing formulations.

Formulation	Initial lipid concentration during extrusion [mg/ml]	Freeze-thaw preparation	GPC	Lipid concentration in wells [mg/ml]	Gd-concentration in wells [mg/ml]
DOPC-Chol-Cl 70:20:10	40	+	w	4	0.27
DOPC-Chol-DOPE 70:20:10	40	+	w	4	0.36
DOPC-Chol-DOTAP 57:33:9	40	+	w	4	0.47
DOPC-DOPE 50:50	40	+	w	4	0.46
FolS-DOPC-Chol 0.13:63:37	40	+	w	4	0.36
Magnevist 0.5	--	--	--	--	0.17
Magnevist	--	--	--	--	0.34
Magnevist 2	--	--	--	--	0.68

4.6.2.6.1 *Toxicity tests*

For toxicity assessment of liposomal NC-element-formulations and free Magnevist, non-irradiated, NC-element-treated cell groups were monitored over the same period as the irradiated cells. Survival values were calculated based on medium control and present the arithmetic mean from three points. In some

cases, the last time point (97 h after irradiation) was not reliable for toxicity assessment due to sudden turning points of the proliferation curves. Non-irradiated controls tended to grow very fast, especially if lipids and sugar-containing Magnevist®-solution were added to the medium. Therefore, media and space for the growing cells were depleted quickly, after which cells entered the plateau phase and died too early in the experiment. The data from these cells could be misleading in regard to cell survival. Consequently, the last time-point was not used for the toxicity tests and the survival was based mostly on irradiated cells (irradiated medium control) except for investigation of the radiation effect on cells alone.

Blank liposomes were non-toxic for both F98 and LN229 cells (fig. 4-54 A and 4-55 A). Similarly, Gd-loaded liposomes also proved to be biocompatible for the two cell lines (mean survival > 88% for F98 cells and > 90% for LN229 cells). The different Gd-containing formulations and their respective survival values are presented in figures 4-54 B and 4-55 B. The individual time points of liposome-treated cells were used as a basis for survival calculations regarding irradiation effect.

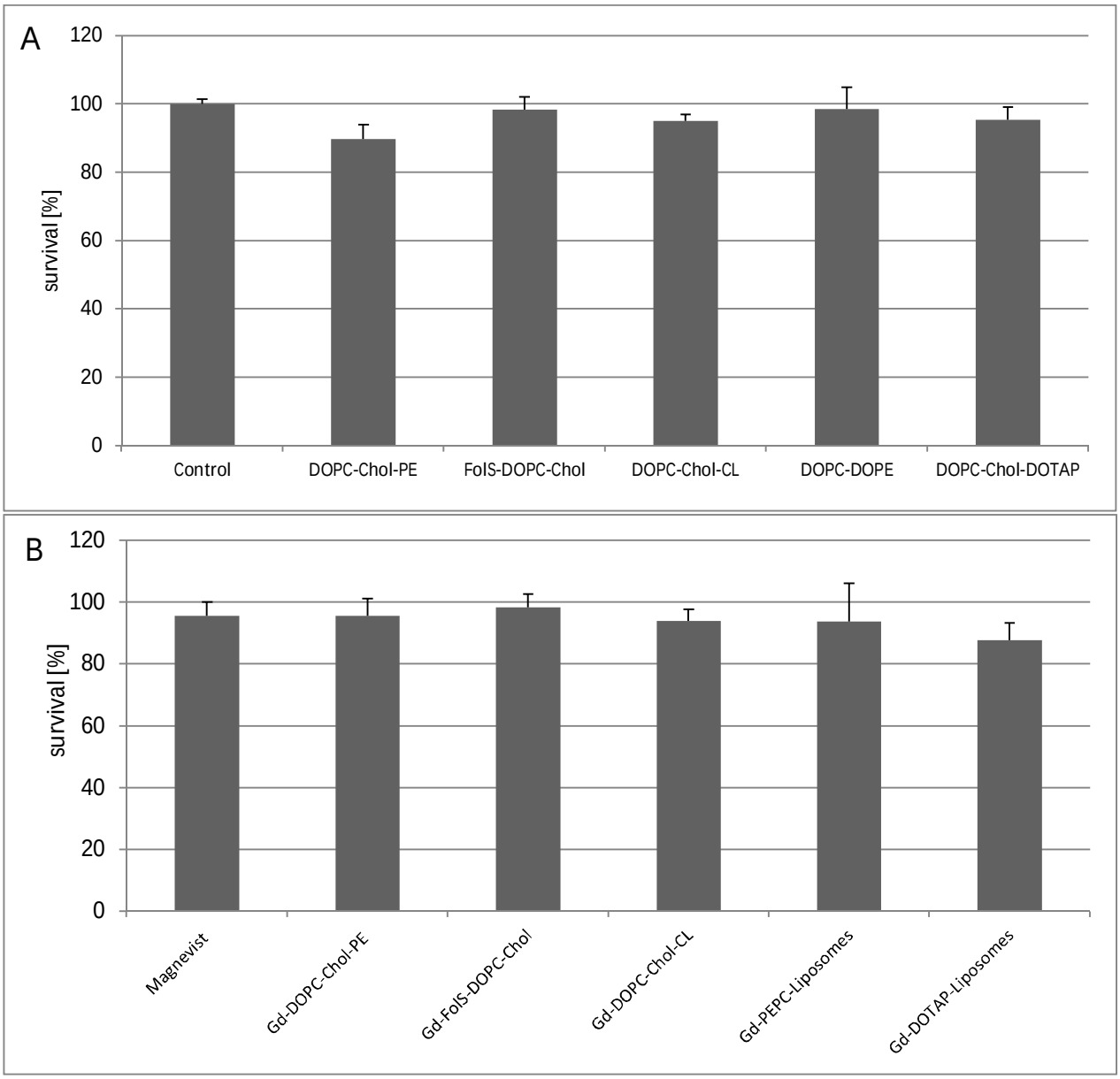

Figure 4-54 Toxicity values of F98 cells for A) blank liposomes, B) Gd-loaded liposome formulations, 3h incubation, arithmetic mean of three time points assessed with MTT assay.

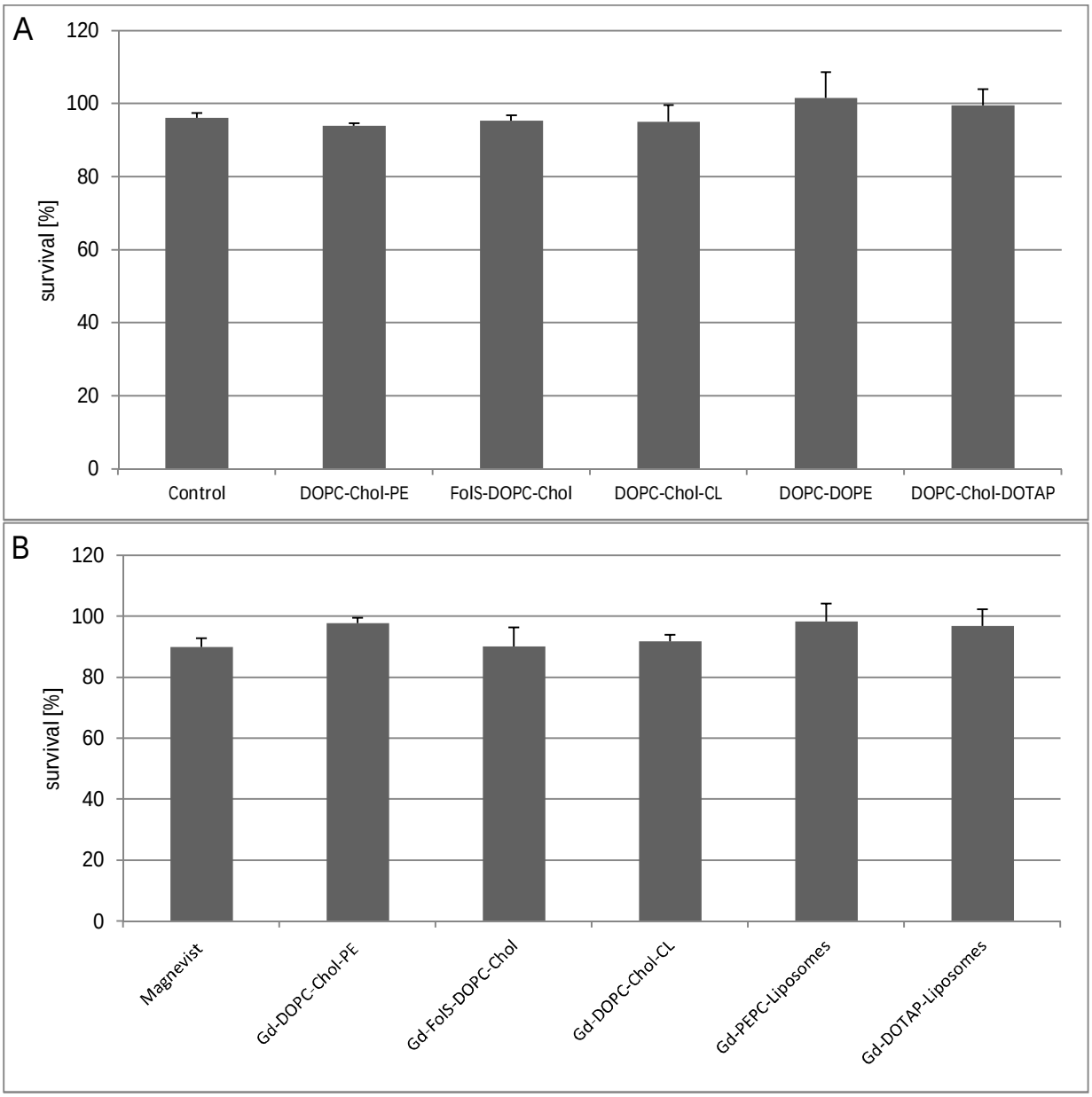

Figure 4-55 Toxicity values of LN229 cells for A) blank liposomes, B) Gd-loaded liposome formulations, 3h incubation, arithmetic mean of three time points assessed with MTT assay.

Two formulations and free Magnevist were chosen for a more thorough toxicity test (see fig. 4-56). Cells were incubated for 3, 8 and 24 hours with different concentrations of liposomes and Magnevist. For both cell lines, the cationic Gd-DOPC-Chol-DOTAP showed the highest toxicity with LD_{50} of approximately 2 mg lipid/ml during 24 h incubation. The folate liposomes caused less than 50% cell death for F98 cells in the tested range, but LN229 cells proved to be more sensitive against the formulation and revealed again a LD_{50} of 2 mg/ml for 24 hours incubation time. Nevertheless, the finally chosen incubation time of three hours with 4 mg/ml lipid remains still biocompatible, even for the higher doses of 6 mg lipid/ml (97% and 93% survival for treatment with folate-liposomes, 106% and 78% with DOTAP-formulation and 91% as well as 88% survival for free Magnevist solution, for F98 and LN229 cells, respectively).

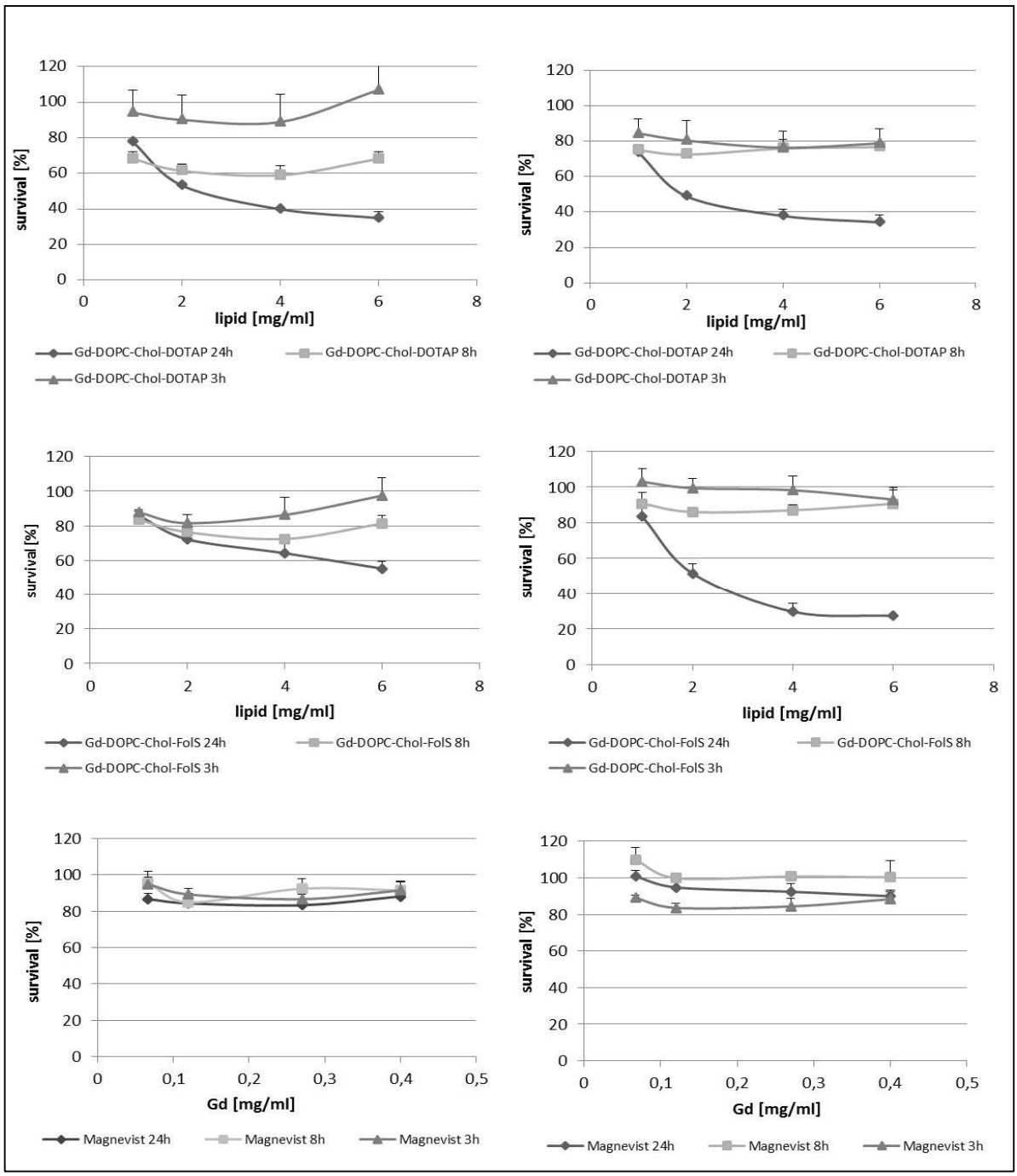

Figure 4-56 Toxicity of selected Gd-containing liposomes and free Magnevist in different concentrations, for incubation times of 3, 8 and 24 h. Left side: F98 cells, right side: LN229 cells.

4.6.2.6.2 Neutron irradiation of NC-element-treated glioma cells

As described above, cells were incubated with various preparations of NC-element Gd-DTPA and respective blanks and irradiated with neutron fluences of $4.14 \cdot 10^{12}$ or $6.21 \cdot 10^{12}$ n/cm². Cell survival as derived from MTT proliferation assay and calculated based on irradiated medium control was examined individually for time points 72 and 97 h after irradiation and for both neutron fluences. For F98 cells, cell survival of Gd-DOPC-DOPE- and Gd-DOPC-Chol-DOTAP- treated cells irradiated with $4.14 \cdot 10^{12}$n/cm² was significantly lower than survival of cells treated with Magnevist, Magnevist 2 and their respective blank

liposomes (fig. 4-57 A), 72h after irradiation). The higher neutron dose lead to significantly lower survival in comparison to Magnevist and Magnevist 2 for three Gd-containing formulations: Gd-FolS-DOPC-Chol, Gd-DOPC-DOPE and Gd-DOPC-Chol-DOTAP (fig. 4-57 B), 97 h after irradiation).

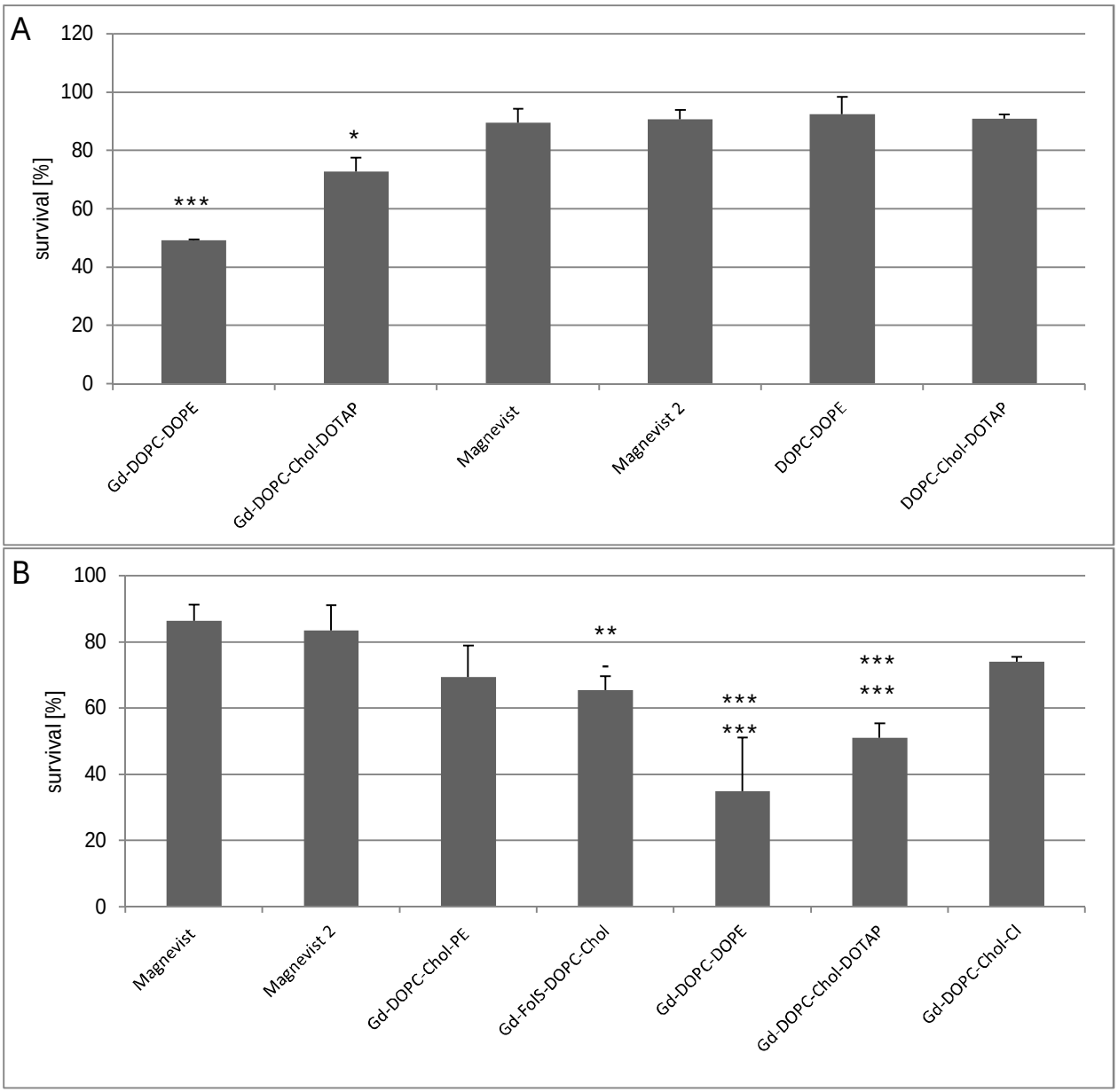

Figure 4-57 Survival of F98 cells after neutron irradiation. A) Fluence: $4.14 \cdot 10^{12}$ n/cm², 72 h after irradiation. B) Fluence $6.21 \cdot 10^{12}$ n/cm², 97 h after irradiation. Error bars present SD.

Figure 4-58 presents survival curves for F98 cells 72 (A) and 97h (B) after irradiation. While the graphs for Gd-containing formulations appear to be similar for the time point 72 h after irradiation, except for the cationic DOTAP and the fusogenic DOPC-DOPE-formulation, the curves grow more distinguished at the later time point. All of the Gd-containing liposomes lead to lower cell survival compared to free Magnevist for both neutron doses at 97 h after irradiation. However, Gd-DOPC-Chol-CL and Gd-DOPC-Chol-DOPE mixtures were not significantly superior to free Magnevist in the experiment. In contrast, the cationic liposomes and the DOPC-DOPE liposomes presented high effects on cell survival throughout all time points and doses. Table 21 shows survival values for irradiated cells in detail.

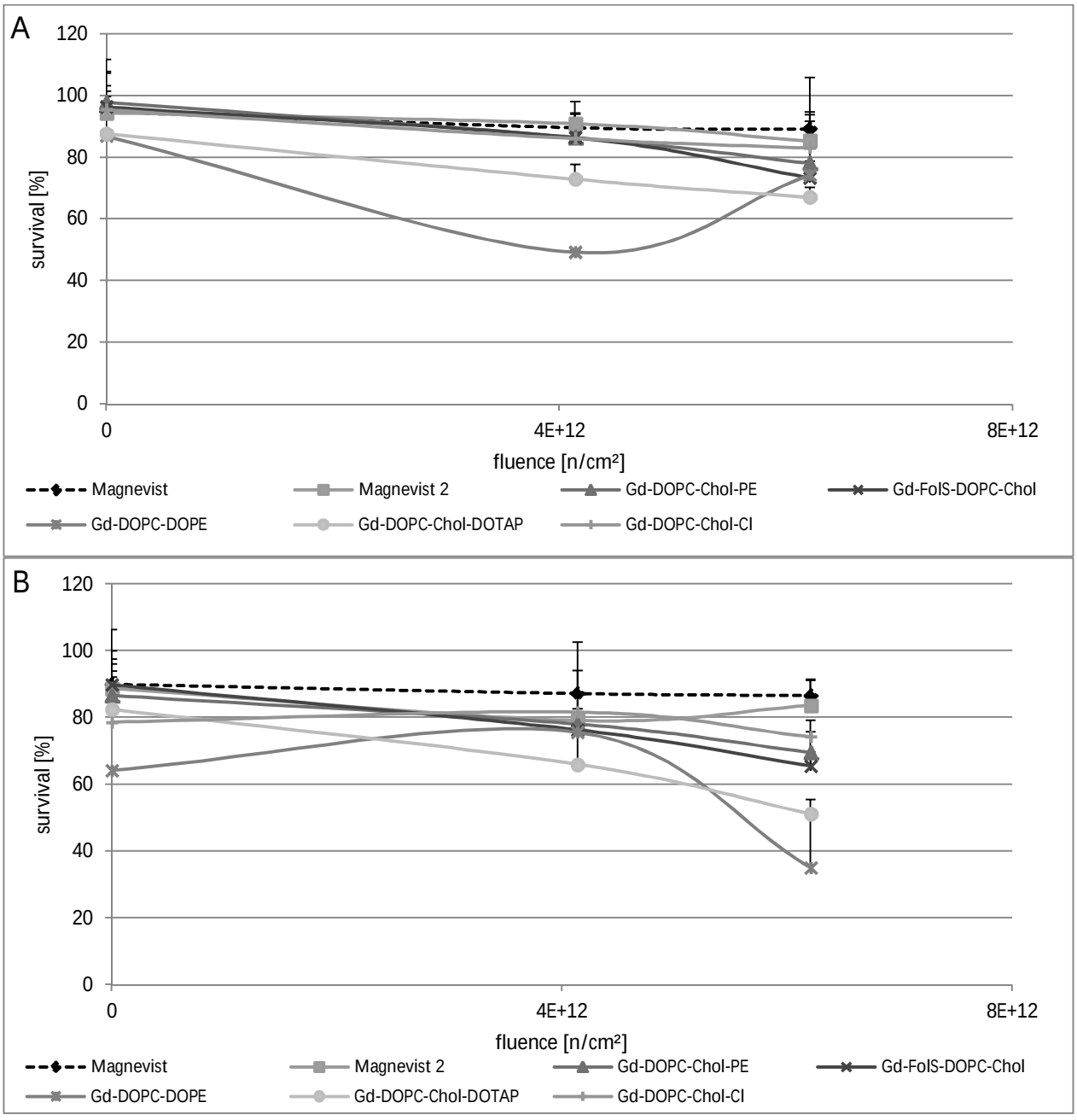

Figure 4-58 Survival curves of Gd-treated F98 cells A) time point 72 h after irradiation, B) 97 h after irradiation.

Table 21 Overview cell survial F98 after neutron irradiation, based on irradiated control.

MTT time point	72 h		97 h	
Fluence [n/cm²]	$4.14 \cdot 10^{12}$	$6.21 \cdot 10^{12}$	$4.14 \cdot 10^{12}$	$6.21 \cdot 10^{12}$
Magnevist	89.6 ± 4.7	89.2 ± 5.4	87.2 ± 4.8	86.6 ± 4.8
Gd-DOPC-Chol-PE	86.4 ± 4.8	78.1 ± 0.6	78.6 ± 4.5	69.5 ± 9.5
Gd-FolS-DOPC-Chol	86.3 ± 11.6	73.4 ± 3.9	76.3 ± 4.6	65.5 ± 4.2
Gd-DOPC-DOPE	49.2 ± 0.4	74.2 ± 31.5	75.5 ± 26.9	34.9 ± 16.2
Gd-DOPC-Chol-DOTAP	72.9 ± 4.7	67.0 ± 3.1	66.0 ± 8.8	51.2 ± 4.3
Gd-DOPC-Chol-Cl	86.0 ± 6.0	83.0 ± 10.8	81.6 ± 5.8	74.2 ± 1.4
Magnevist 2	90.8 ± 3.0	85.3 ± 6.3	79.1 ± 1.4	83.6 ± 7.5
Magnevist 0.5	91.1 ± 4.4	90.4 ± 8.2	77.7 ± 4.9	85.3 ± 4.8

LN229 cells react very similar to F98 cells, when treated with Gd-DOPC-Chol-DOTAP or Gd-DOPC-DOPE liposomes before neutron irradiation. A fluence of $4.14 \cdot 10^{12}$ n/cm² leads then to significant lower survival compared to Magnevist and the respective blank liposomes for all four time points (fig. 4-59, A)). At the higher neutron dose, only Gd-DOPC-DOPE liposomes proved to be significantly better than free Magnevist for both 72 and 97 h after irradiation.

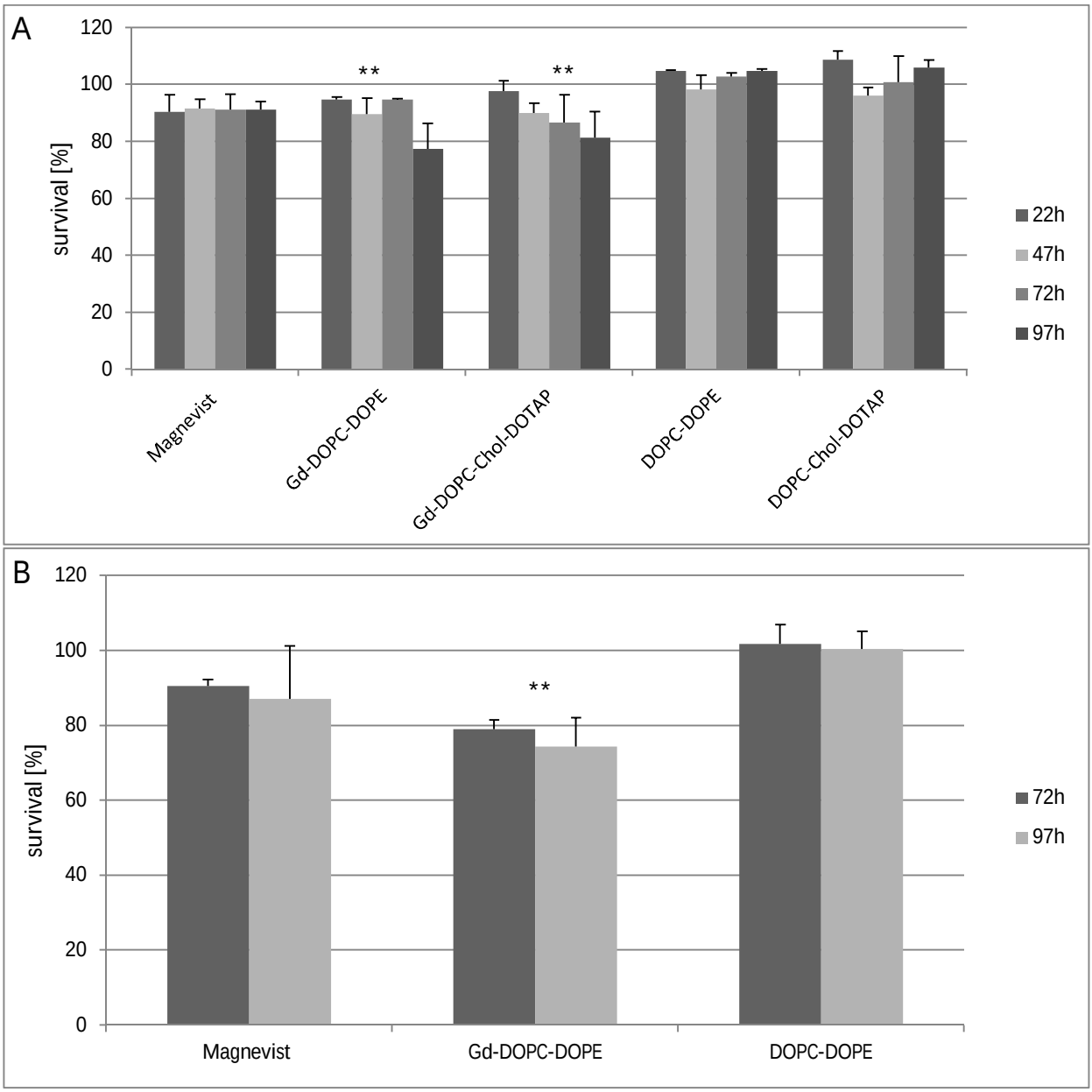

Figure 4-59 Survival data of irradiated LN229 cells, based on irradiated control. A)Fluence: $4.14 \cdot 10^{12}$ n/cm², all time points. B) $6.21 \cdot 10^{12}$ n/cm², 72 and 97h after irradiation. Error bars represent SD.

Regarding the complete survival curves, the liposomal formulations differ only slightly from free Magnevist (fig. 4-60). Especially after 72 h, the curves show very little effect for the liposomal Gd on cell survival. However, after more cell divisions, the distinction becomes clearer: of the five Gd-liposome formulations, Gd-FolS-DOPC-Chol, Gd-DOPC-Chol-DOTAP and Gd-DOPC-DOPE lead to lower cell survival than free Magnevist. While the folate-containing formulation did not accomplish a distinctly superior outcome, both the cationic and the fusogenic formulation improved the irradiation effect on LN229 cells considerably. Detailed values are presented in table 22.

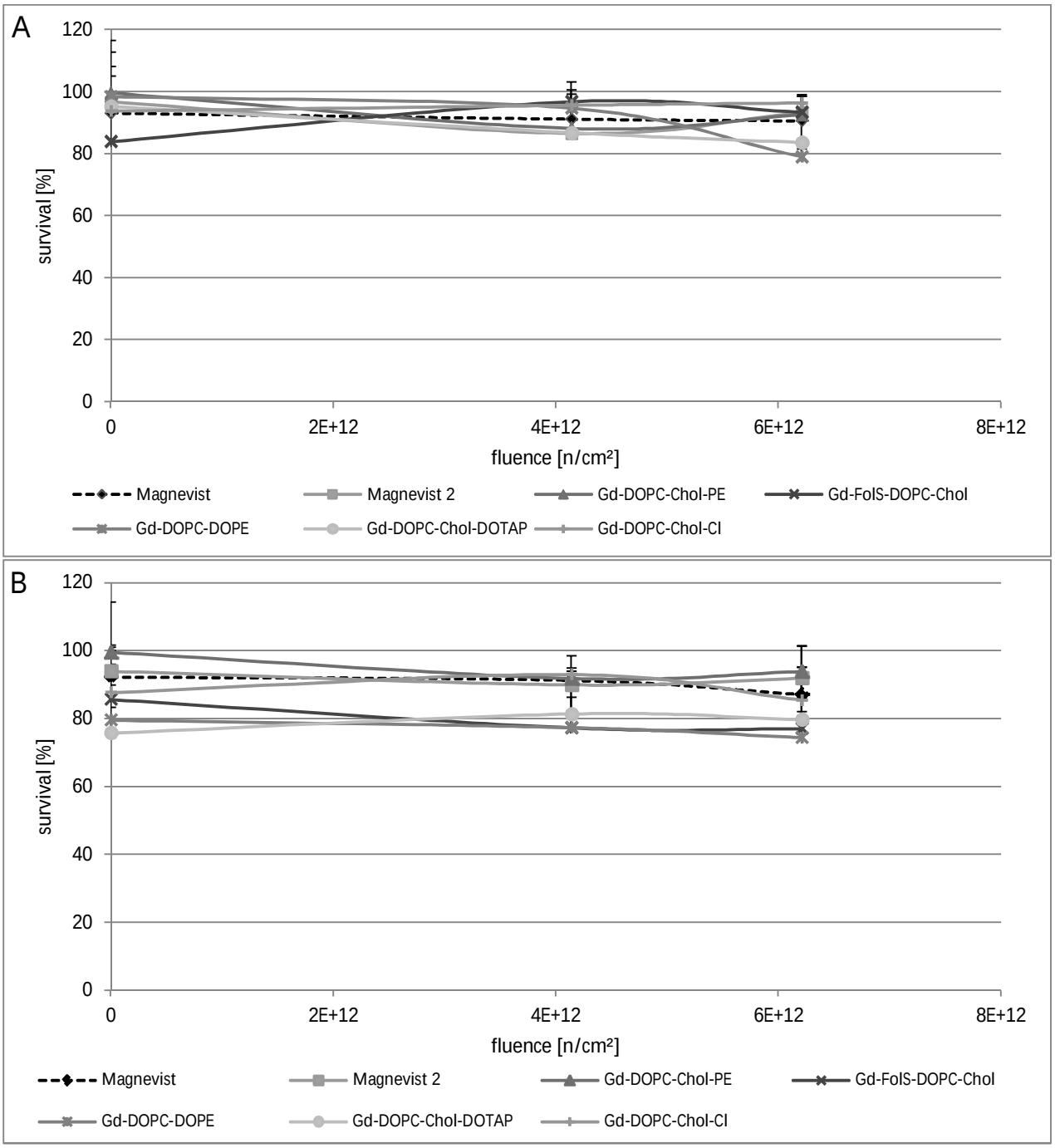

Figure 4-60 Survival curves of LN229 cells, based on irradiated control. A) At time point 72 h after irradiation. B) Time point 97 h after irradiation.

Table 22 Survival values for neutron irradiated LN229 cells, based on respective irradiated medium control.

MTT time point	72 h		97 h	
Fluence [n/cm²]	$4.14 \cdot 10^{12}$	$6.21 \cdot 10^{12}$	$4.14 \cdot 10^{12}$	$6.21 \cdot 10^{12}$
Magnevist	91.1 ± 5.4	90.6 ± 1.7	91.3 ± 2.6	87.1 ± 14.1
Gd-DOPC-Chol-PE	96.8 ± 3.8	92.5 ± 1.8	91.9 ± 3.1	93.9 ± 7.6
Gd-FolS-DOPC-Chol	86.5 ± 16.6	93.3 ± 5.1	77.3 ± 11.1	77.1 ± 9.0
Gd-DOPC-DOPE	94.7 ± 0.3	79.0 ± 2.4	77.4 ± 8.9	74.4 ± 7.6
Gd-DOPC-Chol-DOTAP	86.8 ± 9.6	83.6 ± 7.7	81.4 ± 8.9	79.8 ± 15.5
Gd-DOPC-Chol-Cl	95.6 ± 3.5	96.4 ± 2.6	93.0 ± 5.5	85.5 ± 6.2
Magnevist 2	88.2 ± 5.3	94.2 ± 11.5	90.0 ± 3.2	91.9 ± 3.0
Magnevist 0.5	89.9 ± 3.3	95.6 ± 5.4	91.5 ± 2.8	93.3 ± 3.0

4.6.2.6.3 Analysis of different factors affecting cell survival

The design of the experiments allows an interpretation of the survival outcome with regard to several basic aspects. The main principles of interest are the effect of the NC-Element, the absolute damage due to the radiation and the influence of liposomal carrier for the improvement of drug transport into the cancer cell. To gain information on these aspects, cell survival was calculated based on different controls. For the effect of radiation, survival was related to non-irradiated control treated with the same formulation, the Gd-influence was calculated referring to irradiated blank liposome or medium control and the overall effect of the treatment was gained from the differences between irradiated formulations and non-irradiated medium control. The role of the liposomal transporter can be observed from the divergence between formulations (liposomal Gd versus free Gd). For most experiments, the survival data presented was based on irradiated medium control. Thus, only the effect of the NC-element Gd-DTPA under neutron irradiation is shown, while the basal irradiation effect is already subtracted from the survival.

Table 23 gives an overview of different aspects of survival calculated for F98 cells. A to D represent the variations used in calculation of survival:

A) Survival = irradiated Gd-containing formulation/irradiated blank liposome (or medium in case of free Magnevist)

B) Survival = irradiated Gd-containing formulation/ non-irradiated Gd-containing formulation or free Magnevist

C) Survival = irradiated Gd-containing formulation/ non-irradiated medium control

D) Survival = irradiated Gd-containing formulation/ irradiated medium control

Equation A) gives back the impact of Gd as NC-element, corrected for possible toxicity of the blank liposome and the basal radiation effect and B) accounts for the radiation and Gd-effect which is corrected for the toxicity of the Gd-containing liposomes. Equation C) displays the overall effect of cell irradiation with NC-element Gd without any corrections, while D) gives the result of Gd-influence corrected for the 'underlying' radiation dose (i.e. basal radiation effect). As expected, calculation with equation C) results normally in the lowest survival value for tested formulations, although there are some exceptions for the earlier time point. Equation B also leads to small values, which may account for high cell proliferation of non-irradiated Gd-containing formulations. If the OD at MTT assay of these cells is higher than for medium control, the survival calculated with B will be lower than for C. Results from A and D should be comparable, if the toxicity of the blank formulation is negligible. In most cases, the difference of both values is smaller than 10% and therefore, correlates with the very low cytotoxic effects observed in the toxicity tests. Only for Gd-DOPC-DOPE at the higher dose and 97 h after irradiation is the discrepancy higher than 20%, although the toxicity tests proved the formulation to be biocompatible. It is possible, that the irradiation procedure also has an impact of the blank liposomal carrier, for example may lipids be oxidized or radicals may be generated, thus leading to cell damage originated by the liposomes. If this is the case, the survival calculated via equation A will naturally lead to higher values than C, because these lesions are already accounted for in the evaluation in A though not in C.
The revision of the calculated values gave comparable results for the tested formulations at each time point and neutron dose. To verify if the collected data is in accordance with the real conditions in cells, the data from toxicity studies, the underlying radiation effect (medium irradiated/-medium non-irradiated) and the Gd-effect (from equation A) were multiplied. These survival values were based on different controls (non-irradiated medium and irradiated blank formulation). Theoretically, this calculation should give the value derived from equation C, which is based on its respective irradiated control. In fact, as presented in table 24, the results from both calculations differ only little, in most cases, the variation is less than 6%. This indicates that the survival values presented here are quite harmonious in spite of the inter-plate differences and the variations between wells and that they reflect the actual situation in the glioma cell model very well.

In summary, the analysis of different survival values giving credit to various factors such as radiation effect alone, toxicity of liposomal carriers and the impact of Gd-DTPA as a NC-element proved useful for the review and verification of the collected data.

Table 23 Overview over different survival calculations for F98 cells after neutron irradiation.

	72h				97h			
$4.14 \cdot 10^{12}$ n/cm²	A	B	C	D	A	B	C	D
Magnevist 0.5	91.1	88.9	84.2	91.1	77.7	67.9	59.0	77.7
Magnevist	89.4	83.4	85.0	89.6	84.5	87.3	70.8	87.2
Magnevist 2	90.8	89.7	83.1	90.8	79.1	68.5	62.9	79.1
Gd-DOPC-Chol-DOPE	91.7	88.0	85.9	86.4	86.4	85.8	74.5	78.0
Gd-FolS-DOPC-Chol	91.4	87.5	87.7	86.3	82.3	78.9	66.3	76.3
Gd-DOPC-DOPE	53.3	32.5	41.5	49.2	87.0	73.6	70.8	75.5
Gd-DOPC-Chol-DOTAP	79.7	67.1	60.7	72.9	74.1	85.5	59.5	66.0
Gd-DOPC-Chol-CL	94.8	81.0	77.9	86.0	92.2	83.1	62.2	81.6
$6.21 \cdot 10^{12}$ n/cm²	A	B	C	D	A	B	C	D
Magnevist 0.5	90.3	79.9	81.0	90.4	83.8	77.2	66.6	85.3
Magnevist	85.2	67.3	71.7	89.2	80.9	69.0	63.8	86.6
Magnevist 2	85.4	76.6	78.4	85.3	84.4	75.2	68.7	83.6
Gd-DOPC-Chol-DOPE	81.0	62.5	61.2	78.1	79.6	67.9	58.9	69.5
Gd-FolS-DOPC-Chol	83.4	66.7	68.7	73.4	80.8	62.2	52.5	65.5
Gd-DOPC-DOPE	66.7	53.9	73.7	74.2	56.2	40.3	34.5	34.9
Gd-DOPC-Chol-DOTAP	72.2	54.0	44.0	67.0	56.1	50.2	34.1	51.2
Gd-DOPC-Chol-CL	94.0	64.8	62.1	83.0	84.4	79.9	59.7	74.2

Table 24 Comparison of survival calculated from toxicity, Gd-and irradiation effect based on different controls and survival based on irradiated control.

72h		97h	
Calculated survival value (toxicity·radiation effect·Gd-effect (A))	Survival value based on irradiated control (from equation C)	Calculated survival value (toxicity·radiation effect·Gd-effect (A))	Survival value based on irradiated control (from equation C)
$4.14 \cdot 10^{12}$ n/cm²		$4.14 \cdot 10^{12}$ n/cm²	
81.0	84.2	61.7	59.0
79.6	85.0	67.1	70.8
79.1	83.1	61.5	62.9
81.5	85.9	68.6	74.5
83.7	87.7	67.3	66.3
46.5	41.5	67.7	70.8
65.0	60.7	53.9	59.5
82.9	77.9	71.9	62.2
$6.21 \cdot 10^{12}$ n/cm²		$6.21 \cdot 10^{12}$ n/cm²	
71.7	81.0	61.7	66.6
67.7	71.7	59.6	63.8
66.4	78.4	60.9	68.7
64.3	61.2	50.0	58.9
68.2	68.7	61.3	52.5
51.9	73.7	40.6	34.5
52.6	44.0	34.4	34.1
73.3	62.1	57.8	59.7

4.6.2.6.4 Gadolinium dose calculations via Monte Carlo simulation

Since the neutron capture event should provide most of the dose absorbed in cells, the Gd-dose was calculated based on Monte-Carlo simulation. With respect to the actual Gd-content in the medium, the dose was calculated for each well individually, always including the influence of the environment (i.e. the presence of Gd or medium without additives in adjacent wells).

The Gd-containing liposomes differed slightly in their actual Gd-content, as encapsulation efficiency had different values for each formulation. Figure 4-61 presents the dose derived from Gd, neutrons and photons for each well at the two fluences and for different pipetting schemes (cf. figure 4-46) of the liposome formulations. The exact position of the plate in the stack, the arrangement of the formulations and their respective Gd-content (as measured by ICP-MS, cf. section 4.4) are accounted for in the resulting dose.

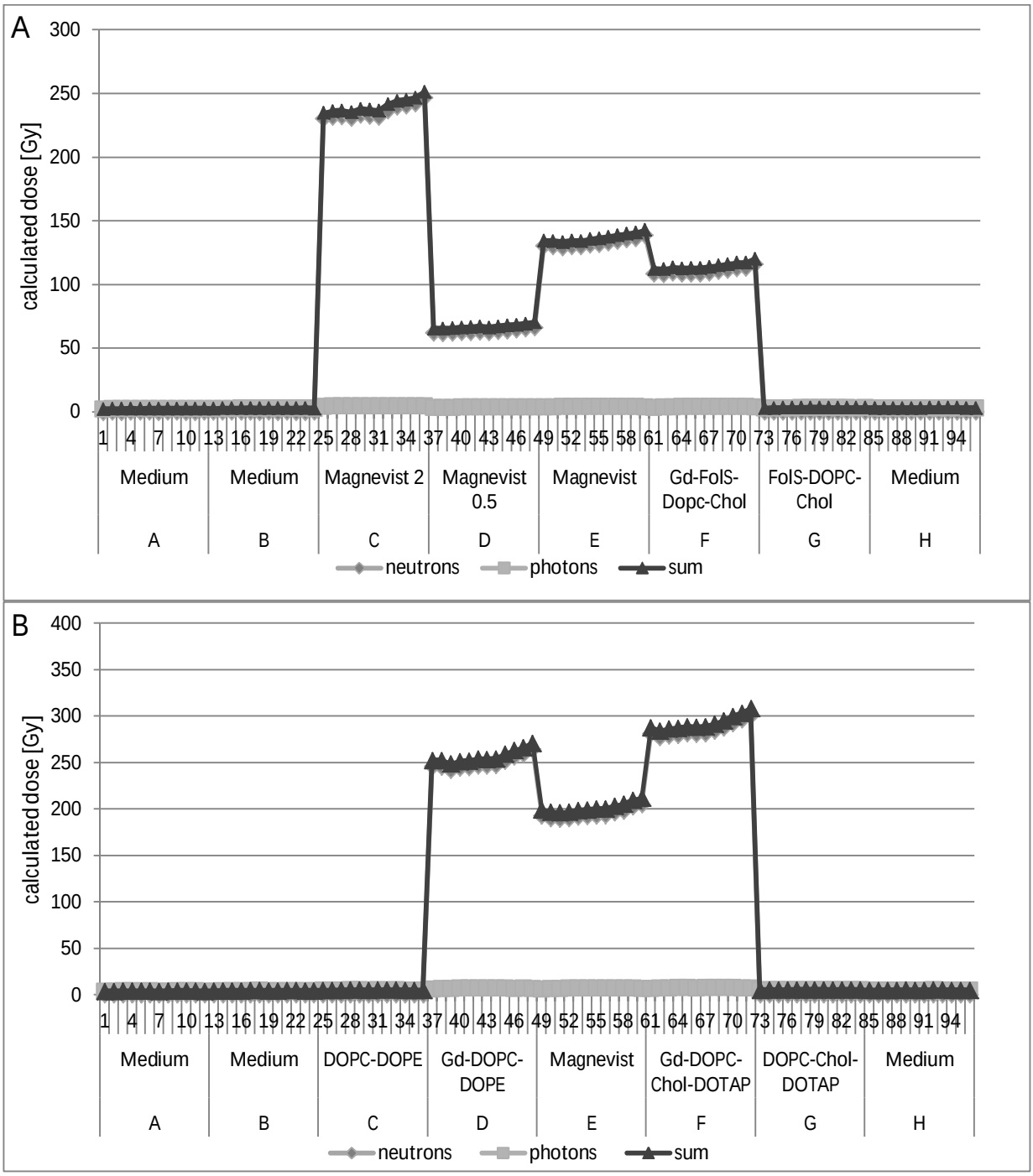

Figure 4-61 Dose calculation for 96 well plates with different formulations, based on Gd-content, neutron dose and photon dose. A) $4.14 \cdot 10^{12}$ n/cm², pipetting scheme 1.B) $6.21 \cdot 10^{12}$ n/cm², scheme 2.

The calculated dose distribution over the wells is very high for Gd-containing formulations. The dose ranges here from 65 to 300 Gy in wells, based on the amount of Gd in the medium above the cells. However, the glioma cells are not killed immediately by this high dose, due to the relatively low uptake of Gd into the cellular body. Although the long-range gamma rays from the Gd-neutron capture event were indeed transported from their origin to the neighboring wells as expected, their energy was still attributed to the calculated dose in the wells of their origin by the Monte Carlo simulations-program, MCNP5. In reality, the total dose in the wells is therefore lower than it appears here, while the relationship between Gd-content and the Gd-derived dose is unaltered. Figure 4-62 displays the

difference in Gd-attributed dose for the whole well and for the amount taken up by an average of 10^6 cells. Values are given in table 25. Based on the Gd amount found in cells by ICP-MS measurement, the Gd-related dose which is generated inside the cell is very small in comparison (approximately 1/1000 of the total dose); even though in case of the cationic DOTAP-formulation, more than 1900 ng Gd were carried into the cells. This amount still accounts for about 5 Gy at $6.21 \cdot 10^{12}$n/cm². In contrast, non-encapsulated Magnevist only delivers a dose of 0.06 Gy to the cells.

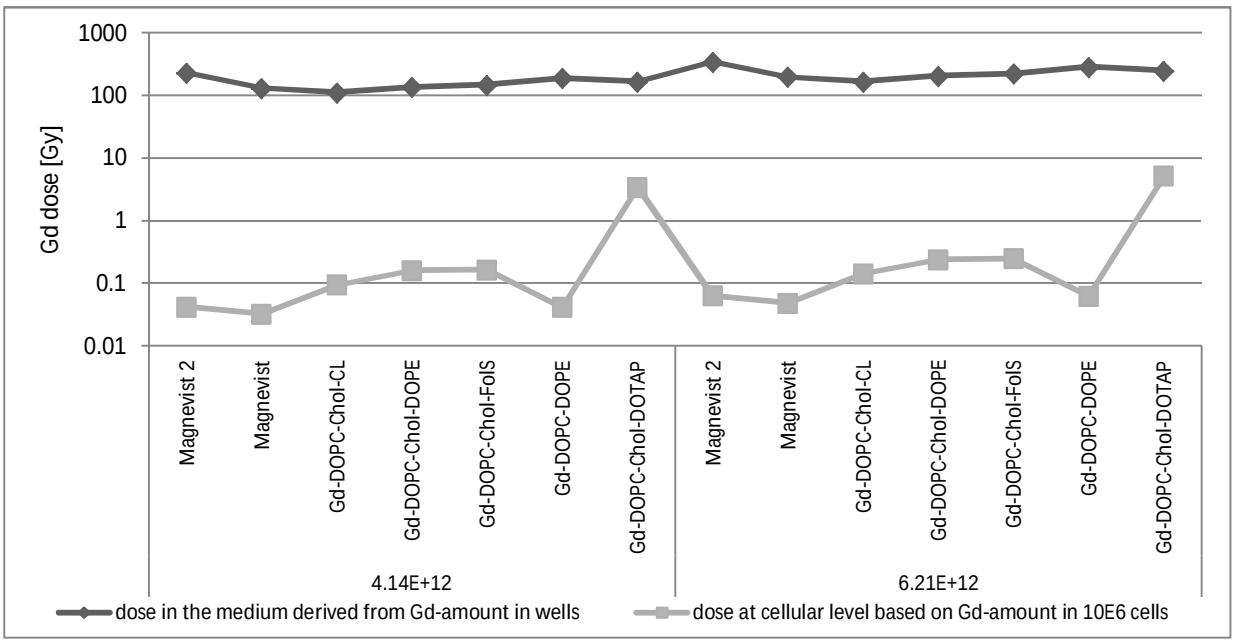

Figure 4-62 Comparison of total Gd-related dose per well (total Gd-amount in media) and dose inside cells based on Gd-uptake into 10^6 F98 cells.

Table 25 Gd-derived dose per formulation for neutron irradiation

Fluence [n/cm²]	Formulation	dose in wells (based on total Gd-amount in medium) [Gy]	dose in cells (based on Gd-amount taken up into 10^6 cells) [Gy]
$4.14 \cdot 10^{12}$	Magnevist 2	230.91	0.04
	Magnevist	131.54	0.03
	Gd-DOPC-Chol-CL	111.01	0.10
	Gd-DOPC-Chol-DOPE	136.63	0.16
	Gd-DOPC-Chol-FolS	148.04	0.16
	Gd-DOPC-DOPE	189.41	0.04
	Gd-DOPC-Chol-DOTAP	166.27	3.44
$6.21 \cdot 10^{12}$	Magnevist 2	346.37	0.06
	Magnevist	197.31	0.05
	Gd-DOPC-Chol-CL	166.51	0.14
	Gd-DOPC-Chol-DOPE	204.94	0.24
	Gd-DOPC-Chol-FolS	222.05	0.25
	Gd-DOPC-DOPE	284.11	0.06
	Gd-DOPC-Chol-DOTAP	249.40	5.16

4.6.2.6.4.1 Correlation between cell survival and different concentrations of free Magnevist

The observed differences in cell survival were considered to depend primarily on the Gd-dose delivered to the glioma cells from intracellular Gd. For the correlation of survival and Gd-content, the overall neutron effect on nitrogen and other isotopes was excluded from survival calculations by the use of irradiated medium as a control.

A preliminary experiment examined the relationship of cell survival and different concentrations of Gd in the medium, while the actual Gd-content in cells was not measured. The correlation of cell survival with different concentrations of free Magnevist (Gd-DTPA) per well shows a homogenous survival curve for both cell lines (fig. 4-63). For F98 cells, the curve shape clearly follows the linear-quadratic model with a small shoulder region at lower Gd-concentrations (representing lower dose) and a declining curve for slightly higher concentrations. In contrast, LN229 cells follow a more linear decline after irradiation with the higher neutron dose. The lower dose does not lead to a continuous decrease in survival. Nevertheless, the results indicate a relationship between Gd-concentration and cell survival which follows at least the exponential part of the linear-quadratic model for survival curves.

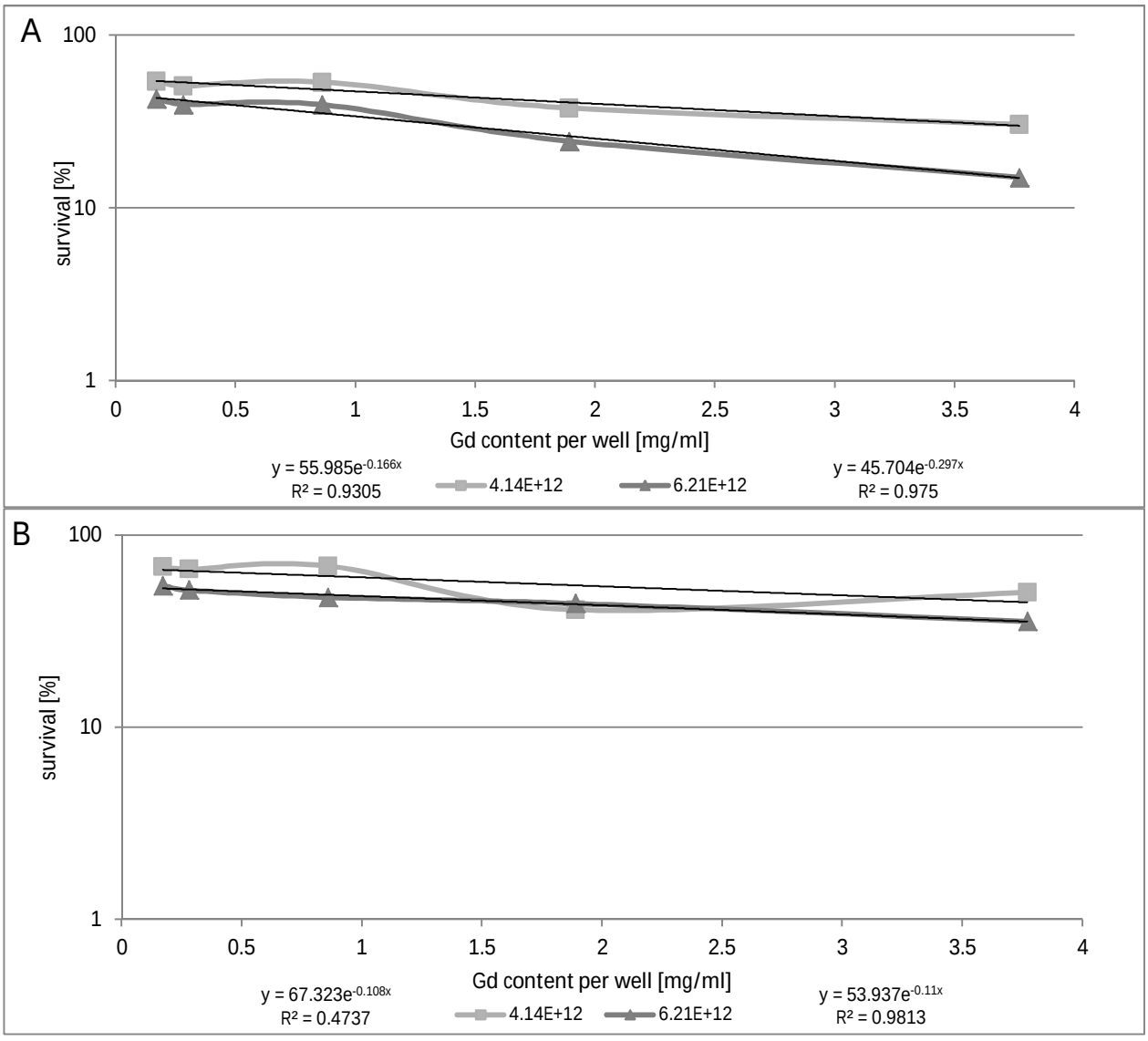

Figure 4-63 Survival curves of F98 (A) and LN229 (B) cells, treated with different concentrations of Gd and irradiated with $4.14 \cdot 10^{12}$ and $6.21 \cdot 10^{12}$ n/cm², 72 h after irradiation, incubation time 3 h.

4.6.2.6.4.2 Correlation of cellular Gd-content and respective survival after neutron irradiation

Since the experiment described above revealed a good correlation between Gd-concentration per well and survival of cells after irradiation, the next step was to study the relationship between the actual Gd-amount taken up into cells and their respective cell survival.

First, the Gd-amount per well for the administered liposomal formulations and free Magnevist® and the respective cell survival was analyzed for the past neutron irradiation experiments. Figure 4-64 shows Gd-content per well plotted against cell survival in the respective wells. Surprisingly, there seemed to be no connection between Gd concentration in the medium and cell survival, in contrast to the previous results with free Magnevist. The attempt to fit the Gd-concentration and survival data with an exponential model led to very poor correlation with coefficients (R^2) below 0.3.

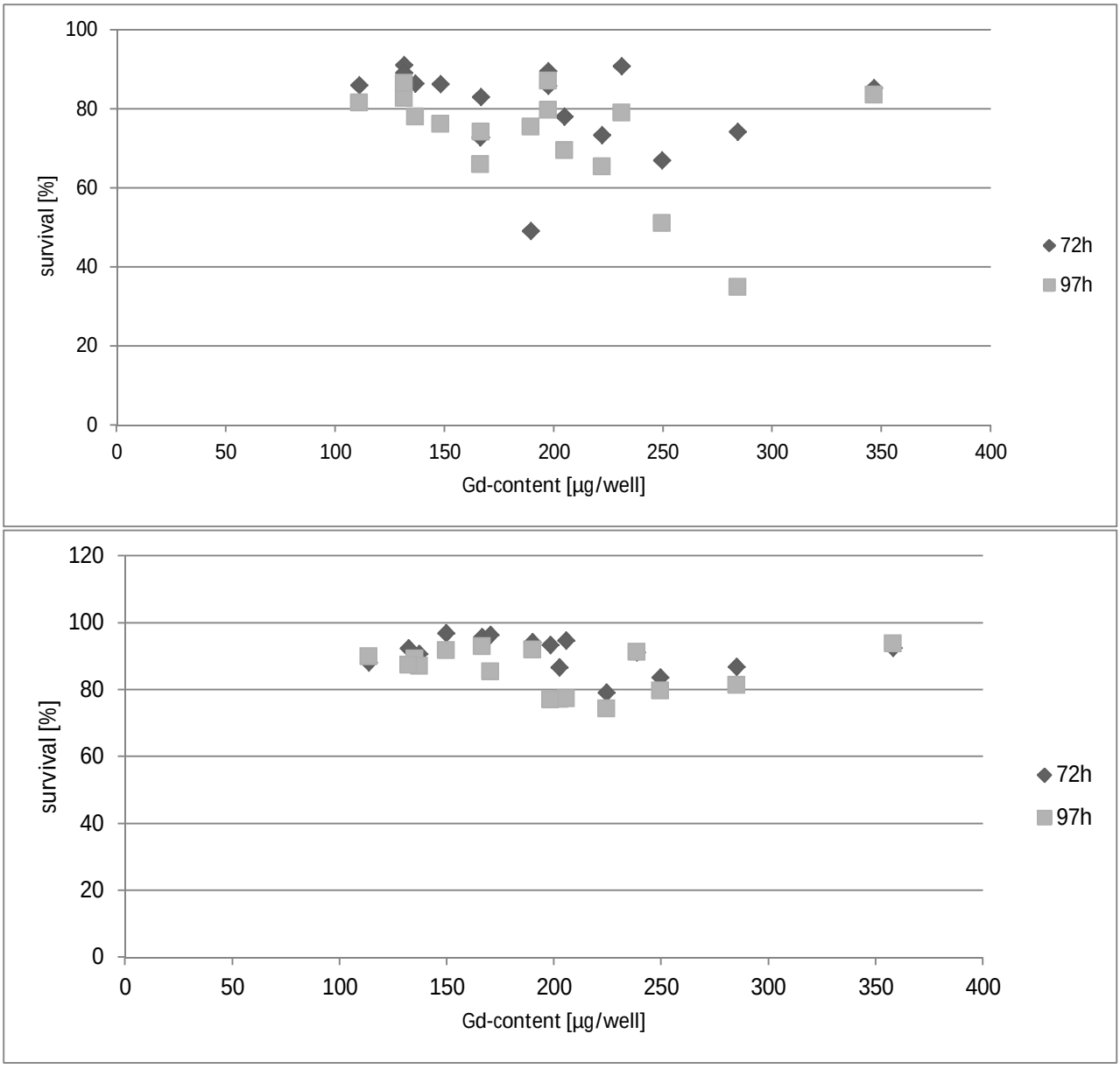

Figure 4-64 Correlation of Gd-content per well and respective cell survival (based on irradiated control). A) F98 cells, B)LN229 cells.

The next step was to correlate the actual Gd-concentration in cells and survival after irradiation. The resulting graphs are presented in figure 4-65. The amount of Gd delivered into cells by liposomes as measured by ICP-MS, was transformed to resulting dose and plotted against the survival of cells treated with the respective formulation. Both neutron doses were included. Although the curves decline for higher doses, the initial part which should follow the linear dose-dependency typical for lower radiation doses is not linear and in some cases, does not decline either (e.g. MTT at 22 h after irradiation, A). This phenomenon is due to a discrepancy in formal Gd-dose delivered to the cells and respective survival. In case of, for example Gd-DOPC-DOPE-liposomes, the uptake into cells is relatively small (20 ng Gd for F98 cells), nonetheless, the survival was reduced to less than 36 per cent. On the other hand, the high amount of Gd carried by DOTAP-liposomes (1900 ng) did not achieve this degree of viability reduction; the resulting survival was still 51 per cent of the control.

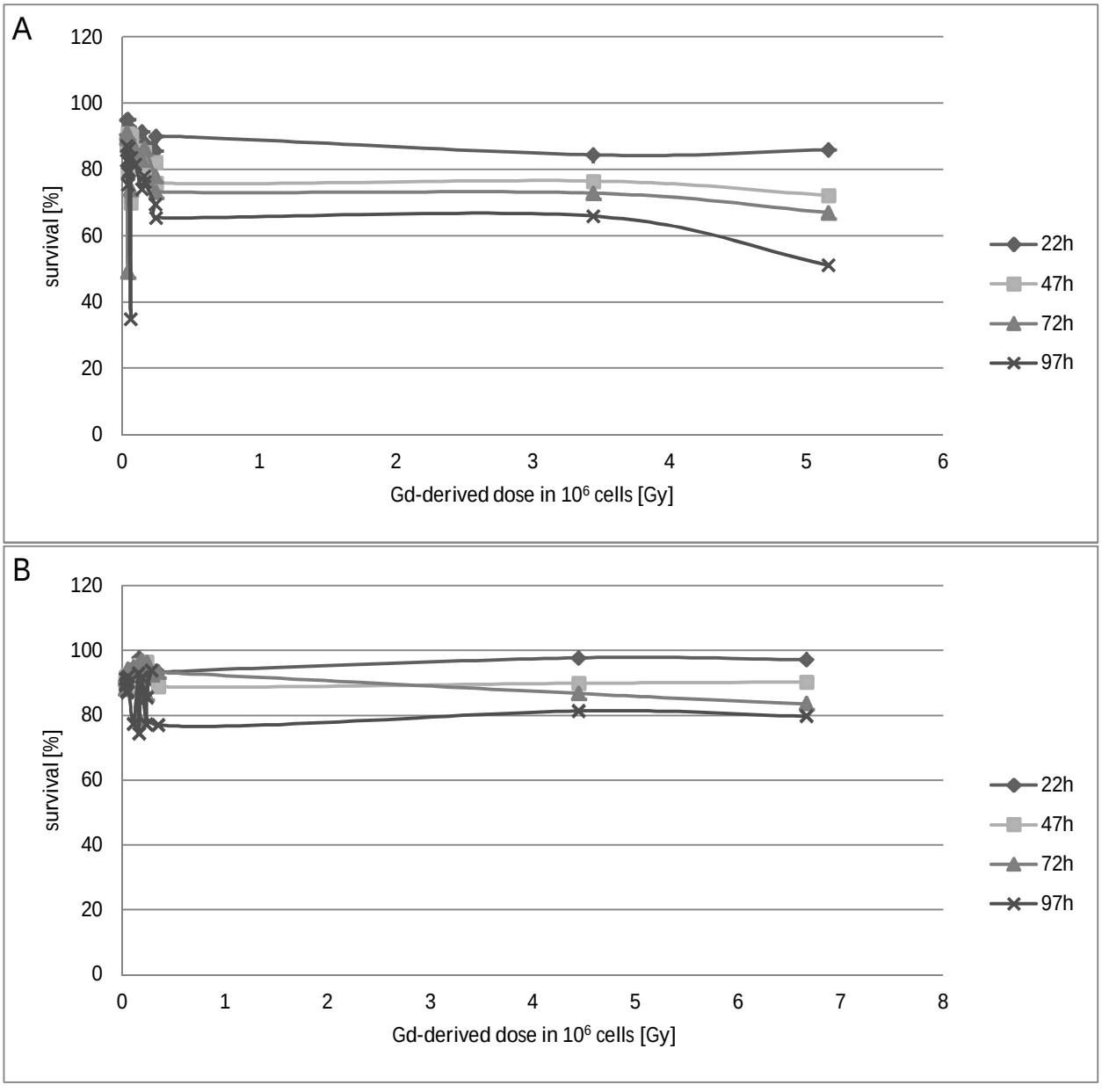

Figure 4-65 Correlation of Gd-related dose, based on Gd-amount taken up into 10^6 cells, and cell survival for all four time points (22, 47, 72 and 97 h after irradiation). A) F98 cells, B) LN229 cells.

Since the Gd-DOPC-DOPE and Gd-FolS-DOPC-Chol survival values were uncommonly low while the delivered Gd-amount was also small, these two pairs were excluded from correlation fitting. Then, the analysis of cell survival against Gd-derived dose in cells allows a simple exponential fit of the curves with good and acceptable coefficients of determination for F98 and LN229 cells, respectively. Resulting trendlines and equations are presented in figure 4-66. Graphs were fit to the exponential part of the linear-quadratic model with the survival being a function of *e* ($S = e^{-D/Do}$), because the doses applied were relatively low and the original model led to poor correlation.

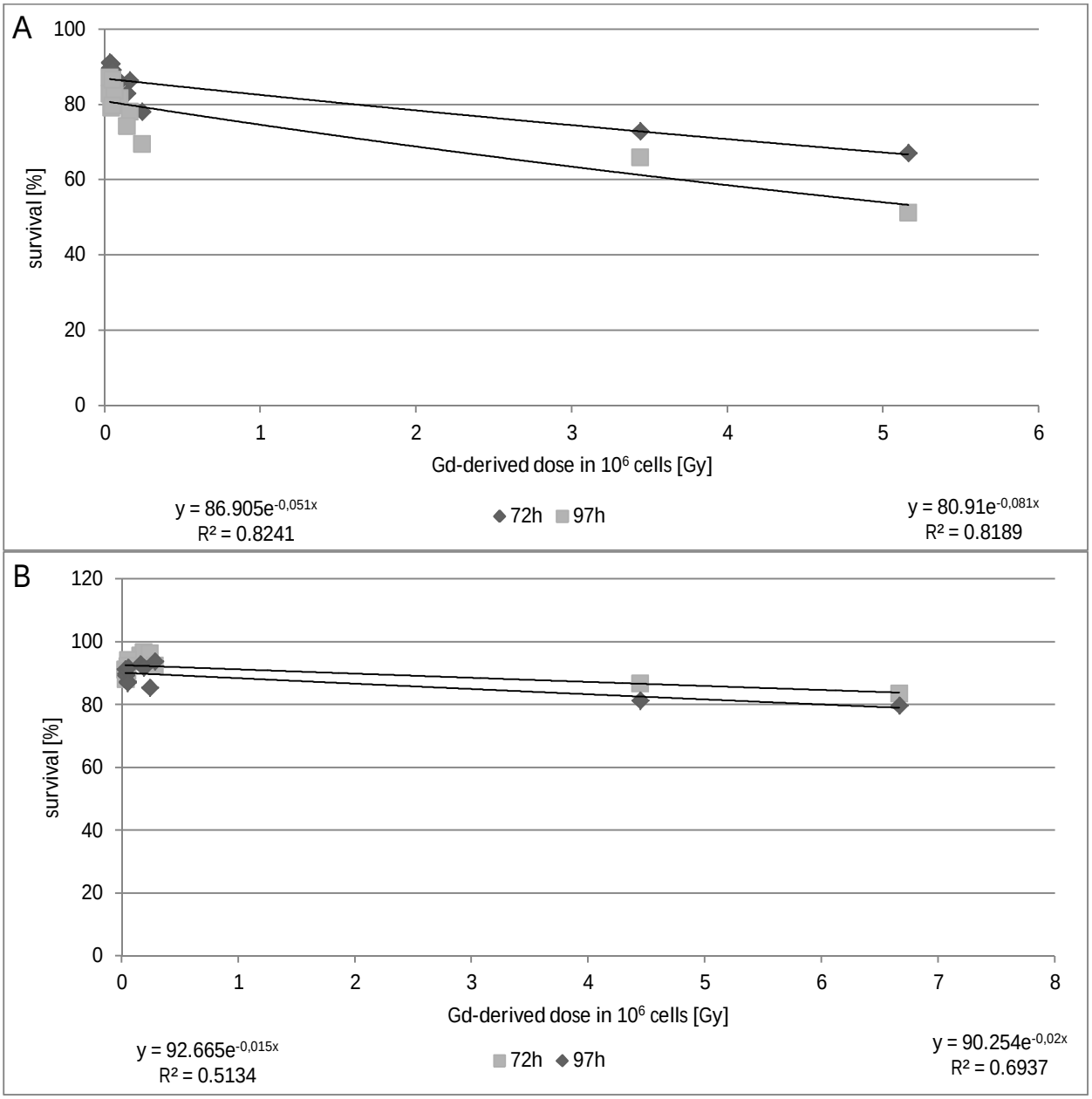

Figure 4-66 Correlation of Gd-related dose, based on Gd-amount taken up into 10^6 cells, and their respective survival. A) F98 cells, B) LN229 cells.

In summary, the survival curves derived from a single kind of formulation, free Magnevist alone in different concentrations, display a more homogenous shape with high similarity to survival curves following the linear-quadratic model and a good fit for exponential equation. On the contrary, the resulting survival curve from different liposomal formulations and free Magnevist could only be fitted to the linear part of the linear-quadratic model after two pairs of values were removed. The formulations Gd-DOPC-DOPE and Gd-DPC-Chol-FolS were excluded from the correlation, as they showed low Gd-delivery into cells while impairing uncharacteristically high effect on cell survival. However, the other Gd-formulations displayed a relatively homogenous relationship of Gd-content delivered into cells and decrease in cell survival.

5 Discussion

5.1 Liposomal formulations of radioenhancer/NC-elements

The development of a liposomal formulation containing the neutron capture element Gd had to meet several conditions to create an applicable compound for neutron capture therapy of glioma. These conditions include reproducibility of the manufacturing process, a narrow size distribution of the liposomes (preferably around 100 to 150 nm), high enough encapsulation efficiency for the drug, the ability to deliver the drug inside the cell and low toxicity.

The lipid/film-extrusion method leads to both reproducible results and monomodal size distribution of the liposomes with mean sizes of approximately 130 nm in diameter for all lipid mixtures tested, even for Folate-PEG and PEG2000-containing liposomes. The size of liposomes was perceived as a crucial point in formulation development, since nanoparticle uptake was reported previously to depend greatly on particle size [18, 44]. Rejman et al. [46] found that internalized beads of 50 to 200 nm were distributed perinuclear in mouse melanoma cell. Additionally, they observed that uptake continued for 3 h, which coincides with the highest amount of cationic liposomes and Gd-DTPA found in F98 and LN229 cells in this study. With all liposome formulations displaying very similar size distribution due to the usage of 100 nm pore membranes for extrusion, further uptake modalities were ascribed solely to lipid composition of the formulations and will be discussed in the uptake section of this work.

As reported before by several other authors [162, 181, 182], freeze-thaw cycles before extrusion enhanced encapsulation efficiency (EE) of water soluble drug considerably. Mayer et al. [161, 162] ascribed this effect to the formation of mostly unilamellar vesicles whose internal volumes were naturally higher than those of multilamellar liposomes. The repeated freeze-thaw process leads to fragmentation of the MLVs to LUV. Thereby, the entrapment efficiency for water-soluble drugs increases while the size of the vesicles grows smaller. Additionally, the raise of lipid concentration for the manufacturing process further increased the EE, as found previously by other groups [163, 181]. The encapsulation efficiency for the five main formulations of neutron capture (NC) element Gd, 7-10% of the initial Gd-amount (5.91 ± 1.74 mg Gd/ml for DOTAP-liposomes), was regarded as sufficient for the intended use, since Le and Cui [183] report only slightly higher entrapment (6.8 ± 0.3 mg Gd/ml) for their pLL-Gd-DTPA-complex in soy HPC liposomes.

The zeta-potential values of cationic DOTAP-formulation and anionic Cardiolipin are high enough to ensure electrostatic repulsion between liposomes and therefore, provide a stable formulation [160]. Addition of PEG-DSPE affected the initially high zeta potential of cationic liposomes and led to lower values, which may be due to insertion of more negative groups at the surface. However, since Cardiolipin liposomes also showed a less negative zeta potential after addition of PEG-DSPE, a shielding effect of the long PEG-chains is a possible explanation for the decrease in zeta potential. Another point in favor for this conclusion is the fact that the potential of Folate-PEG liposome did not change after PEG-addition. Both PEG-chains have approximately the same length and therefore, PEG-DSPE has no influence on the charge provided by Folate-PEG. Chen et al. [184] found that PEG-PE reduced the zeta-potential of charged liposomes close to neutral which was attributed to a shielding effect from or charge neutralization of the liposome surface charge.

Release of Gd-DTPA from liposomal formulations showed a common release profile for liposomes: an initial burst in the first few minutes followed by a slower release. The initial burst was ascribed to already released Magnevist (before experiment begin), since all three formulations showed the same behavior. This phenomenon is also known from other liposomes, albeit multilamellar formulations [185]. Nevertheless, the principle of the fast 'release' of superficially attached drug from the liposome remains the same for unilamellar and multilamellar liposomes. The release kinetic of Gd-DTPA-containing liposomes was found to fit first order kinetic, accounting for diffusion-controlled liberation [186]. As expected of the water-soluble Gd-DTPA, the release from the unilamellar liposomes was relatively fast. Nevertheless, after 180 min, the chosen incubation time for neutron irradiation experiments, DOTAP-liposomes still hold more than 50% of the initial Gd-content, while PEPC-liposomes and Magnevist retained 40%, respectively. These findings are in accordance with results from Wurster [164], who observed that Er-DTPA entrapped in liposomes showed a three-stage-release, depending on the concentration of encapsulated Er-DTPA. Low Er-DTPA concentrations (100 mM) led to a two-stage mechanism, while higher concentrations (250 mM) showed a three-stage behavior. The author ascribed this phenomenon to pore-formation in the liposome membrane due to the high molarity of the Er-DTPA formulation. The Gd-DTPA-liposomes tested here showed similar behavior in regard to the release stages. The molarity of the Gd-DTPA solution (Magnevist®) entrapped is 300 mM and may therefore account for a three-phase release. In contrast, the graph only shows two distinct stages, although another very short phase may be located between the first rapid release and the slower stage. However, this phase is not very distinct. Nevertheless, the overall release rate of Gd-DTPA from liposomes certainly resembles the release of Er-DTPA from liposomes, and the optimal incubation time chosen for the irradiation experiments (3 h), based on these findings and on the results from uptake experiments in particular, is in good agreement with the time frame previously suggested for this kind of experiments [164].

The Sotax CE7 method for liposomal release studies has not been used by other groups who manufactured Gd-liposomes. Le and Cui [183] showed slower release for Gd-DTPA from soy PC:Cholesterol liposomes (30% in 4 h), but employed the conventional dialysis tube method on a plate shaker. The circulating release media of the USP4 apparatus is thought to enhance the release rate, since the fluid flow provides for sink conditions in the Sotax CE7 while the shaker might not achieve this condition [132]. Therefore, it remains questionable if the release profiles from the two methods are actually comparable.

5.2 Cellular uptake of liposomes

5.2.1 Fluorimetric measurements of liposome uptake

Liposomal delivery of drugs into cells and the individual uptake pathway are fields of great interest for the formulation development of new cancer agents. Several authors examined the cellular uptake modalities of cationic, anionic and neutral liposomes and the respective pathways into different cell lines. It is generally believed that liposomes are taken up by clathrin-mediated endocytosis, although size, liposome composition, surface charge, cell type and culture conditions may also have an influence on the extent and the respective pathway of their uptake [44, 187].

In the present study, fluorimetric experiments were conducted to analyze liposome uptake into cells. The method does not exclude the binding of liposomes at the cell surface from the overall uptake of liposomes. Nevertheless, since binding was previously suggested to be the crucial step in endocytotic uptake process [187-189], bound liposomes were counted in for estimation of cellular uptake. In the light of a possible interaction of NBD-PE with the cellular membrane through lipid exchange or degradation of the fluorescent compound, the obtained results from the fluorimetric measurements discussed here exhibit perhaps a more qualitative character than presenting absolute numbers [190-192]. However, as discussed below, the results from these experiments nevertheless provided important insight in possible mechanisms of cellular uptake.

Cationic liposomes were found to be taken up to a greater extent than anionic and neutral mixtures. The surface charge density of DOTAP-liposomes plays an important role in the uptake: lower DOTAP-content led to significantly lower uptake into F98 and LN229 cells. A likely explanation for the preferential uptake of cationic liposomes is the electrostatic attraction between the cationic surface of the liposome and the anionic cell membrane which facilitates the binding step in endocytotic process [49]. Additionally, the fusion of cationic lipoplexes with cell membrane is still being discussed, although this mechanism might in part relay on the helper lipids used in such formulations, cholesterol and DOPE [45, 193]. Nevertheless, since cholesterol is included in the formulations here, the same mechanism could apply for cationic liposomes. Yet, lipoplexes consist normally of far more than the 9 mol% DOTAP that were used in our study. The negative impact of low lipid/DNA charge ratio on transfection efficiency was reported for cationic lipoplexes [194] and is usually thought to be due to low binding of liposomes to cell membrane [19].

Addition of PEG-DSPE led to lower uptake for nearly all tested formulations and in both cell lines, confirming the shielding ability of the PEG chain regardless of the initial liposome composition [29, 30]. As was observed for cationic liposomes, the cellular uptake depended on the density of PEG on the liposome surface, with higher PEG-content leading to lower uptake. Other groups also reported severe uptake-inhibition after addition of PEG to neutral and charged liposomes [184, 195, 196]. Nevertheless, PEG-shielded DOTAP- liposomes were still taken up to a high amount in comparison to neutral and anionic mixtures, a fact in accordance with findings from Miller et al. [187]. It seems clear that the steric barrier of PEG-DSPE on the lipid surface inhibits the liposome-cell association and therefore, prevents uptake of the nanocarrier. Yet, the shielding effect of 1 mol% PEG does not interrupt electrostatic attraction between cationic liposome and anionic cell membrane completely; otherwise the magnitude of cellular uptake would be the same for charged and neutral liposomes. This is only the case for 3 and 5 mol% PEG-DSPE in the liposome. After addition of 1 mol% PEG-DSPE the uptake is still facilitated for cationic liposomes and more than 3 fold higher than for neutral and anionic mixtures. It is debatable if this amount is already sufficient for avoiding the reticuloendothelial system (RES) and prolonging circulation time in the bloodstream. Drummond et al. believe these effects to depend primarily on reduced uptake rather than lesser opsonizaton of stealth liposomes [15]. In this case, the reduced uptake of 1 mol% might be sufficient for passive targeting via EPR-effect, since PEG-liposomes were also found to accumulate preferentially at tumor sites than normal tissues [30]. Although most groups used at least 5 mol% PEG for manufacture of stealth liposomes [21, 184, 187], the higher PEG-amount was possibly chosen because some authors reported aggregation for smaller PEG-contents [197]. Therefore, the required amount of PEG-DSPE for shielding the carrier from macrophages while still leading to high uptake in systemic use of cationic liposomes needs to be further investigated.

Liposomes made of cardiolipin as anionic component, were taken up to very small extent by the cell lines used in the study. Remarkably, Lee et al. [188] found that CV1-cells readily endocytosed anionic liposomes made of 9 mol% PG, PA or PS, and uptake was enhanced more than 20fold in comparison to PC-Chol liposomes. In contrast, insertion of G_{M1} or PI did not increase liposome uptake. These findings indicate that the headgroup of anionic lipids defines the uptake into cells. Cardiolipin was chosen as a new anionic lipid for liposome manufacture because of its presence in glioblastoma and glial cells (2.5% of whole phospholipid in rat glial cells as reported by Witter and Debuch [198]). In addition, it has been observed that CL-containing liposomes fused with cellular membrane of GL15 cells and travelled to cellular mitochondria [199]. Furthermore, it has been shown that similarity between liposome and cellular membranes enhanced uptake and ER-like liposomes were indeed transported to the ER of cells [200]. Therefore, the uptake of 4.5 and 10 mol% CL-liposomes was expected to be relatively high, instead of being the lowest compared to fusogenic and cationic liposomes.

Both DOPE-containing formulations were taken up to a higher extent than anionic, but lower than cationic and folate-targeted liposomes. DOPE is known as a helper lipid for cationic gene delivery and was found to destabilize membranes, thus facilitating membrane fusion and release of liposomal contents from endosomes [49, 201, 202]. As mentioned above, the fusion of cationic/DOPE liposome and cell membrane is still under debate. The uptake via clathrin-mediated pathway is favored, while actual fusion seems to play a minor role in cell uptake [18, 45].

Folate-targeted liposomes were found to enhance liposome uptake into both cell lines compared to anionic and neutral lipid mixtures. In addition, their uptake outranged that of cationic liposomes. These results were unexpected, given that only one of the cell lines in the study was found to express FR α (LN229). F98 cells were in contrast described previously to be FR negative, a status which was confirmed here by qualitative PCR for FR α-mRNA. Nevertheless, uptake of folate-receptor-targeted liposomes was equally high in F98 and in LN229 cells in fluorimetric experiments. Furthermore, the delivery of Gd-DTPA into cells by folate-liposomes was not so much lower in F98 as in LN229 cells (approximately 78 versus 110 ng/10^6 cells). The density of the folate-PEG on the surface might affect the uptake as some authors have reported before [175, 190]. Generally, a density of 0.03 to 0.5 mol% was observed to be optimal for targeting purposes. In this study, the amount of 0.13 mol% was regarded as sufficient, since increase of folate-PEG in the lipid mixture to 0.3 mol% did not enhance liposome uptake in both cell lines (data not shown). Another factor might be the definite number of FR alpha expression. The PCR experiment gave only a qualitative result, while the quantity of receptor expression was not addressed. If the expression was very low in LN229 cells, the enhancing effect for folate-mediated uptake may not be high enough to manifest clearly in the experiments. Although the FR alpha expression was clearly shown for LN229 cells, Parker et al. have found that in general, expression of the receptor is negligible in brain carcinoma [33]. Reddy et al. [175] showed that folate-liposome uptake for FR α positive cells was higher than for FR α negative cells, but the latter still showed some uptake of the liposomes. In addition, low receptor expression-cells were found to exhibit no uptake of the targeted liposomes [203]. It is therefore possible that the relatively high uptake of targeted liposomes into LN229 and F98 cells was not a consequence from introduction of folate-ligand, but some other aspect of the liposome structure. The question remains, why these liposomes would attach to the cellular membrane if there is no FR-receptor present which would facilitate binding, not to mention endocytosis? Non-specific binding of liposomes seems to be too low for the high amount of folate-liposome uptake if compared to the uptake of, for example PEG-shielded DOPC-Chol-liposomes. One could speculate, if some other folate-transporting mechanisms are involved. For instance, the reduced folate carrier is ubiquitous since it provides the amount of folate needed in all cells. Organic anionic transporters also have been reported

to play a role in folate-maintenance. These folate transporters are transmembrane carriers and therefore unlikely to transport folate-liposome through the membrane. The size of the liposomes alone would pose a hindrance. Reddy et al. [204] have stated that the RFC plays no role in folate-targeted transport, because conjugated folates were no substrate for the carrier. Still, it seems that the binding is enhanced by the folate moiety itself, since non-targeted liposomes are taken up to a lower extent. Additionally, PEG-DSPE introduction does not inhibit endocytosis of folate-liposomes as it would if uptake depended on the composition of the residual liposome components. All these findings favor that folate increases uptake into F98 and LN229 cells due to another binding-mechanism than to FRα. It is certainly possible that some other receptor than FRα (e.g. FRβ, γ and δ) is expressed in the F98 and LN229 cell lines, although these receptors are found primarily on other tissue types (i.e. macrophages and T-cells) [205].

Another explanation for the high uptake of (folate-targeted) liposomes may be the phagocytic activity of glial cells, since F98 and LN229 both are of glial origin. Although microglia cells are known as the main immune system of the brain, activated astrocytes were also observed to play a major role in the elimination of synaptic terminals, although the extent of their involvement remains unclear [206]. Furthermore, glial cells (i.e. microglia, astrocytes and ependymal cells) were found to express scavenger and phagocytic receptors enabling these cells to detect and phagocytose pathogens [207]. Therefore, it is possible that the presence of different liposomal structures such as, for example the folate-targeting moiety, triggered a phagocytosis-mechanism for F98 and LN229 cells, leading to high uptake of the respective liposomes.

Interestingly, uptake of liposomes was reported before to be highly cell type-dependent; HeLa (epithelial cervix carcinoma) cells endocytosed cationic liposomes to a greater extent than anionic or neutral ones, while J774 cells (macrophage-like) took up more charged liposomes, regardless of positive or negative charge, than neutral liposomes [187]. In contrast, the cell lines in the present study which were both derived from glioma had very similar uptake modalities. Although F98 cells are of glial and LN229 of epithelial morphology, and the F98 cell line is of murine and LN229 of human origin, the findings in regard to uptake modalities were comparable in both qualitative as quantitative regard. Therefore, the cell lines were regarded as a good model for estimation for the effectiveness of liposomal Gd-DTPA treatment in NCT.

5.2.1.1.1 Fluorescence microscopy

Fluorescence microscopic images were taken to support results from fluorescence spectroscopic measurements in regard of liposome uptake. As mentioned before, the values measured for uptake include also binding of liposomes to cell surface. For fluorescence microscopy, the uptake of DOTAP-liposomes was examined. Pictures showed liposome-cell co-localization clearly and slide images from different cell levels from both cell lines strongly suggest that besides surface attachment, internalization of liposomes took place. Remarkably, the localization of some liposomes was preferably on cell-cell junctures. The attachment of cationic liposomes to adjacent cell membranes reminds of cationic polymers used for tight junction opening in other surroundings [208]. On the other hand, tight junctions which are dominant in the blood brain barrier are known to be downregulated in glioma cells [37]. In fact, transendothelial electrical resistance (TEER) of F98 cells measured in transwell experiments is practically non-existent in comparison to TEER of Caco-2 cells (unpublished data). Nevertheless, it is

possible that even the lower content of tight junction proteins attract preferential binding of cationic liposomes. Since occludin and the claudin-family which are main components of tight junctions, expose several loops to the cell outside, electrostatic attraction between liposome and cell membrane protein might be enhanced at cell-cell barriers.

5.2.1.2 Uptake of Gd-DTPA

Fluorimetric measurements showed a preferential uptake of cationic DOTAP-liposomes which is consistent with the uptake amount of Gd-DTPA measured via ICP-MS. Folate-targeted liposomes also showed high uptake for the fluorimetric measurements, yet the cellular Gd-content was low in comparison to the cationic formulation. As mentioned before, the amount of Gd-DTPA delivered by folate-liposomes into F98 cells was only 30% lower than the amount delivered into LN229 cells which was not expected in regard to FR α expression. Except for free Magnevist accumulation, the Gd-content differed in both cell lines, as did the order from highest to lowest Gd-delivery by liposomes. Nevertheless, the range of Gd-content is similar for both cell lines. It is debatable if the encapsulation efficiency has influence on the final Gd-account in cells. Since CL-liposomes have the smallest EE, the delivery should also be small, but this is not the case for both cell lines. DOPC-DOPE liposomes have one of the highest EE, yet the Gd-content in F98 cells is very low. It is noticeable that neither F98 nor LN229 cells show the same order for uptake from liposomes as in fluorimetric uptake experiments which might be due to the different time points of experiment read-out (3 h versus 4 h). As mentioned before, after 2-4 h there was a maximum in uptake for fluorimetric measurements, but Gd-uptake was for the most part only measured after 3h which seemed to be the adequate incubation time for irradiation experiments. Additionally the magnitude of differences between the values is not the same and correlation of the values was therefore impossible. Interestingly, it seems that the DOPC-DOPE and folate-formulations both are outside the typical pairing of fluorimetric uptake and Gd-delivery. Both liposome-compositions show very high uptake in fluorescence experiments, but comparably low Gd-delivery. It is possible that fluorimetric measurements were influenced by lipid-exchange from liposomes to cell membrane and the mere binding of liposomes on cell surface, without actual internalization [190]. Furthermore, degradation processes of the fluorescent probe NBD-PE and possible pH-dependency may play a role in fluorimetric uptake experiments [191, 192]. However, this also would have played a role for other formulations which contained the same amount of NBD-PE and had similar good binding capabilities, such as DOTAP. In contrast, DOTAP showed high uptake in both fluorescence and ICP-MS measurements which would be unlikely for mere binding. Furthermore, bound liposomes were observed to have a tendency toward leaking their contents and the uptake of free Magnevist was several magnitudes lower than that of liposomal encapsulated Gd-DTPA [209, 210]. Nevertheless, regarding the magnitude of differences in the values for Gd-uptake in comparison to fluorescence measurements, especially in regard of DOTAP-liposomes, these findings might still be a result from variation in the experiments.

Regarding the range of Gd-uptake into cells, results from literature are often expressed as µg Gd/g wet tumor tissue. The conditions for cell uptake experiments are different from those of in vivo tumor models, since the tumor is a three-dimensional heterogeneous mass whereas cells often have only one homogeneous adherent layer. Therefore, the accumulation in tumors might be different from the cell culture model, especially with respect to the EPR-effect which would enhance tumor retention of liposomes *in vivo*. In the present study, Gd-contents in cells were expressed as ng Gd/ 10^6 cells in order

to normalize Gd-uptake and to avert variations due to cell numbers and residual fluids. The expression of Gd-content per wet tumor tissue might include superfluous fluids and very different cell numbers, thus leading to inaccurate assumptions. Therefore, the expression of Gd-content per 10^6 cells was chosen instead (cell sizes of F98 and LN229 cells are approximately 15-20 µm, cf. fluorescence images).

Our results of time- and dose-dependent uptake of Gd are consistent with findings from de Stasio et al. [211]. Furthermore, De Stasio et al. proved that Gd preferentially concentrated in the cell nuclei [211], a fact bringing great benefit for the therapy based on short-range capture products like Auger electrons [99, 102, 212]. Additionally, their working group found a Gd-content of > 250 µg/ml after 24 h when cells were exposed to 10 mg Gd-DTPA/ml (64 mM) for a primary glioma cell suspension of approximately 10^6 cells. This value is astonishing high given that a) the cell lines in our study experienced severe cytotoxic effects if exposed to 10 mg/ml Gd-DTPA (Magnevist from Bayer/Schering which was also used by de Stasio) b) our F98 and LN229 cells contained only 80 and 89 ng Gd/10^6 cells after 24h. However, these discrepancies between results may be due to differences in Gd-measurement, that is in ICP-MS methods. In a second publication, U87 cells which are comparable in size to F98 and LN229 cells, retained roughly 60 ppm Gd from Motexafin compound (accounting for approximately 6.5 µg Gd per 10^6 cells if based on ppm = µg/ml and U87 having a cell volume of 9,200 cells/µl as given in the publication) [85]. However, with the average weight of a mammalian cell being 2-3 ng, 10^6 cells would weigh 2.5 mg [213, 214]. Accordingly, our Gd-content would be around 6.6 µg Gd/g for 3 h incubation of F98 cells with free Magnevist while DOTAP-liposomes would deliver 768 µg/g into the glioma cells. This amount is thought to be more than sufficient for efficient Gd-NCT since it was calculated that 50-200 µg ^{157}Gd/g tumor tissue are needed for successful treatment of glioma [212]. It needs to be specified that this Gd-concentration was calculated for the ^{157}Gd isotope with a cross-section of 255,000 barn for thermal neutrons, not for the natural mixture which only contains 15.6% of the required isotope and has a cross-section of 49,000 barn [90]. Therefore, a ^{157}Gd-enriched solution should be used for the preparation of liposomes. Still, from the spectrum of our tested formulations, DOTAP- liposomes achieved a ^{157}Gd-delivery in this range for both F98 and LN229 cells. If pure isotopes were used, folate-liposomes and DOPC-DOPE-liposomes would also be optimal carriers for Gd-NCT of F98 and LN229 cells, respectively.

Although the comparability of tumor in mice and cancer cell lines is debatable, it should be noted that liposomal Gd-DTPA as prepared by Le and Cui [215] delivered 33 µg Gd/g tumor tissue (TC-1, cervical cancer in mice) 3 h after injection and after 12 h, the liposomal Gd uptake in tumors was significantly higher (over 200fold) than from free Gd. The group of Dewi et al. [93] found 40.3 µg Gd/g tumor uptake of liposomal Gd after 2 h in tumor bearing mice. These findings support the benefits of a liposomal carrier for Gd-DTPA and lead to the assumption that the application of our liposome formulations can greatly improve the conditions for Gd-NCT *in vivo*.

5.3 MTT assay

The MTT assay shows higher survival for irradiated cells than the colony forming assay (CFA). This observation can be ascribed to the time point of experiment read-out. CFA is usually done at least 8 or more days after irradiation, but the MTT is run up to 5 days after the treatment. Since irradiated cells may still divide several times after irradiation before they arrest or die, MTT assay as a single-point assay will show more cells as being alive than CFA [67, 74, 146]. It needs to be discussed if the ability to form colonies is the only important factor in estimation of irradiation success. Cells that are still alive, but not

dividing, for example cells that are in G0-phase of the cell cycle, are not included in CFA. However, these cells may re-enter the cell cycle at a later time point and therefore add to further tumor growth. Furthermore, the quiescent cells may account for tumor recurrence or late metastasis, especially, if these cells are tumor stem cells [216]. The MTT assay on the other hand, accounts for all cells even though their metabolism might be reduced [147]. In assessment of the real biological conditions of tumor growth, the MTT assay may therefore be advantageous against CFA. Furthermore, the expenditure of time is considerably lower for MTT assay than for CFA.

The multiple MTT assay offers another advantage: the visualization of changes in proliferation behavior. Here, the exact time point when cells stop dividing can be read from the curve. Additionally, the curve can be used to gain information about the non-dividing cells which are in cell cycle arrest. These cells would form a 'base' of formazan production, that is the start value, underlying the increasing growth curve. Furthermore, it might be possible to extract information about cells that undergo immediate cell death (interphase death or apoptosis) in contrast to cells that suffer intermitotic death and finally those that survive the radiation treatment by close observation of the resulting growth curve. Unfortunately, some of the graphs depicting proliferation of irradiated cells show non-exponential growth curves with high aberrations or late spurts of cell regrowth, leading to poor curve fitting and negative doubling times. For the application of the multiple MTT assay, the proliferation curve should follow an idealized model for exponential growth. Although some information may still be gained from the non-exponential curves, the analysis would require the introduction of more variables to describe the curve. Thus, the acquired data points are not sufficient to lead to valuable results. As described before, the multiple assay in any event tended to show slightly lower survival than the individual time points. Therefore, the multiple MTT assay was performed nonetheless for visualization of cell proliferation, but the analysis was kept simpler by using individual time points for comparison of irradiation effect.

5.4 Photon irradiation experiments

Photon irradiation experiments were performed to investigate the suitability of Gd-DTPA (as well as other lanthanides) as a radioenhancer for external beam therapy (XRT). Furthermore, the induction of Auger-electron cascades from these high-Z elements through photoelectric interaction of x-rays with electrons of their K-shell also occurs under neutron irradiation. This effect, induced by interaction of the elements with photons of the adequate energy (of the K-absorption edge of the elements), is thought to be the most important attribution to cell killing for gadolinium neutron capture therapy [211, 212]. The gamma-rays released after the Gd-neutron capture can interact with further Gd- or other lanthanide atoms (fig. 5-1). Thus, more reactive species, such as free radicals, peroxides or superoxide anions (O_2^-) are generated, leading to additional cell damage [68]. With synchrotron radiation, the suitable photon energy for the K-absorption edges of lanthanides can be selected and cells previously treated with lanthanide formulations can be irradiated with a monochromatic beam. For clinically used 6 MV linear accelerators, the beam spectrum is not ideal for K-shell absorption, since the central beam composition is shifted to higher photon energies by the use of flattening filters (beam hardening)[177]. In the experiments at the clinical medical center, the outer region of the radiation field, where lower photon energies prevail (due to the insertion of the flattening filter), was used for the study of the radioenhancing effect of Gd-DTPA.

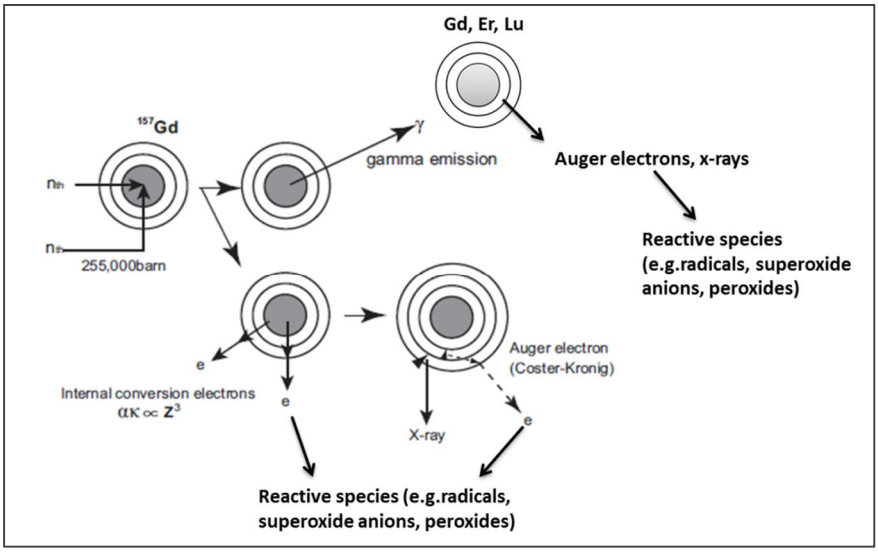

Figure 5-1 Schematic drawing of ^{157}Gd neutron capture reaction (adapted from Dewi et al. [93]). The gamma-rays generated by the NC-event may interact with further lanthanide atoms (Gd, Er, Lu) in their proximity, thus generating still more cell-damaging reactive species.

5.4.1 Synchrotron irradiation experiments

The depth profile for x-rays depends on the x-ray energy: higher energies penetrate deeper into tissue. The region between phantom or body surface and the dose maximum is called the build-up region [68]. The build-up region and the depth profile are a product of the correlation between attenuation of the primary beam due to scattering and absorption and the resulting secondary particles (electrons, photons), depositing their energy in the phantom or body and the depth of the dose maximum is dependent on the range of the secondary electrons.

The variation in irradiation set-ups (agar phantom in front of or behind cells) showed that the secondary particles generated in the build-up material have a pronounced effect of cell survival, even if the phantom is located behind the cells. In addition, the backscatter of photons attributes to the absorbed dose and cannot be neglected in the radiation planning [69]. Nevertheless, the build-up effect is more evident if the agar gel is placed in front of the cells, probably because the formation of secondary particles is higher for higher photon fluences.

Irradiation experiments of F98 and LN229 cells with monochromatic synchrotron radiation showed an effect of energy spectrum on the applicability of radioenhancer. The appropriate energy required to push an electron from K-shell of Gd ('above K-edge') leads to lower survival of irradiated cells in comparison to an energy of 1 keV lower than the K-edge. This phenomenon proves the concept of the enhancing effect of Gd on photon irradiation in vitro and its suitability as radioenhancer for glioma cells.

The application of Gd-DTPA in liposomal form and subsequent synchrotron irradiation (above K-edge) led to a decrease in cell survival of 70% for F98 (DOTAP-liposomes) and 30% for LN229 cells (CL-liposomes) for a dose of 10 Gy, respectively, while irradiation alone reduced survival only by 54 and 15%. LN229 cells were shown previously by other authors to lose colony forming ability completely at a radiation dose of 6 Gy [217] and survival of F98 cells was reduced to 15% after application of only 4 Gy [218]. In the present study, the cell lines proved to be more radioresistant, but it has to be noted that

other publications used the colony forming assay and not the MTT assay for assessment of survival. It was shown before that MTT might overestimate survival [141], especially since the time span for colony assay is much longer than for MTT test, thus allowing more mitotic cell deaths to occur.

Few authors have examined the radioenhancing effect of Gd-DTPA for photon irradiation. Most publications lay out the effects of radiosensitizing/-enhancing compound motexafin-Gd (a porphyrin-like complex of Gd^{3+}) which is generally believed to sensitize cells to irradiation effects by depleting cellular redox-potential and generating reactive oxygen species [87]. However, the radiosensitizing may also result from other mechanisms such as metabolic inhibition of mitochondria [219], inhibition of thioredoxin reductase and heme oxygenase-1 [220], direct radiosensitization and oxygenation of the tumor, not to mention the mechanism of porphyrins [81]. In contrast to the texaphyrin-complex, Gd-DTPA was chosen for his high Z-number and its ability to eject Auger electrons under radiation treatment [221, 222]. De Stasio prepared usage of motexafin-Gd for stereotactic irradiation, but primary under the hypothesis that the Gd-atom would induce Auger electrons and would not reduce cellular metabolites [85]. Régnard et al. [221] and Le Duc et al. [223] found that Gd-DTPA and Gd-DTPA particles enhanced irradiation effects from microbeam radiation therapy (spectrum maxima 83 keV and 90 keV, respectively) for 9L gliosarcoma-bearing mice. Recently, the group showed that 6 MeV irradiation also led to enhancement effect of Gd-particles [224]. Interestingly, the Gd-nanoparticle uptake into tumor was only 2-3 µg Gd/g [222] and 5 µg after 20 min [223] and despite of this low number, median survival time of rats was prolonged. Of course, with microbeam radiation therapy, the doses applied to tumor are roughly a 100fold higher than the doses we worked with. Therefore, the increase of dose might as well have led to higher effect of the radioenhancing agent, similar to our findings that in some cases higher radiation doses resulted in higher effects of Gd-DTPA.

5.4.2 Linear accelerator experiments

The spectrum of the prompt gamma rays deriving from Gd-NC-event with gamma ray energies up to 8 MeV can be compared to the x-ray spectra of clinically used linear accelerators (linacs) (cf. fig. 3-13, prompt gamma ray spectrum Gd and 4-36, photon spectrum 6 MV linac). Both spectra contain the energy of 50.2 keV (K-absorption edge of Gd), which was used for the monochromatic radiation experiments at the synchrotron facility, ESRF. For linear accelerators, the portion of the spectrum made up by lower energies, as 50 keV, is small, due to the flattening filter of the linac which hardens the central beam in the radiation field. Thus, only the outer regions of the radiation field contain higher percentages of lower photon energies and consequently, the spectrum strongly depends on the position in the radiation field.

Irradiation of glioma cells under clinical conditions with linear accelerator Siemens MD2 in the center of the radiation field did not show particularly high effect of the radioenhancing agent (3% for GPC-treated CL-liposomes and 12% for the high concentration of free Magnevist at a dose of 8 Gy, based on irradiated control), but irradiation alone accounted for 52% survival/8 Gy. Therefore, the energy spectrum in the outer regions of the radiation field was used to deliver the required energy range for the K-edge absorption and release of an Auger electron cascade from Gd. Here, the impact of Gd on cell survival was more pronounced (10% reduction for 8 Gy, based on irradiated control). Yet, the radioenhancement was relatively low, although an improvement of 10% of the radiation effect in glioblastoma therapy may be still worth pursuing, given that the mean survival span of the patients is

only about 14 months under optimal treatment conditions. Additionally, the formulations applied here were early prototypes and the later in Gd-NCT successfully used DOTAP and DOPC-DOPE-liposomes were not yet tested. It seemed however, that the high energy spectrum in the center of the radiation field of clinical accelerators was not adequately suited for the approach. However, with the recently published work from Mowat et al. [224], the question of applicable conditions at the clinical linear accelerator has risen again and it remains to be investigated if the newer designed Gd-loaded liposomes are qualified to serve as radioenhancer also under a 6 MeV-spectrum.

The alternate application in place of the radioenhancer for external beam radiation therapy (XRT) is the use of Gd-DTPA in neutron capture therapy as a high cross-section neutron capture element. Since the effects from liposomal Gd-DTPA in XRT were relatively low, further development of the formulations was based primarily on the application of the compound as NCT agent.

5.5 Neutron irradiation experiments

5.5.1 Experimental conditions at D22, Institute Laue-Langevin and TRIGA reactor, Johannes Gutenberg-University – advantages and disadvantages

Experiments at D22 beamline, ILL, did show the potential of Gd-NCT for the treatment of glioma cells and also proved the benefit from supplemented Er-DTPA as second radioenhancer, profiting from the gamma rays derived from Gd-NC-event. Unfortunately, the regulatory and environmental conditions at the beamline were not optimal for our study. Although the beamline offers several advantages, such as the possibility for structural investigations of liposomes and the monochromatic beam, as well as providing cold neutrons and therefore, an even higher cross section of neutron capture element Gd than for thermal neutrons, the disadvantages outweighed the benefits at last. Since users have to apply for the highly demanded beamtime at the instrument, only few and relatively short experiment times can be granted. The work with cell lines requires prolonged stays at the ILL for preparation and follow-up of the experiments, and is therefore associated with considerable expenses, both in time and effort. As an alternative to the organization of beamtime for external users, the possibility to stay for a longer period at the ILL as a visiting researcher may have been exploited.

Regardless of the above mentioned regulatory restrictions, the logistic organization proved to be another drawback. The routine cell work as well as the preparations of the 96 well plates for the irradiations had to be performed at the European Molecular Biology Laboratory (EMBL) which is located on the same site as the ILL, but still considerably far away from the beamline. The transport of cells was associated with a high percentage of cell-detachment of the usually adherent cells from the culture plates. Furthermore, the monochromatic beam at the D22 instrument leads to relatively low neutron flux, and as was observed for the second ILL experiment, the low flux was not sufficient for our experiments.

In contrast, the conditions at the TRIGA reactor in Mainz complied very well with the essential requirements for our study. As the most important factor, the neutron flux is higher, since the irradiation chamber is in closer proximity to the core. Although the flux is slightly inhomogeneous (see neutron spectrum, cf. fig. 3-14 and 3-18) the variation in cell survival of irradiated cells (without NC-agent) between different rows and columns on the 96 well plate is still very low (maximal variation 10

and 6 % for F98 and LN229 cells, respectively). Hence, the conditions at the thermal column were well suited for our experiments. Of course, for Gd-neutron capture, cold neutrons provide a more advantageous cross section than thermal neutrons. Nevertheless, as discussed below, the results we obtained with thermal neutrons at TRIGA reactor are very encouraging, even with the lower Gd-cross section. Other points in favor for the radiation experiments at TRIGA were the close proximity to the cell laboratory at the campus of the Johannes Gutenberg-University Mainz, the high local support, the possibility to conduct more experiments with much less effort regarding logistic and regulatory demands and the higher flexibility of beamtime usage. In summary, the experiments at ILL, though providing valuable insight into the influence of environmental conditions for Gd-NCT, were not reasonably practicable compared to the more convenient experimental conditions at TRIGA and therefore, were not pursued further.

5.5.2 Benefit of liposomal Gd-DTPA for neutron capture therapy

Gadolinium as a liposomal neutron capture element for treatment of glioblastoma cells in vitro led to very promising results. The application of Gd-DTPA encapsulated in liposomal carriers achieved high uptake rates into glioma cells while offering low cytotoxicity and short incubation times. Cell survival was for both cell lines reduced to 80% with irradiation alone ($6.21 \cdot 10^{12}$ n/cm², 97 h after irradiation). Application of liposomal formulations (DOPTAP- and DOPC-DOPE-formulation) led to another decrease of 49 and 65% based on irradiated medium control for F98 cells. For LN229 cells, the effect was lower, but treatment with Gd-liposomes achieved still an additional 20-25% reduction of cell survival compared to irradiation alone (folate, DOPC-DOPE- and DOTAP-formulation of Magnevist). Free Magnevist solution only reduced survival for additional 13 % (both cell lines) compared to irradiation alone. De Stasio et al. 2001 irradiated glioma cells with $1.8 \cdot 10^{10}$ n/cm² and achieved a reduction in cell survival of about 20% which corresponds to the value we measured for our experiment. She found that the application of 1 and 5 mg/ml Gd-DTPA for 72 h led to a decrease of additional 9 and 35%. In comparison, our liposomal formulations contained merely 0.27 - 0.47 mg Gd/well (corresponding to 1.4-2.4 mg/ml) and cells were left to incubate for only 3 h, less than 1/20 of the time used by de Stasio. Therefore, the benefit of employing the newly developed Gd-containing liposomes consists not only of higher delivery of Gd to cells and thus higher decrease of cell survival in regard of initial Gd-concentration, but also of reduction of treatment time for more than 80%.

5.5.3 Different liposomal formulations for Gd-NCT

Gd-NCT is believed to primarily depend on induction of double strand breaks by high LET-radiation. For the Gd-neutron capture event, Auger electrons are the most likely particles to induce these lesions in cellular DNA [102]. The results from our study strongly suggest that Gd was taken up into the cellular body and remained in close proximity to the nucleus. The range of Auger electrons is very limited and therefore, proximity to DNA is an absolute requirement to inflict double strand breaks (dsb). The concept of introducing another high-Z element like erbium as a radioenhancer for the neutron capture-derived gamma rays was presented for the first time to our best knowledge. The addition of Er-DTPA in liposomes besides the NC-element Gd clearly added to the cell killing after neutron irradiation

(experiments at ILL). Nevertheless, further experiments were performed without the supplement, due to practical reasons: unlike Gd-DTPA, Er-DTPA is not FDA-approved and consequently, the medical application would require much higher expenses for clinical studies than an already approved drug for human use. Therefore, the concept was deferred for the moment, as Gd naturally also serves as provider of Auger-electrons after photoelectric interaction with gamma rays from another Gd-atom. This effect was shown by the decrease in cell survival after introduction of the Gd-loaded gel behind the 96 well plates under neutron irradiation.

The magnitude of cell survival reduction for different Gd-DTPA formulations invites to form conjectures about the exact position of Gd-DTPA in the cell. Some of the formulations had relatively low Gd-concentrations delivered into glioma cells, but nevertheless, led to severe reduction in cell survival. The question arises how cell survival is related to Gd-presence in the cell, because the simple 'the more, the better' does not seem to apply in this case. One could speculate, if the effect is related to the respective pathway (or intracellular fate) the liposomes were subjected to after being endocytosed. DOPC-DOPE liposomes were likely to escape endosomes, since DOPE is known as a fusogenic lipid and often used to enhance delivery of liposome cargo into the cytosol, especially in gene delivery [202]. Consequently, the chance of Gd-atoms to be released from liposomes near the nucleus would be higher than for liposome compositions without the helper lipid. These formulations were likely to be retained in endosomes and dissipated in lysosomes after their clathrin-mediated uptake into cells. For folate-targeted liposomes, the pathway of caveolae-mediated uptake was suggested [49]. This uptake mechanism can lead to a non-destructive pathway headed for the endoplasmatic reticulum in the cell, thus preventing the cargo to end up in lysosomes for degradation. Therefore, the Gd-delivery by such folate-targeted liposomes might also be more easily dispatched into the cytosol where Gd-atoms could accumulate near the nucleus. In addition, it has been shown for free Magnevist that Gd-DTPA reached cell nuclei and accumulated there [211]. This finding accounts for the relatively high success of free Magnevist in decreasing cell survival given that the uptake rate into cells is also rather low in comparison to liposomal formulations.

As Magnevist® is composed of gadopentetate-dimeglumine, the characteristics of the salt need to be discussed in regard to possible scavenger effects. Several aliphatic alcohols such as ethanol, glycerol and mannitol as well as antioxidant vitamin c are known to have radioprotective properties due to their ability to 'capture' free radicals [225, 226]. Meglumine contains five hydroxyl-groups and therefore unquestionably may act as scavenger for free radicals generated under neutron- or x-ray-irradiation. What is more, the concentration of meglumin in Magnevist® solution is relatively high (1 mmol/ml, cf. references, additional websites: *Magnevist®*). In contrast, lanthanide-DTPA formulations with tris-acetate or -citrate as counter ions (Nanovel) should exhibit less pronounced scavenger characteristics, since both acetate and citrate have none or less free hydroxyl-groups than meglumine, respectively. Nevertheless, these formulations also contain relatively high concentrations of tris, another aliphatic alcohol with three hydroxyl-groups which might act as radical scavenger. Hence, the advantage of citrate or acetate as counter ions probably will be diminished by the application of tris, although all formulations tested here (Magnevist® and Nanovel-solutions) showed satisfying results under neutron irradiation. However, another compound for radioenhancing without further additions, erbium citrate, proved to be very effective in enhanced XRT [142] in comparison to Magnevist®, showing that the influence of scavenger molecules should not be neglected. Therefore, the development of further different lanthanide formulations without supplementation of scavenging molecules certainly seems promising in regard to their application in both neutron capture and external beam radiation therapy.

5.5.4 Gadolinium neutron capture therapy

Some working groups have investigated the effect of (liposomal) Gd in NCT for tumor-bearing animals and received very positive results. Akine et al. [227] found significant tumor reduction of subcutaneous VX-2 carcinoma in rabbits after intra-arterial injection of gadopentetate. Dewi et al. [93] came to similar results for tumor-bearing mice after application of liposomal Gd and irradiation in comparison to irradiation alone. Further studies had the objective to compare boron- and gadolinium-NCT, although it is difficult to objectively compare the two forms of NCT, due to not fully investigated uptake and distribution characteristics of the NCT-compounds boron and gadolinium. Tokuuye et al. [92] tried to enhance the effects of Gd-NCT in V79 cells with addition of boron, but observed less than additive effects. Gd alone was more effective than boron alone in reduction of cell survival. The unexpectedly small improvement by boron-gadolinium combination resulted probably from the high cross section of Gd which would act like a shield against other materials. Later, Matsumura et al. [228] discovered that the effect of combined B- and GdNCT in fact depends greatly on the respective concentration of the elements; the authors gained additive effects in V79 cells only for a Gd-concentration up to 1600 ppm whereas higher concentrations showed no benefit from boron addition. They suggested therefore that Gd should act as the additional element for BNCT to prevent an excess of neutron capture elements and thus negative results in clinical outcome. In addition it was proposed that Gd may be useful for treatment of cells that do not incorporate the boron compounds, but can be reached with the long-range X-rays from Gd neutron capture event.

Mitin et al. [112] finally compared the effectiveness of boron and gadolinium neutron capture therapy for melanoma and osteosarcoma in dogs, where they observed higher benefit for osteosarcoma treatment with Gd-NCT than with the boron equivalent. On the other hand, melanoma treatment was more successful by means of BNCT. The authors believed that this outcome was due to the additional radiation effect from secondary gamma emission of Gd whose long flight range would be beneficial in cancer types such as osteosarcoma, but not in the more superficial melanoma. In addition to these findings in favor of GdNCT over BNCT, Hwang et al. [106] observed that Gd-containing carbon particles performed better in reducing survival of HeLa cells after neutron irradiation than the equivalent boron compound. Of course, the much higher cross section for Gd in comparison to B will have a great influence on the outcome of these experiments.

In summary, the question if GdNCT is more beneficial than B-NCT has not yet been answered completely. In our study, equimolar amounts of Gd and B achieved different results in cell survival. Boron compounds led to lower cell survival than Gd, but the difference was very small. Nevertheless, the higher energy release in the neutron capture event led us to expect higher effect from Gd than from boron, although some authors suggested that the overall effect may be equal for both NC-elements for similar molecular concentrations [92]. It is possible that the induction of dsb by Auger and internal conversion electrons in this case was not sufficient to prove superiority to boron treatment, and the long gamma rays from Gd neutron capture were lost for infliction of DNA damage because of their path length. The fission products of boron in contrast have short path lengths and stay therefore mostly intracellular if boron was taken up by the cell. On the other hand, gamma rays from GdNCT are certainly useful in treatment of heterogeneous tumor mass when the distribution of NC-element tends to be uneven. These products from Gd neutron capture may also induce cellular damage if Gd is extracellular, because of their long travel path in tissues. Furthermore, the interaction of these gamma rays with additional high-Z elements, such as in the concept with erbium (or more gadolinium) in- or outside the cell may induce more Auger-electron cascades, thus still adding to cellular damage.

5.5.5 Shape of survival curves

Franken et al. [229] have stated that Gd acts as a enhancer for lung tumor cells under thermal neutron but not under gamma-ray irradiation. In their study, survival curves from neutrons with and without Gd-DTPA treatment showed no initial shoulder region, similar to reports from Maki et al. [77]. Nevertheless, Franken et al. [229] and Yasui et al. [100] fitted survival curves according to the linear-quadratic model. In contrast, Tokuuye et al. [230] found a shoulder region for neutron-irradiated cells only after application of Gd and survival curves of irradiation alone were fitted by simple exponential fit.

Since only two neutron irradiation fluences were applied in the later TRIGA experiments with the 'stacked plates'-set-up, the data was not sufficient for fitting with a two-variable model and only tendencies could be observed. In some cases, a shoulder region was found, although the shape was not very distinctive. The survival curves from the preliminary TRIGA experiments for neutrons alone, where more fluences were included, may rather be described as curves with a shoulder region than as straight lines. For ILL experiments, survival curves appeared linear (data not shown), although the effects of the neutron irradiation were scarcely distinguishable, due to the low neutron flux. However, since neutrons as high-LET particles are expected to form more linear survival curves for irradiated cells [69, 76], our survival curves were fitted with the simple exponential model. The cell survival seems to follow an exponential line and is therefore regarded as being in conformity with the findings reported before.

In contrast, x-ray irradiation curves from both ESRF and clinical center showed the expected shoulder region for small doses for both our cell lines. Interestingly, the shoulder region was indeed less noticeable after application of Gd-formulation, clearly indicating the effect of the enhancer as a high-LET Auger-electron donator.

5.5.6 Correlation between Gd-content in cells, Gd-related dose and cell survival

The correlation between Gd-amount taken up into F98 and LN229 cells, the deriving dose from this Gd-content, calculated by Monte Carlo simulations and the respective survival was done for the first time to our best knowledge. Although several publications have examined the uptake of NC-elements into cells, the correlation between element concentration and consequently achieved effect was seldom analyzed. As was already observed in the experiments at ILL, the different dose components of the Gd-neutron capture event, the Auger-electron cascades and the long-range gamma rays which may interact with further high-Z lanthanides (e.g. Er) in the environment and add to cellular damage, must be taken into account for the estimation of the total dose on the cellular level (fig. 5-2). The second radioenhancer can be located inside or outside the target cell and nevertheless attribute to the lesions inflicted to a cell.

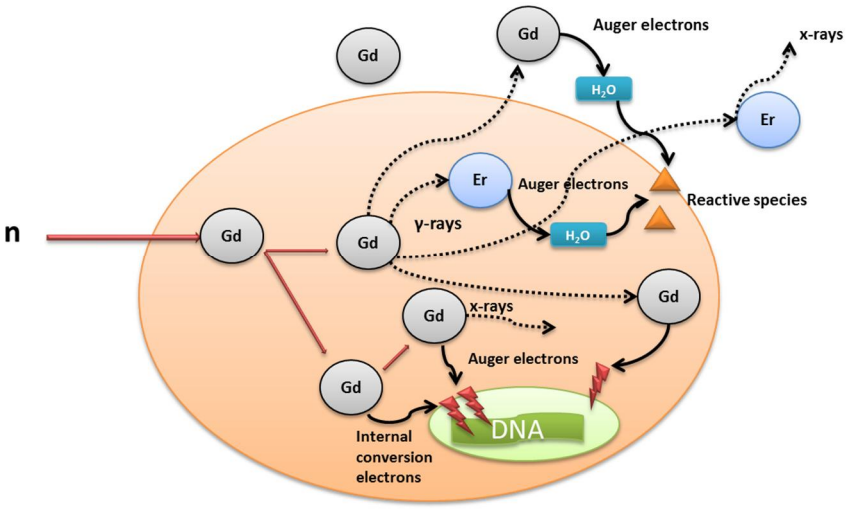

Figure 5-2 Schematic drawing of Gd-neutron capture event and subsequent interactions of resulting prompt gamma rays and Auger- and internal conversion electrons in- and outside the target cell. Simplified drawing according to scheme for indirect radiation therapy, Nawroth, Langguth, Decker at http://mpsd.de/irt/IRT.html. Reactive species may include amongst others radicals, superoxide anions or peroxides.

As described above, the fitting of survival curves from this study to the linear-quadratic model was not possible. Consequently, the model was also not adequate for the correlation of survival and Gd-derived dose. The poor correlation of results may be due to the inhomogeneity of the formulations, since different liposomal Gd-DTPA carrier were included in one survival curve based on the Gd-related dose. Nevertheless, the fit with a simple exponential function was satisfactory, if one concession was made: the exclusion of the DOPC-DOPE and the folate-liposomes. The survival data strongly indicate the dependence of cell survival on the intracellular location of Gd. Since correlation of Gd in wells (overall concentration regardless of uptake) and survival did not succeed, it was concluded that mostly high-LET Auger and internal conversion electrons from intracellular Gd were responsible for cell killing. This conclusion was also drawn by other authors [103, 211, 212]. The concept of the additional high-Z element Er as a second radioenhancer, absorbing gamma rays and releasing further Auger-electrons on the cellular level, thus increasing the dose and reducing cell survival to a greater extent than with Gd alone, was based on the same assumption.

The differences between individual liposomal formulations of Gd-DTPA and their influence on cell killing were not taken into account before. The exclusion of the two formulations from correlation between Gd-content in cells and respective cell survival led to reasonable good correlation. This indicates that these liposomes delivered their cargo to different cell compartments than other formulations, thus bringing Gd in closer proximity to cellular DNA. As described above, all other formulations did either have small effect while Gd-content was also small or high effect for high Gd-amount. Interestingly, the DOPE-formulation with 10 mol% DOPE did not achieve such high decrease in cell survival as the 50 mol% mixture. However, cationic liposomes for gene delivery traditionally content 50 mol% of the helper lipid and our findings confirm the assumption that lower contents do not enhance cytosolic delivery sufficiently. The correlation of free Magnevist (Gd-content per well) and cell survival was surprisingly good, regarding that the Gd-content per well of different liposomal formulations and free Magnevist did not correlate at all. There are two possible explanations for this phenomenon: first, the gamma-rays from Gd-neutron capture event have an impact on cell survival after all, i.e. higher concentration of Gd in the medium results in lower cell survival, or second, the good correlation simply derives from the nearly linear uptake kinetics of free Magnevist into cells. Thus, the higher the concentration in the

medium, the higher the uptake into cells would be. The latter seems to be the more likely conclusion, given that in general, the gamma rays are more or less neglected in GdNCT and we, among others, have found that a change of Gd-containing medium before neutron irradiation did not alter the outcome of cell survival (data not shown). It is still not clear in what way the long-range gamma rays from the Gd-capture event contribute to cell killing. From our point of view, the impact may be relatively small, since the high Gd-amounts in cell media practically have no influence on cell survival. On the other hand, the presence of an additional lanthanide in the ILL experiments resulted in increased cell killing – this effect should also occur with further Gd-atoms, interacting with gamma rays from another Gd-NC-event. Monte Carlo simulation showed extraordinarily high Gd-derived dose in the medium above cells during irradiation. Maximum doses were approximately 350 Gy in the well, based on the total Gd-amount, but cell survival was not diminished accordingly. For such high dose, one would expect complete cell killing. Instead, cell survival was for the most part merely reduced for 20 to 50 percent. Of course, the Gd-derived dose was estimated too high in the wells, due to the inclusion of the long gamma rays which travel further in tissue and will not depose all their energy at their origin. Nevertheless, these findings are in favor of high attribution from only the Gd-amount taken up into cells, rather than from the Gd-amount in the medium above the cells.

The sharp dose decline at the edge of the well showed that the simulation neglected parts of the long-range gamma rays generated from the Gd-NC-event which definitely would reach the adjacent wells due to their high energy. The energy shown as absorbed in the wells does not represent the actual dose delivered. Interactions of photons with matter, such as photoelectric effect, Compton scattering and pair creation may occur along the path of the gamma rays, but the mean free path in water of, for example, 500 keV photons is already as long as 10 cm [231]. Furthermore, the depth of the dose maximum of a 6 MV beam whose energy spectrum is comparable to the spectrum emitted by Gd after neutron capture, lies in approximately 1.5 cm tissue depth [69]. Consequently, the energy deposition shown by the Monte Carlo simulations here needs to be adjusted and shifted towards lower doses in the wells, probably with a less sharp dose decline at their edges. In contrast, the Auger- and conversion electrons (approximately 5 and 0.6 per neutron capture event, with energies of 4.2 and 46.3 keV, respectively [103]) will deposit their energy in a range of possibly less than 100 nm, that is, still in the tumor cell where the Gd-atom is located [232]. Nonetheless, for three-dimensional tumors, it is conceivable that γ-rays may help to reduce tumor tissue, especially if they also interact with Gd outside the cell and release secondary short-range electrons (cf. fig. 5-2). In the tumor environment, the long-range gamma rays also could add up when coming from inside and outside the tumor, thus indeed inflicting serious DNA damage and leading to cell death. At the same time, one has to bear in mind that by this means the long-range photons could also damage healthy tissue around the tumor, which is the main drawback of GdNCT in comparison to BNCT.

The results of the study state that the achievement of high Gd-delivery into cells alone does not necessarily result in high effects for cell irradiation with thermal neutrons. The intracellular position of Gd-atoms or other high-Z elements has a great influence on DNA damage and therefore, intracellular delivery must be carefully orchestrated to ensure Gd-accumulation in proximity to the nucleus. The addition of a second radioenhancer such as erbium can improve the cell killing effect from Gd-NCT. The liposomal formulations developed for Gd-NCT and Gd as radioenhancing element in photon irradiation have been proven to solidly ameliorate Gd-uptake into cells, thereby enhancing irradiation effect for F98 and LN229 glioma cells significantly. The impact on cell survival was different for individual liposome-mixtures and did not depend solely on Gd-delivery into cells, but obviously also on the intracellular depositing of Gd.

6 Summary

The improvement of radiation therapy via application of liposomal radioenhancer or neutron capture element has been the main objective of this study, integrated in the BMBF-project "Indirect radiation therapy with target nanoparticles". Several new liposome-based formulations of gadolinium-DTPA were developed, characterized and successfully tested at different radiation facilities for radiation treatment of our in vitro model for glioblastoma multiforme (F98 and LN229 cell lines).

The development of liposomes entrapping Gd-DTPA included close monitoring of several factors for liposome characterization, such as size (100-150 nm), entrapment efficiency, liberation of Gd-DTPA, uptake and thereby delivery of Gd-DTPA into glioma cells, toxicity and performance under treatment conditions. Five liposomal formulations of Magnevist® (DOTAP-, Cl-, DOPC-DOPE-, folate- and DOPE-liposomes) were optimized for the application in neutron capture therapy and tested for their suitability and efficacy in Gd-NCT.

The proof-of-principle for the radioenhancing effect of Gd-DTPA was given through experiments with synchrotron radiation at the ESRF, France. The irradiation of cells treated with Magnevist® above the K-absorption edge of Gd resulted in significantly lower cell survival than with radiation below the K-edge. The 'on-switch' of the Auger-electron cascade after photoelectric interaction of photons of a defined energy (above K-edge, 51.2 keV) with electrons of Gd-shell led to higher cell death than application of photons of slightly lower energy (below K-edge, 49.2 keV) which do not possess suitable energy to promote Auger electron formation by K-shell ionization. Here, the application of Gd-DTPA distinctly showed beneficial effect on cell survival reduction. Liposomal formulations of Magnevist® further reduced cell survival and highest effects on F98 cells were additional 30% lower survival for a dose of 8 Gy (based on irradiated control, cardiolipin-formulation). Although these results with photon irradiation were very promising, the experiments in the university clinical center with clinically used linear accelerators did not lead to the same satisfying results. As expected from the synchrotron experiments, the energy spectrum of the applied photons plays a major role in the successful radioenhancement with Gd-DTPA. It was suspected that the spectrum in the central field of a clinical linear accelerator with high proportions of high energy photons (up to 6 MeV) would not be as suitable for our formulations as the monochromatic beam of 51.2 keV at the ESRF. Experiments conducted in the outer region of the radiation field (i.e. off-axis from the central beam) where the fluence of photons with lower relative spectral energy is higher than in the center, confirmed the hypothesis. The effect of liposomal Magnevist® on cell survival was more pronounced here than in the main irradiation field, due to the higher proportion of adequate photon energy for photoelectric interaction with the Gd-Kedge and subsequent Auger electron-release. Nevertheless, the overall effect of the radioenhancer Gd was still relatively low (approximately 10% for 8 Gy, F98 cells, cardiolipin-liposomes).

The small effects of the liposomal radioenhancer Gd-DTPA under conventional external beam irradiation led to a stronger focus on alternative radiation therapies for glioblastoma multiforme, more precisely on neutron capture therapy. Since ^{157}Gd is a very potent neutron capture agent with a cross-section for thermal neutrons 66 times higher than 10-boron, liposomal formulations of Magnevist® were expected to significantly influence cell survival under neutron irradiation. The feasibility of the Gd-NCT approach with cold neutrons, for which Gd has an even higher cross section than for thermal neutrons, has been shown for our model cell line F98 at the D22 beamline of the Institute Laue-Langevin (ILL), Grenoble.

Here, the first application of the additional radioenhancer erbium besides gadolinium showed a distinct benefit in cell survival reduction. The high-Z element erbium may interact photoelectrically with gamma rays from the Gd-neutron capture event and release Auger electrons. Thus, further damage is inflicted to the cell, resulting in enhanced cell killing of the tumor cells.

Gadolinium neutron capture experiments with thermal neutrons were carried out at TRIGA reactor, Mainz. The irradiation experiments at the thermal column of TRIGA reactor showed a very high impact of the Gd-compound on cell survival for both our model cell lines (up to 65% lower cell survival based on irradiated control, F98 cells, DOPC-DOPE-formulation). Further investigations had the aim to decipher observed differences in regard to cell survival reduction between liposomal formulations. Therefore, the uptake and Gd-DTPA-delivery into cancer cells was analyzed by fluorimetric measurements of labeled liposomes and ICP-MS determination of Gd-content in F98 and LN229 cells. The liposomal formulations differed considerably in their ability to enter cells and deposit their cargo in the cell interior. DOTAP liposomes achieved highest Gd-accumulation in both cell lines and consequently reduced cell survival to a great extent, but folate-targeted and DOPC-DOPE liposomes led despite low Gd-deposition as well to extremely low cell survival. The discrepancy between those findings was ascribed to different uptake modalities of the liposomes. As different uptake pathways can lead to dissimilar fates of the endocytosed particles we suggest that folate-and DOPC-DOPE liposomes enter cells by a more favorable path and deposit their cargo of Gd-DTPA in closer proximity to cellular DNA, thus leading to relatively higher cell reduction. The proximity to DNA is mandatory for successful Gd-NCT, since primarily short-ranged Auger and internal conversion electrons are made responsible for DNA destruction and subsequent cell death.

Correlation of intracellular Gd-content and respective cell survival support this hypothesis, while the experiments at ILL with the second radioenhancer erbium also showed the influence of the prompt gamma rays from the Gd-neutron capture event. Still, the increase of the radiation effect is based on the formation of further high-LET secondary electrons, this time from the second radioenhancer erbium. Apart from folate- and DOPC-DOPE liposomes, the Gd-content/Gd-derived dose and the cell survival could be interrelated according to exponential fit and led to satisfactory correlation. To our knowledge, ours was the first time that biologically assessed cell survival after treatment with neutron capture-agent Gd and neutron irradiation was successfully set in relation to the Gd-derived dose, calculated by Monte Carlo simulations based on cellular Gd-uptake. The findings underline the importance of Auger electrons to DNA damage and cell death, and consequently also of the exact location of Gd inside the target cell. Nevertheless, the prompt gamma rays could be used for administration of an even higher dose, if there is the possibility of interaction with other high-Z elements in the tumor mass.

In conclusion, the application of the newly developed liposomal Gd-DTPA formulations was found to be highly beneficial for in vitro neutron capture therapy of glioblastoma cells. The concept of introducing a second radioenhancer to interact with gamma rays from the Gd-neutron capture event was proved to be successful and a promising tool for future applications. The variances in treatment enhancement observed from five different liposome compositions for transport of Gd-DTPA tested here emphasize the significance of designing and choosing the right transport vehicle for the destined application, matched to the respective requirements of drug delivery and therapy.

7 Appendix

A. Synchrotron irradiation experiments

Experiment MD 287

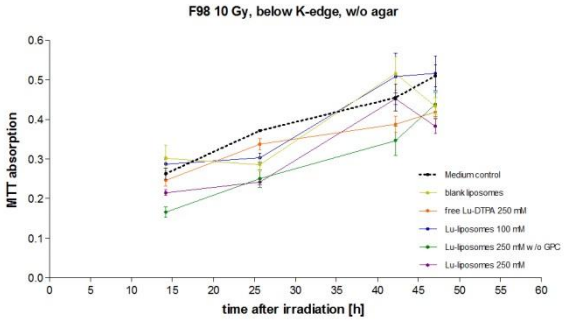

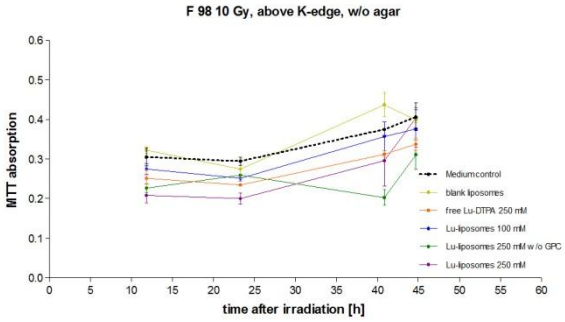

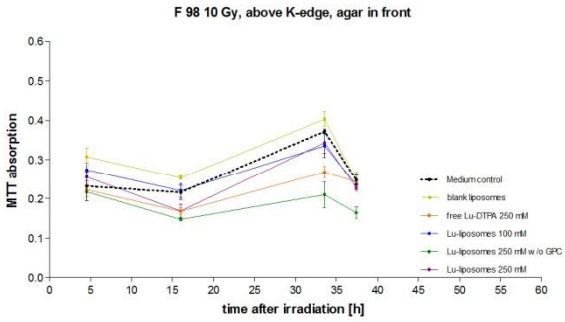

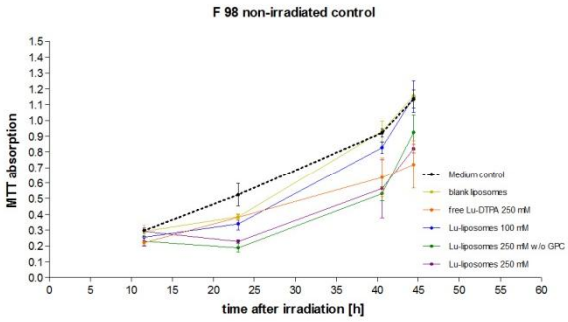

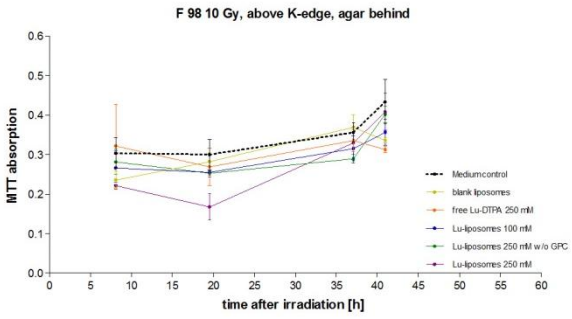

Experiment MD 485 **A**

a. Proliferation curves of F98 cells after irradiation with synchrotron radiation (above Gd-K-edge: +, below Gd-K-edge: -).

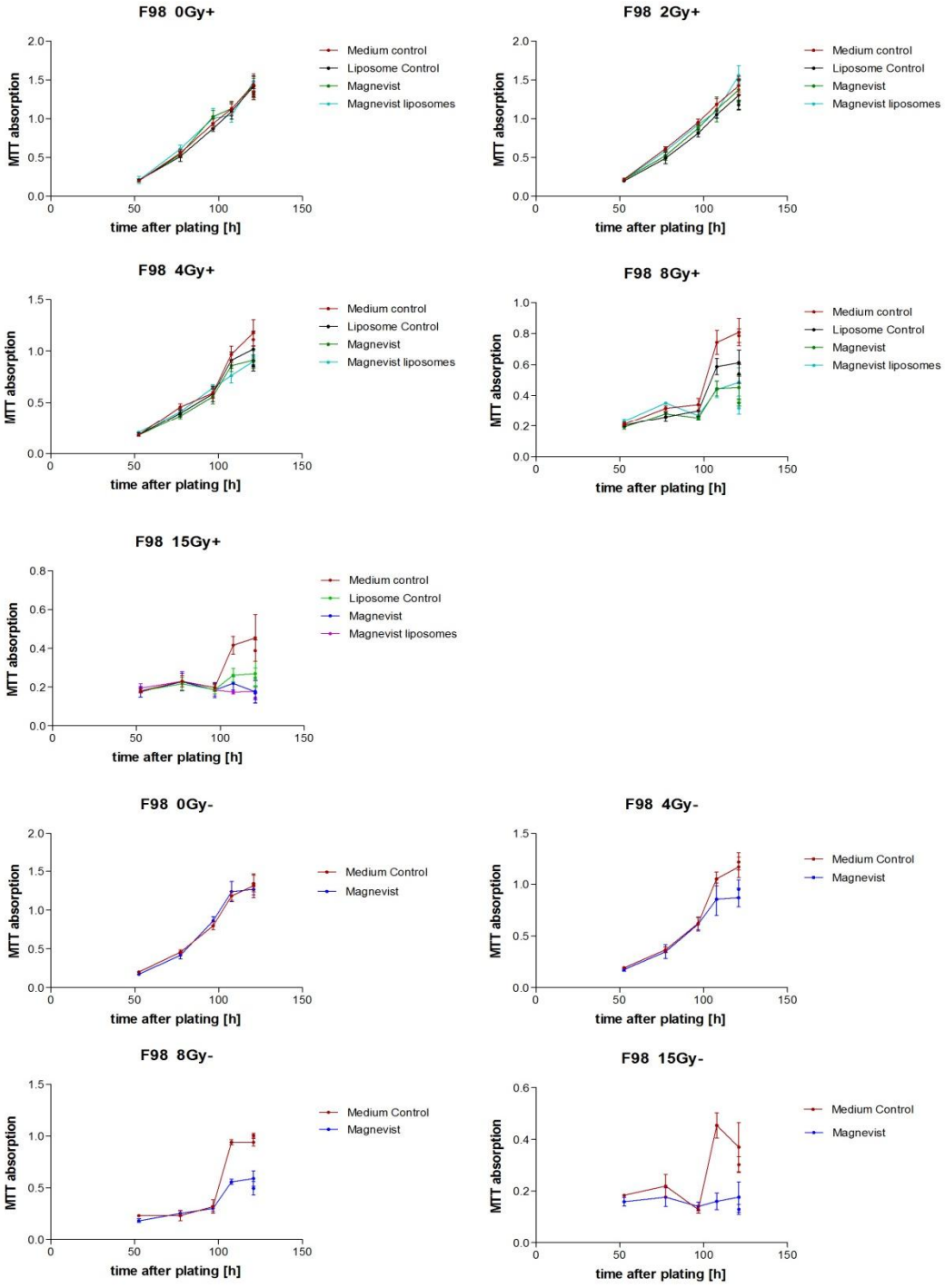

Experiment MD 485 **B**

a. Proliferation curves of irradiated F98 cells (above Gd-K-edge).

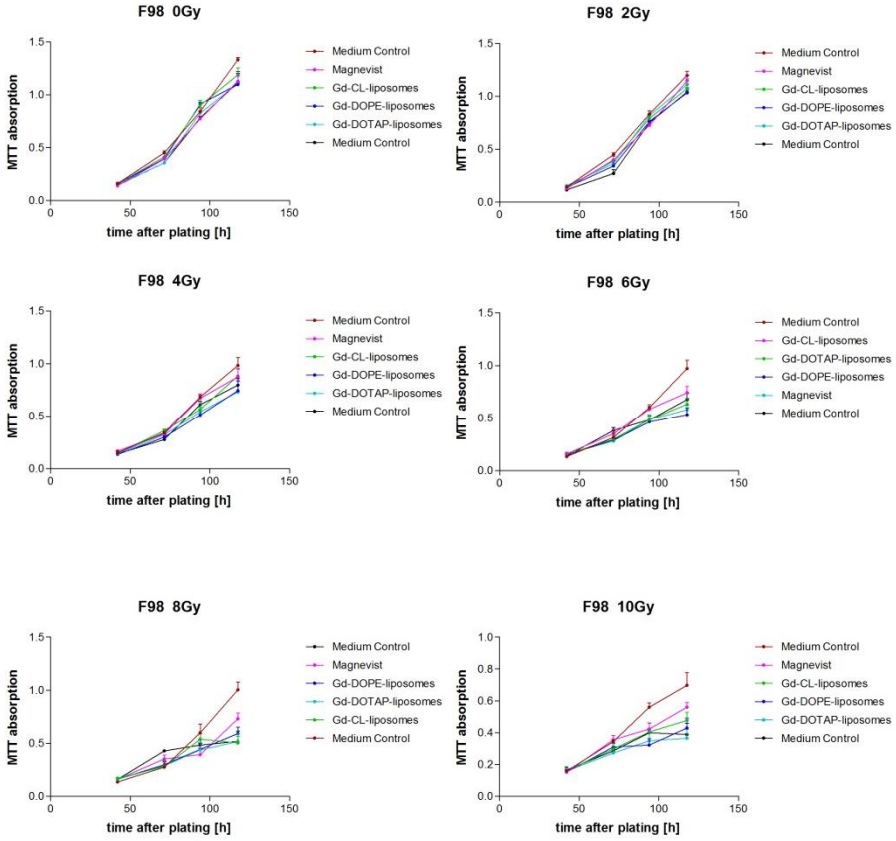

b. Proliferation curves of irradiated LN229 cells (above Gd-K-edge).

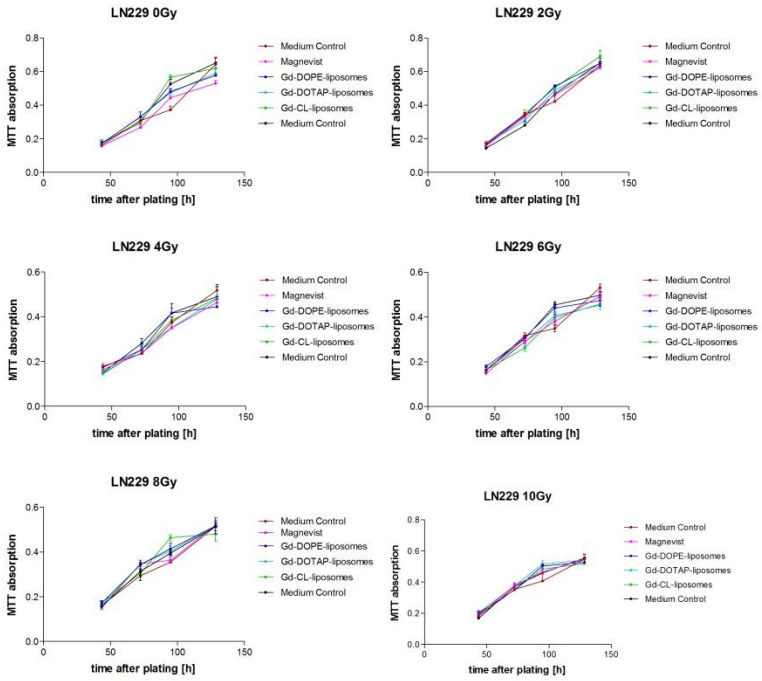

B. Linac irradiation at University Medical Center (Johannes Gutenberg-University Mainz)

a. Proliferation curves of F98 cells

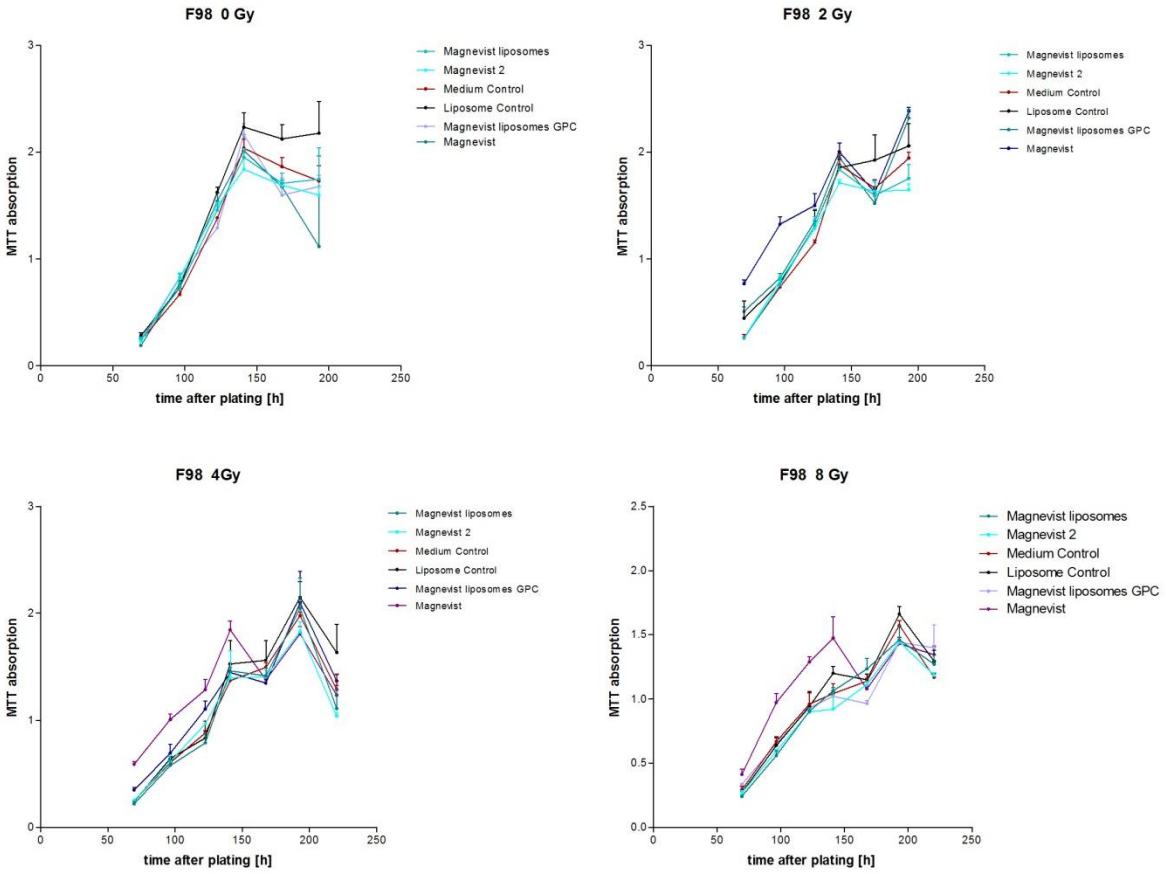

b. Proliferation curves of irradiated F98 cells, effect of energy spectrum (outer region of radiation field)

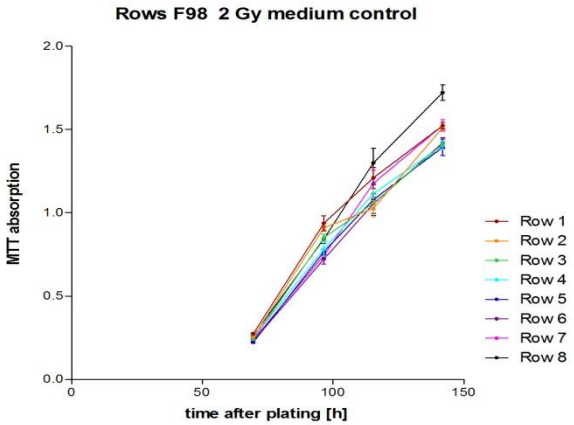

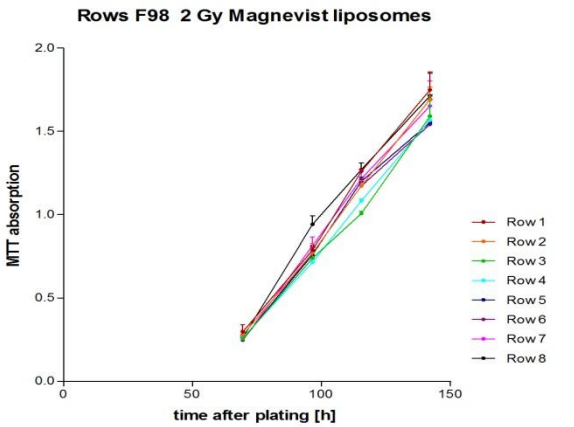

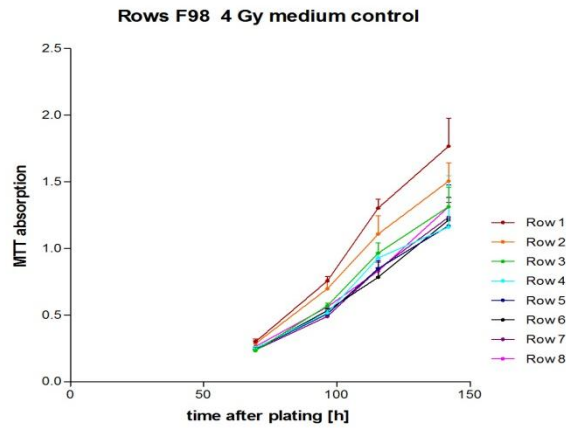

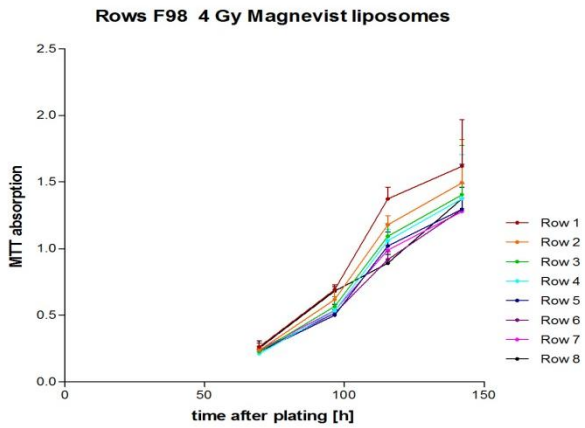

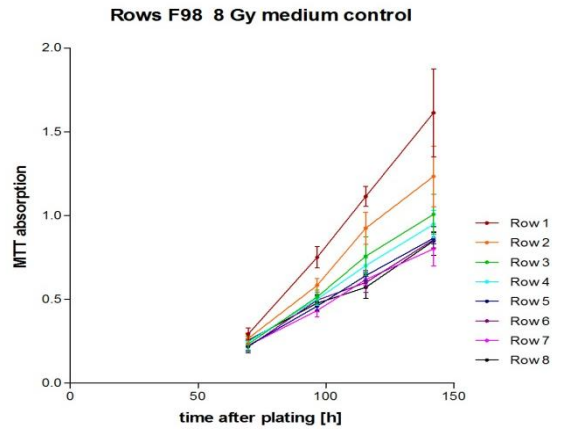

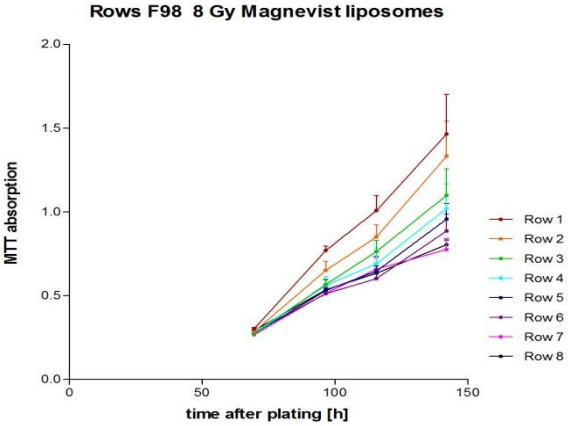

C. Neutron irradiation experiments at D22, ILL

Experiment BAG-8-4

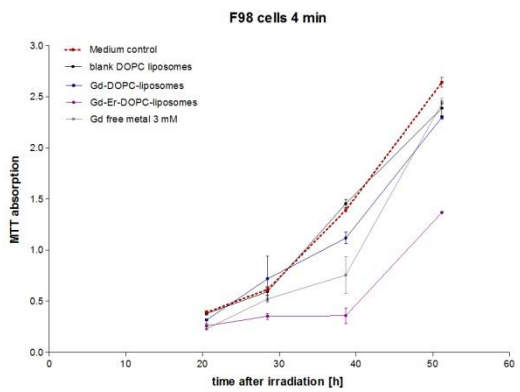

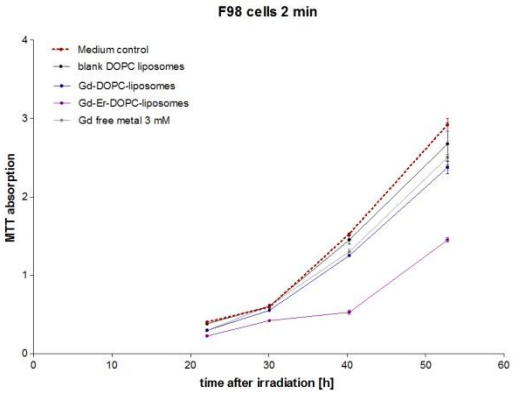

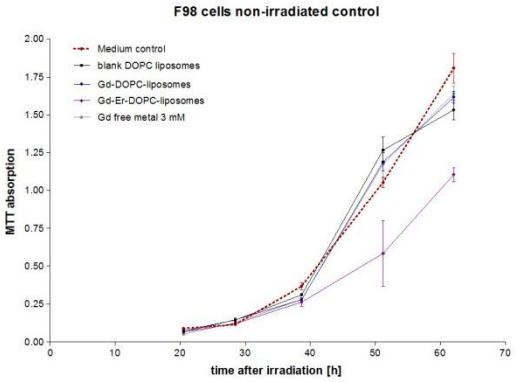

Experiment LTP-8-1

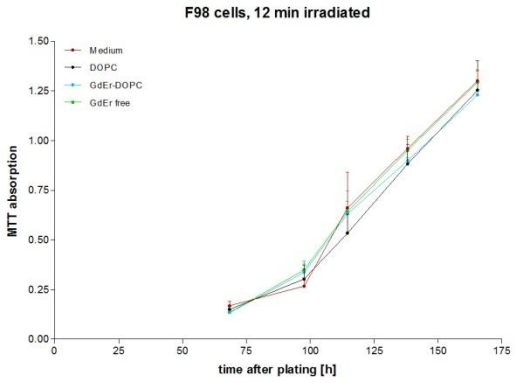

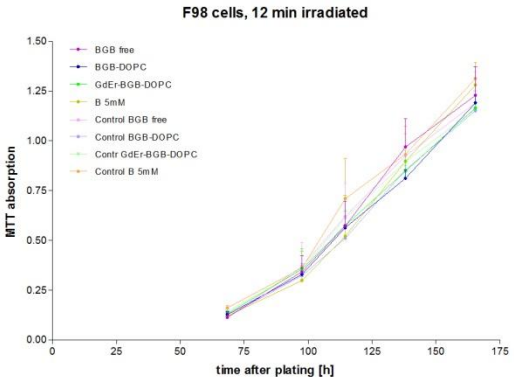

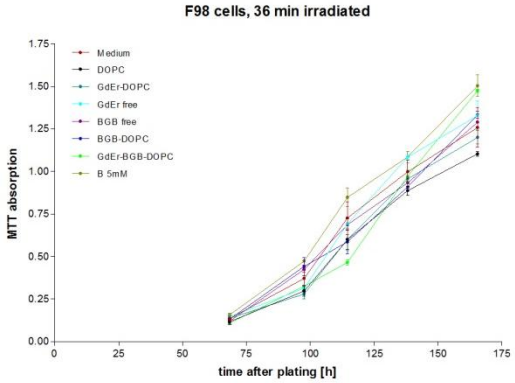

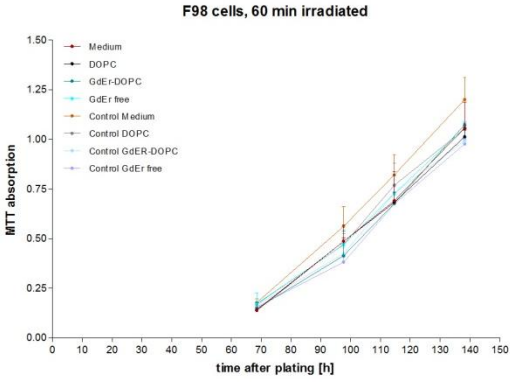

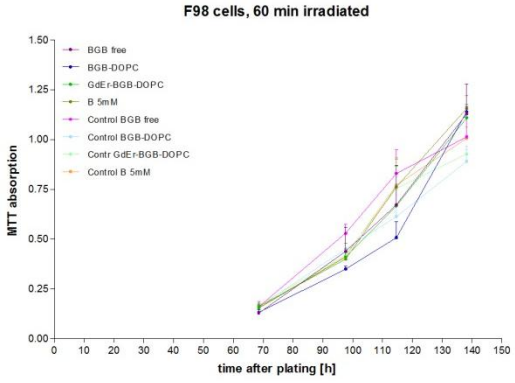

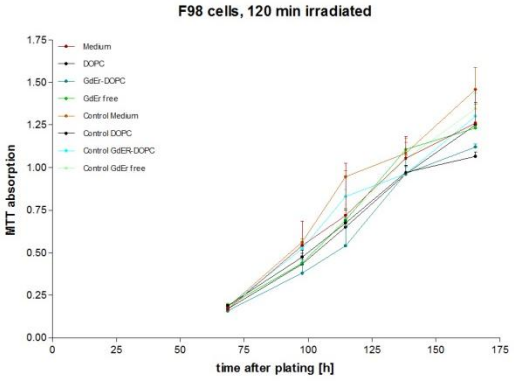

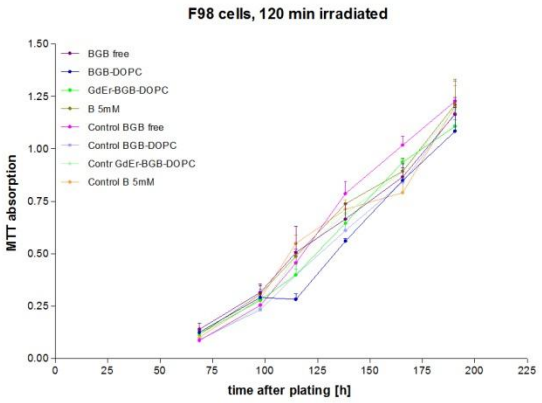
F98 cells, 120 min irradiated
BGB free
BGB-DOPC
GdEr-BGB-DOPC
B 5mM
Control BGB free
Control BGB-DOPC
Contr GdEr-BGB-DOPC
Control B 5mM
MTT absorption
time after plating [h]

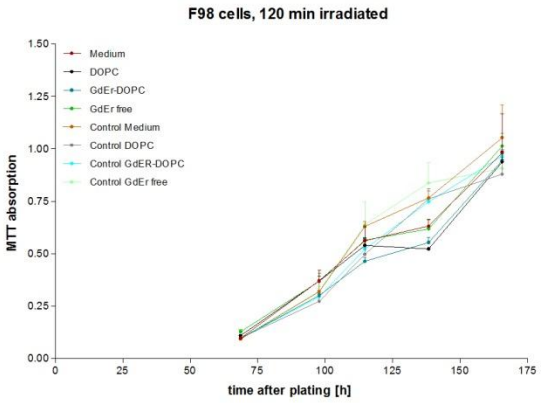
F98 cells, 120 min irradiated
Medium
DOPC
GdEr-DOPC
GdEr free
Control Medium
Control DOPC
Control GdER-DOPC
Control GdEr free
MTT absorption
time after plating [h]

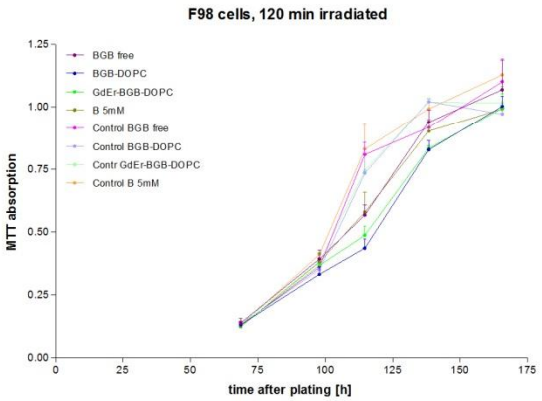
F98 cells, 120 min irradiated
BGB free
BGB-DOPC
GdEr-BGB-DOPC
B 5mM
Control BGB free
Control BGB-DOPC
Contr GdEr-BGB-DOPC
Control B 5mM
MTT absorption
time after plating [h]

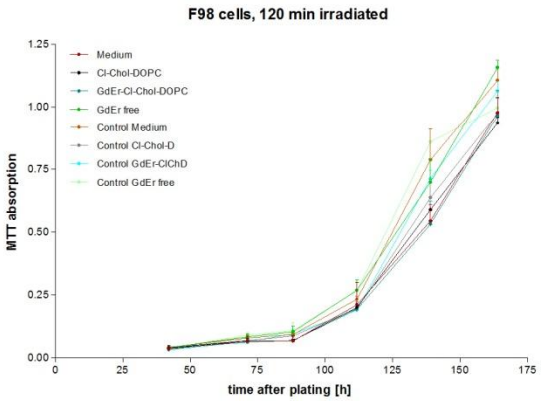
F98 cells, 120 min irradiated
Medium
Cl-Chol-DOPC
GdEr-Cl-Chol-DOPC
GdEr free
Control Medium
Control Cl-Chol-D
Control GdEr-ClChD
Control GdEr free
MTT absorption
time after plating [h]

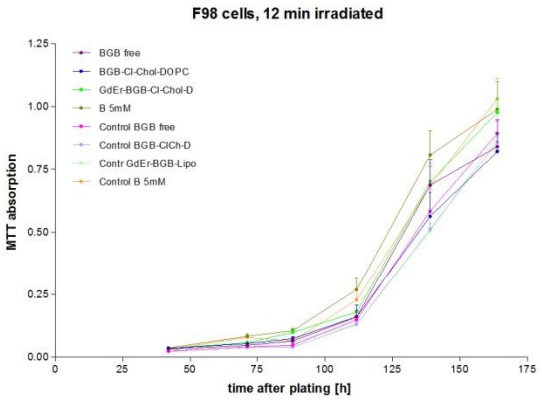
F98 cells, 12 min irradiated
BGB free
BGB-Cl-Chol-DOPC
GdEr-BGB-Cl-Chol-D
B 5mM
Control BGB free
Control BGB-ClCh-D
Contr GdEr-BGB-Lipo
Control B 5mM
MTT absorption
time after plating [h]

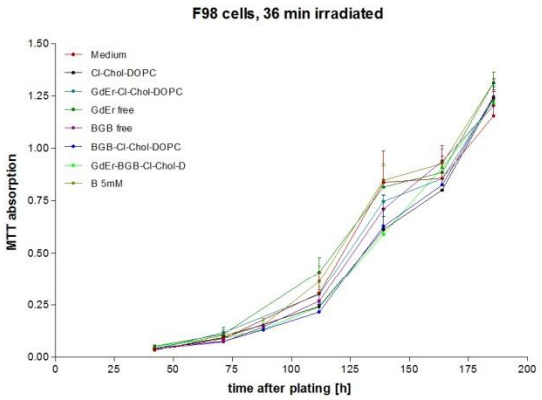
F98 cells, 36 min irradiated
Medium
Cl-Chol-DOPC
GdEr-Cl-Chol-DOPC
GdEr free
BGB free
BGB-Cl-Chol-DOPC
GdEr-BGB-Cl-Chol-D
B 5mM
MTT absorption
time after plating [h]

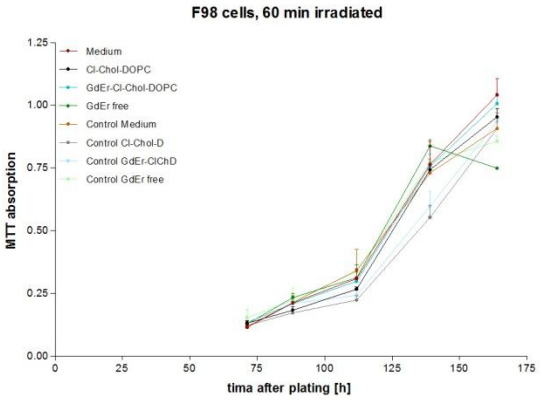
F98 cells, 60 min irradiated
Medium
Cl-Chol-DOPC
GdEr-Cl-Chol-DOPC
GdEr free
Control Medium
Control Cl-Chol-D
Control GdEr-ClChD
Control GdEr free
MTT absorption
tima after plating [h]

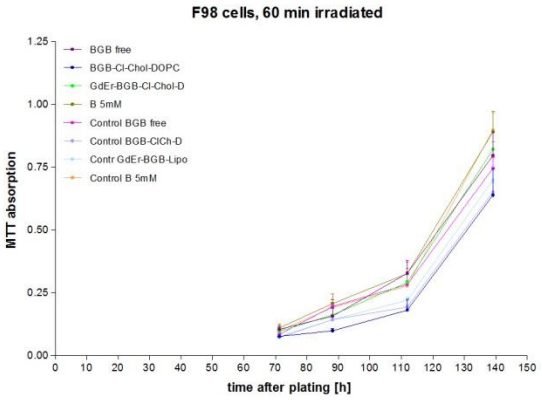
F98 cells, 60 min irradiated
BGB free
BGB-Cl-Chol-DOPC
GdEr-BGB-Cl-Chol-D
B 5mM
Control BGB free
Control BGB-ClCh-D
Contr GdEr-BGB-Lipo
Control B 5mM
MTT absorption
time after plating [h]

Experiment LTP-8-1: Irradiation in Gd-environment

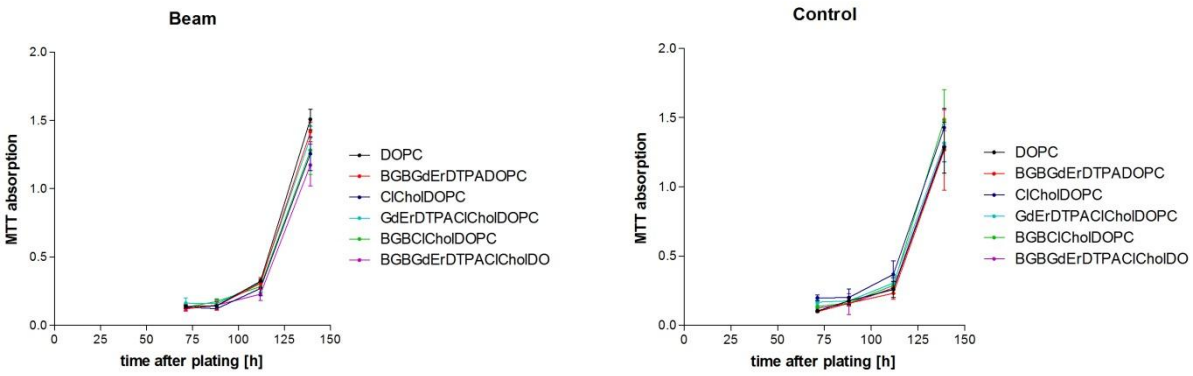

D. Neutron irradiation experiments at TRIGA reactor

a. Feasibility of NC-element approach. Proliferation curves of neutron-irradiated F98 and LN229 cells.

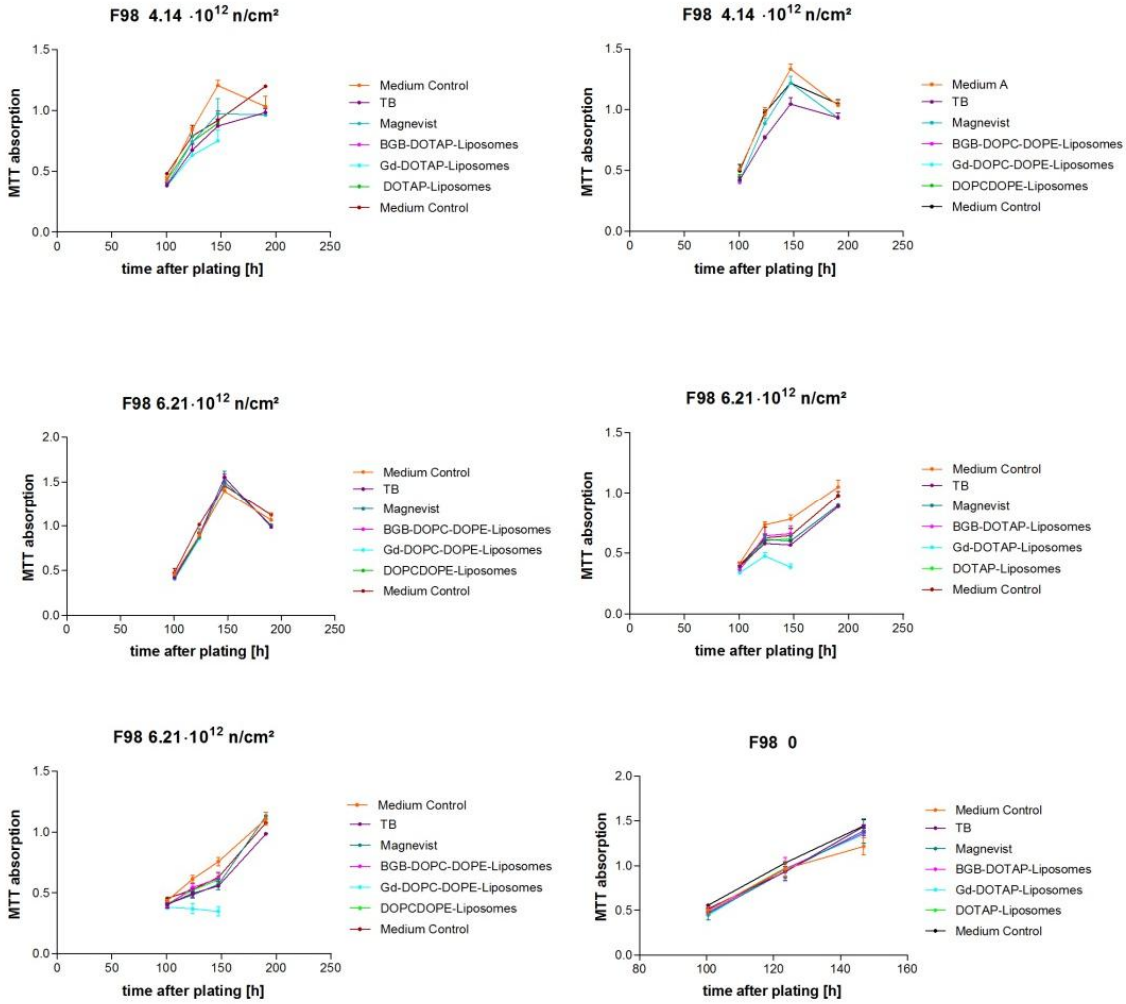

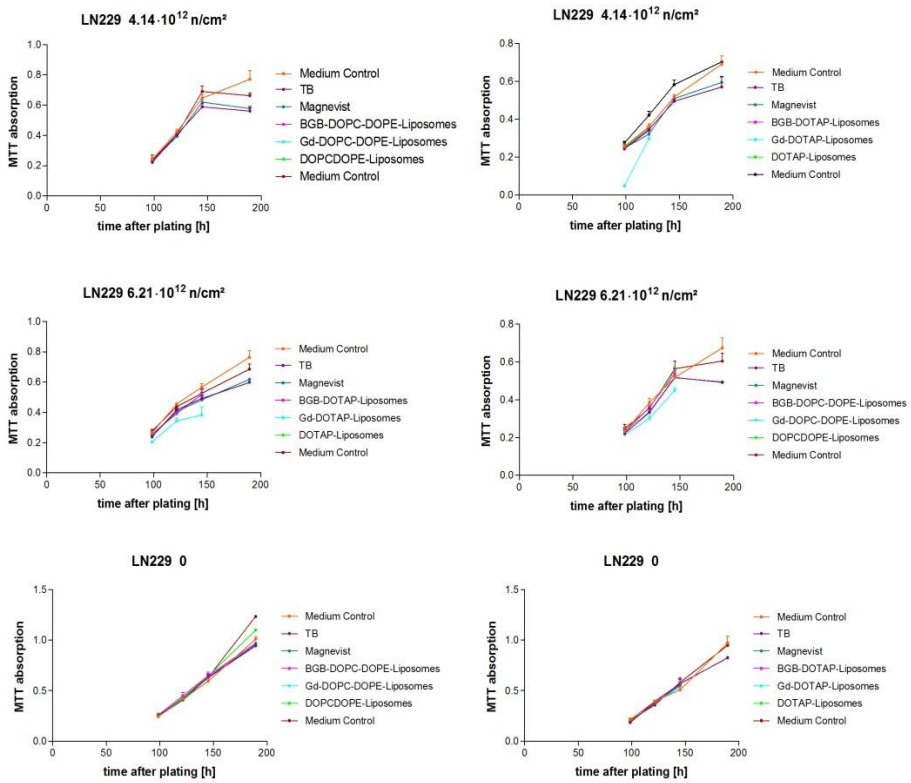

b. Proliferation curves of neutron-irradiated F98 and LN229 cells.

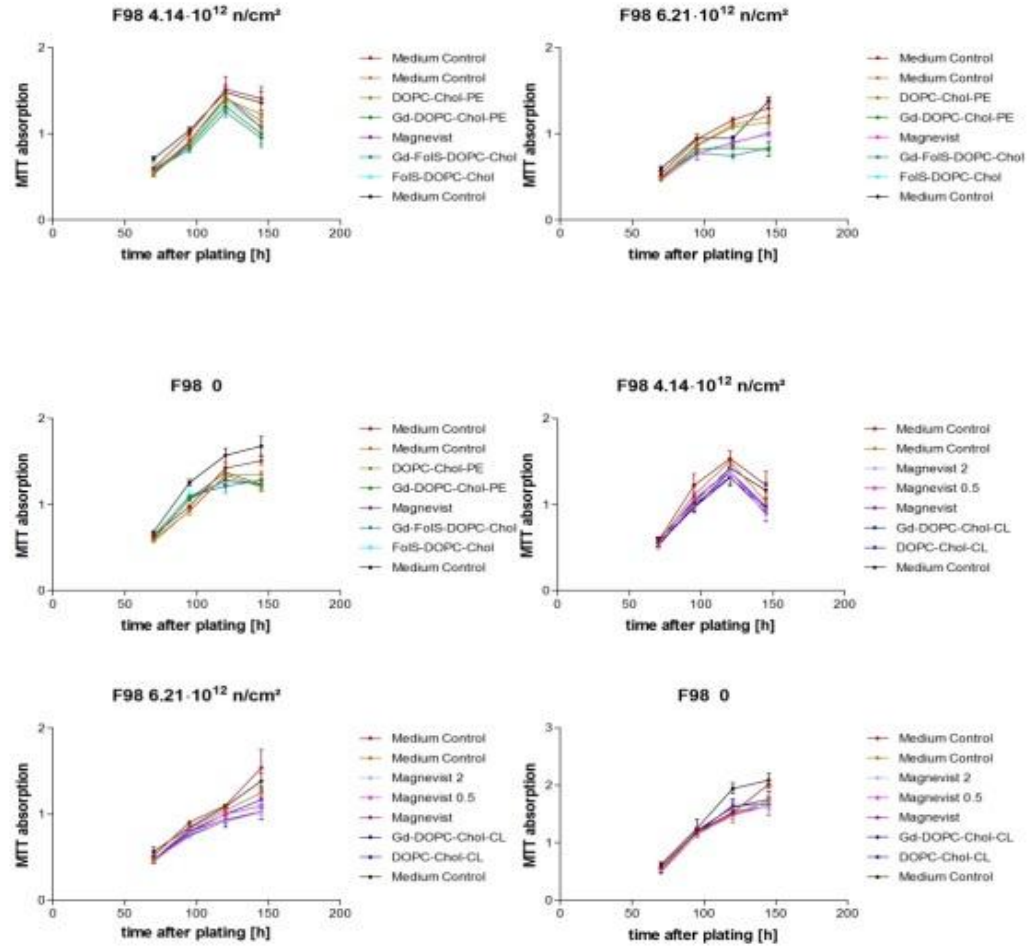

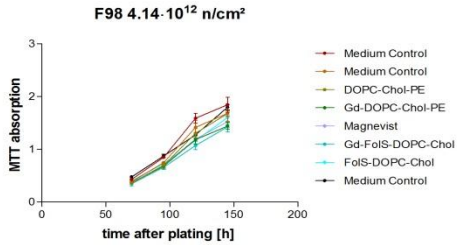
F98 4.14·10^12 n/cm²
MTT absorption
time after plating [h]
Medium Control
Medium Control
DOPC-Chol-PE
Gd-DOPC-Chol-PE
Magnevist
Gd-FolS-DOPC-Chol
FolS-DOPC-Chol
Medium Control

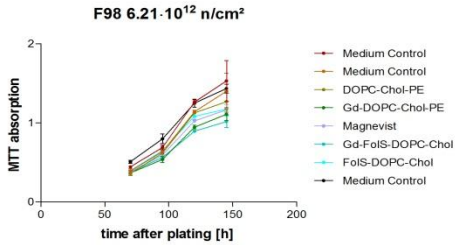
F98 6.21·10^12 n/cm²
MTT absorption
time after plating [h]
Medium Control
Medium Control
DOPC-Chol-PE
Gd-DOPC-Chol-PE
Magnevist
Gd-FolS-DOPC-Chol
FolS-DOPC-Chol
Medium Control

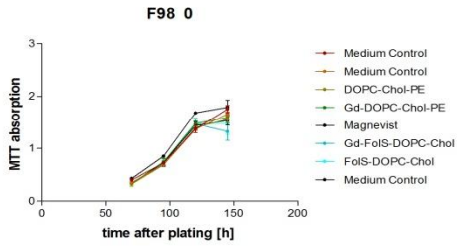
F98 0
MTT absorption
time after plating [h]
Medium Control
Medium Control
DOPC-Chol-PE
Gd-DOPC-Chol-PE
Magnevist
Gd-FolS-DOPC-Chol
FolS-DOPC-Chol
Medium Control

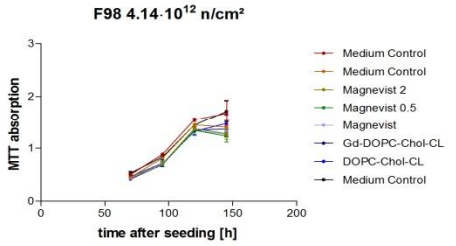
F98 4.14·10^12 n/cm²
MTT absorption
time after seeding [h]
Medium Control
Medium Control
Magnevist 2
Magnevist 0.5
Magnevist
Gd-DOPC-Chol-CL
DOPC-Chol-CL
Medium Control

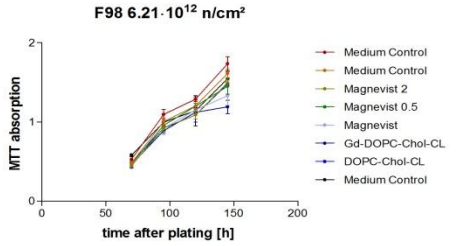
F98 6.21·10^12 n/cm²
MTT absorption
time after plating [h]
Medium Control
Medium Control
Magnevist 2
Magnevist 0.5
Magnevist
Gd-DOPC-Chol-CL
DOPC-Chol-CL
Medium Control

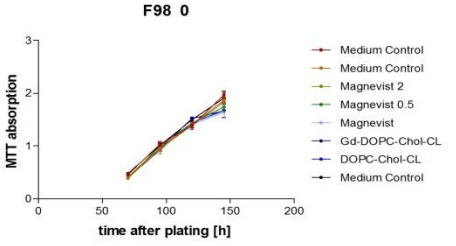
F98 0
MTT absorption
time after plating [h]
Medium Control
Medium Control
Magnevist 2
Magnevist 0.5
Magnevist
Gd-DOPC-Chol-CL
DOPC-Chol-CL
Medium Control

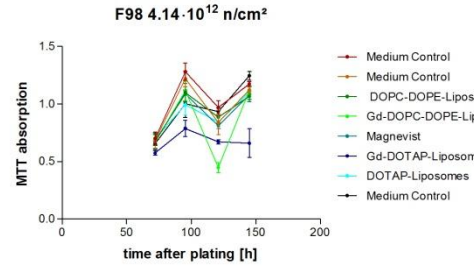
F98 4.14·10^12 n/cm²
MTT absorption
time after plating [h]
Medium Control
Medium Control
DOPC-DOPE-Liposomes
Gd-DOPC-DOPE-Liposomes
Magnevist
Gd-DOTAP-Liposomes
DOTAP-Liposomes
Medium Control

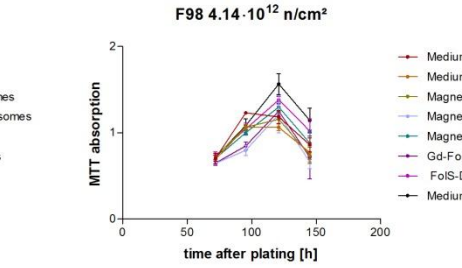
F98 4.14·10^12 n/cm²
MTT absorption
time after plating [h]
Medium Control
Medium Control
Magnevist 2
Magnevist 0.5
Magnevist
Gd-FolS-DOPC-Chol-Liposomes
FolS-DOPC-Chol-Liposomes
Medium Control

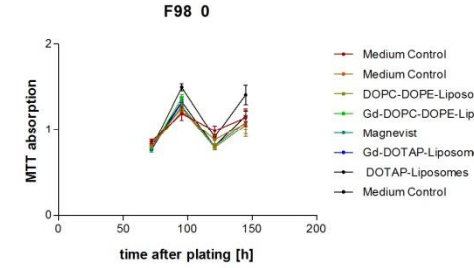
F98 0
MTT absorption
time after plating [h]
Medium Control
Medium Control
DOPC-DOPE-Liposomes
Gd-DOPC-DOPE-Liposomes
Magnevist
Gd-DOTAP-Liposomes
DOTAP-Liposomes
Medium Control

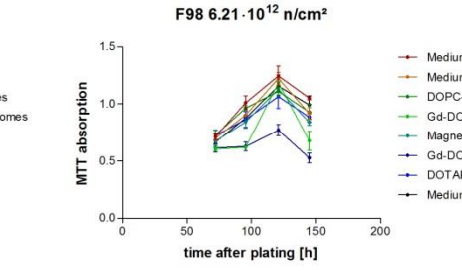
F98 6.21·10^12 n/cm²
MTT absorption
time after plating [h]
Medium Control
Medium Control
DOPC-DOPE-Liposomes
Gd-DOPC-DOPE-Liposomes
Magnevist
Gd-DOTAP-Liposomes
DOTAP-Liposomes
Medium Control

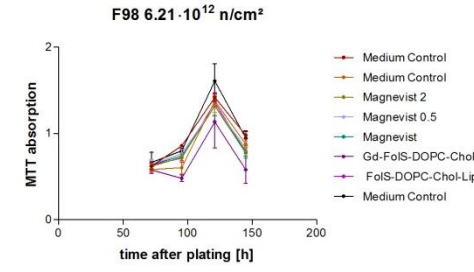
F98 6.21·10^12 n/cm²
MTT absorption
time after plating [h]
Medium Control
Medium Control
Magnevist 2
Magnevist 0.5
Magnevist
Gd-FolS-DOPC-Chol-Liposomes
FolS-DOPC-Chol-Liposomes
Medium Control

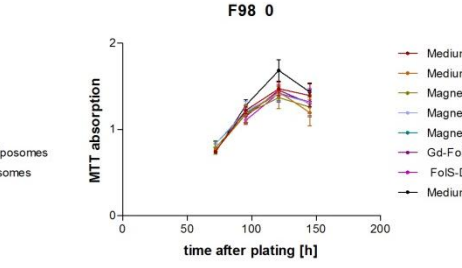
F98 0
MTT absorption
time after plating [h]
Medium Control
Medium Control
Magnevist 2
Magnevist 0.5
Magnevist
Gd-FolS-DOPC-Chol-Liposomes
FolS-DOPC-Chol-Liposomes
Medium Control

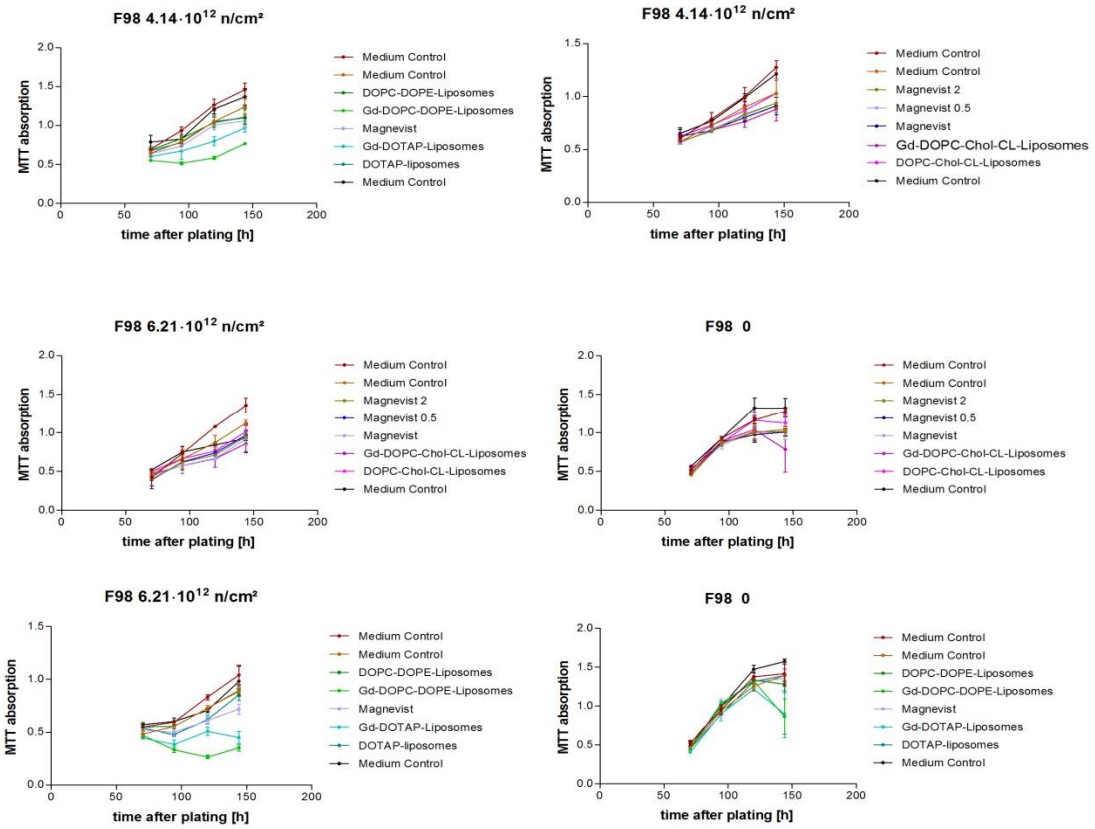

c. Proliferation curves of irradiated LN229 cells after treatment with NC-element Gd-DTPA.

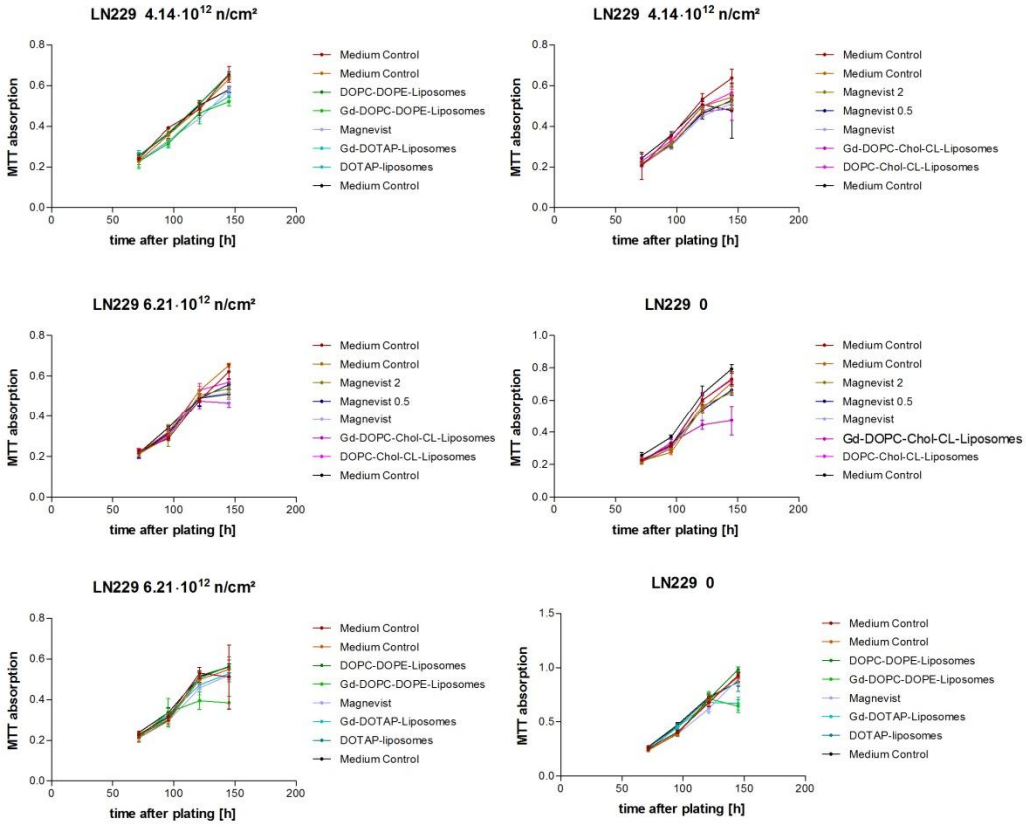

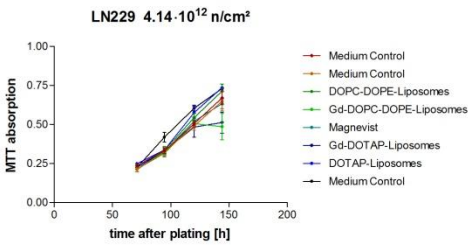
LN229 4.14·10^12 n/cm²
MTT absorption
time after plating [h]
Medium Control
Medium Control
DOPC-DOPE-Liposomes
Gd-DOPC-DOPE-Liposomes
Magnevist
Gd-DOTAP-Liposomes
DOTAP-Liposomes
Medium Control

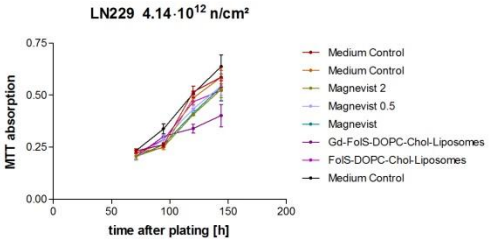
LN229 4.14·10^12 n/cm²
MTT absorption
time after plating [h]
Medium Control
Medium Control
Magnevist 2
Magnevist 0.5
Magnevist
Gd-FolS-DOPC-Chol-Liposomes
FolS-DOPC-Chol-Liposomes
Medium Control

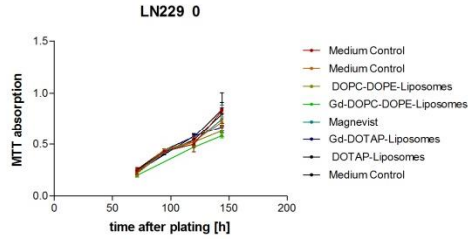
LN229 0
MTT absorption
time after plating [h]
Medium Control
Medium Control
DOPC-DOPE-Liposomes
Gd-DOPC-DOPE-Liposomes
Magnevist
Gd-DOTAP-Liposomes
DOTAP-Liposomes
Medium Control

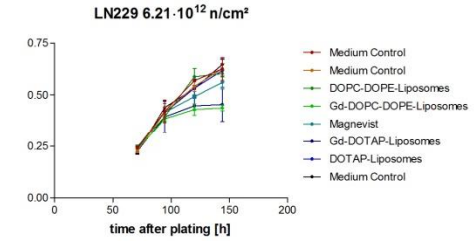
LN229 6.21·10^12 n/cm²
time after plating [h]
Medium Control
Medium Control
DOPC-DOPE-Liposomes
Gd-DOPC-DOPE-Liposomes
Magnevist
Gd-DOTAP-Liposomes
DOTAP-Liposomes
Medium Control

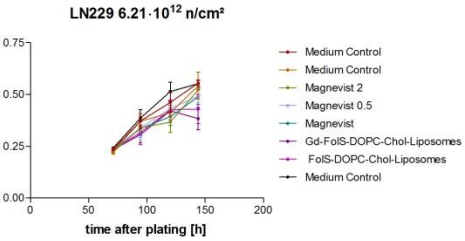
LN229 6.21·10^12 n/cm²
time after plating [h]
Medium Control
Medium Control
Magnevist 2
Magnevist 0.5
Magnevist
Gd-FolS-DOPC-Chol-Liposomes
FolS-DOPC-Chol-Liposomes
Medium Control

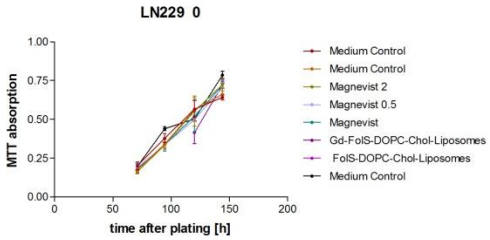
LN229 0
MTT absorption
time after plating [h]
Medium Control
Medium Control
Magnevist 2
Magnevist 0.5
Magnevist
Gd-FolS-DOPC-Chol-Liposomes
FolS-DOPC-Chol-Liposomes
Medium Control

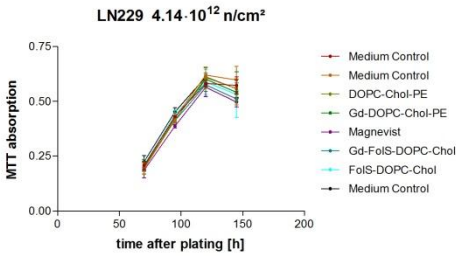
LN229 4.14·10^12 n/cm²
MTT absorption
time after plating [h]
Medium Control
Medium Control
DOPC-Chol-PE
Gd-DOPC-Chol-PE
Magnevist
Gd-FolS-DOPC-Chol
FolS-DOPC-Chol
Medium Control

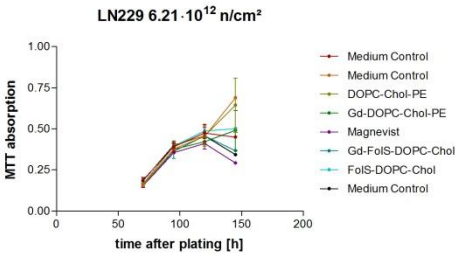
LN229 6.21·10^12 n/cm²
MTT absorption
time after plating [h]
Medium Control
Medium Control
DOPC-Chol-PE
Gd-DOPC-Chol-PE
Magnevist
Gd-FolS-DOPC-Chol
FolS-DOPC-Chol
Medium Control

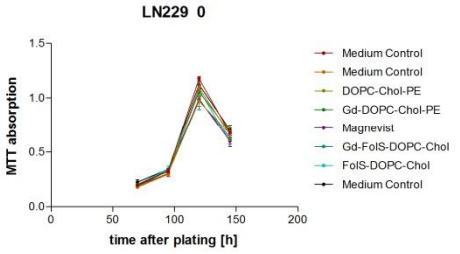
LN229 0
MTT absorption
time after plating [h]
Medium Control
Medium Control
DOPC-Chol-PE
Gd-DOPC-Chol-PE
Magnevist
Gd-FolS-DOPC-Chol
FolS-DOPC-Chol
Medium Control

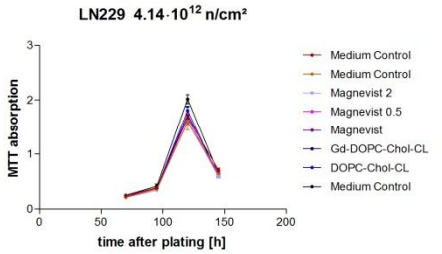
LN229 4.14·10^12 n/cm²
MTT absorption
time after plating [h]
Medium Control
Medium Control
Magnevist 2
Magnevist 0.5
Magnevist
Gd-DOPC-Chol-CL
DOPC-Chol-CL
Medium Control

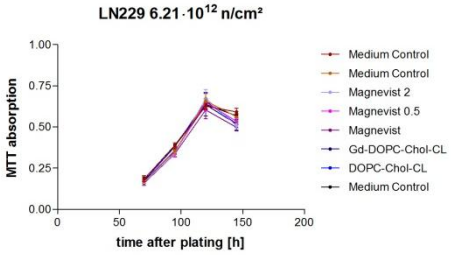
LN229 6.21·10^12 n/cm²
MTT absorption
time after plating [h]
Medium Control
Medium Control
Magnevist 2
Magnevist 0.5
Magnevist
Gd-DOPC-Chol-CL
DOPC-Chol-CL
Medium Control

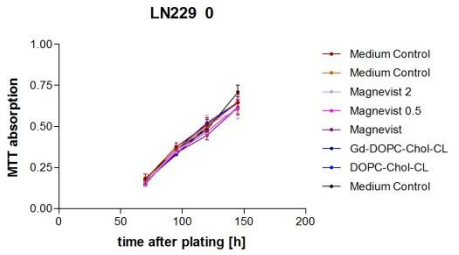
LN229 0
MTT absorption
time after plating [h]
Medium Control
Medium Control
Magnevist 2
Magnevist 0.5
Magnevist
Gd-DOPC-Chol-CL
DOPC-Chol-CL
Medium Control

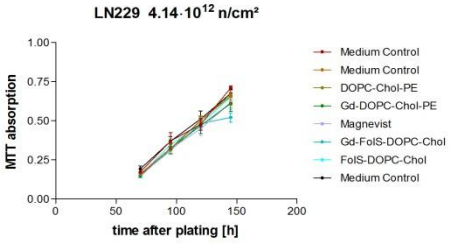
LN229 4.14·10^12 n/cm²
MTT absorption
time after plating [h]
Medium Control
Medium Control
DOPC-Chol-PE
Gd-DOPC-Chol-PE
Magnevist
Gd-FolS-DOPC-Chol
FolS-DOPC-Chol
Medium Control

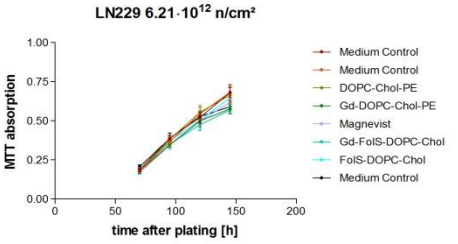
LN229 6.21·10^12 n/cm²
MTT absorption
time after plating [h]
Medium Control
Medium Control
DOPC-Chol-PE
Gd-DOPC-Chol-PE
Magnevist
Gd-FolS-DOPC-Chol
FolS-DOPC-Chol
Medium Control

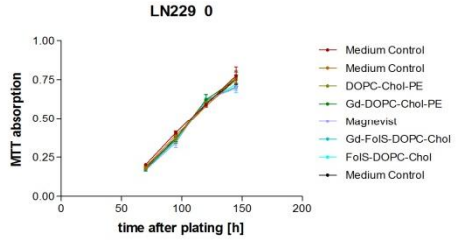
LN229 0
MTT absorption
time after plating [h]
Medium Control
Medium Control
DOPC-Chol-PE
Gd-DOPC-Chol-PE
Magnevist
Gd-FolS-DOPC-Chol
FolS-DOPC-Chol
Medium Control

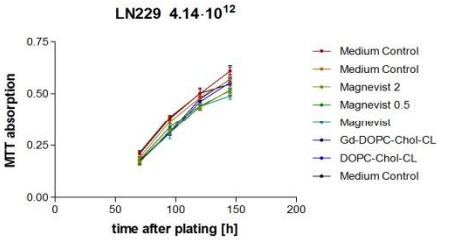
LN229 4.14·10^12
MTT absorption
time after plating [h]
Medium Control
Medium Control
Magnevist 2
Magnevist 0.5
Magnevist
Gd-DOPC-Chol-CL
DOPC-Chol-CL
Medium Control

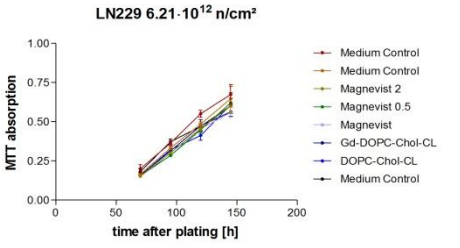
LN229 6.21·10^12 n/cm²
MTT absorption
time after plating [h]
Medium Control
Medium Control
Magnevist 2
Magnevist 0.5
Magnevist
Gd-DOPC-Chol-CL
DOPC-Chol-CL
Medium Control

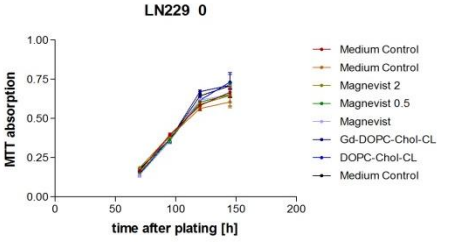
LN229 0
MTT absorption
time after plating [h]
Medium Control
Medium Control
Magnevist 2
Magnevist 0.5
Magnevist
Gd-DOPC-Chol-CL
DOPC-Chol-CL
Medium Control

8 References

1. Jesorka, A. and O. Orwar, *Liposomes: technologies and analytical applications.* Annu Rev Anal Chem (Palo Alto Calif), 2008. 1: p. 801-32.
2. Chen, Z. and R.P. Rand, *The influence of cholesterol on phospholipid membrane curvature and bending elasticity.* Biophys J, 1997. 73(1): p. 267-76.
3. Lapinski, M.M., et al., *Comparison of liposomes formed by sonication and extrusion: rotational and translational diffusion of an embedded chromophore.* Langmuir, 2007. 23(23): p. 11677-83.
4. Bangham, A.D., M.M. Standish, and J.C. Watkins, *Diffusion of univalent ions across the lamellae of swollen phospholipids.* J Mol Biol, 1965. 13(1): p. 238-52.
5. Papahadjopoulos, D., S. Nir, and S. Oki, *Permeability properties of phospholipid membranes: effect of cholesterol and temperature.* Biochim Biophys Acta, 1972. 266(3): p. 561-83.
6. Alberts, B.B., D.; Hopkin, K.; Johnson, A.; Lewis, J.; Raaff, M.; Roberts, K.; Walter, P., *Essential Cell Biology*. 3 ed. 2010, New York, USA: Garland Science. 731.
7. Papahadjopoulos, D., G. Poste, and B.E. Schaeffer, *Fusion of mammalian cells by unilamellar lipid vesicles: inflluence of lipid surface charge, fluidity and cholesterol.* Biochim Biophys Acta, 1973. 323(1): p. 23-42.
8. Blok, M.C., et al., *The effect of chain length and lipid phase transitions on the selective permeability properties of liposomes.* Biochim Biophys Acta, 1975. 406(2): p. 187-96.
9. Papahadjopoulos, D., M. Cowden, and H. Kimelberg, *Role of cholesterol in membranes. Effects on phospholipid-protein interactions, membrane permeability and enzymatic activity.* Biochim Biophys Acta, 1973. 330(1): p. 8-26.
10. Mozafari, M.R., *Liposomes: an overview of manufacturing techniques.* Cell Mol Biol Lett, 2005. 10(4): p. 711-9.
11. Szoka, F., Jr. and D. Papahadjopoulos, *Comparative properties and methods of preparation of lipid vesicles (liposomes).* Annu Rev Biophys Bioeng, 1980. 9: p. 467-508.
12. Lasch, J.W., V; Brandl, M, *Preparation of liposomes*, in *Liposomes*, V.P.W. Torchilin, V, Editor. 2003, Oxford University Press: New York. p. 3-29.
13. Torchilin, V.P., *Recent advances with liposomes as pharmaceutical carriers.* Nat Rev Drug Discov, 2005. 4(2): p. 145-60.
14. Immordino, M.L., F. Dosio, and L. Cattel, *Stealth liposomes: review of the basic science, rationale, and clinical applications, existing and potential.* Int J Nanomedicine, 2006. 1(3): p. 297-315.
15. Drummond, D.C., et al., *Optimizing liposomes for delivery of chemotherapeutic agents to solid tumors.* Pharmacol Rev, 1999. 51(4): p. 691-743.
16. Barenholz, Y., *Doxil(R)--the first FDA-approved nano-drug: lessons learned.* J Control Release, 2012. 160(2): p. 117-34.
17. Chang, H.I. and M.K. Yeh, *Clinical development of liposome-based drugs: formulation, characterization, and therapeutic efficacy.* Int J Nanomedicine, 2012. 7: p. 49-60.
18. Zuhorn, I.S. and D. Hoekstra, *On the mechanism of cationic amphiphile-mediated transfection. To fuse or not to fuse: is that the question?* J Membr Biol, 2002. 189(3): p. 167-79.
19. Choi, J.S., et al., *New cationic liposomes for gene transfer into mammalian cells with high efficiency and low toxicity.* Bioconjug Chem, 2001. 12(1): p. 108-13.
20. Strieth, S., et al., *Paclitaxel encapsulated in cationic liposomes increases tumor microvessel leakiness and improves therapeutic efficacy in combination with Cisplatin.* Clin Cancer Res, 2008. 14(14): p. 4603-11.
21. Dabbas, S., et al., *Importance of the liposomal cationic lipid content and type in tumor vascular targeting: physicochemical characterization and in vitro studies using human primary and transformed endothelial cells.* Endothelium, 2008. 15(4): p. 189-201.
22. Cai, S., et al., *Lymphatic drug delivery using engineered liposomes and solid lipid nanoparticles.* Adv Drug Deliv Rev, 2011. 63(10-11): p. 901-8.

23. Medina, L.A., et al., *Avidin/biotin-liposome system injected in the pleural space for drug delivery to mediastinal lymph nodes.* J Pharm Sci, 2004. 93(10): p. 2595-608.
24. Proulx, S.T., et al., *Quantitative imaging of lymphatic function with liposomal indocyanine green.* Cancer Res, 2010. 70(18): p. 7053-62.
25. Jain, R., P. Dandekar, and V. Patravale, *Diagnostic nanocarriers for sentinel lymph node imaging.* J Control Release, 2009. 138(2): p. 90-102.
26. Gunaseelan, S., et al., *Surface modifications of nanocarriers for effective intracellular delivery of anti-HIV drugs.* Adv Drug Deliv Rev, 2010. 62(4-5): p. 518-31.
27. Matsumura, Y. and H. Maeda, *A New Concept for Macromolecular Therapeutics in Cancer Chemotherapy: Mechanism of Tumoritropic Accumulation of Proteins and the Antitumor Agent Smancs.* Cancer Research, 1986. 46(12 Part 1): p. 6387-6392.
28. Gabizon, A. and D. Papahadjopoulos, *Liposome formulations with prolonged circulation time in blood and enhanced uptake by tumors.* Proc Natl Acad Sci U S A, 1988. 85(18): p. 6949-53.
29. Woodle, M.C. and D.D. Lasic, *Sterically stabilized liposomes.* Biochim Biophys Acta, 1992. 1113(2): p. 171-99.
30. Milla, P., F. Dosio, and L. Cattel, *PEGylation of proteins and liposomes: a powerful and flexible strategy to improve the drug delivery.* Curr Drug Metab, 2012. 13(1): p. 105-19.
31. Mu, X. and Z. Zhong, *Preparation and properties of poly(vinyl alcohol)-stabilized liposomes.* Int J Pharm, 2006. 318(1-2): p. 55-61.
32. Gabizon, A.A., H. Shmeeda, and S. Zalipsky, *Pros and cons of the liposome platform in cancer drug targeting.* J Liposome Res, 2006. 16(3): p. 175-83.
33. Parker, N., et al., *Folate receptor expression in carcinomas and normal tissues determined by a quantitative radioligand binding assay.* Anal Biochem, 2005. 338(2): p. 284-93.
34. Koshkaryev, A., et al., *Immunoconjugates and long circulating systems: origins, current state of the art and future directions.* Adv Drug Deliv Rev, 2013. 65(1): p. 24-35.
35. Yang, W., et al., *Boron neutron capture therapy of EGFR or EGFRvIII positive gliomas using either boronated monoclonal antibodies or epidermal growth factor as molecular targeting agents.* Appl Radiat Isot, 2009. 67(7-8 Suppl): p. S328-31.
36. Maruyama, K., *Intracellular targeting delivery of liposomal drugs to solid tumors based on EPR effects.* Adv Drug Deliv Rev, 2011. 63(3): p. 161-9.
37. Wolburg, H., et al., *The disturbed blood-brain barrier in human glioblastoma.* Mol Aspects Med, 2012. 33(5-6): p. 579-89.
38. Craparo, E.F., et al., *Nanoparticulate systems for drug delivery and targeting to the central nervous system.* CNS Neurosci Ther, 2011. 17(6): p. 670-7.
39. Gao, J.Q., et al., *Glioma targeting and blood-brain barrier penetration by dual-targeting doxorubincin liposomes.* Biomaterials, 2013. 34(22): p. 5628-39.
40. Smith, M.W. and M. Gumbleton, *Endocytosis at the blood-brain barrier: from basic understanding to drug delivery strategies.* J Drug Target, 2006. 14(4): p. 191-214.
41. Fenart, L., et al., *Evaluation of effect of charge and lipid coating on ability of 60-nm nanoparticles to cross an in vitro model of the blood-brain barrier.* J Pharmacol Exp Ther, 1999. 291(3): p. 1017-22.
42. Krauze, M.T., et al., *Real-time imaging and quantification of brain delivery of liposomes.* Pharm Res, 2006. 23(11): p. 2493-504.
43. Groothuis, D.R., *The blood-brain and blood-tumor barriers: A review of strategies for increasing drug delivery.* Neuro-Oncology, 2000. 2(1): p. 45-59.
44. Ziello, J.E., Y. Huang, and I.S. Jovin, *Cellular endocytosis and gene delivery.* Mol Med, 2010. 16(5-6): p. 222-9.
45. Xiang, S., et al., *Uptake mechanisms of non-viral gene delivery.* J Control Release, 2012. 158(3): p. 371-8.
46. Rejman, J., et al., *Size-dependent internalization of particles via the pathways of clathrin- and caveolae-mediated endocytosis.* Biochem J, 2004. 377(Pt 1): p. 159-69.
47. McMahon, H.T. and E. Boucrot, *Molecular mechanism and physiological functions of clathrin-mediated endocytosis.* Nat Rev Mol Cell Biol, 2011. 12(8): p. 517-33.

48. Bareford, L.M. and P.W. Swaan, *Endocytic mechanisms for targeted drug delivery.* Adv Drug Deliv Rev, 2007. 59(8): p. 748-58.
49. Hillaireau, H. and P. Couvreur, *Nanocarriers' entry into the cell: relevance to drug delivery.* Cell Mol Life Sci, 2009. 66(17): p. 2873-96.
50. Düzgünes, N., Simoes, S., Lopez-Mesas, M., Pedroso de Lima, M.C., *Intracellular delivery of therapeutic oligonucleotides in pH-sensitive and cationic liposomes*, in *Liposome Technology, Third Edition, Volume III Interactions of Liposomes with the Biological Milieu*, G. Gregoriadis, Editor. 2007, Informa Health Care USA, Inc.: New York, USA. p. 253-275.
51. Peschka-Suss, R., Schubert, R., *pH-sensitive liposomes*, in *Liposomes*, V.P.W. Torchilin, V, Editor. 2003, Oxford University Press: New York, USA. p. 305-318.
52. Koltover, I., et al., *An inverted hexagonal phase of cationic liposome-DNA complexes related to DNA release and delivery.* Science, 1998. 281(5373): p. 78-81.
53. Simoes, S., et al., *On the mechanisms of internalization and intracellular delivery mediated by pH-sensitive liposomes.* Biochim Biophys Acta, 2001. 1515(1): p. 23-37.
54. Simoes, S., et al., *On the formulation of pH-sensitive liposomes with long circulation times.* Adv Drug Deliv Rev, 2004. 56(7): p. 947-65.
55. Ferlay, J., et al., *Cancer incidence and mortality patterns in Europe: estimates for 40 countries in 2012.* Eur J Cancer, 2013. 49(6): p. 1374-403.
56. NCI. *SEER Cancer Statistics Review*. 1975-2010 [cited 2013 01.08.2013].
57. ABTA, *Glioblastoma and Malignant Astrocytoma*, A.B.T. Association, Editor 2012, American Brain Tumor Association: http://www.abta.org/secure/glioblastoma-brochure.pdf.
58. Wang, Y. and T. Jiang, *Understanding high grade glioma: molecular mechanism, therapy and comprehensive management.* Cancer Lett, 2013. 331(2): p. 139-46.
59. Bruce, J.N.K., B.M. *Glioblastoma multiforme*. 2013 02/04/2013 [cited 2013 01.08.2013].
60. Kesari, S., et al., *DNA damage response and repair: insights into strategies for radiation sensitization of gliomas.* Future Oncol, 2011. 7(11): p. 1335-46.
61. Lima, F.R., et al., *Glioblastoma: therapeutic challenges, what lies ahead.* Biochim Biophys Acta, 2012. 1826(2): p. 338-49.
62. Chang, J.E., et al., *Radiotherapy and radiosensitizers in the treatment of glioblastoma multiforme.* Clin Adv Hematol Oncol, 2007. 5(11): p. 894-902, 907-15.
63. Rolle, K., et al., *Promising human brain tumors therapy with interference RNA intervention (iRNAi).* Cancer Biol Ther, 2010. 9(5): p. 396-406.
64. Short, S.C., et al., *DNA repair after irradiation in glioma cells and normal human astrocytes.* Neuro Oncol, 2007. 9(4): p. 404-11.
65. Kil, W.J., et al., *In vitro and in vivo radiosensitization induced by the DNA methylating agent temozolomide.* Clin Cancer Res, 2008. 14(3): p. 931-8.
66. Auffinger, B., et al., *New therapeutic approaches for malignant glioma: in search of the Rosetta stone.* F1000 Med Rep, 2012. 4: p. 18.
67. Hermann, T.B., M., *Klinische Strahlenbiologie: kurz und bündig*. Vol. 3. 1997, Jena: Gustav Fischer Verlag. 187.
68. Richter, E.F., T., *Grundlagen der Strahlentherapie*. 2 ed. 2002, Berlin/Heidelberg, Germany: Springer Verlag. 462.
69. Washington, C.M.L., D., *Principles and practice of radiation therapy*. 3 ed. 2010, St. Louis, Missouri, USA: Mosby Elsevier. 984.
70. Sancar, A., et al., *Molecular mechanisms of mammalian DNA repair and the DNA damage checkpoints.* Annu Rev Biochem, 2004. 73: p. 39-85.
71. Zhuang, H.Q., et al., *The biological effect of 125I seed continuous low dose rate irradiation in CL187 cells.* J Exp Clin Cancer Res, 2009. 28: p. 12.
72. Maity, A., W.G. McKenna, and R.J. Muschel, *The molecular basis for cell cycle delays following ionizing radiation: a review.* Radiother Oncol, 1994. 31(1): p. 1-13.
73. Han, W.Y., KN, *Ionizing radiation, DNA double strand break and mutation*, in *Advances in Genetics Research*, K. Urbano, Editor. 2011, Nova Science Publishers, Inc. p. 197-210.
74. Ross, G.M., *Induction of cell death by radiotherapy.* Endocr Relat Cancer, 1999. 6(1): p. 41-4.

75. Miret, S., E.M. De Groene, and W. Klaffke, *Comparison of in vitro assays of cellular toxicity in the human hepatic cell line HepG2.* J Biomol Screen, 2006. 11(2): p. 184-93.
76. Chadwick, K.H. and H.P. Leenhouts, *A molecular theory of cell survival.* Phys Med Biol, 1973. 18(1): p. 78-87.
77. Maki, H., *Lethal effect and potentially lethal damage recovery in cultured mammalian cells irradiated by neutron-capture beams.* Int J Radiat Biol, 1989. 55(3): p. 397-409.
78. Thariat, J., et al., *Past, present, and future of radiotherapy for the benefit of patients.* Nat Rev Clin Oncol, 2013. 10(1): p. 52-60.
79. Laramore, G.E., *Role of particle radiotherapy in the management of head and neck cancer.* Curr Opin Oncol, 2009. 21(3): p. 224-31.
80. Maucort-Boulch, D., et al., *Rationale for carbon ion therapy in high-grade glioma based on a review and a meta-analysis of neutron beam trials.* Cancer Radiother, 2010. 14(1): p. 34-41.
81. Wardman, P., *Chemical radiosensitizers for use in radiotherapy.* Clin Oncol (R Coll Radiol), 2007. 19(6): p. 397-417.
82. Poggi, M.M., C.N. Coleman, and J.B. Mitchell, *Sensitizers and protectors of radiation and chemotherapy.* Curr Probl Cancer, 2001. 25(6): p. 334-411.
83. Bencokova, Z., J. Balosso, and N. Foray, *Radiobiological features of the anti-cancer strategies involving synchrotron X-rays.* J Synchrotron Radiat, 2008. 15(Pt 1): p. 74-85.
84. Rousseau, J., et al., *Efficacy of intracerebral delivery of cisplatin in combination with photon irradiation for treatment of brain tumors.* J Neurooncol, 2010. 98(3): p. 287-95.
85. De Stasio, G., et al., *Motexafin-gadolinium taken up in vitro by at least 90% of glioblastoma cell nuclei.* Clin Cancer Res, 2006. 12(1): p. 206-13.
86. Dugas, J.P., et al., *Monochromatic beam characterization for Auger electron dosimetry and radiotherapy.* Eur J Radiol, 2008. 68(3 Suppl): p. S137-41.
87. Viani, G.A., et al., *Whole brain radiotherapy with radiosensitizer for brain metastases.* J Exp Clin Cancer Res, 2009. 28: p. 1.
88. Houldsworth, J., et al., *The response of ataxia-telangiectasia lymphoblastoid cells to neutron irradiation.* Radiat Res, 1991. 125(3): p. 277-82.
89. Britten, R.A., L.J. Peters, and D. Murray, *Biological factors influencing the RBE of neutrons: implications for their past, present and future use in radiotherapy.* Radiat Res, 2001. 156(2): p. 125-35.
90. Enger, S.A., et al., *Dosimetry for gadolinium neutron capture therapy (GdNCT).* Radiation Measurements, 2013(0).
91. Fujimoto, T., et al., *Accumulation of MRI contrast agents in malignant fibrous histiocytoma for gadolinium neutron capture therapy.* Appl Radiat Isot, 2009. 67(7-8 Suppl): p. S355-8.
92. Tokuuye, K., et al., *Comparison of radiation effects of gadolinium and boron neutron capture reactions.* Strahlenther Onkol, 2000. 176(2): p. 81-3.
93. Dewi, N., et al., *Tumor growth suppression by gadolinium-neutron capture therapy using gadolinium-entrapped liposome as gadolinium delivery agent.* Biomed Pharmacother, 2013. 67(6): p. 451-7.
94. Cerullo, N., D. Bufalino, and G. Daquino, *Progress in the use of gadolinium for NCT.* Appl Radiat Isot, 2009. 67(7-8 Suppl): p. S157-60.
95. Miller, G.A.J., et al., *Gadolinium neutron capture therapy.* Journal Name: Nuclear Technology; (United States); Journal Volume: 103:3, 1993: p. Medium: X; Size: Pages: 320-331.
96. Barth, R.F., et al., *Boron neutron capture therapy of cancer: current status and future prospects.* Clin Cancer Res, 2005. 11(11): p. 3987-4002.
97. Goorley, T. and H. Nikjoo, *Electron and photon spectra for three gadolinium-based cancer therapy approaches.* Radiat Res, 2000. 154(5): p. 556-63.
98. Salt, C., et al., *Boron and gadolinium neutron capture therapy.* Russian Chemical Bulletin, 2004. 53(9): p. 1871-1888.
99. De Stasio, G., et al., *Are gadolinium contrast agents suitable for gadolinium neutron capture therapy?* Neurol Res, 2005. 27(4): p. 387-98.

100. Yasui, L.S., et al., *Gadolinium neutron capture in glioblastoma multiforme cells.* Int J Radiat Biol, 2008. 84(12): p. 1130-9.
101. Laster, B.H., et al., *The biological effects of Auger electrons compared to alpha-particles and Li ions.* Acta Oncol, 1996. 35(7): p. 917-23.
102. Martin, R.F., et al., *Induction of DNA Double-Strand Breaks by 157Gd Neutron Capture.* Pigment Cell Research, 1989. 2(4): p. 330-332.
103. Goorley, T., R. Zamenhof, and H. Nikjoo, *Calculated DNA damage from gadolinium Auger electrons and relation to dose distributions in a head phantom.* Int J Radiat Biol, 2004. 80(11-12): p. 933-40.
104. Soloway, A.H., et al., *The Chemistry of Neutron Capture Therapy.* Chem Rev, 1998. 98(4): p. 1515-1562.
105. Yanagie, H., et al., *Application of drug delivery system to boron neutron capture therapy for cancer.* Expert Opin Drug Deliv, 2008. 5(4): p. 427-43.
106. Hwang, K.C., et al., *Neutron capture nuclei-containing carbon nanoparticles for destruction of cancer cells.* Biomaterials, 2010. 31(32): p. 8419-25.
107. Yasui, L.S.O.K., *Necrosis is not induced by gadolinium neutron capture in glioblastoma multiforme cells.* International Journal of Radiation Biology, 2012. 88(12): p. 980-990.
108. Barth, R.F., et al., *Current status of boron neutron capture therapy of high grade gliomas and recurrent head and neck cancer.* Radiat Oncol, 2012. 7: p. 146.
109. Pisarev, M.A., M.A. Dagrosa, and G.J. Juvenal, *Boron neutron capture therapy in cancer: past, present and future.* Arq Bras Endocrinol Metabol, 2007. 51(5): p. 852-6.
110. Capala, J., et al., *Boron Neutron Capture Therapy for Glioblastoma Multiforme: Clinical Studies in Sweden.* Journal of Neuro-Oncology, 2003. 62(1): p. 135-144.
111. Watanabe, T., H. Ichikawa, and Y. Fukumori, *Tumor accumulation of gadolinium in lipid-nanoparticles intravenously injected for neutron-capture therapy of cancer.* Eur J Pharm Biopharm, 2002. 54(2): p. 119-24.
112. Mitin, V.N., et al., *Comparison of BNCT and GdNCT efficacy in treatment of canine cancer.* Appl Radiat Isot, 2009. 67(7-8 Suppl): p. S299-301.
113. Bortolussi, S. and S. Altieri, *Thermal neutron irradiation field design for boron neutron capture therapy of human explanted liver.* Med Phys, 2007. 34(12): p. 4700-5.
114. Prusinski, P.P., S; Borysiewicz, M; Kowal, K; Kwiatkowski, T; Prusinski, AM, *CFD analysis of the safety related thermal hydraulic parameters describing a flow domain of an experimental medical installation (BNCT converter) inside of the Research Reactor MARIA.* Journal of Power Technologies, 2012. 92(4): p. 227-240.
115. Kankaanranta, L., et al., *Boron neutron capture therapy in the treatment of locally recurred head and neck cancer.* Int J Radiat Oncol Biol Phys, 2007. 69(2): p. 475-82.
116. Halfon, S., et al., *High-flux neutron source based on a liquid-lithium target.* AIP Conference Proceedings, 2013. 1525(1): p. 511-515.
117. Menichetti, L., et al., *In vitro neutron irradiation of glioma and endothelial cultured cells.* Appl Radiat Isot, 2009. 67(7-8 Suppl): p. S336-40.
118. Matsuda, M., et al., *Dose distribution and clinical response of glioblastoma treated with boron neutron capture therapy.* Appl Radiat Isot, 2009. 67(7-8 Suppl): p. S19-21.
119. Ko, L., A. Koestner, and W. Wechsler, *Morphological characterization of nitrosourea-induced glioma cell lines and clones.* Acta Neuropathol, 1980. 51(1): p. 23-31.
120. Barth, R.F., *Rat brain tumor models in experimental neuro-oncology: the 9L, C6, T9, F98, RG2 (D74), RT-2 and CNS-1 gliomas.* J Neurooncol, 1998. 36(1): p. 91-102.
121. Clendenon, N.R., et al., *Boron neutron capture therapy of a rat glioma.* Neurosurgery, 1990. 26(1): p. 47-55.
122. Goodman, J.H., et al., *Inhibition of tumor growth in a glioma model treated with boron neutron capture therapy.* Neurosurgery, 1990. 27(3): p. 383-8.
123. Knedlitschek, G., et al., *Radioresistance of rat glioma cell lines cultured as multicellular spheroids. Correlation with electrical cell-to-cell-coupling.* Strahlenther Onkol, 1990. 166(2): p. 164-7.

124. Frei, K., et al., *Ex vivo malignant glioma cells are sensitive to Fas (CD95/APO-1) ligand-mediated apoptosis.* Journal of Neuroimmunology, 1998. 87(1–2): p. 105-113.
125. Fry, D.W., J.C. White, and I.D. Goldman, *Rapid separation of low molecular weight solutes from liposomes without dilution.* Anal Biochem, 1978. 90(2): p. 809-15.
126. Grohganz, H., et al., *Quantification of various phosphatidylcholines in liposomes by enzymatic assay.* AAPS PharmSciTech, 2003. 4(4): p. E63.
127. Ingebrigtsen, L. and M. Brandl, *Determination of the size distribution of liposomes by SEC fractionation, and PCS analysis and enzymatic assay of lipid content.* AAPS PharmSciTech, 2002. 3(2): p. E7.
128. Nakamura, M., K. Tsujii, and J. Sunamoto, *Liposome-induced release of cell membrane proteins from intact tissue epithelium.* Med Biol Eng Comput, 1998. 36(5): p. 645-53.
129. Oksendal, A.N. and P.A. Hals, *Biodistribution and toxicity of MR imaging contrast media.* J Magn Reson Imaging, 1993. 3(1): p. 157-65.
130. Chidambaram, N. and D.J. Burgess, *A novel in vitro release method for submicron sized dispersed systems.* AAPS PharmSci, 1999. 1(3): p. E11.
131. Zolnik, B.S., J.-L. Raton, and D.J. Burgess, *Application of USP apparatus 4 and in situ fiber optic analysis to microsphere release testing.* Dissolution Technologies, 2005. 12(2).
132. Bhardwaj, U. and D.J. Burgess, *A novel USP apparatus 4 based release testing method for dispersed systems.* Int J Pharm, 2010. 388(1-2): p. 287-94.
133. *N-(7-Nitrobenz-2-Oxa-1,3-Diazol-4-yl)-1,2-Dihexadecanoyl-sn-Glycero-3-Phosphoethanolamine, Triethylammonium Salt (NBD-PE)* 2013 2013-12-04].
134. Smith, P.K., et al., *Measurement of protein using bicinchoninic acid.* Anal Biochem, 1985. 150(1): p. 76-85.
135. Lowry, O.H., et al., *Protein measurement with the Folin phenol reagent.* J Biol Chem, 1951. 193(1): p. 265-75.
136. Tuszynski, G.P. and A. Murphy, *Spectrophotometric quantitation of anchorage-dependent cell numbers using the bicinchoninic acid protein assay reagent.* Anal Biochem, 1990. 184(1): p. 189-91.
137. Berridge, M.V. and A.S. Tan, *Characterization of the cellular reduction of 3-(4,5-dimethylthiazol-2-yl)-2,5-diphenyltetrazolium bromide (MTT): subcellular localization, substrate dependence, and involvement of mitochondrial electron transport in MTT reduction.* Arch Biochem Biophys, 1993. 303(2): p. 474-82.
138. Gonzalez, R.J. and J.B. Tarloff, *Evaluation of hepatic subcellular fractions for Alamar blue and MTT reductase activity.* Toxicol In Vitro, 2001. 15(3): p. 257-9.
139. Mosmann, T., *Rapid colorimetric assay for cellular growth and survival: application to proliferation and cytotoxicity assays.* J Immunol Methods, 1983. 65(1-2): p. 55-63.
140. Carmichael, J., et al., *Evaluation of a tetrazolium-based semiautomated colorimetric assay: assessment of chemosensitivity testing.* Cancer Res, 1987. 47(4): p. 936-42.
141. Buch, K., et al., *Determination of cell survival after irradiation via clonogenic assay versus multiple MTT Assay--a comparative study.* Radiat Oncol, 2012. 7: p. 1.
142. Buch, K., *Lanthanide-loaded nanoparticles as a novel radioenhancer in radiation therapy of cancer*, in *Fachbereich Chemie, Pharmazie und Geowissenschaften der Johannes Gutenberg - Universität Mainz*2012, Johannes Gutenberg - Universität Mainz: Mainz.
143. Price, P. and T.J. McMillan, *Use of the tetrazolium assay in measuring the response of human tumor cells to ionizing radiation.* Cancer Res, 1990. 50(5): p. 1392-6.
144. Nikkhah, G., et al., *The MTT assay for chemosensitivity testing of human tumors of the central nervous system. Part I: Evaluation of test-specific variables.* J Neurooncol, 1992. 13(1): p. 1-11.
145. Carmichael, J., et al., *Evaluation of a tetrazolium-based semiautomated colorimetric assay: assessment of radiosensitivity.* Cancer Res, 1987. 47(4): p. 943-6.
146. Ramsay, J., R. Ward, and N.M. Bleehen, *Radiosensitivity testing of human malignant gliomas.* Int J Radiat Oncol Biol Phys, 1992. 24(4): p. 675-80.

147. Wasserman, T.H. and P. Twentyman, *Use of a colorimetric microtiter (MTT) assay in determining the radiosensitivity of cells from murine solid tumors.* Int J Radiat Oncol Biol Phys, 1988. 15(3): p. 699-702.
148. Franken, N.A., et al., *Clonogenic assay of cells in vitro.* Nat Protoc, 2006. 1(5): p. 2315-9.
149. Pauwels, B., et al., *Comparison of the sulforhodamine B assay and the clonogenic assay for in vitro chemoradiation studies.* Cancer Chemother Pharmacol, 2003. 51(3): p. 221-6.
150. Kerr, S.A., et al., *Elemental concentrations in geochemical reference samples by neutron capture prompt gamma-ray spectroscopy.* Journal of Radioanalytical and Nuclear Chemistry, 1987. 113(1): p. 249-258.
151. Rauch, H., et al., *Giant Absorption Cross Section of Ultracold Neutrons in Gadolinium.* Physical Review Letters, 1999. 83(24): p. 4955-4958.
152. van Eijk, C.W.E., A. Bessière, and P. Dorenbos, *Inorganic thermal-neutron scintillators.* Nuclear Instruments and Methods in Physics Research Section A: Accelerators, Spectrometers, Detectors and Associated Equipment, 2004. 529(1–3): p. 260-267.
153. Sakurai, Y., Kobayashi, T., *Experimental verification of the nuclear data of gadolinium for neutron capture therapy.* Journal of Nuclear Science and Technology, 2002. August 2002(Supplement 2): p. 1294-1297.
154. Fouquet, D.M., J. Razvi, and W.L. Whittemore, *TRIGA research reactors: A pathway to the peaceful apllications of nuclear energy.* Nuclear News, 2003. 46(12): p. 46-56.
155. Hampel, G., et al., *Irradiation facility at the TRIGA Mainz for treatment of liver metastases.* Appl Radiat Isot, 2009. 67(7-8 Suppl): p. S238-41.
156. Schmitz, T., et al., *Dose calculation in biological samples in a mixed neutron-gamma field at the TRIGA reactor of the University of Mainz.* Acta Oncol, 2010. 49(7): p. 1165-9.
157. Vogtlander, L., *Untersuchung von Photonendosis und Neutronenfluss im 20 x 20 x 127cm3 Bestrahlungskanal in der thermischen Säule des TRIGA Reaktors an der Johannes Gutenberg-Universität Mainz*, in *Institute for Nuclear Chemistry*2009, Johannes Gutenberg - University Mainz: Mainz. p. 90.
158. Schmitz, T., et al., *Dose determination using alanine detectors in a mixed neutron and gamma field for boron neutron capture therapy of liver malignancies.* Acta Oncol, 2011. 50(6): p. 817-22.
159. Blaickner, M., et al., *Dosimetric feasibility study for an extracorporeal BNCT application on liver metastases at the TRIGA Mainz.* Appl Radiat Isot, 2012. 70(1): p. 139-43.
160. Crommelin, D.J., *Influence of lipid composition and ionic strength on the physical stability of liposomes.* J Pharm Sci, 1984. 73(11): p. 1559-63.
161. Mayer, L.D., et al., *Solute distributions and trapping efficiencies observed in freeze-thawed multilamellar vesicles.* Biochim Biophys Acta, 1985. 817(1): p. 193-6.
162. Mayer, L.D., M.J. Hope, and P.R. Cullis, *Vesicles of variable sizes produced by a rapid extrusion procedure.* Biochim Biophys Acta, 1986. 858(1): p. 161-8.
163. Hope, M.J., et al., *Production of large unilamellar vesicles by a rapid extrusion procedure: characterization of size distribution, trapped volume and ability to maintain a membrane potential.* Biochim Biophys Acta, 1985. 812(1): p. 55-65.
164. Wurster, E.-C., *Entwicklung und Erprobung einer Methode zur Bestimmung der Wirkstofffreisetzung aus therapeutischen Nanopartikeln*, in *Institute of Pharmacy and Biochemistry*2010, Johannes Gutenberg-University, Mainz: Mainz, Germany. p. 84.
165. Sibenaller, Z.A., et al., *Genetic characterization of commonly used glioma cell lines in the rat animal model system.* Neurosurg Focus, 2005. 19(4): p. E1.
166. Stark, M., J.E. Wolff, and A. Korbmacher, *Modulation of glial cell differentiation by exposure to lead and cadmium.* Neurotoxicol Teratol, 1992. 14(4): p. 247-52.
167. Sudimack, J.J., et al., *Folate receptor-mediated liposomal delivery of a lipophilic boron agent to tumor cells in vitro for neutron capture therapy.* Pharm Res, 2002. 19(10): p. 1502-8.
168. Barth, R.F., et al., *Molecular targeting of the epidermal growth factor receptor for neutron capture therapy of gliomas.* Cancer Res, 2002. 62(11): p. 3159-66.
169. Barth, R.F., W. Yang, and J.A. Coderre, *Rat brain tumor models to assess the efficacy of boron neutron capture therapy: a critical evaluation.* J Neurooncol, 2003. 62(1-2): p. 61-74.

170. Ciesielski, M.J., et al., *Cellular antitumor immune response to a branched lysine multiple antigenic peptide containing epitopes of a common tumor-specific antigen in a rat glioma model.* Cancer Immunol Immunother, 2005. 54(2): p. 107-19.
171. Ren, Y., et al., *MicroRNA-21 inhibitor sensitizes human glioblastoma cells U251 (PTEN-mutant) and LN229 (PTEN-wild type) to taxol.* BMC Cancer, 2010. 10: p. 27.
172. Zhou, X., et al., *Downregulation of miR-21 inhibits EGFR pathway and suppresses the growth of human glioblastoma cells independent of PTEN status.* Lab Invest, 2010. 90(2): p. 144-55.
173. Yue, X., et al., *Interruption of beta-catenin suppresses the EGFR pathway by blocking multiple oncogenic targets in human glioma cells.* Brain Res, 2010. 1366: p. 27-37.
174. Combs, S.E., et al., *In vitro responsiveness of glioma cell lines to multimodality treatment with radiotherapy, temozolomide, and epidermal growth factor receptor inhibition with cetuximab.* Int J Radiat Oncol Biol Phys, 2007. 68(3): p. 873-82.
175. Reddy, J.A., et al., *Folate-targeted, cationic liposome-mediated gene transfer into disseminated peritoneal tumors.* Gene Ther, 2002. 9(22): p. 1542-50.
176. Ko, L., A. Koestner, and W. Wechsler, *Characterization of cell cycle and biological parameters of transplantable glioma cell lines and clones.* Acta Neuropathol, 1980. 51(2): p. 107-11.
177. Scheithauer, M., *Erhöhung der Genauigkeit bei der Ermittlung des Bremsstrahlungsspektrums klinischer Linearbeschleuniger*, in *Fakultät für Informatik und Automatisierung der Technischen Universität Ilmenau*2004, Technical University Ilmenau: Ilmenau. p. 147.
178. Remeikis, V. and A. Jurkevicius, *Evolution of the neutron sensor characteristics in the RBMK-1500 reactor neutron flux.* Nuclear Engineering and Design, 2004. 231(3): p. 271-282.
179. Nawroth, T., Poynor, M., *Boron entrapping and iron deposition inside magnetic liposomes - timeresolved neutron scattering* in *Experimental report*2004, ILL, Grenoble: https://club.ill.fr/cv/servlet/ReportInPDF?command=view&typeProposal=final&issuer=ReportFind2. p. 2.
180. Grunewald, C., *Bestimmung der Sensitivität von Leberkrebszellen bei Bestrahlungsversuchen zur Neutronentherapie*, in *Fachbereich Sozialwissenschaften, Medien und Sport*2010, Johannes Gutenberg-Universität Mainz: Mainz.
181. Schneider, T., et al., *Generation of conrtast-carrying liposomes of defined size with a new continuous high pressure extrusion mehtod.* Int J Pharm, 1995. 117: p. 1-12.
182. Berger, N., et al., *Filter extrusion of liposomes using different devices: comparison of liposome size, encapsulation efficiency, and process characteristics.* Int J Pharm, 2001. 223(1-2): p. 55-68.
183. Le, U.M. and Z. Cui, *Long-circulating gadolinium-encapsulated liposomes for potential application in tumor neutron capture therapy.* Int J Pharm, 2006. 312(1-2): p. 105-12.
184. Chen, Y., et al., *Uptake of liposomes by cultured cardiomyocytes.* Pharmazie, 2005. 60(11): p. 844-8.
185. Nounou, M.M., et al., *In vitro release of hydrophilic and hydrophobic drugs from liposomal dispersions and gels.* Acta Pharm, 2006. 56(3): p. 311-24.
186. Elorza, B., et al., *Characterization of 5-fluorouracil loaded liposomes prepared by reverse-phase evaporation or freezing-thawing extrusion methods: study of drug release.* Biochim Biophys Acta, 1993. 1153(2): p. 135-42.
187. Miller, C.R., et al., *Liposome-cell interactions in vitro: effect of liposome surface charge on the binding and endocytosis of conventional and sterically stabilized liposomes.* Biochemistry, 1998. 37(37): p. 12875-83.
188. Lee, K.D., K. Hong, and D. Papahadjopoulos, *Recognition of liposomes by cells: in vitro binding and endocytosis mediated by specific lipid headgroups and surface charge density.* Biochim Biophys Acta, 1992. 1103(2): p. 185-97.
189. Lee, K.D., S. Nir, and D. Papahadjopoulos, *Quantitative analysis of liposome-cell interactions in vitro: rate constants of binding and endocytosis with suspension and adherent J774 cells and human monocytes.* Biochemistry, 1993. 32(3): p. 889-99.
190. Shmeeda, H., et al., *Intracellular uptake and intracavitary targeting of folate-conjugated liposomes in a mouse lymphoma model with up-regulated folate receptors.* Mol Cancer Ther, 2006. 5(4): p. 818-24.

191. Sleight, R.G. and R.E. Pagano, *Transbilayer movement of a fluorescent phosphatidylethanolamine analogue across the plasma membranes of cultured mammalian cells.* Journal of Biological Chemistry, 1985. 260(2): p. 1146-1154.
192. Stegmann, T. and J.-Y. Legendre, *Gene transfer mediated by cationic lipids: lack of a correlation between lipid mixing and transfection.* Biochimica et Biophysica Acta (BBA) - Biomembranes, 1997. 1325(1): p. 71-79.
193. Almofti, M.R., et al., *Cationic liposome-mediated gene delivery: biophysical study and mechanism of internalization.* Arch Biochem Biophys, 2003. 410(2): p. 246-53.
194. Zou, Y., et al., *Development of cationic liposome formulations for intratracheal gene therapy of early lung cancer.* Cancer Gene Ther, 2000. 7(5): p. 683-96.
195. Bellavance, M.A., M.B. Poirier, and D. Fortin, *Uptake and intracellular release kinetics of liposome formulations in glioma cells.* Int J Pharm, 2010. 395(1-2): p. 251-9.
196. Düzgüneş, N. and S. Nir, *Mechanisms and kinetics of liposome–cell interactions.* Advanced Drug Delivery Reviews, 1999. 40(1–2): p. 3-18.
197. Gjetting, T., et al., *In vitro and in vivo effects of polyethylene glycol (PEG)-modified lipid in DOTAP/cholesterol-mediated gene transfection.* Int J Nanomedicine, 2010. 5: p. 371-83.
198. Witter, B. and H. Debuch, *On the phospholipid metabolism of glial cell primary cultures: cell characterization and their utilization of 1-alkyl-glycerophosphoethanolamine.* J Neurochem, 1982. 38(4): p. 1029-37.
199. Buratta, M., et al., *Loss of cardiolipin in palmitate-treated GL15 glioblastoma cells favors cytochrome c release from mitochondria leading to apoptosis.* J Neurochem, 2008. 105(3): p. 1019-31.
200. Pollock, S., et al., *Uptake and trafficking of liposomes to the endoplasmic reticulum.* FASEB J, 2010. 24(6): p. 1866-78.
201. Huth, U.S., R. Schubert, and R. Peschka-Suss, *Investigating the uptake and intracellular fate of pH-sensitive liposomes by flow cytometry and spectral bio-imaging.* J Control Release, 2006. 110(3): p. 490-504.
202. Lv, H., et al., *Toxicity of cationic lipids and cationic polymers in gene delivery.* J Control Release, 2006. 114(1): p. 100-9.
203. Bothun, G.D., et al., *Multicomponent folate-targeted magnetoliposomes: design, characterization, and cellular uptake.* Nanomedicine, 2011. 7(6): p. 797-805.
204. Reddy, J.A., V.M. Allagadda, and C.P. Leamon, *Targeting therapeutic and imaging agents to folate receptor positive tumors.* Curr Pharm Biotechnol, 2005. 6(2): p. 131-50.
205. Zhao, X., H. Li, and R.J. Lee, *Targeted drug delivery via folate receptors.* Expert Opin Drug Deliv, 2008. 5(3): p. 309-19.
206. Aldskogius, H., L. Liu, and M. Svensson, *Glial responses to synaptic damage and plasticity.* J Neurosci Res, 1999. 58(1): p. 33-41.
207. Griffiths, M.R., P. Gasque, and J.W. Neal, *The multiple roles of the innate immune system in the regulation of apoptosis and inflammation in the brain.* J Neuropathol Exp Neurol, 2009. 68(3): p. 217-26.
208. Lemmer HJR, H., JH, *Paracellular drug absorption enhancement through tight junction modulation.* Expert Opinion on Drug Delivery, 2013. 10(1): p. 103-114.
209. Daleke, D.L., K. Hong, and D. Papahadjopoulos, *Endocytosis of liposomes by macrophages: binding, acidification and leakage of liposomes monitored by a new fluorescence assay.* Biochim Biophys Acta, 1990. 1024(2): p. 352-66.
210. Straubinger, R.M., D. Papahadjopoulos, and K.L. Hong, *Endocytosis and intracellular fate of liposomes using pyranine as a probe.* Biochemistry, 1990. 29(20): p. 4929-39.
211. De Stasio, G., et al., *Gadolinium in human glioblastoma cells for gadolinium neutron capture therapy.* Cancer Res, 2001. 61(10): p. 4272-7.
212. Shih, J.L. and R.M. Brugger, *Gadolinium as a neutron capture therapy agent.* Med Phys, 1992. 19(3): p. 733-44.
213. Buselmaier, W., *Biologie für Mediziner*. 2007, Heidelberg, Germany: Springer Medizin Verlag. 520.

214. Park, K., et al., *'Living cantilever arrays' for characterization of mass of single live cells in fluids.* Lab on a Chip, 2008. 8(7): p. 1034-1041.
215. Le, U.M. and Z. Cui, *Biodistribution and tumor-accumulation of gadolinium (Gd) encapsulated in long-circulating liposomes in tumor-bearing mice for potential neutron capture therapy.* Int J Pharm, 2006. 320(1-2): p. 96-103.
216. Jordan, C.T., M.L. Guzman, and M. Noble, *Cancer Stem Cells.* New England Journal of Medicine, 2006. 355(12): p. 1253-1261.
217. Reichert, M., et al., *Modulation of growth and radiochemosensitivity of human malignant glioma cells by acidosis.* Cancer, 2002. 95(5): p. 1113-9.
218. Bencokova, Z., et al., *Molecular and cellular response of the most extensively used rodent glioma models to radiation and/or cisplatin.* J Neurooncol, 2008. 86(1): p. 13-21.
219. Xu, S., et al., *Effects of Motexafin gadolinium on tumor metabolism and radiation sensitivity.* Int J Radiat Oncol Biol Phys, 2001. 49(5): p. 1381-90.
220. Thomas, S.R. and D. Khuntia, *Motexafin gadolinium injection for the treatment of brain metastases in patients with non-small cell lung cancer.* Int J Nanomedicine, 2007. 2(1): p. 79-87.
221. Regnard, P., et al., *Enhancement of survival of 9L gliosarcoma bearing rats following intracerebral delivery of drugs in combination with microbeam radiation therapy.* Eur J Radiol, 2008. 68(3 Suppl): p. S151-5.
222. Miladi, I., et al., *Biodistribution of ultra small gadolinium-based nanoparticles as theranostic agent: Application to brain tumors.* J Biomater Appl, 2012.
223. Le Duc, G., et al., *Toward an image-guided microbeam radiation therapy using gadolinium-based nanoparticles.* ACS Nano, 2011. 5(12): p. 9566-74.
224. Mowat, P., et al., *In vitro radiosensitizing effects of ultrasmall gadolinium based particles on tumour cells.* J Nanosci Nanotechnol, 2011. 11(9): p. 7833-9.
225. Seto, A., C.J. Gatt, Jr., and M.G. Dunn, *Radioprotection of tendon tissue via crosslinking and free radical scavenging.* Clin Orthop Relat Res, 2008. 466(8): p. 1788-95.
226. Nair, C.K., D.K. Parida, and T. Nomura, *Radioprotectors in radiotherapy.* J Radiat Res, 2001. 42(1): p. 21-37.
227. Akine, Y., et al., *Suppression of rabbit VX-2 subcutaneous tumor growth by gadolinium neutron capture therapy.* Jpn J Cancer Res, 1993. 84(8): p. 841-3.
228. Matsumura, A., et al., *Combination of boron and gadolinium compounds for neutron capture therapy. An in vitro study.* J Exp Clin Cancer Res, 2005. 24(1): p. 93-8.
229. Franken, N.A., et al., *Gadolinium enhances the sensitivity of SW-1573 cells for thermal neutron irradiation.* Oncol Rep, 2006. 15(3): p. 715-20.
230. Tokuuye, K., et al., *Biological Dosimetry for Gadolinium Neutron Capture Reaction*, in *Advances in Neutron Capture Therapy*, A. Soloway, R. Barth, and D. Carpenter, Editors. 1993, Springer US. p. 245-248.
231. Tavernier, S., *Experimental Techniques in Nuclear and Particle Physics.* 2010, Heidelberg, Germany: Springer Verlag. 306.
232. Meesungnoen, J., et al., *Low-energy electron penetration range in liquid water.* Radiat Res, 2002. 158(5): p. 657-60.

Additional websites:

Lipids:

Cardiolipin
http://avantilipids.com/index.php?option=com_content&view=article&id=334&Itemid=246&catnumber=840012

Cholesterol
http://avantilipids.com/index.php?option=com_content&view=article&id=401&Itemid=162&catnumber=700000
DOPC
http://avantilipids.com/index.php?option=com_content&view=article&id=231&Itemid=207&catnumber=850375
DOPE
http://avantilipids.com/index.php?option=com_content&view=article&id=565&Itemid=228&catnumber=850725
DOTAP
http://avantilipids.com/index.php?option=com_content&view=article&id=946&Itemid=156&catnumber=890890
Folate mPEG 2000
http://avantilipids.com/index.php?option=com_content&view=article&id=1104&Itemid=153&catnumber=880124
MPEG 2000 18:0
http://avantilipids.com/index.php?option=com_content&view=article&id=1088&Itemid=448&catnumber=880120

LabAssay:

http://www.wakodiagnostics.com/pi/pi_phospholipids_c.pdf

Magnevist®:

http://www.fachinfo.de/FachInfo/data/fi/pdf/00/23/002374.pdf

9 Publications and presentations

Publications

Hühn, E. Peters, T., Nwroth, T. Langguth, P.
Liposomale Trägerstoffe als supramolekulare Transportsysteme
Natur & Geist. 2010; 25 (1): 17-20

Buch, K., Peters, T., Nawroth, T., Sänger, M., Schmidberger, H., Langguth, P.
Determination of cell survival after irradiation via clonogenic assay versus multiple MTT Assay – a comparative study. Radiat. Oncol. 2012 Jan 3;7:1.

In preparation:

Peters, T., Nawroth, T., Schmidberger, H., Le Duc, G., Bravin, A., Langguth, P.
Radioenhancing properties of liposomal Gd-DTPA – an in vitro study

Peters, T., Grunewald, C., Nawroth, T., Schütz, C., Iffland, D., Ziegner, M., Blaickner, M., Hampel, G., Langguth, P.
Novel Gd-DTPA liposomes for the application in neutron capture therapy of glioblastoma multiforme

Poster and oral presentations

Peters, T., Glube, N., Nawroth, T., Schmidberger, H., Langguth, P.
Manufacture and characterization of nanoparticulate formulations for the improvement of radiation therapy
Poster presentation at the annual DPhG Meeting 2008 in Bonn

Peters, T., Glube, N., Grunewald, C., Callow, P., Hampel, G., Nawroth, T., Schmidberger, H., Langguth, P.
Radiotherapeutic strategies for brain cancer – NCT development based on a glioblastoma cell model
Oral presentation at the Young Researcher BNCT Meeting 2009, Mainz

Peters, T. , Nawroth, T., Grunewald, C., Hampel, G., Langguth, P.
Development and in vitro testing of liposomes for boron neutron capture therapy
Poster presentation at the APV World Meeting 2010, Malta

Peters, T. , Grunewald, C., Hampel, G., Nawroth, T., Langguth, P.
Liposomal Drug Carriers for Neutron Capture Therapy - Influence of Lipid Composition on Liposome Uptake in Glioblastoma Cells
Oral presentation at the OEPhG and DPhG Meeting 2011, Innsbruck

Selected presentations (Co-author):

Glube, N.D., Peters, T., Nawroth, T., Langguth, P., Schmidberger, H., Corde, S., Bravin, A., Le Duc, G.
Cell culture tests and electron boost effect in Nano-IRT with synchrotron radiation
Oral presentation at Synchrotron light and Microbeam Radiation Therapy-SYRAD workshop 2008, Grenoble

Nawroth, T., Peters, T, Glube, N.D., Buch, P., Langguth, P.,Pairet, B., Decker, H., Schmidberger, H., Alexiou, C., Corde, S., Lauss, B., Jentschel, M., May, R.P., Callow, P.

Indirect Radiation Therapy of Cancer by Gadolinium NCT
Presentation at Deutsche Neutronenstreu-Tagung 2008, München

Nawroth, T., Peters, T., Buch, P., Buch, K., Hühn, E., Glube, N., Langguth, P.,Pairet, B., Meesters, C., Decker, H., Bickes-Kelleher, D., Schmidberger, H., Lauss, B., Jentschel, M., Gähler, R., May, R.P., Callow, P., Corde, S., Boesecke, P., Bravin, A., Le Duc, G.
Nano-RT: Radiation Therapy and Imaging with Target Liposomes and Nanoparticles.
Poster presentation at Symposium on Phospholipids in Pharmaceutical Research 2009, Heidelberg.

Nawroth, T., Peters, T., Wurster, E., Buch, K., Buch, P., Hühn, E., Langguth, P., Decker, Hampel, G., Hofmann, A.M., Frey, H. Schmidberger, Alexiou, C., May, R.P., Callow, P., Schweins, R., Boesecke, P. , Le Duc, G., Bravin, A.
Target Nanoparticles - Drug Carriers for Enhancer Radiation Therapy of Cancer
Poster presentation at DPhG/GDCh Münster 2010

Nawroth, T., Peters, T., Wurster, E.C., Buch, K., Buch, P., Hühn, E., Langguth, P., Decker, H., Hampel, G., Hofmann, A.M., Frey, H., Schmidberger, H., Alexiou, C., May, R., Callow, P., Schweins, R., Boesecke, P., Le Duc, G., Bravin, A. Target
Nanoparticles – Drug Carriers for Enhancer Radiation Therapy of Cancer.
Poster presentation at Frontiers in Medicinal Chemistry 2010, Münster.

Nawroth, T., Buch, K., Peters, T., Wurster, E., Langguth, P., Pairet, B., Decker, H., Hofmann, A.M., Frey, H., Hampel, G., Sänger, M., Schmidberger, H., Alexiou, C., Goerig, G., Boesecke, P., Bravin, A., Requardt, H., Le duc, G., May, R.P., Callow, P., Schweins, R.
Enhancer Radiation Therapy – development for a patient-specific medicine
Presentation at Neutrons in Biology 2011, Grenoble

Neutron therapy development with target nanoparticles – B and Gd, Er liposomes and polymer at ILL Grenoble and TRIGA Mainz
Nawroth, T., Peters,T., Langguth, P. Grunewald, C., Hampel, G., Schmidberger, H., Schweins, R.
Presentation at IAEA meeting Mainz, 2013

Blaickner, M., Ziegner, M. , Böck, H., Khan, R., Peters, T., Grunewald, C., Hampel, G.
Monte Carlo dose assessment in cell cultures after enrichment with Gadolinium and irradiation in the neutron field of the TRIGA Mainz
Presentation at IAEA Meeting 2013, Mainz.

Ziegner, M., Blaickner, M., Böck, H., Khan, R., Peters, T., Grunewald, C., Hampel, G.
Monte Carlo dose assessment in cell cultures after enrichment with Gadolinium and irradiation in the neutron field of the TRIGA Mainz
Presentation at YRBNCT Meeting 2013, Granada

Curriculum vitae